The Role of Seminal Fluid Extracellular Vesicles in Human Endometrial Receptivity



Helena Rodríguez Caro

St Peter's College

University of Oxford

Supervised by:

Dr. Ingrid Granne

Dr. Jennifer Helen Southcombe

Nuffield Department of Women's and Reproductive Health

A thesis submitted for the degree of *Doctor of Philosophy*
Michaelmas Term 2018

Dedicatoria

A:

Mis padres Diego y Carmen *por ser el pilar fundamental de mi persona, por estar conmigo en cada paso del camino de mi vida, por quererme, apoyarme y educarme. Muchísimas gracias por enseñarme a luchar por mis sueños y no darme por vencida. Vosotros sois la razón por la que este trabajo ha sido posible.*

Mis abuelos maternos Diego y María *por estar siempre cerca de mí, incluso en la distancia, por ser un gran modelo a seguir y enseñarme que en esta vida hay que seguir para adelante, adaptarse a los tiempos y que nunca es tarde para seguir aprendiendo y seguir creciendo como persona. Sois un gran ejemplo de vitalidad y amor, espero parecerme a vosotros en el futuro.*

A mis tíos Alonso y Juan *por ser tanto mis tíos como mis amigos, por quererme y apoyarme en todo momento, por cuidar de mí. Gracias por estar ahí siempre que lo necesito.*

Abstract

The Role of Seminal Fluid Extracellular Vesicles in Human Endometrial Receptivity

Helena Rodríguez Caro

Michaelmas Term 2018, St Peter's College
A thesis submitted in partial fulfilment of the requirements for the degree of Doctor of Philosophy at the University of Oxford.

Embryo implantation is a key limiting factor to In Vitro Fertilization (IVF) success, the main treatment of subfertility. A successful embryo implantation requires the endometrium to be receptive, which involves embryo-endometrium crosstalk, decidualisation, and modulation of the maternal immune system. Research data showed maternal exposure to seminal fluid improved clinical pregnancy rates. The seminal fluid contains extracellular vesicles that facilitate cell-cell communication through their cargo. This thesis aimed to investigate seminal fluid extracellular vesicles (SF-EVs) and their role in human endometrial receptivity.

SF-EVs, isolated by ultracentrifugation, were characterised and purified using size-exclusion chromatography. SF-EVs ranged between 15 to 300 nm and were a heterogenous group of EVs. Four populations were described based upon morphology while protein expression identified three $CD63^+$ SF-EV populations and suggested another four populations by co-localization and correlation studies respectively. Importantly, purified SF-EVs were demonstrated to be a good representation of physiological SF-EVs after analysing extracellular vesicles in unprocessed seminal fluid.

The role of SF-EVs in endometrial receptivity was then investigated. Bio-maleimide labelled SF-EVs bound to Ishikawa cells (endometrial adenocarcinoma cell line) and primary endometrial epithelial and stromal cells. SF-EVs bound more to untreated than progesterone treated Ishikawa cells, and, unlike previously described for progesterone-treated cells, SF-EVs did not induce dephosphorylation of CREB S133 in untreated Ishikawa cells. In addition, SF-EVs enhanced endometrial stromal cells secretion of prolactin throughout the days of decidualisation and increased total HCK Tyr411 phosphorylation in non-decidualised stromal cells. Bio-maleimide labelled SF-EVs also bound to primary endometrial immune cells. $CD4^+$ and $CD8^+$ T cells bound more SF-EVs than NK cells and regulatory $CD4^+$ T (Treg) cells showed higher SF-EV binding than non-regulatory $CD4^+$ T cells. SF-EVs did not change CD3 and CD25 Treg cell expression levels, which are involved in T cell receptor (TCR) mediated activation. Endometrial Treg cells also did not increase TGF-β1 expression after TCR mediated activation.

These DPhil thesis reports for the first time that SF-EVs interact with endometrial cells and play a role in endometrial receptivity suggesting they might be used as adjuvants to assist human embryo implantation in IVF. It also highlights the need for further research to understand endometrial Treg cellular physiology.

Acknowledgments

First of all, I would like to thank my supervisor Dr. Ingrid Granne for giving me the opportunity to undertake a DPhil at The University of Oxford with her. This DPhil has been a once in a life-time experience, an exciting journey filled with ups and downs that have helped me become a better scientist and person. Thanks for believing in me, for your guidance and for your constant support. I could not have asked for a better, strong-female role model. I am also hugely grateful to my second supervisor Dr. Jen Southcombe for her guidance and persistent help, this thesis would not have been possible without her. Thanks for all the fun memories in the lab, for your warm encouragement, and for always checking how I was doing. Thanks also to Dr. Rebecca Dragovic who has been like a third supervisor to me. It has been a privilege to have access to your expertise in the field of extracellular vesicles, thank you very much for all your guidance, support, and enthusiasm.

Heartfelt thanks go to The Rafael del Pino Foundation and St Peter's College for funding my DPhil studies and letting me be part of such wonderful and inspiring communities of people, which I hope to be involved with for many years.

I am also deeply grateful to all the patients from Oxford Fertility who participated in these studies, and to Dr. Tim Child and all the nurses and embryologists who were amazing at recruiting patients and collecting the samples, especially Ms. Ginny Mounce and Ms. Kate Field. Thanks also to Dr. Daniel Lunn for his advice and teaching in statistics, I really enjoyed learning more about this field. In addition, thanks to Dr. Errin Johnson for performing the electron microscopy. I would also like to express my gratitude to Mr. Andrew Malloy, Dr. George Daaboul, and Dr. Michael Senior for giving me the opportunity to collaborate with NanoView Bioscience, and Oxford Nanoimaging.

I would also like to thank all my colleagues at The John Radcliffe Hospital, special mention should be made to Dr. Gavin Collett and Ms. Janet Carver for all their help in the laboratory – thanks also to Janet for providing some endometrial stromal cells for these studies. In addition, I am grateful to have had such fantastic office mates, thanks for all the memories, the laughs, and making my days so enjoyable. Thanks also to Dr. Karin Hellner for teaching me how to isolate endometrial epithelial cells and to Dr. Robert A. Hirst and Mr. Abdulkhaliq Alsaadi for their advice on how to optimise this epithelial cell culture.

During this DPhil journey I have had the honour of making new friends that have helped me in this adventure. I especially want to thank Dr. Belinda Lo, Ms. Eszter Dombi, Ms. Madison Pearce, and Dr. Dhruti Babariya for all your support and advice, for keeping me sane and making me laugh; for being there for me. P.S. thanks also to Eszter for helping me with the IN Cell Analyser.

Finally, but most importantly, my heartfelt thanks go to my beloved family, especially to my father Mr. Diego Rodriguez Ropero and my mother Ms. Carmen Caro Gallego. Thanks for making me the person I am today, for your love, encouragement and support, and for teaching me to not give up and fight for my dreams.

Table of Contents

List of Figures *1*

List of Tables *6*

List of Abbreviations *8*

1 Introduction *10*

1.1 Human embryo implantation **11**

1.2 Seminal fluid role in embryo implantation **13**

1.3 The male reproductive system and seminal fluid **14**

1.4 Extracellular vesicles **18**

1.5 Aims and hypothesis of this thesis **22**

2 Analysis of Seminal Fluid Extracellular Vesicles (SF-EVs) *24*

2.1 Introduction **24**

2.1.1 Characterisation of SF-EVs: size & morphology 25

2.1.2 Molecular composition of SF-EVs 28

2.1.3 Functions of SF-EVs 29

2.1.4 SF-EVs as diagnostics and therapeutic tools 32

2.1.4.1 SF-EVs for non-invasive diagnosis of male subfertility: obstructive azoospermia Vs azoospermia due to spermatogenesis failure 32

2.1.4.2 SF-EVs for Human Immunodeficiency Virus (HIV) treatment 33

2.1.4.3 Prostasomes for non-invasive diagnose of prostate cancer 33

2.2 Aims of the chapter **35**

2.3 Methods **36**

2.3.1 Subject Recruitment 36

2.3.2 Isolation of SF-EVs 36

2.3.3 Characterisation of individual SF-EV samples 36

2.3.3.1 Nanoparticle tracking analysis (NTA) 37
2.3.3.2 Western blotting 38
2.3.4 SF-EV purification 39
2.3.4.1 Bio-maleimide labelling 39
2.3.4.2 Proteinase K treatment 40
2.3.5 Characterisation of purified pooled SF-EV preparations 41
2.3.5.1 Electron microscopy 41
2.3.5.2 ExoView analysis (NanoView Biosciences) 41
2.3.6 Statistical analysis 42
2.3.6.1 Characterization of individual SF-EV samples 42
2.3.6.1.1 NTA 42
2.3.6.1.2 Western blotting 43
2.3.6.1.3 Correlation analysis 43
2.3.6.2 SF-EV purification & Characterisation of SF-EV size in SF-EV preparations 43
2.4 Results 44
2.4.1 Characterisation of individual SF-EV preparations 44
2.4.1.1 NTA analysis of patients SF-EVs 44
2.4.1.2 Western blot analysis of patients SF-EVs 45
2.4.2 Correlations between SF-EV characteristics and patient's age and sperm analysis 46
2.4.3 SF-EVs are successfully purified using size-exclusion chromatography 51
2.4.4 Characterisation of purified pooled SF-EV preparations 57
2.4.4.1 Electron microscopy analysis of SF-EVs 58
2.4.4.1.1 SF-EVs comprise four morphologically different populations of extracellular vesicles 58
2.4.4.1.2 The majority of SF-EVs range from 20 to 80 nm 62
2.4.5 Purified pooled SF-EVs are similar to unprocessed seminal fluid SF-EVs (NanoView Biosciences Collaboration) 65
2.4.5.1 SF-EVs comprise three different $CD63^+$ populations of extracellular vesicles 65
2.4.5.2 The majority of SF-EVs range from 50 to 100 nm 67
2.5 Discussion 69

2.5.1 SF-EV sizes range from 15 to 300 nm ... 69
2.5.2 SF-EVs exhibit 4 different morphologies ... 71
2.5.3 SF-EVs populations and their biogenesis ... 73
2.5.3.1 Correlation study ... 73
2.5.3.2 Co-localization study ... 75
2.5.4 SF-EVs' CD9 level positively correlates with sperm count ... 77
2.5.5 Purified pooled SF-EVs are similar to unprocessed seminal fluid SF-EVs ... 78

3 The role of SF-EVs on luminal endometrial epithelial cell (EEC) receptivity to embryo implantation ... 80

3.1 Introduction ... 80
3.1.1 Development of luminal EEC receptivity to embryo implantation ... 80
3.1.1.1 Loss of apico-basal cell polarity ... 83
3.1.1.2 Pinopodes formation ... 84
3.1.1.3 Molecular changes ... 86
3.1.2 Failed luminal EEC receptivity to embryo implantation and subfertility ... 87
3.1.3 The role of seminal fluid on EEC receptivity to embryo implantation ... 87
3.1.3.1 SF-EVs effect on Ishikawa cells ... 88

3.2 Aims of the chapter ... 90

3.3 Methods ... 91
3.3.1 *In vitro* culture of Ishikawa cells ... 91
3.3.2 Subject Recruitment ... 91
3.3.3 Isolation and *in vitro* culture of primary luminal EECs ... 92
3.3.3.1 Bright field microscopy ... 94
3.3.4 SF-EV isolation and purification ... 95
3.3.5 Binding studies ... 95
3.3.5.1 Flow cytometry of Ishikawa cells ... 95
3.3.5.2 Flow cytometry of primary EECs ... 96
3.3.5.3 Fluorescence microscopy of Ishikawa cells (IN Cell 1,000 Analyser) ... 98
3.3.5.4 Fluorescence microscopy of Ishikawa cells (Nanoimager) ... 99

3.3.6 Molecular studies on Ishikawa cell activation 100
3.3.6.1 Western blot..... 101
3.3.7 Statistical analysis..... 101
3.3.7.1 In vitro culture of primary EECs – survival rates..... 101
3.3.7.2 Binding and Molecular studies 102
3.4 Results..... 103
3.4.1 SF-EVs bind to Ishikawa cells..... 103
3.4.1.1 SF-EV binding to Ishikawa cells increases with longer incubation times 103
3.4.1.2 Ishikawa cells binding of SF-EVs increased with higher EV:cell ratios. 106
3.4.1.3 SF-EV binding to Ishikawa cells decreased with increasing exposure time to progesterone and cAMP. 109
3.4.2 Analysis of CREB phosphorylation at S133 and HSP60 expression in untreated Ishikawa cells upon SF-EV exposure 114
3.4.3 Optimisation of isolation and *in vitro* culture of primary EECs..... 116
3.4.4 Primary luminal EECs bind SF-EVs 117
3.5 Discussion 123
3.5.1 EECs bind SF-EVs..... 123
3.5.2 Increased survival rates of *in vitro* culture primary luminal EECs..... 124
3.5.3 SF-EVs induce differential changes in CREB phosphorylation at S133 in Ishikawa cells during the implantation window..... 126
4 The role of SF-EVs on endometrial stromal cell (ESC) decidualisation..... 128
4.1 Introduction..... 128
4.1.1 Decidualisation of ESCs..... 128
4.1.1.1 The role of dESCs in endometrial immune modulation 131
4.1.1.2 Defective ESC decidualisation and subfertility..... 134
4.1.2 The role of seminal fluid on ESC decidualisation..... 134
4.2 Aims of the chapter 135
4.3 Methods 136

4.3.1 Subject Recruitment 136
4.3.2 Isolation and culture of ESCs 136
4.3.3 SF-EV isolation and purification 136
4.3.4 Binding studies 137
4.3.4.1 Flow cytometry 137
4.3.4.2 Fluorescence microscopy 138
4.3.5 Functional studies 138
4.3.5.1 Prolactin and IGFBP-1 ELISAs 139
4.3.5.2 Bright field microscopy 140
4.3.6 Molecular studies on ESC activation 140
4.3.6.1 Human phospho-kinase array 140
4.3.6.2 Western blot validation 141
4.3.7 Statistical analysis 142
4.3.7.1 Binding studies 142
4.3.7.2 Functional studies 143
4.3.7.3 Molecular studies 144
4.4 Results 145
4.4.1 SF-EVs bind to ESCs 145
4.4.2 ESC decidualisation is enhanced after SF-EV exposure 150
4.4.2.1 ESCs morphological differentiation into round-secretory cells is not affected by SF-EV treatment 150
4.4.2.2 ESC prolactin secretion increases after SF-EV treatment 152
4.4.2.3 ESCs IGFBP-1 secretion does not change after SF-EV treatment 153
4.4.3 Analysis of signalling pathways in ESCs upon SF-EV exposure 154
4.4.3.1 Total HCK Tyr411 phosphorylation in ESCs augments after SF-EV treatment 157
4.4.3.2 SF-EV treatment of ESC does not affect S2448 mTOR phosphorylation 161
4.4.3.3 HSP60 expression in ESCs does not change after SF-EV treatment 162
4.5 Discussion 164
4.5.1 SF-EVs bind to ESC 164
4.5.2 ESC decidualisation is enhanced after SF-EV exposure 164

4.5.3 ESCs protein phosphorylations vary after SF-EV exposure 167

5 The role of SF-EVs on maternal tolerance during the implantation window .. 172

5.1 Introduction 172

5.1.1 Endometrial T cells 176

5.1.1.1 Regulatory T cells 178

5.1.2 Endometrial regulatory T cells in reproductive pathologies 181

5.1.3 Seminal fluid effect on maternal tolerance 182

5.1.3.1 Immunoregulatory roles of SF-EVs 182

5.2 Aims of the chapter 185

5.3 Methods 186

5.3.1 *In vitro* culture of JY cells 186

5.3.2 Subject Recruitment 186

5.3.3 Isolation of primary endometrial immune cells 186

5.3.4 Isolation of Peripheral Blood Mononuclear Cells (PBMCs) 187

5.3.5 Isolation and *in vitro* culture of expanded endometrial Treg cells 187

5.3.5.1 Bright field microscopy 189

5.3.6 SF-EV isolation and purification 189

5.3.7 Flow cytometry binding studies 189

5.3.7.1 Cell membrane staining 190

5.3.7.2 Intracellular staining for nuclear proteins 190

5.3.7.3 Identification of endometrial uNK cells, $CD4^+$ T cells, and $CD8^+$ T cytotoxic cells 192

5.3.7.4 Identification of endometrial non-Treg $CD4^+$ T cells and Treg cells 193

5.3.8 Flow cytometry functional studies 194

5.3.8.1 Endometrial $CD4^+$ T cells 194

5.3.8.1.1 Intracellular cytokine staining 195

5.3.8.1.2 Identification of $CD4^+$ T cells 196

5.3.8.2 In vitro expanded Treg cells 197

5.3.8.2.1 Identification of Treg cells 198

5.3.9 Statistical analysis 198
5.3.9.1 Binding and Functional studies 198
5.4 Results 200
5.4.1 EICs bind SF-EVs 200
5.4.2 Endometrial $CD4^+$ T cell activation is not stimulated by SF-EVs 204
5.4.2.1 SF-EVs do not affect membrane CD3 and CD25 expression in endometrial $CD4^+$ T cells 204
5.4.2.2 SF-EVs do not affect membrane CD3 expression in endometrial T regulatory cells 206
5.4.3 Endometrial TGF-β1 secretion by $CD4^+$ T cells does not increase after stimulation 207
5.4.3.1 Intracellular expression of TGF-β1 in endometrial $CD4^+$ T cells 209
5.4.3.2 Membrane expression of TGF-β1 in endometrial Treg cells 211
5.5 Discussion 213
5.5.1 SF-EVs bind to EICs 213
5.5.2 SF-EVs do not activate endometrial Treg cells through the canonical TCR/CD3 complex-dependent pathway 213
5.5.3 Endometrial Treg cell activation does not increase TGF-β1 expression 215
6 Final Discussion 219
6.1 Comprehensive characterisation of human SF-EVs (aim 1) 219
6.1.1 SF-EVs alterations as markers of pathological conditions 220
6.2 Integrative model of SF-EVs role in human endometrial receptivity (aim 2 & aim 3) 222
6.2.1 SF-EVs as potential adjuvants to assist embryo implantation in IVF 226
6.3 Physiology of endometrial regulatory T cells (aim 3 derived research) 227
7 Final Discussion 229
8 Appendices 231
8.1 Appendix 1 231

8.2 Appendix 2..... 233

8.3 Appendix 3..... 236

8.4 Appendix 4..... 238

8.5 Appendix 5..... 239

References*..... *240

List of Figures

Fig 1.1 Embryo implantation..... 12

Fig 1.2 Male reproductive tract 16

Fig 1.3 Biogenesis of EVs..... 20

Fig 2.1 Morphology of SF-EVs: electron microscopy diagrams..... 27

Fig 2.2 Functional roles of SF-EVs. 30

Fig 2.3 Nanoparticle tracking analysis (NTA) of SF-EVs samples 1 to 21..... 45

Fig 2.4 Western blots of ALIX, CD9 and syntenin-1 in SF-EV samples 46

Fig 2.5 Expression of ALIX, CD9 and syntenin-1 in SF-EV samples 46

Fig 2.6 Correlation analyses of SF-EV concentrations..... 48

Fig 2.7 Correlation analyses between ALIX, CD9 and syntenin-1 SF-EV expression, and SF-EV mean & mode size. 50

Fig 2.8 Correlation analyses of ALIX, CD9 and syntenin-1 expression in SF-EVs with patients' characteristics. 51

Fig 2.9 Purification of SF-EV preparation # 2 by size-exclusion chromatography. 53

Fig 2.10 Purification of SF-EV preparation # 3 by size-exclusion chromatography. 54

Fig 2.11 Purification of bio-maleimide labelled SF-EV preparations # 1 and # 4 by size-exclusion chromatography. 55

Fig 2.12 Efficiency of SF-EV purification by size-exclusion chromatography..... 57

Fig 2.13 Electron microscopy of SF-EV preparation # 1..... 59

Fig 2.14 Electron microscopy of SF-EV preparation # 2..... 60

Fig 2.15 Electron microscopy of SF-EV preparation # 3..... 61

Fig 2.16 Electron microscopy of bio-maleimide labelled SF-EV preparation # 4. 62

Fig 2.17 SF-EV size distribution determined by nanoparticle tracking analysis (NTA) and electron microscopy. 64

Fig 2.18 Co-localization of SF-EV exosomal markers CD81, CD63 and CD9: ExoView. 66
Fig 2.19 Representative images of SF-EV size distribution: ExoView. 68
Fig 2.20 Morphology of SF-EVs: electron microscopy diagrams. 72
Fig 2.21 Potential SF-EV biogenesis pathways. 77
Fig 3.1 Development of receptivity to embryo implantation in luminal EECs. 81
Fig 3.2 Protein expression of p-CREB (S133) and HSP60 in day 7 progesterone treated Ishikawa cells after SF-EV treatment. 89
Fig 3.3 Isolation of primary EECs. 92
Fig 3.4 Flow cytometry identification of isolated primary luminal EECs on passage 0 or 2 (Protocol 2). 97
Fig 3.5 Flow cytometry identification of live primary luminal EECs isolated with protocol 3. 98
Fig 3.6 Representative flow cytometry histograms of SF-EV binding to Ishikawa cells: time-dependent experiment. 104
Fig 3.7 SF-EVs bind to Ishikawa cells at different incubation times: mean fluorescence intensity. 105
Fig 3.8 SF-EV binding to Ishikawa cells increases with longer incubation. 106
Fig 3.9 Representative flow cytometry histograms of SF-EV binding to Ishikawa cells: concentration-dependent experiment. 107
Fig 3.10 SF-EVs bind to Ishikawa cells at different ratios of EV:cell 108
Fig 3.11 Increased SF-EV binding to Ishikawa cells with increasing EV:cell ratio. ... 108
Fig 3.12 Morphology of Ishikawa cells under progesterone treatment. 109
Fig 3.13 Representative flow cytometry histogram of SF-EV binding to Ishikawa cells at different days of progesterone treatment 110

Fig 3.14 SF-EVs bind to Ishikawa cells at different days of progesterone treatment: mean fluorescence intensity..... 111

Fig 3.15 SF-EV binding to Ishikawa cells decreases when cells have been treated with progesterone. 112

Fig 3.16 SF-EVs associated with Ishikawa cells: Fluorescence microscopy..... 113

Fig 3.17 Western blotting analysis of CREB phosphorylation at S133 and HSP60 levels in untreated Ishikawa cells after SF-EV exposure..... 115

Fig 3.18 Optimization of isolation and *in vitro* culture of primary luminal EECs..... 117

Fig 3.19 Flow cytometry histograms of SF-EV binding to primary luminal EECs isolated with protocol 2 ($5x10^{10}$ SF-EVs/10^6 cells)..... 119

Fig 3.20 SF-EV binding to primary luminal EECs at passage 0 ($5x10^{10}$ SF-EVs/10^6 cells). 120

Fig 3.21 Flow cytometry histograms of SF-EV binding to primary luminal EECs isolated with protocol 3..... 121

Fig 3.22 SF-EV binding to primary luminal EECs isolated with protocol 3 ($1x10^{11}$ SF-EVs/10^6 cells). 122

Fig 3.23 SF-EV regulation of CREB signalling in luminal EECs receptive to embryo implantation..... 127

Fig 4.1 cAMP signalling pathway. 130

Fig 4.2 Immunoregulation by decidualised ESCs (dESCs). 133

Fig 4.3 Representative flow cytometry histogram of SF-EV binding to primary ESCs ($5x10^{10}$ SF-EVs/10^6 cells). 145

Fig 4.4 SF-EVs bind to primary ESCs: Mean fluorescence intensity. 147

Fig 4.5 SF-EVs bind to primary ESCs at different days of decidualisation..... 148

Fig 4.6 SF-EVs bind to primary ESCs: Fluorescence microscopy..... 149

Fig 4.7 Morphological ESCs differentiation into round secretory cells after single or multiple SF-EV exposure. 151
Fig 4.8 Percentage of decidualised ESCs at day 7 of decidualisation induction after SF-EV exposure. 152
Fig 4.9 Concentration of ESCs supernatant prolactin after single or multiple SF-EV exposure. 153
Fig 4.10 Concentration of ESCs supernatant IGFBP-1 after single or multiple SF-EV exposure. 154
Fig 4.11 Phosphorylation profiles of ESCs after SF-EV exposure. 156
Fig 4.12 Expression of HCK phosphorylation at Tyr411 in primary ESCs after SF-EV exposure: Western blots. 158
Fig 4.13 Expression of HCK phosphorylation at Tyr411 in primary ESCs after SF-EV exposure: dot plots. 159
Fig 4.14 Expression of HCK in primary ESCs after SF-EV exposure: dot plots..... 160
Fig 4.15 Western blotting and densitometry analysis of mTOR phosphorylation at S2448 in primary ESCs after SF-EV exposure. 162
Fig 4.16 Expression of HSP60 in primary ESCs after SF-EV exposure. 163
Fig 4.17 SRC family kinases signalling pathway and its relationship with dESCs prolactin gene. 170
Fig 5.1 Regulatory T cells (Treg) mechanisms of immune suppression. 180
Fig 5.2 TCR/CD3 complex-dependent pathway in $CD4^+$ T cells. 184
Fig 5.3 Flow cytometry identification of primary endometrial $CD4^+$ and $CD8^+$ T cells, and NK cells. 193
Fig 5.4 Flow cytometry identification of primary endometrial non-Treg $CD4^+$ T cells and T regulatory cells. 194

Fig 5.5 Flow cytometry identification of live primary endometrial $CD4^+$ T cells. 197

Fig 5.6 Flow cytometry identification of *in vitro* expanded endometrial T regulatory cells. 198

Fig 5.7 SF-EVs bind to primary EICs. 201

Fig 5.8 SF-EVs bind more to endometrial T cells than uNK cells. 202

Fig 5.9 SF-EVs bind to endometrial $CD4^+$ T cells. 203

Fig 5.10 SF-EVs bind more to endometrial T regulatory cells than non-Treg $CD4^+$ T cells. 204

Fig 5.11 SF-EVs effect on endometrial $CD4^+$ T cells expression of membrane CD3.. 205

Fig 5.12 SF-EVs effect on endometrial $CD4^+$ T cells expression of membrane CD25.206

Fig 5.13 SF-EVs effect on endometrial T regulatory cells expression of membrane CD3. 207

Fig 5.14 SF-EVs effect on intracellular TGF-β1 expression in endometrial $CD4^+$ T cells. 209

Fig 5.15 Intracellular TGF-β1 expression in endometrial $CD4^+$ T cells. 210

Fig 5.16 Representative image of TGF-β1 expression in endometrial and blood T regulatory cells. 212

Fig 5.17 Membrane TGF-β1 expression in endometrial T regulatory cells. 212

Fig 6.1 Integrative model of SF-EVs role in human endometrial receptivity 223

Fig 8.1 Representative flow cytometry histograms of Ishikawa cells treated with purified bio-maleimide labelled PBS (Negative control) 237

List of Tables

Table 2.1 Primary and secondary antibodies used for Western blotting. 38

Table 2.2 Characteristics of purified pooled SF-EV preparations..... 40

Table 2.3 Primary antibodies used for ExoView analysis. 42

Table 2.4 SF-EV mean and mode size of SF-EV preparations # 1, # 2, and # 3 63

Table 2.5 SF-EV populations based upon expression of CD9, ALIX and syntenin-1 ... 74

Table 2.6 SF-EV populations based upon expression of CD63, CD9 and CD81 76

Table 3.1 Fluorescence dye, primary and secondary antibodies used for flow cytometry and fluorescence microscopy studies. 100

Table 3.2 Primary and secondary antibodies used for Western blot on Ishikawa cells. 101

Table 4.1 Fluorescence dye, primary and secondary antibodies used for flow cytometry and fluorescence microscopy studies. 138

Table 4.2 Primary and secondary antibodies used for Western blot validation of phospho-kinase array on ESCs. 142

Table 5.1 Examples of cytokines and chemokines involved in the immune environment 174

Table 5.2 Main characteristics of T cell subtypes. 177

Table 5.3 Antibody-fluorochrome combinations used to identify (Panel 1) uNK cells, $CD4^+$ T cells, $CD8^+$ T cells, and (Panel 2) non-Treg $CD4^+$ T cells and Treg cells. 190

Table 5.4 Fluorescence conjugated antibodies used for flow cytometry. 191

Table 5.5 Antibody-fluorochrome combinations used to identify membrane CD3 and CD25, and intracellular TGF-β1 expression in $CD4^+$ T cells 195

Table 5.6 Fluorescence conjugated antibodies used for flow cytometry. 196

Table 5.7 Antibody-fluorochrome combinations used to identify CD3 and CD25 expression in Treg cells..... 198

Table 8.1 Clinical characteristics of patients recruited for sperm samples..... 231

Table 8.2 Clinical characteristics of patients recruited for EEC isolation. 233

Table 8.3 Clinical characteristics of patients recruited for ESC isolation. 238

Table 8.4 Clinical characteristics of patients recruited for EIC isolation. 239

List of Abbreviations

ADPR-cyclases	Adenosine diphosphate ribosyl cyclases
AIDS	Acquired immune deficiency syndrome
APCs	Antigen presenting cells
BCA	Bicinchoninic acid
BSA	Bovine serum albumin
cAMP	Cyclic adenosine monophosphate
COX2	Cyclooxygenase-2
CREB	cAMP response element binding
CV	Coefficient of variation
dESCs	Decidualised endometrial stromal cells
DMEM	Dulbecco's Modified Eagle's Medium
DMEM-F12	DMEM/Nutrient Mixture F-12 Ham
DLS	Dynamic light-scattering
ECACC	European Collection of Authenticated Cell Cultures
ECL	Enhanced chemiluminescence
ECM	Extracellular matrix
EDTA	Ethylenediaminetetraacetic acid
EEC	Endometrial epithelial cell
EICs	Endometrial immune cells
EpCam	Epithelial cell adhesion molecule
ESC	Endometrial stromal cell
ESCRT	Endosomal-sorting complex required for transport
EVs	Extracellular vesicles
EVT	Extravillous cytotrophoblast
FCS	Fetal calf serum
FGF2	Fibroblast growth factor 2
FoxP3	Forkhead box P3
GM-CSF	Granulocyte-macrophage colony-stimulating factor
GVHD	Graft-versus-host disease
HCK	Hematopoietic cell kinase
HFEA	Human Fertilisation & Embryology Authority
HIV	Human immunodeficiency virus
HLA	Human leukocyte antigen
HRP	Horseradish peroxidase
HSP60	60 kDa heat shock protein
IDO	Indoleamine 2,3-dioxygenase
IFNγ	Interferon γ
IGFBP-1	Insulin like growth factor binding protein 1
IL	Interleukin
ILVs	Intraluminal vesicles
IPB	Intracellular staining perm wash buffer

ITAMs	Immunoreceptor tyrosine-based activation motifs
IVF	*In vitro* fertilization
LAP	Latency-associated peptide
LIF	Leukemia inhibitory factor
MCP-1	Monocyte chemoattractant protein 1
MeFI	Median fluorescence intensity
MFI	Mean fluorescence intensity
MHC	Major histocompatibility complex
MMPs	Metalloproteases
mTOR	mammalian target of rapamycin
MUC1	Mucin 1
MVB	Multivesicular bodies
NCDs	Non-communicable diseases
NCS	Nucleolar channel systems
NTA	Nanoparticle tracking analysis
PB	Transcription factor 1X perm buffer
PBMCs	Peripheral blood mononuclear cells
PBS	Phosphate-buffered saline
PBS-T	PBS - 0.05 % Tween-20
PEG	Polyethylene glycol
PGE2	Prostaglandin E2
PK	Proteinase K
PKC	Protein kinase C
PMSF	Phenylmethylsulfonyl fluoride
PRLR$^{-/-}$	Prolactin receptor knockout
PSCA	Prostate stem-cell antigen
RIF	Recurrent implantation failure
RPL	Recurrent pregnancy loss
RT	Room temperature
SF-EVs	Seminal fluid extracellular vesicles
SFK	SRC family kinases
STAT	Signal transducer and activator of transcription
STB	Syncytiotrophoblast
TCR	T cell receptor
TGF-β1	Transforming growth factor β1
Th1	T helper 1
Th2	T helper 2
Th17	T helper 17
TIMP	Tissue inhibitors of metalloproteases
TNFα	Tumor necrosis factor α
Treg cell	Regulatory T cell
uNK cell	Uterine natural killer cell

1 Introduction

Subfertility is a global health issue (WHO, 2002, 2006) defined as the inability to conceive after two years or more of regular unprotected sexual intercourses (WHO, 2006, Child, 2013), which can lead to reduced quality of life (Chachamovich *et al.*, 2010). Subfertility affects 15 % of couples trying to conceive (WHO, 2002, Lletget, 2011), with an estimated 50 million subfertile couples around the world (Mascarenhas *et al.*, 2012). According to the 'Trends and figures report, 2014-2016' by The Human Fertilisation & Embryology Authority (HFEA), in the UK, data from couples seeking medical care for assisted reproduction, indicated 37 % of cases were attributed to male infertility, 31 % had female infertility, and 32 % were unexplained (HFEA, 2018).

In Vitro Fertilization (IVF) is the most common intervention for the treatment of infertility, and although it has allowed many couples to achieve pregnancy, the success rates are still low with approximately 21 % of the cycles resulting in live pregnancy (HFEA, 2018). Embryo implantation is a key limiting factor of IVF success with only 36 % of all transferred embryos implanting according to data from cycles in the UK in 2014 (HFEA, 2016). Even the transfer of a good quality day 5 embryo, defined by morphology, results in no more than a 60 % implantation rate (Gardner *et al.*, 2004). These data highlight the need for further research in embryo implantation and therapies to increase implantation and associated IVF success rates, because, as stated in the Universal Declaration of Human Rights[1], 1948 (Article 16) "men and women of full age, …, have the right… to found a family".

[1] Universal Declaration of Human Rights (www.un.org/en/universal-declaration-human-rights/)

1.1 Human embryo implantation

Embryo implantation is the process by which the conceptus is embedded into the maternal endometrium (Fig 1.1). After fertilization the conceptus travels through the fallopian tube reaching the uterus 5 days later at the blastocyst stage. Thereafter, the blastocyst hatches from the zona pellucida (Shankar Srinivas, 2013). On approximately day 6 the embryo starts implanting (Shankar Srinivas, 2013). The process of implantation consists of a series of sequential steps: 1) apposition - the embryo positions near the implantation site with the inner mass towards the side of contact, 2) adhesion – the embryo attaches to the luminal endometrial epithelium; 3) invasion - the embryo breaches and penetrates into the maternal endometrium which eventually surrounds the conceptus (Cha *et al.*, 2012). This intrusive process can only occur during the implantation window, a specific time-span when the endometrium is receptive (Fig 1.1).

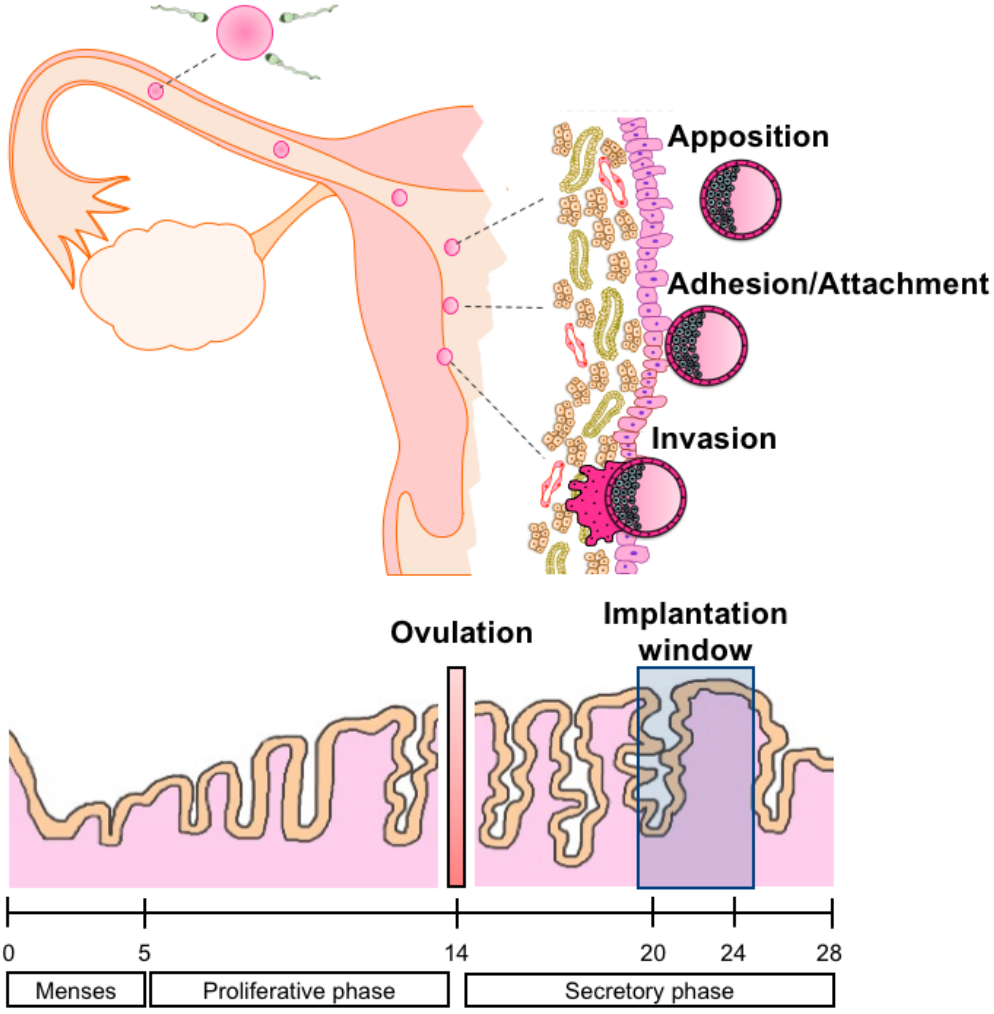


Fig 1.1 Embryo implantation
Diagram detailing the process of embryo implantation (top panel). Briefly, the embryo is fertilised in the fallopian tube, travels to the uterus and then implants in 3 sequential steps: apposition, adhesion/attachment, and invasion. This can only happen at a certain point of the menstrual cycle (bottom panel), during the implantation window of the secretory phase.

Endometrial receptivity refers to the phenotypical and functional transformations of endometrial cells to facilitate embryo-endometrium crosstalk, decidualisation, and maternal immune modulation (Cha *et al.*, 2012). Broadly, decidualisation refers to changes in the endometrium to support pregnancy. Receptivity in the oestrogen-primed endometrium is stimulated by the rise in progesterone after ovulation. Later during the secretory phase this process is assisted by factors from the blastocyst and the receptive

endometrial cells (Fazleabas and Strakova, 2002). In humans this receptive implantation window lasts around 4 days, therefore, in a normal 28 days menstrual cycle it ranges from day 20 to day 24 of the cycle (Fig 1.1) (Wilcox *et al.*, 1999, Cha *et al.*, 2012, Szamatowicz, 2016). In the following chapters the acquisition of receptivity in luminal epithelium, the decidualisation of stromal cells, and the regulation of immune cells in the maternal endometrium to achieve receptivity to embryo implantation will be discussed in detail.

Importantly, asynchrony between endometrial receptivity and embryo development can lead to implantation failure and/or recurrent implantation failure[2] (Ruiz-Alonso *et al.*, 2013, Teh *et al.*, 2016, Valdes *et al.*, 2017). This asynchrony can also result in other reproductive pathologies such as recurrent pregnancy loss[3] and pre-eclampsia[4] (Redman and Sargent, 2010, Salker *et al.*, 2010).

1.2 Seminal fluid role in embryo implantation

Evidence suggests maternal exposure to seminal fluid promotes human embryo implantation, although results are controversial. In 1986, Bellinge *et al.* showed that semen injection after oocyte pick up increased implantation rates by positively influencing the maternal endometrium (Bellinge *et al.*, 1986). In 2000, Tremellen *et al.*, reported that sexual intercourse during an IVF cycle also increased the chances of embryo implantation (Tremellen *et al.*, 2000). In addition, Chicea *et al.*, 2013 showed that maternal insemination with seminal fluid at the time of egg retrieval significantly

[2] Repeated implantation failure: a pathological condition defined as the inability to achieve clinical pregnancy after three IVF cycles.
[3] Recurrent pregnancy lost: a pathological condition defined as the loss of two or more pregnancies.
[4] Pre-eclampsia: an inflammatory pathology of pregnancy characterised by maternal hypertension and proteinuria.

increased implantation rates (Chicea *et al.*, 2013). However, other studies have not been able to corroborate these findings (Friedler *et al.*, 2013, von Wolff *et al.*, 2013). Interestingly, two meta-analysis of clinical trials recently showed that seminal fluid exposure during the cycle significantly increased clinical pregnancy rate (Crawford *et al.*, 2015, Ata *et al.*, 2018), suggesting that seminal fluid most likely facilitates embryo implantation. However, neither of these two studies observed any increase in live birth/ongoing pregnancy rates after exposure to seminal fluid, although the amount of data available was very limited (Crawford *et al.*, 2015, Ata *et al.*, 2018).

1.3 The male reproductive system and seminal fluid

The male reproductive system houses the synthesis, maintenance and transport of sperm and seminal fluid and facilitates their delivery into the female reproductive tract. It also produces and secretes androgens, such as testosterone, to ensure male reproductive function (Joaquin Gadea, 2013).

The male reproductive tract consist of the testes, the epididymides, the vas deferens, the urethra, the accessory glands (prostate gland, seminal vesicles, bulbourethral glands, and peri-urethral glands) and the penis (Fig 1.2) (Joaquin Gadea, 2013, Mawhinney and Mariotti, 2013). The testes are organs that make sperm, this process is termed spermatogenesis and takes 64 days in humans. Testes are ovid glands surrounded by the tunica albuginea and are suspended in the scrotum (Fig 1.2). Each teste is divided by two sections: the seminiferous tubules and the interstitium. Spermatogenesis occurs in the seminiferous tubules, which constitute 95 % of the testes. The multiple layers of sperm at different developmental stages are found within Sertoli cells, these cells provide nutritional and mechanical support. The interstitium contains blood and lymphatic cells,

connective tissue and several other cell types, including Leydig Cells which are the major source of testosterone (Joaquin Gadea, 2013, Mawhinney and Mariotti, 2013). The epididymides are coiled organs that transport sperm from the testes to the vas deferens, a process that takes approximately two weeks. They are located along the superior edge of the testes (Fig 1.2). Each epididymis is divided into the caput, the corpus, and the cauda. The caput is the segment closest to the teste and comprises between 10 to 15 efferent ducts with origin in the testes, that join together to form the epididymal duct. At the caput, fluids from the testes are absorbed and replaced with secretions from the epididymal epithelium. Importantly, sperm from the testes is fully differentiated but not fully mature. Sperm maturation happens during epidydimal transportation – this involves acquisition of sperm motility as well as the ability to recognise, bind and fuse with the oocyte. Mature sperm is stored at the cauda of the epididymis until ejaculation when it is released into the vas deferens (Joaquin Gadea, 2013, Lotti and Maggi, 2015). The vas deferens are single ducts that connect the epididymides to the urethra (Fig 1.2) (Joaquin Gadea, 2013). The urethra is a duct that extends from the bladder to the end of the penis and is a common path for urine and semen out of the body (Fig 1.2) (Joaquin Gadea, 2013). During ejaculation mature sperm travels from the vas deferens to the urethra where it is mixed with the seminal fluid and delivered into the female reproductive tract (Joaquin Gadea, 2013).

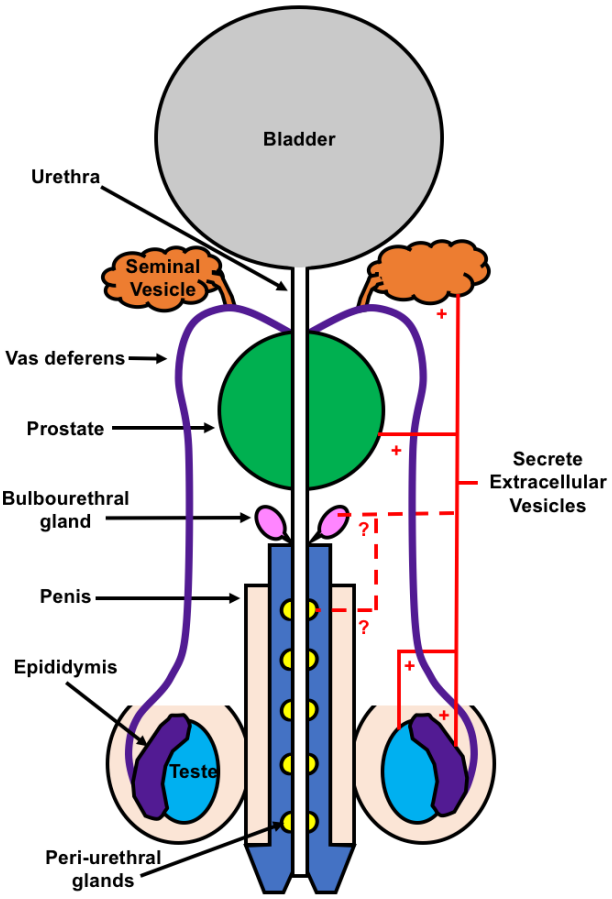


Fig 1.2 Male reproductive tract
Diagram detailing the structure of the male reproductive tract, that consists of the testes, the epididymides, the vas deferens, the urethra, the accessory glands (prostate gland, seminal vesicles, bulbourethral glands, and peri-urethral glands) and the penis. This diagram also illustrates which glands secrete extracellular vesicles (red lines).

90 % of the semen is seminal fluid, which contains a series of secretions from the accessory glands that provide sperm nutrition and modulate sperm function and interaction with the female reproductive tract (Mawhinney and Mariotti, 2013, Lotti and Maggi, 2015). The prostate gland is an organ located bellow the bladder surrounding the first segment of the urethra, in adults it has the size of a walnut (Fig 1.2) (Joaquin Gadea, 2013, Mawhinney and Mariotti, 2013, Lotti and Maggi, 2015). It secretes approximately 1/3 of the seminal fluid (Joaquin Gadea, 2013, Lotti and Maggi, 2015). Specifically, the prostate gland produces a barely acid fluid, rich in citric acid, zinc, calcium, acid phosphatase, and seminal plasmin (Joaquin Gadea, 2013, Mawhinney and Mariotti,

2013). The seminal vesicles are a paired of lobe-type glands located superior and posterior to the prostate, between the bladder and the rectum, just at the end of each vas deferens (Fig 1.2) (Joaquin Gadea, 2013, Mawhinney and Mariotti, 2013, Lotti and Maggi, 2015). They secrete an alkaline fluid that constitute between 50-80 % of the seminal fluid (Ramchandani *et al.*, 1993, Kim *et al.*, 2009, Joaquin Gadea, 2013). This fluid contains fructose, prostaglandins, flavins, vitamin C, mucus, and phosphorylcholine to nourish and stabilise the sperm. The prostatic acid phosphatase is an enzyme that hydrolases phosphorylcholine from the seminal vesicles to choline that is a sperm nutrient (Joaquin Gadea, 2013). The seminal vesicles also secrete semenogellins that form the gelatinous substrates of semen; these substrates are liquefied by prostatic prostate specific antigen (Mawhinney and Mariotti, 2013, Lotti and Maggi, 2015). The alkaline fluid from the seminal vesicles helps to neutralise the slightly acid prostate secretion and the acid environment in the vagina. The bulbourethral glands, also called Cowper's glands, are located distally to the prostate and they release their secretion at the root of the penis (Fig 1.2). Their secretion is an alkaline, viscous, clear mix of mucin, sialic acid and galactose, this mix acts as lubricant during sexual intercourse, protects the urethra and helps to neutralise the vaginal acid pH (Joaquin Gadea, 2013).

As described here, the molecular composition of the seminal fluid is varied including inorganic ions, proteins, lipids, glycans, oligosaccharides, small metabolites, and free genomic material (RNA, miRNA and DNA) (Joaquin Gadea, 2013, Mawhinney and Mariotti, 2013, Drabovich *et al.*, 2014, Druart and de Graaf, 2018, Samanta *et al.*, 2018). More information on the seminal fluid proteome can be found at Drabovich *et al.*, 2014, Druart and de Graaf, 2018, Samanta *et al.*, 2018. Importantly, the seminal fluid also contains large quantities of extracellular vesicles (EVs) (Poliakov *et al.*, 2009, Hoog and

Lotvall, 2015). These EVs are more likely a mix of EVs from the different organs of the male reproductive tract (Fig 1.2). The prostate gland and the seminal vesicles, which contribute to the largest volume of seminal fluid, are known to secrete EVs. In addition, approximately 10 % of the seminal fluid comes from the testes and the epididymides, and evidence suggests these organs also secrete EVs - therefore there might by epidydimal or testicular EVs in seminal fluid (Sullivan *et al.*, 2007, Sullivan and Saez, 2013, Aalberts *et al.*, 2014, Drabovich *et al.*, 2014, Tannetta *et al.*, 2014, Gao *et al.*, 2018). Up until now, no studies in the literature have investigated if the bulbouretral and peri-urethral glands produce EVs, it might be possible that a small proportion of seminal fluid EVs are secreted by these organs.

1.4 Extracellular vesicles

Extracellular vesicles (EVs) are membrane-enclosed complexes involved in cellular communication through their cargoes. They carry proteins, lipids and nucleic acids to target cells regulating multiple physiological processes (Raposo and Stoorvogel, 2013, Yanez-Mo *et al.*, 2015). EVs have been described in several body fluids such as plasma (Caby *et al.*, 2005, Lasser *et al.*, 2011), urine (Pisitkun *et al.*, 2004), and saliva (Lasser *et al.*, 2011). In addition, EVs play an important role in the development of multiple diseases, such as cancer (Greening *et al.*, 2015) and asthma (Mortaz *et al.*, 2018). EV cargoes in normal and pathological conditions are listed in ExoCarta[5], EVpedia[6] and Vesiclepedia[7] databases.

[5] ExoCarta (www.exocarta.org)
[6] EVpedia (www.evpedia.info)
[7] Vesiclepedia (www.microvesicle.org)

The main types of EVs are exosomes (30-100 nm), microvesicles (100 nm – 1 μm) and apoptotic bodies (1 – 5 μm) (Fig 1.3) (Raposo and Stoorvogel, 2013, D'Souza-Schorey and Schorey, 2018, Simon *et al.*, 2018). Apoptotic bodies are shed from the plasma membrane of cells undergoing programmed cell death (Kerr *et al.*, 1972, Simon *et al.*, 2018). Microvesicles are also shed from the plasma membrane, but from live cells (Chargaff and West, 1946, Raposo and Stoorvogel, 2013), in addition microvesicles, that are larger than 1 μm, shed by cancer cells have been described and are called oncosomes (Minciacchi *et al.*, 2017, Simon *et al.*, 2018). Exosomes are EVs released from the fusion of multivesicular bodies (MVB) with the plasma membrane (Raposo *et al.*, 1996, Raposo and Stoorvogel, 2013, Simon *et al.*, 2018). The biogenesis of exosomes is detailed in Fig 1.3 (McKelvey *et al.*, 2015, D'Souza-Schorey and Schorey, 2018, Juan and Furthauer, 2018, van Niel *et al.*, 2018). In short, exosomes formation starts with the membrane invagination of late endosomes, termed at this stage as MVBs, forming intraluminal vesicles (ILVs). During this invagination new cargo is transferred into the MVBs through different mechanisms. For example, proteins can be sorted through the canonical endosomal-sorting complex required for transport (ESCRT) pathway in which ubiquitinated proteins are recognised by ESCRT-0, that recruits ESCRT-I. ESCRT-I then activates ESCRT-II and binds ALIX[8]. ALIX will link ESCRT-I to ESCRT-III triggering the invagination of the MVB membrane with the cargo (Hurley, 2008, McKelvey *et al.*, 2015, Juan and Furthauer, 2018, van Niel *et al.*, 2018). Other ESCRT dependent/independent pathways can be involved, e.g.: the ALIX/Syntenin/Syndecan pathway, and the ESCRT independent dependent pathway of MVB membrane ceramide-rich regions (Trajkovic *et al.*, 2008, Baietti *et al.*, 2012, Juan and Furthauer, 2018, van Niel *et al.*, 2018). After the ILVs are formed the MVBs dock at the plasma membrane

[8] ALIX: ALG-2-interacting protein X

where they fuse releasing the ILVs, these secreted ILVs are now termed exosomes. Proteins involved in the above-mentioned process are used as markers of exosomes since they are enriched in these EVs, although some markers, for example CD9, are not exclusively expressed by exosomes and can also be found in microvesicles (Tannetta *et al.*, 2014). It is common practice to identify exosomes and microvesicles analysing protein markers and EV size and shape.

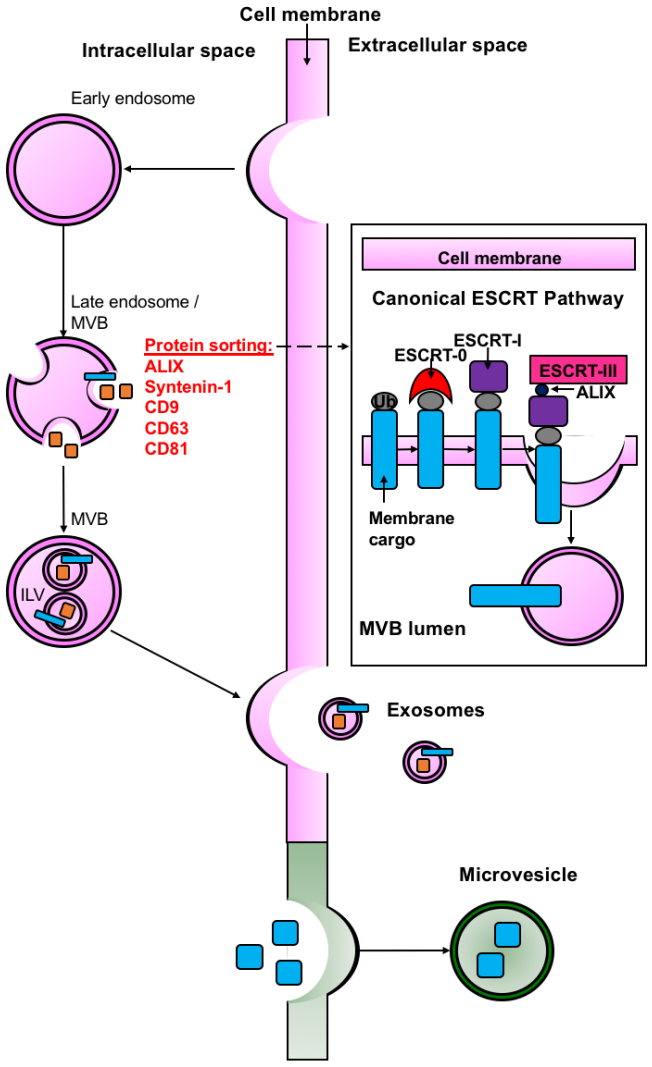


Fig 1.3 Biogenesis of EVs

Diagram detailing the biogenesis of exosomes and microvesicles. Exosomes are produced by the invagination of the late endosome/multivesicular body (MVB) forming intraluminal vesicles (ILVs). The MVB then fuse with the plasma membrane releasing the ILVs, now called exosomes. Proteins are sorted in the MVB by e.g. the canonical endosome sorting complex required for transport (ESCRT) pathway. Ub = ubiquitinated.

In the field of reproductive science there is a growing interest surrounding EVs (Tannetta *et al.*, 2014, Simon *et al.*, 2018). EVs have been described in multiple reproductive fluids, such as breast milk (Lasser *et al.*, 2011), amniotic fluid (Asea *et al.*, 2008), follicular fluid (Franz *et al.*, 2016), and seminal fluid (Poliakov *et al.*, 2009, Hoog and Lotvall, 2015). In addition, evidence showed that they can regulate human fertility and play a role in reproductive pathologies, e.g.: pre-eclampsia, polycystic ovarian syndrome, and sexually transmitted infections (Sang *et al.*, 2013, Tannetta *et al.*, 2014, Madison and Okeoma, 2015, Tannetta *et al.*, 2017, Simon *et al.*, 2018). Interestingly, in reproduction EVs facilitate cell-cell interactions between cells of the same organism and between organisms (male-female EV transfer). In this DPhil project I am interested in EVs transported from the male to the female reproductive tract – I hypothesise these EVs might assist embryo implantation. Therefore, only EVs present in the seminal fluid will be discussed, recent review articles detail information on other reproductive EVs (Tannetta *et al.*, 2014, Simon *et al.*, 2018).

1.5 Aims and hypothesis of this thesis

The introduction to this thesis has described the process of human embryo implantation and endometrial receptivity, and highlighted the importance of further research to improve implantation rates during IVF cycles. Evidence suggests seminal fluid can enhance implantation rates, which has been attributed to the presence of soluble proteins, such as transforming growth factor β-1 (Chang *et al.*, 2008), prostaglandin E2 (Frank *et al.*, 1994), and relaxin (Lane *et al.*, 1994). The seminal fluid also contains extracellular vesicles that play an important role in cellular communication and are known to regulate reproductive physiology. **I hypothesise that seminal fluid extracellular vesicles (SF-EVs) regulate maternal endometrial receptivity to facilitate successful embryo implantation.**

The overall aim of this thesis is to investigate the role of SF-EVs in human endometrial receptivity. To address this goal, this thesis aims:

1. **To characterise SF-EVs**: chapter 2 provides a comprehensive characterisation of SF-EVs and describes the preparation and purification of pooled SF-EV preparations that will be used in the following chapters. In addition, SF-EVs and patients' characteristics were analysed to determine if there were correlations.
2. **To evaluate the effect of SF-EVs on the receptivity of endometrial epithelium and stroma to embryo implantation**: chapter 3 describes the role of SF-EVs on luminal endometrial epithelial cells' receptivity. This chapter initially assesses SF-EV binding to Ishikawa cells, an endometrial epithelial cancer cell line, and their effect on Ishikawa cells' molecular signalling. Secondly, this chapter provides an

optimised protocol for isolation and *in vitro* culture of primary endometrial epithelial cells to confirm SF-EVs bind to the endometrial epithelium under normal conditions. Chapter 4 defines the role of SF-EVs on the regulation of endometrial stromal cell decidualisation. This chapter investigates SF-EV binding to primary endometrial stromal cells, and then analyses the effect of SF-EVs on stromal cell decidualisation and the molecular mechanisms involved.

3. **To investigate the effect of SF-EVs on maternal immunotolerance:** chapter 5 investigates SF-EV binding to endometrial immune cells subtypes, including uterine Natural Killer cells, $CD8^+$ T cells, $CD4^+$ T cells (non-regulatory $CD4^+$ T cells and regulatory $CD4^+$ T cells). Then, the effect of SF-EVs on the activation of endometrial $CD4^+$ T cells, specifically regulatory T cells, is analysed. The expression pattern of the immunosuppressive cytokine Transforming Growth Factor β1 (TGF-β1) in the latter cells is also characterised.

MSc declaration

The work of this DPhil thesis is a continuation of my MSc Clinical Embryology (University of Oxford) Research Project titled "Immune regulatory functions of prostasomes". The MSc data presented in this thesis is highlighted in the corresponded subsections. In short, SF-EV samples 1 to 11 were isolated and characterized by NTA and Western blotting during my MSc (chapter 2). In addition, chapter 3 work is based upon the dephosphorylation effect of SF-EV on CREB signalling in progesterone treated Ishikawa cells which was discovered during my MSc.

2 Analysis of Seminal Fluid Extracellular Vesicles (SF-EVs)

2.1 Introduction

The seminal fluid contains trillions of extracellular vesicles per millilitre. Traditionally, scientists have termed all EVs in the seminal fluid prostasomes. However, as mentioned in the introduction, evidence suggests these EVs are not exclusively from the prostate, therefore this description is inaccurate. Seminal fluid EVs are a mix of exosomes and microvesicles secreted from different organs of the male reproductive tract, including the epididymis, the seminal vesicles and the prostate (Sullivan *et al.*, 2007, Sullivan and Saez, 2013, Aalberts *et al.*, 2014, Tannetta *et al.*, 2014). EVs from the epididymis and the prostate are called as epididymosomes and prostasomes respectively (Sullivan and Saez, 2013, Aalberts *et al.*, 2014, Tannetta *et al.*, 2014).

Evidence for the presence of multiple SF-EV subpopulations with alternative function comes from a study in humans that showed both seminal fluid EVs and prostate cancer EVs (isolated from prostate cancer bone metastases) increased the number of sperm with forward motility, while prostasomes isolated from healthy prostatic tissue, obtained from patients with adenocarcinoma of the uterine bladder, did not (Carlsson *et al.*, 2003). This suggested EVs not originating from the prostate exert this effect. In addition, less than 40 % of EVs isolated from seminal fluid of vasectomized men - which contain secretions from the seminal vesicles and the prostate but not from the testes and the epididymis - expressed prostate stem-cell antigen (PSCA), a marker of prostasomes. This suggests some of these EVs might have come from the seminal vesicles (Aalberts *et al.*, 2012).

Acknowledging the multiple tissue origins of the EVs in seminal fluid, I have referred to them in this thesis as Seminal Fluid Extracellular Vesicles (SF-EVs).

2.1.1 Characterisation of SF-EVs: size & morphology

SF-EV diameters are measured between 50 to 500 nm with a mean size of 150 nm and a mode size of 120 nm (Ronquist and Nilsson, 2004, Tannetta *et al.*, 2014). This range is based on multiple characterization techniques. Nanoparticle tracking analysis (NTA) analysis showed SF-EVs from 50 to 350 nm, mode size of 120 nm (Tannetta *et al.*, 2014) and mean size of 146 nm (Garcia-Rodriguez *et al.*, 2018). Electron microscopy studies of isolated SF-EVs and human ejaculates also revealed SF-EVs ranged from 50 to 300 nm, mean size of 120 nm (Poliakov *et al.*, 2009, Hoog and Lotvall, 2015). Similarly, quasi-elastic light scattering showed SF-EVs size ranged from 150 to 200 nm (Arienti *et al.*, 1997, Carlini *et al.*, 1997), of note SF-EVs smaller than 150 nm might not have been detected due to the detection limit of the technique. Interestingly, Chiasserini *et al*. has recently analysed SF-EVs using dynamic light-scattering (DLS) and observed 2 SF-EV populations with different sizes; one population had a mean size of approximately 80 nm and the other of approximately 300 nm (Chiasserini *et al.*, 2015). This suggests SF-EV size distribution profiles might have higher concentration of smaller SF-EVs than previously described, or that there are smaller SF-EVs that have not been detected with some techniques.

SF-EVs are characterised by a trilamellar membrane and diverse morphology (Poliakov *et al.*, 2009). Multiple groups have described high and low electron-dense SF-EVs (Poliakov *et al.*, 2009, Ronquist *et al.*, 2012, Hoog and Lotvall, 2015, Garcia-Rodriguez *et al.*, 2018). A detailed analysis of isolated SF-EVs by cryo-electron microscopy

revealed 3 different SF-EV populations based on morphology (Fig 2.1) (Poliakov *et al.*, 2009): Type 1) 50 % are round high-electron dense SF-EVs with asymmetric distribution of a dark substance and one or more secondary vesicles inside. Type 2) 25 – 30 % are round low-electron dense SF-EVs with cauliflower protrusions and sometime secondary vesicles inside. Type 3) 20 - 25 % are elongated or pear-shaped low-electron dense SF-EVs (Poliakov *et al.*, 2009).

Human ejaculates of 1 patient were also analysed by cryo-electron microscopy (Hoog and Lotvall, 2015). The authors of this study identified multiple structures including small high electron-dense particles and EVs. The different SF-EV populations described are detailed in Fig 2.1: Type 1) high-electron dense double SF-EVs with dark material inside asymmetrically distributed. Type 4) low electron-dense single, double and multivesicular SF-EVs. Some of these vesicles presented double trilamellar membranes closely opposed to each other. 90% of the structures observed were classified as small high-electron dense particles with no clear membrane bilayer (Hoog and Lotvall, 2015).

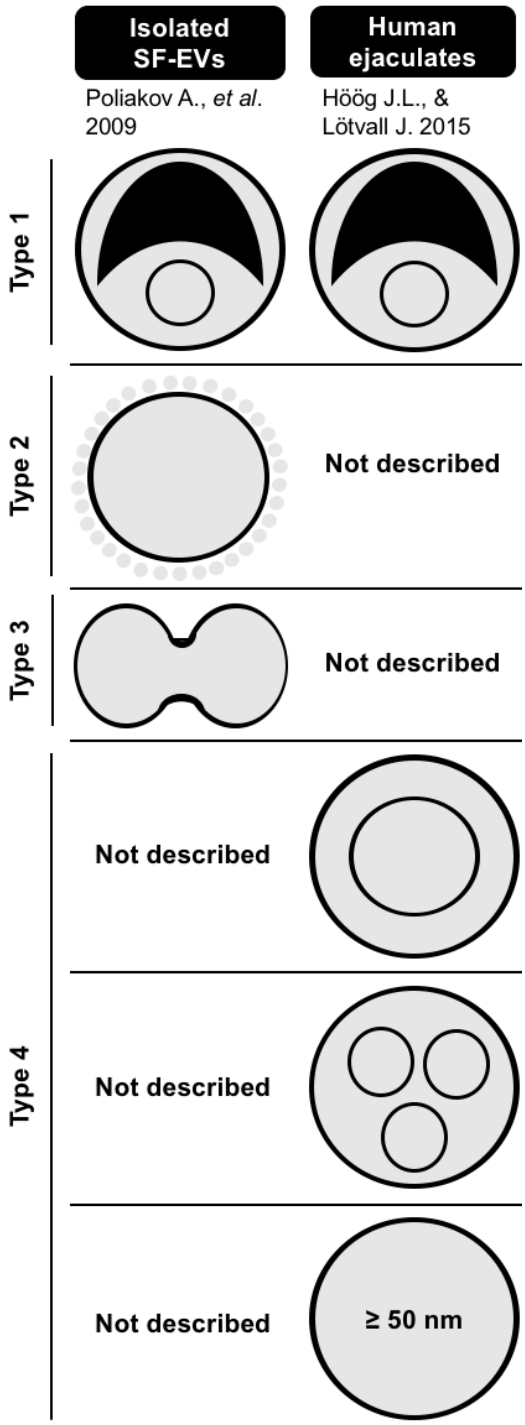


Fig 2.1 Morphology of SF-EVs: electron microscopy diagrams.
4 types of SF-EVs were described in isolated SF-EVs (Poliakov *et al.*, 2009, Hoog and Lotvall, 2015). **Type 1)** Round high-electron dense SF-EVs with asymmetric distribution of a dark substance and one or more secondary vesicles inside. **Type 2)** Round low-electron dense SF-EVs with cauliflower protrusions sometimes containing secondary vesicles inside. **Type 3)** Elongated or pear-shaped low-electron dense SF-EVs. A study in human ejaculates confirm type 1 SF-EVs but did not detect type 2 and type 3. In addition, **Type 4)** round low-electron dense SF-EVs without or with one or more secondary vesicles inside, were described in human ejaculates.

2.1.2 Molecular composition of SF-EVs

The outer membrane of SF-EVs has a characteristic lipid composition with high cholesterol/phospholipid ratio of approximately 2:1 (Carlsson *et al.*, 2003, Chiasserini *et al.*, 2015). This trilamellar membrane is rich in cholesterol and sphingomyelin and contains mainly saturated or monounsaturated fatty acids. High cholesterol levels stabilise the membrane (Ronquist and Nilsson, 2004, Aalberts *et al.*, 2014, Chiasserini *et al.*, 2015). Unlike SF-EVs, epididymosomes have a cholesterol/phospholipid ratio of 0.5:1 and sphingomyelin concentration increases throughout the epididymis reaching high levels by the cauda in mice (Rejraji *et al.*, 2006, Girouard *et al.*, 2011). Like SF-EVs, SF-EVs of normal and vasectomised patients and prostasomes from ex-vivo metastatic prostate tissue, isolated from prostate cancer bone metastases, have approximately 2:1 cholesterol/phospholipid ratio, with high levels of cholesterol and sphingomyelin (Carlsson *et al.*, 2003, Brouwers *et al.*, 2013).

SF-EVs contain genomic material including DNA and RNA (Ronquist *et al.*, 2009, Ronquist *et al.*, 2012). DNA levels in SF-EVs varied between populations ranging from 50 to 160 ng/µL and 31 % of the DNA corresponded to gene sequences (Ronquist *et al.*, 2012). Regarding RNA, seminal fluid from healthy donors carried YWAHZ[9] and HSP90ß[10] mRNA (Thimon *et al.*, 2008). Epididymosomes also contained mRNA encoding 90 % of the proteins found in these EVs (Thimon *et al.*, 2008). In addition prostasomes isolated from serum of mice grafted with human prostate cancer xenografts,

[9] YWAHZ: 14-3-3 protein zeta/delta
[10] HSP90ß: Heat shock protein 90ß

were shown to carry prostate cancer-specific fusion gene TMPRSS2[11]:ERG mRNA (Jansen *et al.*, 2009).

SF-EVs carry a wide range of proteins and multiple comprehensive proteomic studies have been performed to identify protein cargoes (Utleg *et al.*, 2003, Poliakov *et al.*, 2009, Ronquist *et al.*, 2013). To date more than 400 SF-EV proteins have been discovered using these proteomic studies, including enzymes, protein kinases and chaperones (Utleg *et al.*, 2003, Poliakov *et al.*, 2009). Some of these proteins are found in all epididymosomes, prostasomes and seminal vesicles EVs, but other are specific, serving as markers of cell origin. In general, SF-EVs contain tetraspanins (e.g. CD9), annexin 2 and PGAM2[12]. Only epididymosomes express CRISP1[13] and NPC2 (Thimon *et al.*, 2008), suggesting epididymosomes carrying the latter proteins are likely uptaken during sperm maturation in the epididymis. Prostasomes also express PSCA, CD26 and CD13, which are absent in seminal vesicles EVs (Sahlen *et al.*, 2010, Aalberts *et al.*, 2012). On the contrary, seminal vesicles EVs carry CD55 and CD70 while prostasomes do not (Sahlen *et al.*, 2010).

2.1.3 Functions of SF-EVs

The functional role of SF-EVs is not yet fully understood, known roles are summarised in Fig 2.2. SF-EVs are known to carry information from cells of the male reproductive tract to sperm, regulating sperm capacitation, acrosome reaction, and motility. SF-EVs adhere to sperm but only fuse at an acidic pH (4 – 6.5) but not at pH 7 and above (Ronquist *et al.*, 1990, Arienti *et al.*, 1997, Carlini *et al.*, 1997). This fusion is exclusively pH-

[11] TMPRSS2: Transmembrane Serine Protease 2
[12] PGAM2: Phosphoglycerate Mutase 2
[13] CRISP1: Cysteine Rich Secretory Protein 1

dependent and addition of Ca^{2+} or other divalent cations do not exert effects, unlike with other EVs, e.g.: rat liposomes mixed with sperm (Arienti *et al.*, 1997).

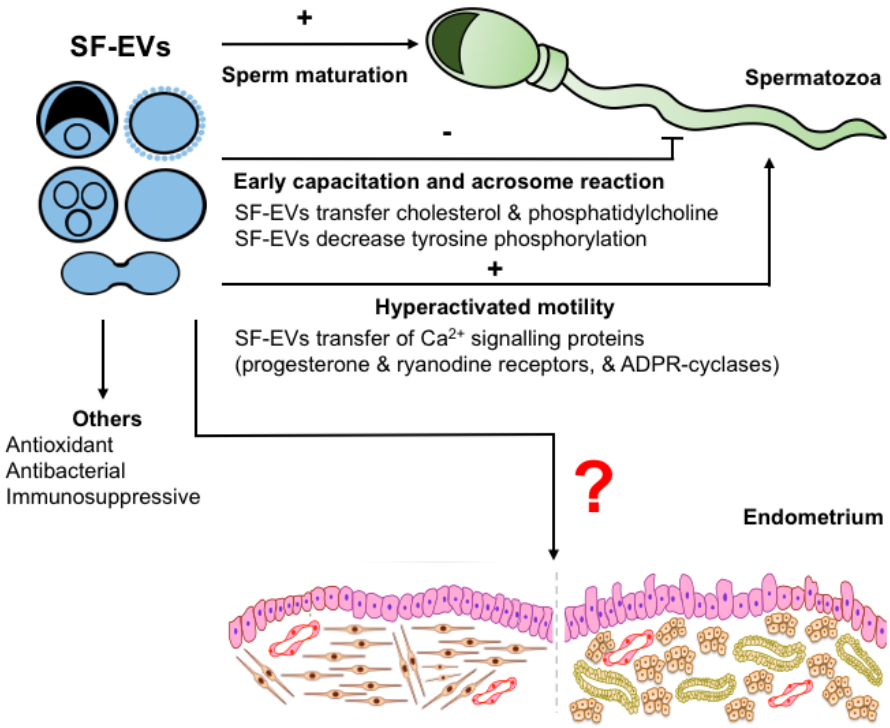


Fig 2.2 Functional roles of SF-EVs.
SF-EVs promote sperm maturation in the epididymis, inhibit early sperm capacitation and acrosome reaction, and promote sperm hyperactivated motility by transferring proteins involved in calcium signalling. Apart from regulating sperm function, SF-EVs are antioxidant, antibacterial and immunosuppressive. Currently, the functional effect of SF-EVs on the maternal endometrium is unknown. ADPR-cyclases = adenosine diphosphate ribosyl cyclases

In the female reproductive tract the sperm must undergo capacitation, acquisition of hyperactivated motility, and the acrosome reaction to be able to fertilize the oocyte. SF-EVs prevent early capacitation and acrosome reaction, which is a known cause of subfertility (Tesarik, 1989, Chemes and Rawe, 2003); a lower proportion of sperm undergo these modifications after SF-EV fusion (Pons-Rejraji *et al.*, 2011). Capacitation involves a decrease in cholesterol levels of the sperm membrane to increase fluidity (Pons-Rejraji *et al.*, 2011). Interestingly, SF-EV fusion to sperm leads to the transfer of lipids from SF-EVs to sperm decreasing sperm membrane fluidity (Carlini *et al.*, 1997).

Cholesterol and phosphatidylcholine levels are higher in sperm fused with SF-EVs (Bechoua *et al.*, 2011). Capacitation and the acrosome reaction are also involved with changes in protein phosphorylations (Bechoua *et al.*, 2011, Pons-Rejraji *et al.*, 2011), SF-EVs decreased tyrosine phosphorylation of P80 and P110 proteins which are markers of sperm capacitation in human (Pons-Rejraji *et al.*, 2011). In addition, SF-EVs also decreased tyrosine phosphorylation of P107 which is a sperm protein phosphorylated during the acrosome reaction (Bechoua *et al.*, 2011). SF-EVs promote sperm hyperactivated motility (under progesterone stimulation), characterised by asymmetrical flagellar beating with high amplitude (Park *et al.*, 2011). This motility is activated by Ca^{2+} signalling, SF-EVs transfer multiple proteins involved in this signalling pathway to the sperm including, progesterone receptors, ryanodine receptors, and adenosine diphosphate ribosyl cyclases (ADPR-cyclases) (Park *et al.*, 2011), which confers higher ADPR-cyclase activity to sperm (Park *et al.*, 2011).

In addition, SF-EVs are antioxidant and immunosuppresive protecting sperm against reactive oxygen species, and the female immune system. SF-EVs also show antibacterial capability (Fig 2.2) (Ronquist and Nilsson, 2004, Ronquist *et al.*, 2012, Aalberts *et al.*, 2014, Tannetta *et al.*, 2014). Up until now the immunosuppressive effect of SF-EVs has mainly been studied on blood derived immune cells, and their effect on endometrial immune cells is unknown – for more information go to chapter 5. To our knowledge there is no published data on the functional effect of SF-EVs on the endometrium (Fig 2.2).

.

2.1.4 SF-EVs as diagnostics and therapeutic tools

2.1.4.1 SF-EVs for non-invasive diagnosis of male subfertility: obstructive azoospermia Vs azoospermia due to spermatogenesis failure

As SF-EVs play an important role in sperm regulation, it has been hypothesized that SF-EV populations might also be altered in male subfertility. A study showed that the protein content of SF-EVs varied between non-normozoospermic and normozoospermic patients but no differences in SF-EV size or concentration were found (Garcia-Rodriguez *et al.*, 2018). SF-EVs from non-normozoospermic patients carried CHMP2B[14], exportin-1, and 40S ribosomal protein S19, while SF-EVs from normozoospermic patients did not. On the contrary, non-normozoospermic SF-EVs did not express Ras-related protein Rab-22A or 26S protease regulatory subunit 10B, while normozoospermic SF-EVs did (Garcia-Rodriguez *et al.*, 2018).

SF-EV miRNA also varies between normozoospermic and azoospermic individuals (Barcelo *et al.*, 2018), with reduced miR-122-5p, piR58527 and miR-539-5p in azoospermia. In addition, miR-205-5p and miR-31-5p levels were decreased in SF-EVs from obstructive azoospermia but not in SF-EVs from patients with azoospermia due to spermatogenic failure. Interestingly, this study showed that analysing SF-EV miR-31-5p the type of azoospermia can be predicted with 92.9 % of sensitivity and 90 % of specificity. High expression levels of these miRNAs were associated with azoospermia due to spermatogenic failure (Barcelo *et al.*, 2018). Currently, only invasive diagnostic test biopsies are used to determine if a patient suffers of obstetric azoospermia or spermatogenic failure, and the result obtained determines the treatment. Analysis of SF-

[14] CHMP2B: charged multivesicular body protein 2b

EV miR-31-5p is a promising non-invasive diagnostic approach but it needs further validation.

2.1.4.2 SF-EVs for Human Immunodeficiency Virus (HIV) treatment

HIV is responsible for the Acquired Immune Deficiency Syndrome (AIDS) and is diagnosed in approximately 1.8 million patients each year (UNAIDS, 2018). HIV is predominantly transmitted through sexual interactions, including anal, vaginal and oral sex, and semen is the primary transmission vector - sexual transmission of this virus through vaginal intercourse seems to require multiple sexual exposure, suggesting a defensive mechanism in the reproductive tract (Nicolosi *et al.*, 1994, Byrn *et al.*, 1997, Royce *et al.*, 1997, Vernazza *et al.*, 1999, Varghese *et al.*, 2002, Patel *et al.*, 2014). Madison *et al*. 2014 showed SF-EVs inhibited HIV replication in different cell lines exposed to HIV before, at the same time, or after SF-EV treatment. This effect was exclusively attributed to SF-EVs, and no inhibition was observed with blood EVs (Madison *et al.*, 2014). This same group showed SF-EVs inhibited transmission of HIV from vaginal epithelial cells to other cells and also inhibited HIV crossing through the vaginal epithelial barrier in *in vitro* studies (Madison *et al.*, 2015). In addition, SF-EVs restricted murine AIDS virus intravaginal transmission and propagation in *in vivo* studies (Madison *et al.*, 2015).

2.1.4.3 Prostasomes for non-invasive diagnose of prostate cancer

Prostate cancer is the most common cancer in males, it is estimated that around 30 % of men over 65 years old are diagnosed with this cancer (Stangelberger *et al.*, 2008, Ferlay *et al.*, 2010). Currently, prostate cancer diagnosis is invasive, involving rectal examination and prostate biopsy, and has low accuracy; 23 – 45 % of the cases are missed

and 50 % of diagnosis are at advanced stages (Horwich *et al.*, 2013). A non-invasive accurate diagnostic method that discriminates between benign prostatic disease and invasive prostatic cancer is required.

Transformed prostatic cells lose their polarity, secreting molecules and prostasomes not only into the prostate ducts but also into the blood circulatory system. Prostasomes from prostate carcinoma cells might promote progression and invasiveness of the tumour due to their immunosuppressive and angiogenic properties (Ronquist and Nilsson, 2004). This has led to the investigation of prostasomes in prostate cancer cells and their potential role as diagnostic tools of prostate cancer, reviewed in (Tompkins *et al.*, 2015, Zijlstra and Stoorvogel, 2016).

In 2016, Biggs *et al*., published a paper showing that quantifying prostasomes levels in plasma using nanoscale flow cytometry accurately differentiated patients with high risk of prostate cancer (Gleason Score $\geq$ 8) from patients with intermediate or low risk. Prostasomes levels were significantly increased in plasma from patients with Gleason Score $\geq$ 8 compared to patients with lower scores. Treatment of these high-risk patients with radical prostatectomy significantly reduced prostasome concentrations in plasma 3 weeks after surgery (Biggs *et al.*, 2016). This preliminary data suggests prostasomes are a promising non-invasive tool to diagnose high-burden prostate cancer.

SF-EVs are a promising diagnostic and therapeutic tool of the above medical conditions and might also regulate endometrial receptivity (this thesis hypothesis). Therefore, further research on SF-EVs is needed to understand this heterogeneous population of EVs.

2.2 Aims of the chapter

1) To provide a comprehensive characterisation of SF-EVs using well-known and state of the art techniques
2) To determine if there is any correlation between SF-EV characteristics and sperm analysis
3) To purify pooled SF-EVs for the experiments in the following chapters

2.3 Methods

2.3.1 Subject Recruitment

Ethical approval for seminal fluid samples were obtained from the South Central Research Board - #12/SC/0468. All patients gave written informed consent. Human seminal fluids were collected from patients at Oxford Fertility (n = 38). Patient characteristics are described in appendix 1.

2.3.2 Isolation of SF-EVs

Human seminal fluid samples were centrifuged at 1,000 x g for 10 min at room temperature (RT) to remove sperm, and then at 10,000 x g for 10 min at RT to remove cellular debris. The supernatants were then collected and stored at - 80°C before use. Afterwards, the supernatants were diluted in a total volume of 11 mL with phosphate-buffered saline (PBS) (Sigma-Aldrich, USA) and ultracentrifugation performed at 100,000 x g for 2 hrs at 4°C using a L-80 ultracentrifuge with a Sorval TH-641 swing out rotor (Beckman Coulter, UK). The pellets were then resuspended in 500 µl of PBS and the SF-EV preparations were stored at - 80°C.

2.3.3 Characterisation of individual SF-EV samples

Individual SF-EV preparations were analysed by NTA and by Western blotting. Prior to the Western blotting, the protein content of SF-EVs was determined using a bicinchoninic acid (BCA) protein assay (Thermo Scientific, USA).

Individual seminal fluid samples from patient number 1 to 11 were isolated and characterized by NTA and Western blotting by me during my MSc research project (MSc Clinical Embryology, Oxford).

Individual seminal fluid samples from patient number 22 to 31 were isolated and characterized by NTA and Western blotting by Srishti Sawney, an MSc Clinical Embryology student whom I co-supervised.

2.3.3.1 Nanoparticle tracking analysis (NTA)

SF-EV samples were analysed by NTA using a NanoSight LM10 with a 405 nm laser (Malvern, UK). SF-EV preparations were diluted in PBS to reach concentrations inside the precision range of the NTA machine ($2x10^8$ to $10x10^8$ particles/ml). EVs were measured at camera level 12 (Camera shutter speed: 15ms, camera gain: 350) using the following script: PRIME, DELAY 5, CAPTURE 60, REPEAT 5, in total 5 videos of 60 sec were taken per sample. These videos were analysed using NanoSight NTA 2.3 software (Malvern, UK) or NanoSight NTA 3.1 software (Malvern, UK).

During my DPhil project the department changed NTA software from NanoSight NTA 2.3 software (Malvern, UK) to NanoSight NTA 3.1 software (Malvern, UK). Therefore, I had to start using NanoSight NTA 3.1 on January 2017. Results obtained with different software are not comparable. All the SF-EVs used in each experiment were analysed by the same software. SF-EVs samples 1 – 21 were analysed using NanoSight NTA 2.3 software, and samples 22 – 36 were analysed with NanoSight NTA 3.1.

2.3.3.2 Western blotting

10 µg of protein per sample was separated by electrophoresis using NuPAGE 4 - 12 % Bis-Tris Gels (Life technologies™, USA) under reducing conditions. Proteins were then transferred onto Immuno-Blot® PVDF Membranes (BIO-RAD, USA) using a BIORAD semidry Western blot apparatus and nonspecific binding was blocked with 5 % dried skimmed milk (Marvel, UK) in PBS - 0.05 % Tween-20 (PBS-T). Afterwards, membranes were incubated overnight with primary antibodies towards exosomal markers (Table 2.1). Membranes were then washed and incubated with appropriate secondary antibodies conjugated to horseradish peroxidase (HRP) (Table 2.1). All antibodies were diluted 1:1,000 in 5 % milk/PBS-T. Proteins were developed using EZ-ECL enhanced chemiluminescence (ECL) detection kit for HRP (Biological Industries, Israel) and Amersham Hyperfilm™ ECL (GE Healthcare, UK). Results were analysed using Image J software version 1.43v.

Table 2.1 Primary and secondary antibodies used for Western blotting.
Approx. MW = Approximated Molecular Weight

Antibody	Approx. MW	Source	Clone	Company
Anti-ALIX	100 KDa	Mouse	3A9	Cell Signalling, USA
Anti-CD9	20 KDa	Rabbit	EPR2949	Abcam®, UK
Anti-Syntenin-1	32 KDa	Rabbit	EPR8102	Abcam®, UK
Anti-CD63	26 KDa	Mouse	MEM-259	Abcam®, UK
Anti-CD81	30 KDa	Rabbit	Polyclonal	Abcam®, UK
anti-Mouse IgG-HRP	-	Goat	Polyclonal	Dako, Denmark
anti-Rabbit IgG-HRP	-	Goat	Polyclonal	Dako, Denmark

2.3.4 SF-EV purification

SF-EV individual preparations were pooled together and proteins not associated with extracellular vesicles were removed by size-exclusion chromatography following a modified protocol from (Welton *et al.*, 2015). In brief, 100 µL of each sample was mixed to create pooled SF-EV samples – 4 different pools were created (n = 11, n = 10, n = 10, n =10) (Table 2.2). After mixing, 80 µL was stored as the non-purified fraction and the rest was purified using the Exo-spin^{TM} columns (CELL guidance systems, UK). The columns were initially equilibrated twice with 10 mL of PBS, pooled SF-EV samples were then applied to the columns and EVs were eluted with 15 mL of PBS - 30 sequential fractions of 500 µL were collected. Each fraction was then analysed by NTA and BCA protein assay to determine the location of the SF-EVs and EV associated or free protein. The fractions containing SF-EVs were then put together as purified pooled SF-EV preparations and their vesicle concentrations were measured by NTA – expression of the exosomal markers ALIX, CD9 and syntenin-1 after purification was also confirmed by Western blotting.

SF-EVs for binding and molecular studies were labelled with the dye bio-maleimide or treated with the enzyme proteinase K (PK) before Exo-spin^{TM} purification to remove the excess of dye and enzyme at the same time as the free protein.

2.3.4.1 Bio-maleimide labelling

Fluorescent SF-EVs were generated by labelling EVs with bio-maleimide, as previously described by (Dragovic *et al.*, 2013). EV dye bio-maleimide (BODIPY FL N-(2-aminoethyl)-maleimide) (Molecular probes, USA) was filtered using a 0.2 µm Nanosep

MF centrifugal device (Pall, USA) at 1,400 x g for 3 min to eliminate contamination. The dye was then resuspended in PBS to a final 100X concentration. Finally, pooled SF-EVs samples were treated with 2 µM of the filtered bio-maleimide for 30 min at RT in the dark.

2.3.4.2 Proteinase K treatment

Pooled SF-EV samples were treated with 10 µg/mL PK (Sigma-Aldrich, USA) for 1.5 hrs at 37°C. Proteinase activity was then inhibited adding 5 mM phenylmethylsulfonyl fluoride (PMSF) (Sigma-Aldrich, USA) for 10 min at RT. Both, PK and PMSF had been passed through a 0.2 µm filter (Starsted, Germany).

Table 2.2 Characteristics of purified pooled SF-EV preparations.
Patient's SF-EVs used in different pooled SF-EV preparations are in bold. NTA software for the analysis of EVs concentration and size is shown in brackets. * Pooled SF-EV preparation 1 was reanalyzed with NTA software 3.1 to compare NTA results to electron microscopy studies.

SF-EV preparation name	Number of patients	Patient numbers	Treatments
1 (NTA 2.3)	11	1 - 11	• Non-treated* • Bio-maleimide labelled • PK-treated
2 (NTA 3.1)	10	22 - 31	• Non-treated • PK-treated
3 (NTA 3.1)	10	**17 - 21,** + 32 - 36	• Non-treated • PK-treated
4 (NTA 3.1)	10	12 - 16, + **17 - 21**	• Bio-maleimide labelled

2.3.5 Characterisation of purified pooled SF-EV preparations

2.3.5.1 Electron microscopy

SF-EV preparations # 1, # 2 and # 3, and bio-maleimide labelled SF-EV preparation # 4 were processed by Dr. Errin Johnson (Sir William Dunn School of Pathology, University of Oxford) for electron microscopy. Briefly, 10 µl of SF-EV preparations were applied to 300 mesh Cu grids coated with a carbon film, which had been freshly glow discharged, and incubated for 2 mins. The grids were then quickly blotted and stained with 2 % uranyl acetate (aqueous) for 10 sec, blotted and air dried. Afterwards, the grids were imaged using a 120kV FEI Technai12 Transmission Electron Microscope (FEI company, USA) with a Gatan OneView digital camera (GATAN, USA).

2.3.5.2 ExoView analysis (NanoView Biosciences)

SF-EV preparations # 1, # 2 and # 3 were diluted in PBS-T to reach a final concentration of $1x10^{10}$ SF-EVs/mL. Seminal fluid samples # 37 and # 38, after removing the sperm and cellular debris, were diluted 1/10 in ethylenediaminetetraacetic acid (EDTA) solution (NanoView Biosciences, USA). 35 µl of each SF-EV preparations and unprocessed seminal fluid samples were added to the NanoView microarray, a tetraspanin chip (NanoView Biosciences, USA), and incubated overnight at RT – this chip contained capture antibodies against CD81, CD63 and CD9. Afterwards, the microarray was washed three times with PBS and stained with secondary fluorescence labelled antibodies (Table 2.3) for 2 hrs at RT in the dark. The microarray was then washed three times with PBS. Finally, SF-EVs bound to the microarray and their fluorescence were detected by the ExoView (NanoView Biosciences, USA) – a newly developed platform for EVs analysis (https://www.nanoviewbio.com/). To date the ExoView is the only platform available in the market that can analyse non-purified EV samples and determine at the

same time EV concentration, size and expression of multiple membrane proteins. In brief, EVs are captured by antibodies against EVs membrane proteins (e.g.: CD63, CD9) on the surface of the affinity microarray and then incubated with fluorescence antibodies against other membrane proteins. Finally, using brightfield and fluorescence microscopy, the Exoview detects EVs bound to the microarray through Single Particle Interferometric Reflectance Imaging Sensing (NanoView Biosciences, USA).

Table 2.3 Primary antibodies used for ExoView analysis.

Antibody	Final Concentration	Antibody Clone	Company
Anti-CD81 (Alexa Fluor® 555)	1 µg/mL	N/A	NanoView Biosciences, USA
Anti-CD63 (Alexa Fluor® 488)	1 µg/mL	N/A	NanoView Biosciences, USA
Anti-CD9 (Alexa Fluor® 647)	1 µg/mL	N/A	NanoView Biosciences, USA

2.3.6 Statistical analysis

2.3.6.1 Characterization of individual SF-EV samples

2.3.6.1.1 NTA

Statistical analysis was performed using GraphPad Prism 7.01 (GraphPad Software, USA). D'Agostino & Pearson tests were used to confirm normality of the data. Parametric data was then analysed using one-way ANOVA tests and nonparametric data was analysed using a Kruskal-Wallis test. Experimental groups were always compared controlling the False Discovery Rate (Pawluk-Kolc *et al.*, 2006) using the Two-stage step-up method of Benjamini, Krieger and Yekutieli. Data were represented as mean ± SD and median ± IQR. Differences were considered significant if $p < 0.05$.

2.3.6.1.2 Western blotting

The coefficient of variation (CV) were calculated using GraphPad Prism 7.01 (GraphPad Software, USA).

2.3.6.1.3 Correlation analysis

Statistical analysis was performed using GraphPad Prism 7.01 (GraphPad Software, USA). D'Agostino & Pearson tests were used to confirm normality of the data. Parametric data was then analysed using Pearson correlation tests and nonparametric data was assessed using Spearman correlation tests. Correlations were considered significant if $p < 0.05$.

2.3.6.2 SF-EV purification & Characterisation of SF-EV size in SF-EV preparations

Statistical analysis was performed using GraphPad Prism 7.01. Normality of the data was confirmed again using Shapiro-Wilk tests. Parametric data was then analysed using paired Student's *t*-test. Data were represented as mean ± SD. Differences were considered significant if $p < 0.05$.

2.4 Results

2.4.1 Characterisation of individual SF-EV preparations

Human seminal fluid samples were centrifuged to remove sperm and SF-EVs were then isolated by ultracentrifugation. To characterise SF-EV samples, SF-EV sizes and concentrations of 21 samples were determined by NTA. In addition, SF-EVs expression of well-known exosomal markers were also analysed by Western blotting (n = 21).

2.4.1.1 NTA analysis of patients SF-EVs

Individual SF-EV samples were analysed using NanoSight NTA 2.3 software (n = 21). SF-EV size distribution profiles of samples 12 to 21 were similar and SF-EVs between 50 to 500 nm were detected (Fig 2.3 a) - as previously described for SF-EV samples 1 to 11 (Rodriguez-Caro, MSc dissertation 2015). The analysis of all 21 samples showed SF-EV concentrations varied between individual preparations ranging from $5.3x10^{11}$ to $6.4x10^{12}$ SF-EVs/mL (n = 21) (Fig 2.3 b). On the contrary the mean and mode size of SF-EVs were similar between individual preparations (n = 21) (Fig 2.3 c). The average modal size of SF-EVs was 120 ± 9 nm and the average SF-EV mean size was 148 ± 7 nm.

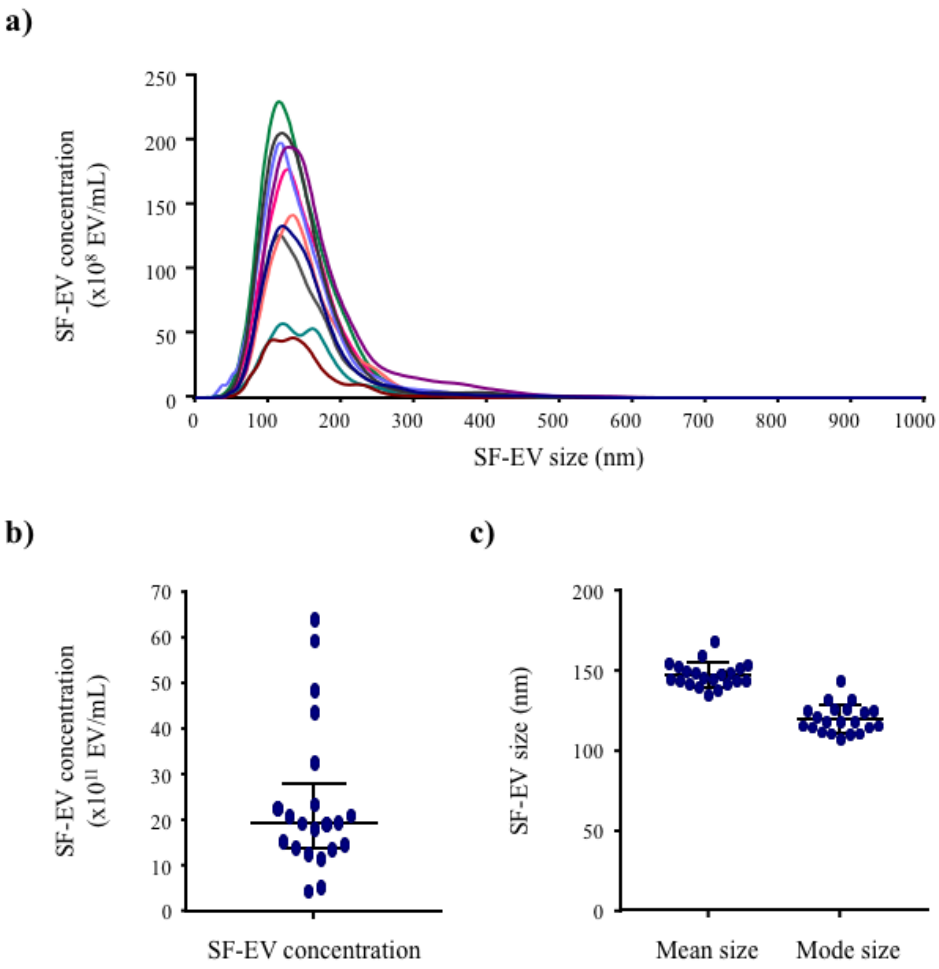


Fig 2.3 Nanoparticle tracking analysis (NTA) of SF-EVs samples 1 to 21.
SF-EVs isolated by ultracentrifugation were analysed by NTA using NanoSight NTA 2.3 software. **(a)** size distribution profile of SF-EVs samples 12 to 21 (n = 10). Graphs of **(b)** SF-EV concentration, and **(c)** SF-EV mean and mode size (n = 21). Bars represent **(b)** median ± IQR, or **(c)** mean ± SD.

2.4.1.2 Western blot analysis of patients SF-EVs

The exosomal protein markers ALIX, CD9 and syntenin-1 were found in all SF-EV samples (n = 21) - Western blot images of SF-EV samples 11 to 21 are shown in figure 2.4. ALIX and CD9 expression were variable between SF-EV samples (Fig 2.5 a, b) – for instance sample numbers 11 and 14, showed higher expression of ALIX and CD9 while others were lower (Fig 2.4). On the contrary syntenin-1 seemed to be less variably expressed between these samples (Fig 2.5 c). Accordingly, the CV of ALIX (72.23 %)

and CD9 (77.51 %) were higher than syntenin-1 CV (24.98 %). Therefore, the CV data suggest syntenin-1 expression in SF-EVs seems to be less variable than ALIX and CD9.

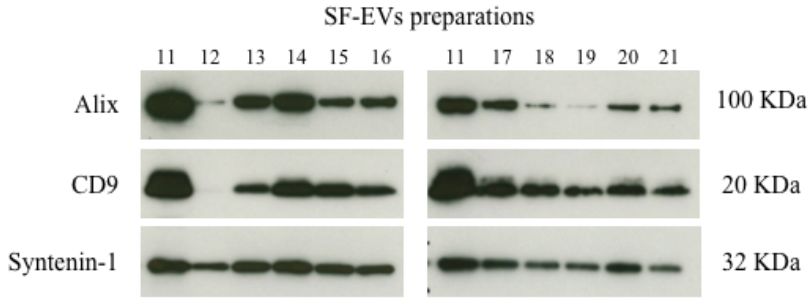


Fig 2.4 Western blots of ALIX, CD9 and syntenin-1 in SF-EV samples
10 µg of SF-EV protein, isolated by ultracentrifugation, was analysed by Western blotting (n = 10). When 2 membranes were used an SF-EV sample was repeated to normalise results by densitometry. These figures show ALIX, CD9 and syntenin-1 Western blot images of SF-EV samples 11 to 21, SF-EV 11 was repeated.

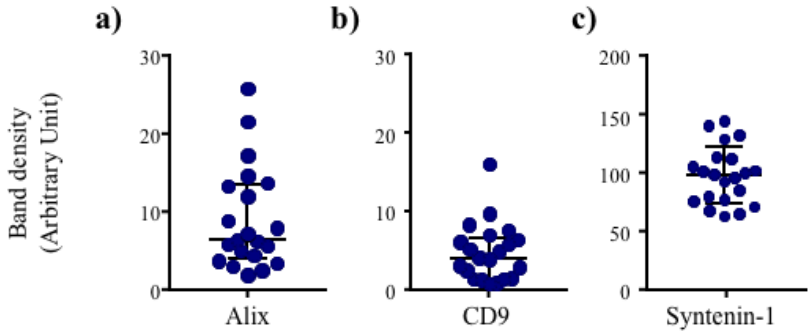


Fig 2.5 Expression of ALIX, CD9 and syntenin-1 in SF-EV samples
10 µg of SF-EV protein, isolated by ultracentrifugation, were analysed by Western blotting (n = 21). Band density was measured by Image J. These figures show the expression levels of **(a)** ALIX, **(b)** CD9, and **(c)** syntenin-1 in SF-EV samples 1 to 21. Bars represent **(a, b)** median ± IQR, or **(c)** mean ± SD.

2.4.2 Correlations between SF-EV characteristics and patient's age and sperm analysis

After showing variable vesicle concentration and exosomal marker expression in the individual SF-EV samples, correlation studies were performed to identify potential relationships between the aforementioned SF-EV characteristics (n = 21), and patient data

including age, sperm count and sperm progressive motility (n = 15). Only data for 15 patients was available.

SF-EV concentrations positively correlated with the expression of the exosomal markers ALIX ($p = 0.0035$, $r^2 = 0.37$), CD9 ($p = 0.0075$, $r^2 = 0.32$) and syntenin-1 ($p = 0.0161$, $r^2 = 0.27$) (n = 21) (Fig 2.6). No significant correlations were found between SF-EV concentration and SF-EV size, patient age, sperm count or sperm progressive motility (Fig 2.6).

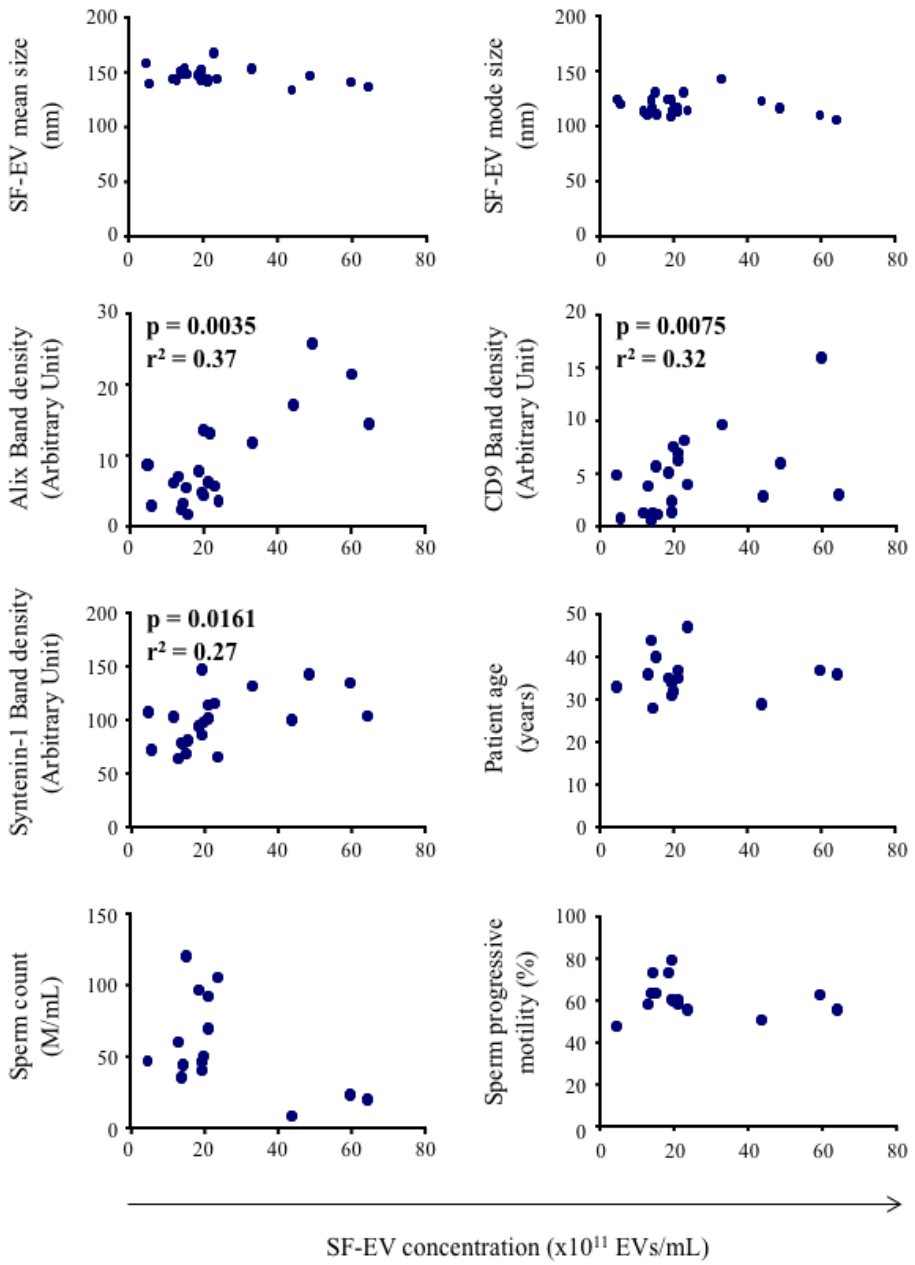


Fig 2.6 Correlation analyses of SF-EV concentrations.
SF-EV concentrations (NTA) were compared to: SF-EV mean and mode sizes (NTA) (n = 21), expression levels of ALIX, CD9 and syntenin-1 (Western blotting) (n = 21); and patients' age, sperm count and sperm progressive motility (n = 15).

After correcting for the effect of SF-EV concentration on ALIX, CD9 and syntenin-1 expression, a positive correlation was found between ALIX and CD9 expression in SF-EVs ($p = 0.0080$, $r^2 = 0.32$) (Fig 2.7). No relationships were found between the other exosomal markers and syntenin-1 or SF-EV size (Fig 2.7). Regarding patient

characteristics, no correlations were found between the exosomal markers (ALIX, CD9 and syntenin-1), and age or sperm progressive motility (Fig 2.8). On the contrary, sperm count positively correlated with SF-EVs' CD9 expression ($p = 0.0072$, $r^2 = 0.46$) but not with ALIX and syntenin-1 (Fig 2.8).

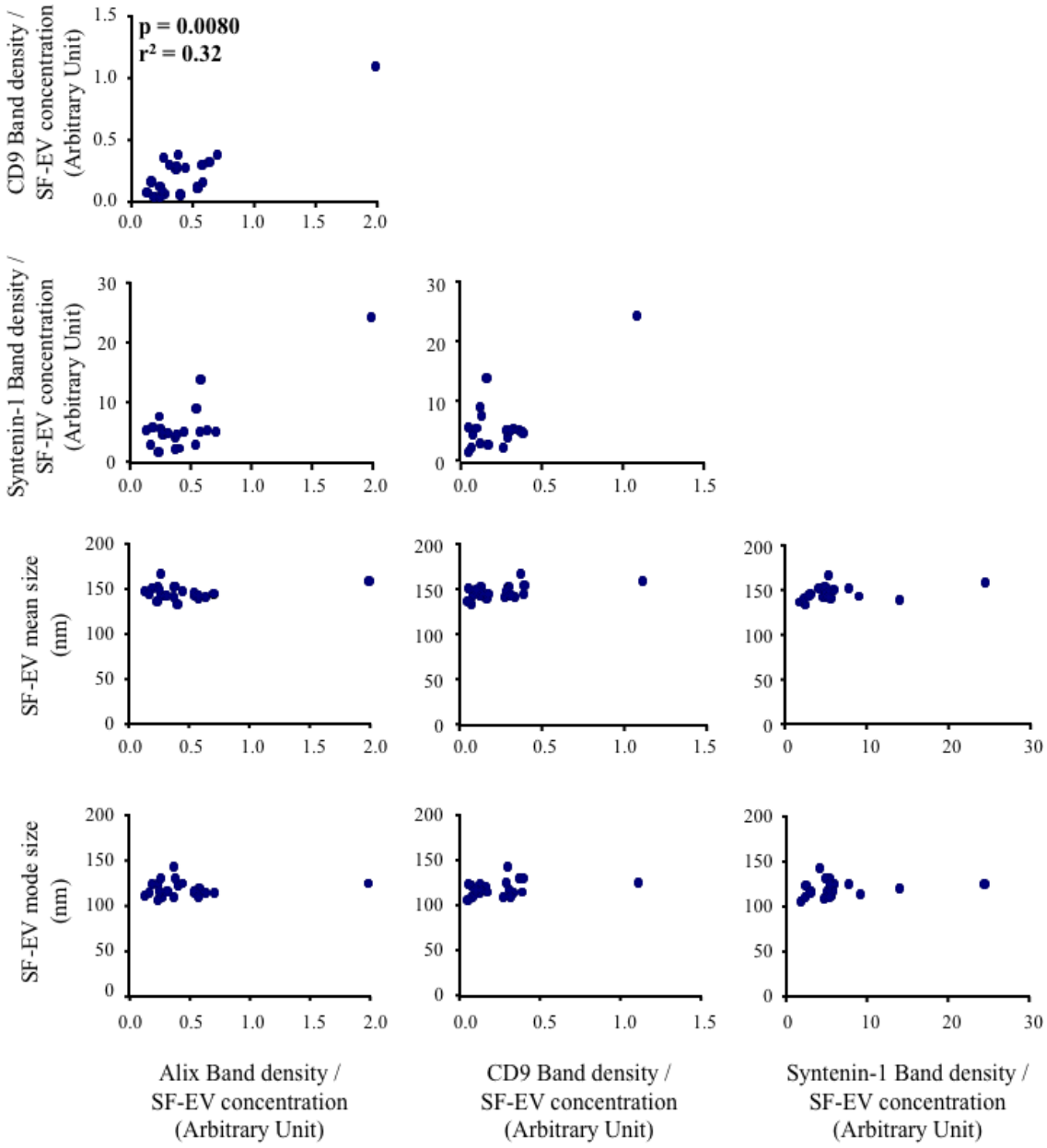


Fig 2.7 Correlation analyses between ALIX, CD9 and syntenin-1 SF-EV expression, and SF-EV mean & mode size.

SF-EV expression levels of ALIX, CD9 and syntenin-1 were determined by Western blotting (10 μg of sample) and compared between them and to SF-EV mean and mode size determined by NTA (n = 21).

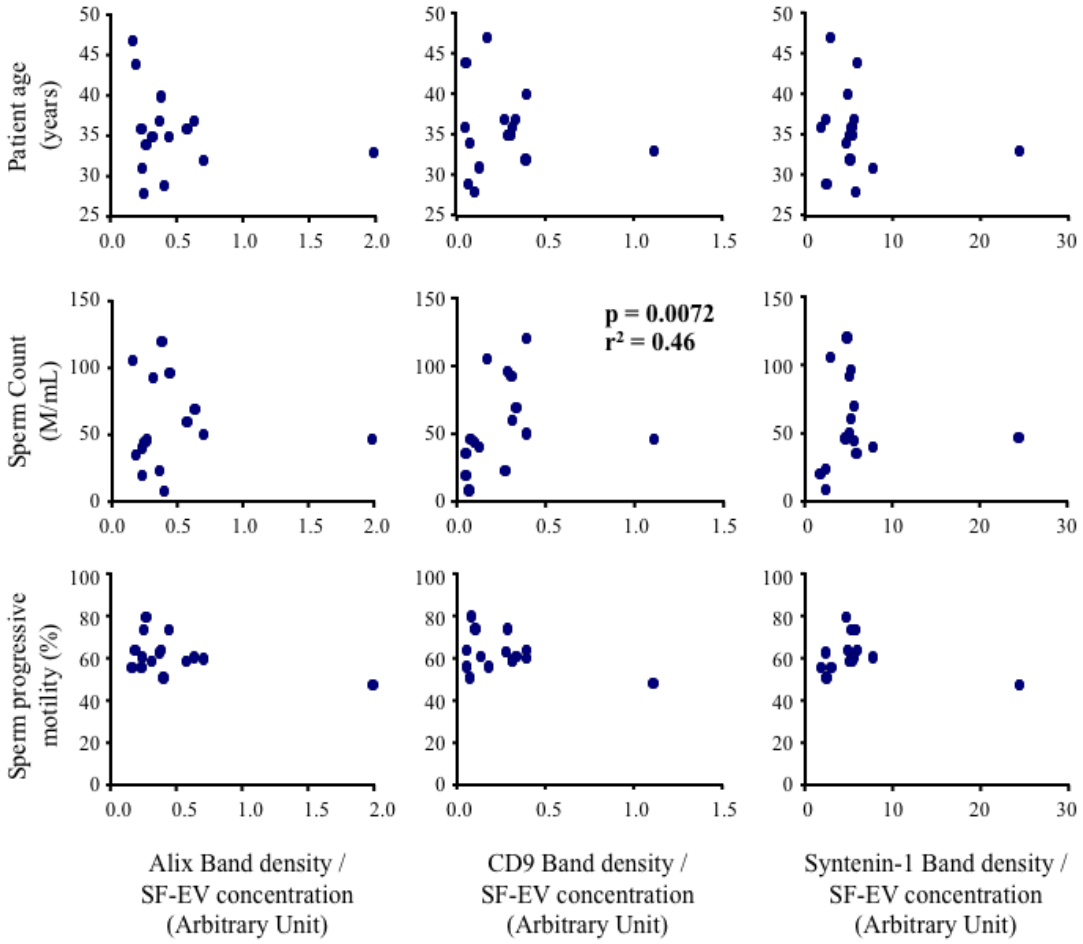


Fig 2.8 Correlation analyses of ALIX, CD9 and syntenin-1 expression in SF-EVs with patients' characteristics.

SF-EV expression levels of ALIX, CD9 and syntenin-1 were determined by Western blotting (10 µg of sample) and compared with patients' age, sperm count and sperm progressive motility (n = 15).

2.4.3 SF-EVs are successfully purified using size-exclusion chromatography

SF-EVs were further purified using size-exclusion chromatography to remove residual seminal fluid proteins not associated to extracellular vesicles to prevent non-EVs interactions in later binding, functional and molecular studies. SF-EVs were pooled and 30 fractions of 500 µl were collected from the Exo-spin™ columns, SF-EV and protein concentrations of each fraction were then determined by NTA and BCA protein assay. 4 different pools of SF-EVs were created and, in addition, pools were prepared with bio-

maleimide labelling for binding studies or PK treatment for molecular studies. PK treatment removes membrane proteins on the surface of the EVs (Gangalum *et al.*, 2011, Phoonsawat *et al.*, 2014). To prepare the above-mentioned SF-EV pools further SF-EVs were isolated and analysed by NTA and Western blotting confirming size distribution and expression of exosomal markers (data not shown).

Non-treated and PK-treated SF-EV preparations # 1 were prepared and described previously at Rodriguez-Caro, MSc dissertation 2015. In both non-treated (Fig 2.9 a) and PK-treated (Fig 2.9 b) SF-EV preparations # 2, vesicles were secreted in fraction 6 to 10. Proteins were eluted in 2 peaks, the first one corresponded to SF-EV associated proteins. The second peak contained minimal numbers of SF-EVs and likely contained soluble seminal fluid proteins. Fractions 6 to 10 were pooled together for future experiments. The protein concentration associated with the SF-EV peak was notably lower in PK-treated than in non-treated SF-EV preparation # 2 (Fig 2.9 a, b). In addition, both non-treated and PK-treated SF-EV preparation # 2 expressed the intravesicular protein syntenin-1, but only the non-treated SF-EV preparation # 2 expressed membrane tetraspanin CD9 (Fig 2.9 c).

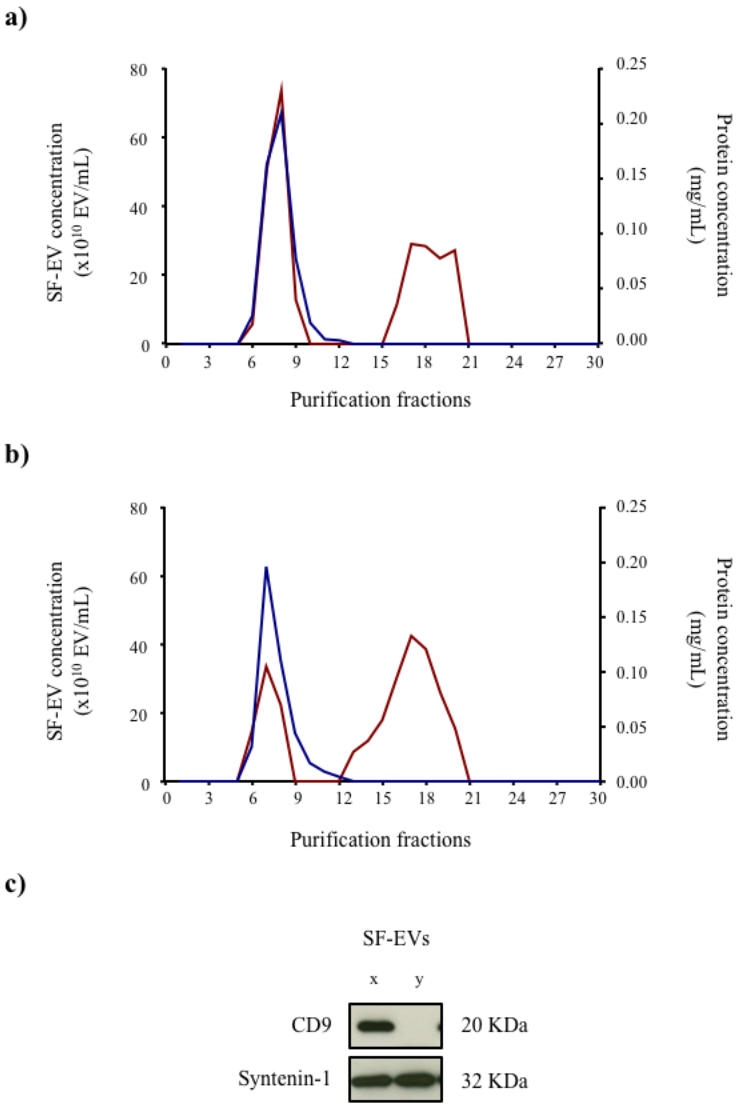


Fig 2.9 Purification of SF-EV preparation # 2 by size-exclusion chromatography. SF-EV samples were pooled together (n = 10) and **(a)** non-treated or **(b)** treated with proteinase K. Pooled SF-EVs were then eluted with PBS and 30 fractions of 500 µl collected. Protein concentrations (red) were determined using a BCA assay and SF-EV concentrations (blue) measured by NTA. **(c)** Western blot (10 µg of sample) analysis of exosomal markers CD9 and syntenin-1 in SF-EV preparations (x) before and (y) after treatment with proteinase K and purification.

The Exo-spin^{TM} column purification strategy was consistent between SF-EV pools. Similarly, in non-treated (Fig 2.10 a) and PK-treated (Fig 2.10 b) SF-EV preparations # 3, SF-EVs were also detected between fractions 6 to 10. As observed in the previous pool of SF-EVs, proteins were eluted in 2 peaks and the protein concentration in the vesicle-associated peak was reduced in PK-treated respect non-treated SF-EV preparation # 3

(Fig 2.10 a, b). Similarly, CD9 was expressed in non-treated SF-EVs preparation # 3 but not after PK-treatment, while syntenin-1 was expressed in both (Fig 2.10 c). Fractions 6 to 10 were pooled together.

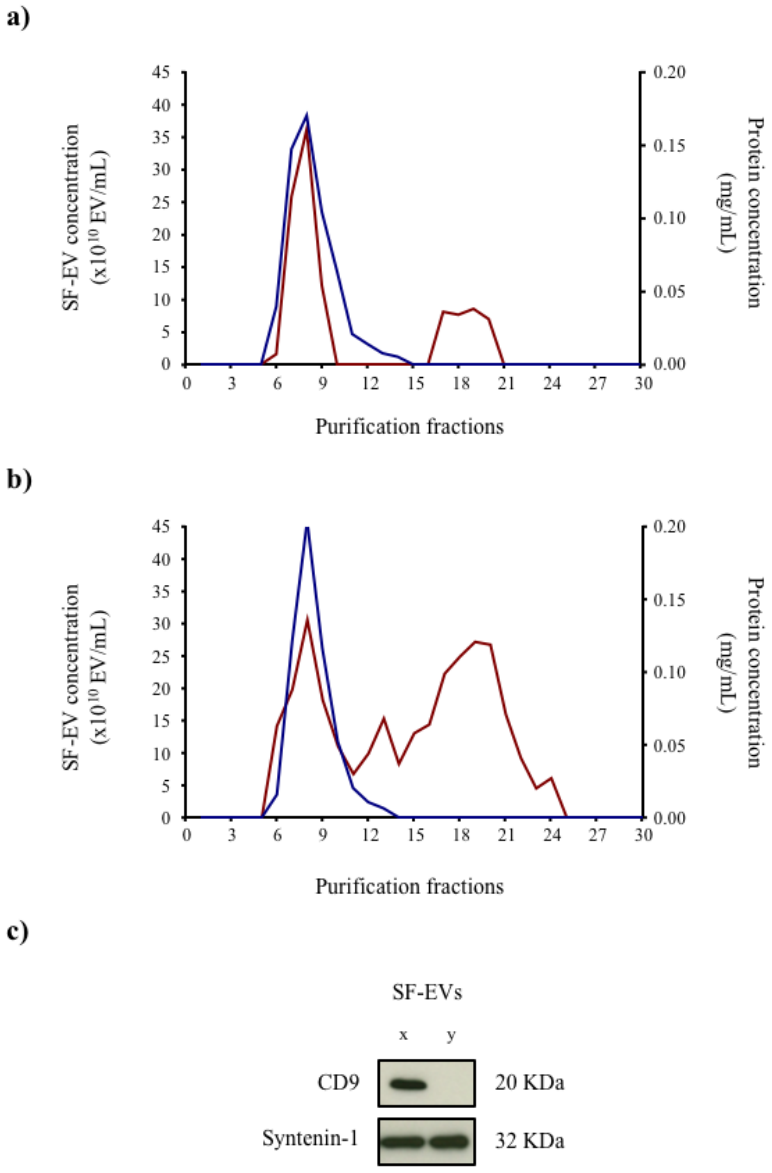


Fig 2.10 Purification of SF-EV preparation # 3 by size-exclusion chromatography. SF-EV samples were pooled together (n = 10) and **(a)** non-treated or **(b)** treated with proteinase K. Pooled SF-EVs were then eluted with PBS and 30 fractions of 500 µl collected. Protein concentrations (red) were determined using a BCA assay and SF-EV concentrations (blue) measured by NTA. **(c)** Western blot (10 µg of sample) analysis of exosomal markers CD9 and syntenin-1 in SF-EV preparations (x) before and (y) after proteinase K treatment and purification.

Two batches of bio-maleimide labelled SF-EV preparation # 1 (Fig 2.11 a), and 3 batches of bio-maleimide labelled SF-EV preparation # 4 (Fig 2.11 b) were prepared for binding experiments. SF-EVs were detected between fractions 5 to 9, which were pooled together for future experiments. Proteins not associated to SF-EVs were secreted in later fractions, approximately fraction 12 to 21. The third batch of bio-maleimide labelled SF-EV preparation # 4 only showed SF-EVs in fractions 6 to 9, however, fractions 5 to 9 were pooled for consistency, this change coincided with a new batch of Exo-spin™ columns (Fig 2.11 b).

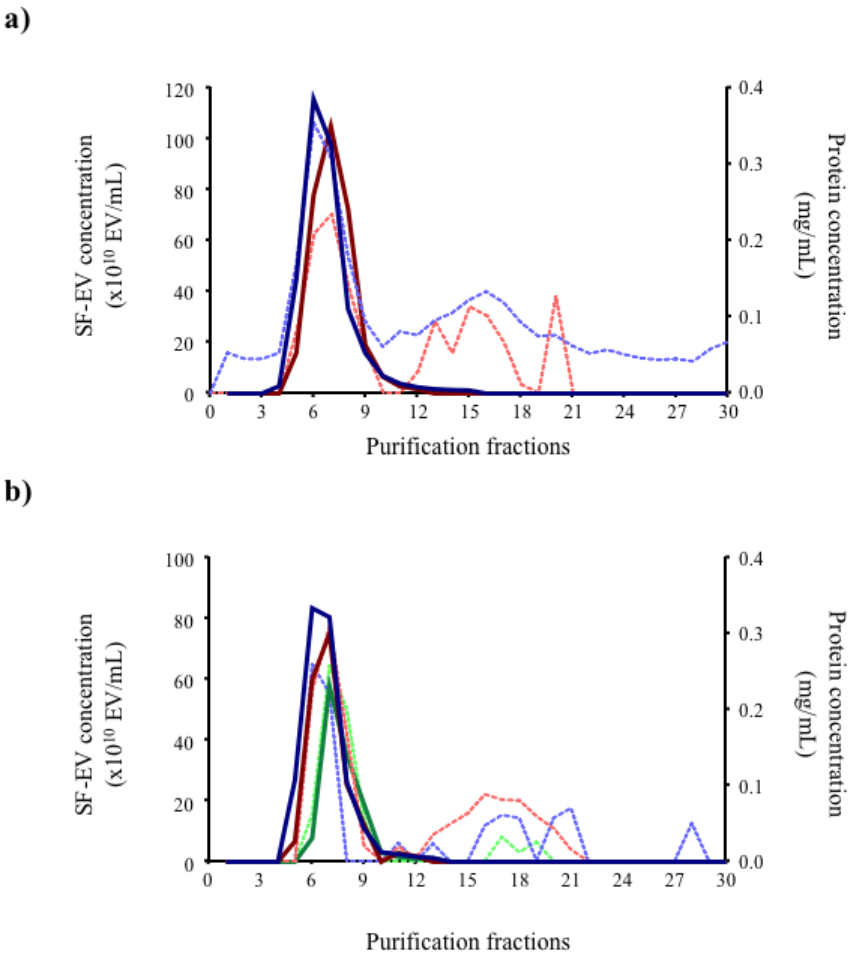


Fig 2.11 Purification of bio-maleimide labelled SF-EV preparations # 1 and # 4 by size-exclusion chromatography.
SF-EV samples were pooled together and labelled with bio-maleimide. Pooled SF-EVs were then eluted with PBS and 30 fractions of 500 µl collected. Protein concentrations

(dashed lines) were determined using a BCA assay and SF-EV concentrations (solid lines) measured by NTA. **(a)** 2 batches of bio-maleimide labelled SF-EV preparation # 1 were prepared. Batch 1 = blue, batch 2 = red **(b)** 3 batches of bio-maleimide labelled SF-EV preparation # 4 were prepared. Batch 1 = blue, batch 2 = red, batch 3 = green.

The average purification yield of SF-EVs using Exo-spin^{TM} columns was 61 % (n = 6) (Fig 2.12 a). Both non-purified and purified SF-EVs expressed ALIX, CD9 and syntenin-1 (Fig 2.12 b). In addition, SF-EV mean and mode sizes did not significantly vary between before and after Exo-spin^{TM} purification (n = 6) (Fig 2.12 c, d). Non-purified pooled SF-EVs had an average mean size of 178 ± 6 nm and an average mode size of 144 ± 7 nm. Purified SF-EV preparations had an average mean size of 180 ± 8 nm and an average mode size of 144 ± 10 nm.

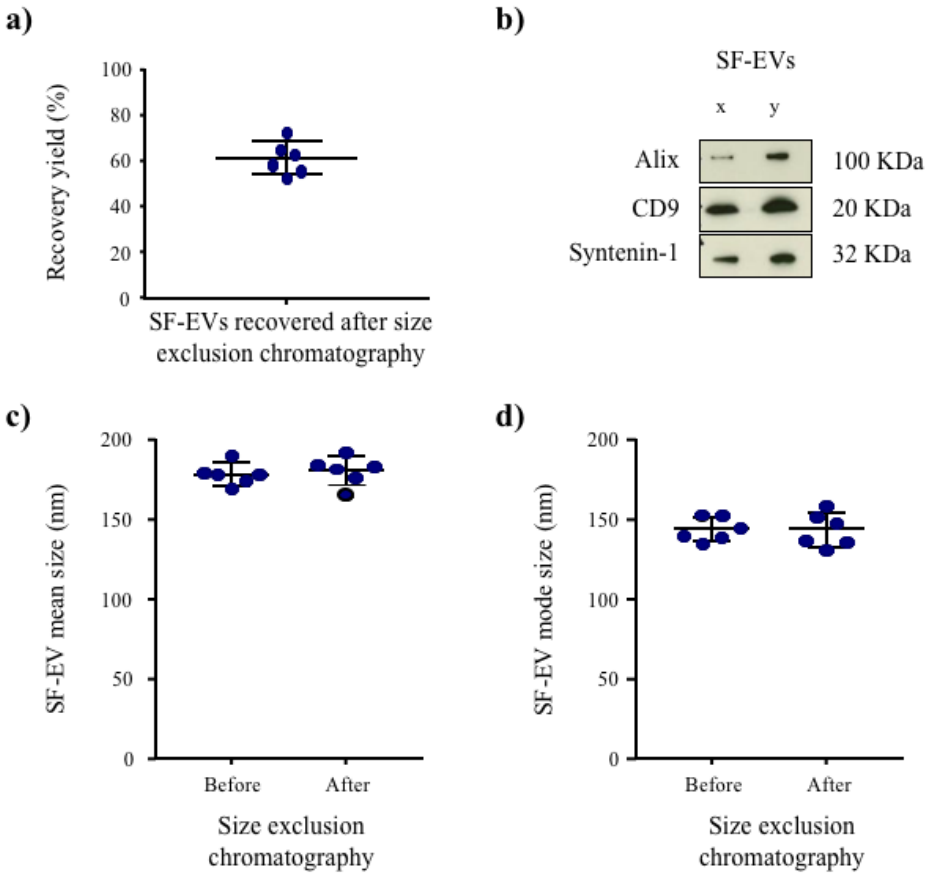


Fig 2.12 Efficiency of SF-EV purification by size-exclusion chromatography.
SF-EV preparations were eluted with PBS and 30 fractions of 500 µl collected. Fractions containing SF-EVs were pooled for future experiments. **(a)** Graph of the recovery yield of SF-EVs after purification by Exo-spin™ columns determined by NTA (n = 6) **(b)** Representative Western blot (10 µg of sample) image of exosomal markers ALIX, CD9 and syntenin-1 in SF-EVs (x) before and (y) after purification. Graphs of **(c)** mean and **(d)** mode size of SF-EVs before and after purification determined by NTA and analysed with NTA 3.1 software (n = 6). Bars represent mean ± SD.

2.4.4 Characterisation of purified pooled SF-EV preparations

Purified pooled SF-EV preparations were further characterised using electron microscopy. Electron microscopy gives detailed morphological and sizing information of EVs and can be used to complement the data obtained with the NTA.

2.4.4.1 Electron microscopy analysis of SF-EVs

SF-EV preparations # 1, # 2, and # 3, as well as bio-maleimide labelled SF-EV preparation # 4 were visualised by electron microscopy. Importantly, electron microscopy images showed minimal background free-protein and did not show widespread protein aggregation in both, SF-EV preparations and bio-maleimide labelled SF-EV preparation (Fig 2.13, 14, 15, 16).

2.4.4.1.1 SF-EVs comprise four morphologically different populations of extracellular vesicles

Electron microscopy images revealed 4 morphologically different populations of SF-EVs (Fig 2.13, 14, 15, 16): Non-electron dense-single membrane SF-EVs, electron dense-multiple membrane SF-EVs, non-electron dense-multiple membrane SF-EVs and non-electron dense cauliflower-like SF-EVs. Non-electron dense-single membrane SF-EVs (solid black arrows) were the most predominant type of SF-EVs, the majority were the smallest SF-EVs detected. Some electron dense-multiple membranes SF-EVs (solid red arrows) showed asymmetric distribution of a dark substance and internal vesicles (e.g.: Fig 2.13 E, F; 14 D, E; 15 E, H). Cauliflower-like SF-EVs (dotted black arrows) were the less common SF-EVs in the preparations - only 6 of them were observed (Fig 2.13 H; 15 D, F, G; 16 D).

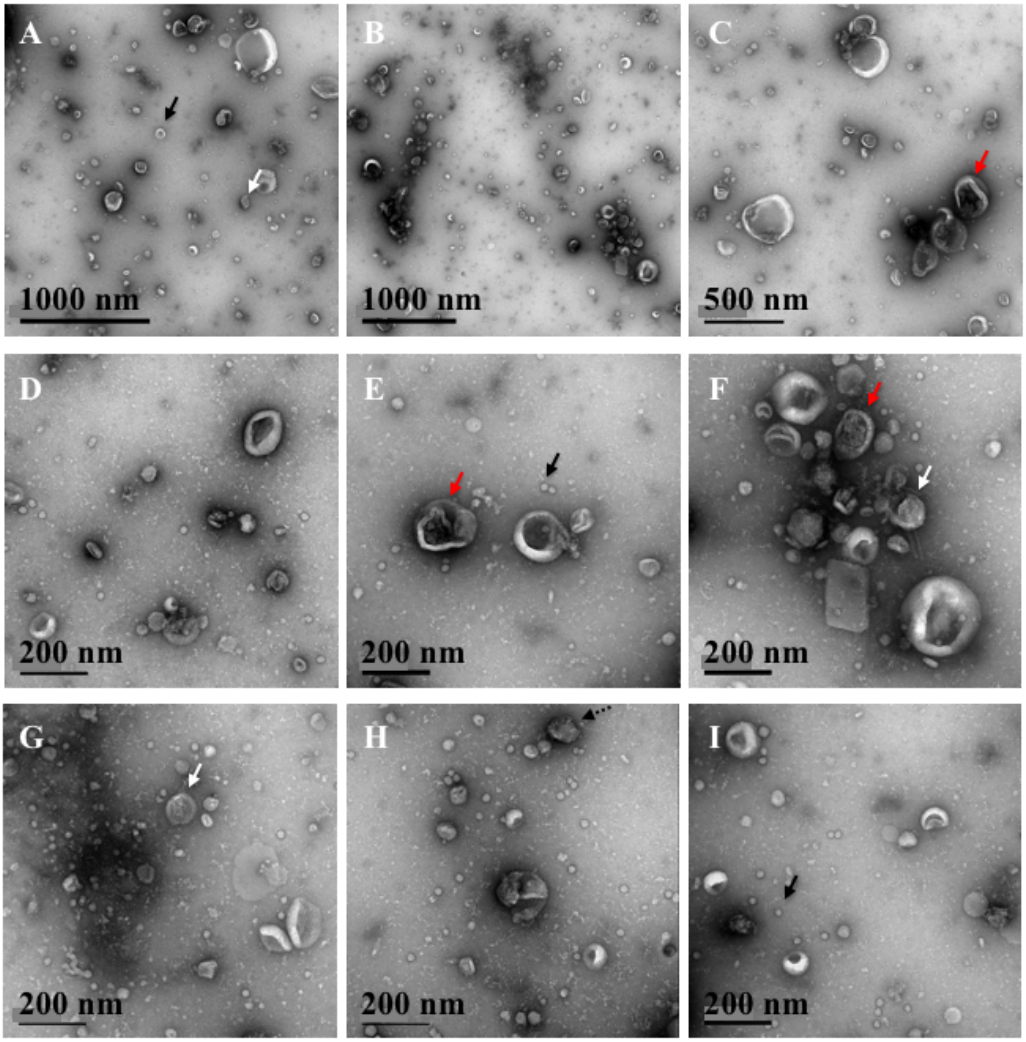


Fig 2.13 Electron microscopy of SF-EV preparation # 1.

Transmission electron microscopy images of SF-EV preparation # 1 with non-electron dense-single membrane SF-EVs (solid black arrows), electron dense-multiple membrane SF-EVs (solid red arrows), non-electron dense-multiple membrane SF-EVs (solid white arrows), and cauliflower-like SF-EVs (dotted black arrows). Scale bars are **(A, B)** 1000 nm, **(C)** 500 nm, and **(D - I)** 200 nm.

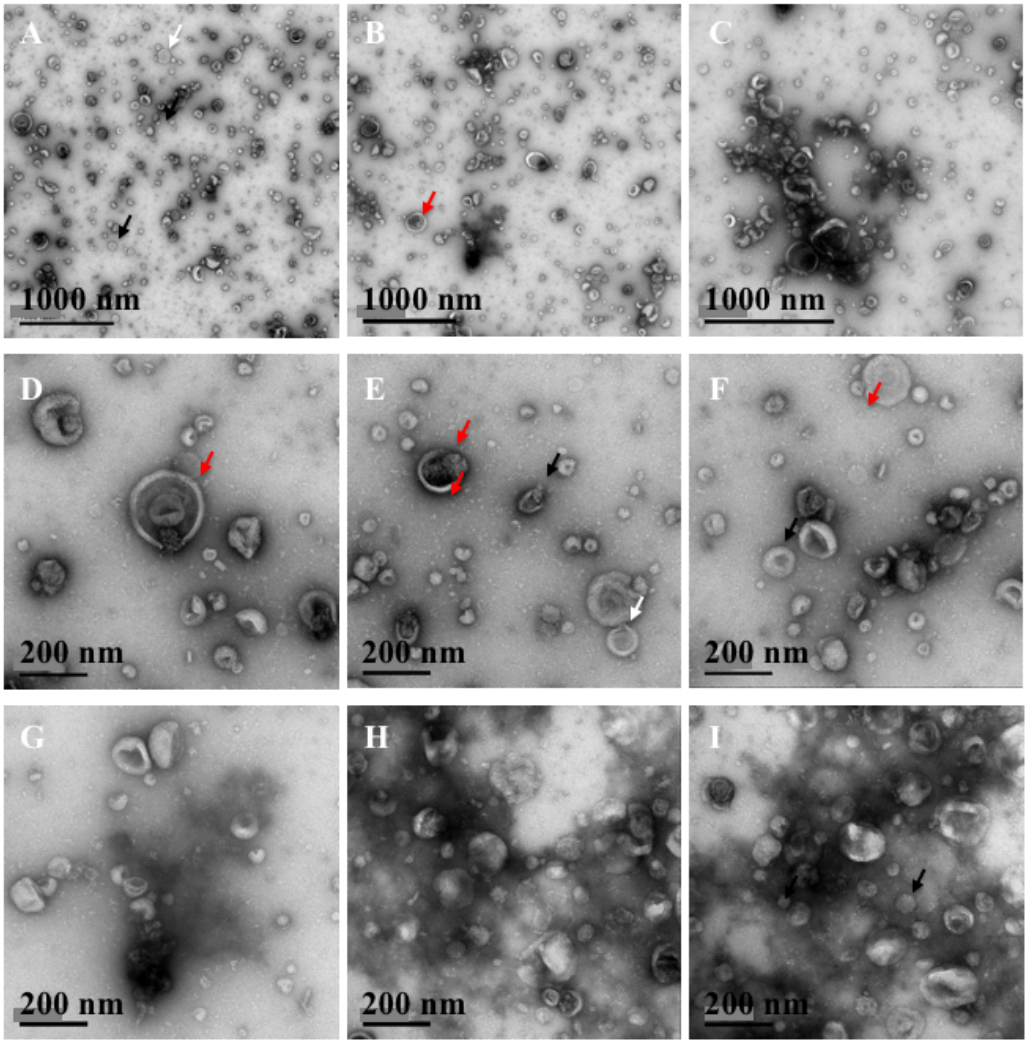


Fig 2.14 Electron microscopy of SF-EV preparation # 2.
Transmission electron microscopy images of SF-EV preparation # 2 with non-electron dense-single membrane SF-EVs (solid black arrows), electron dense-multiple membrane SF-EVs (solid red arrows), and non-electron dense-multiple membrane SF-EVs (solid white arrows). Scale bars represent **(A - C)** 1000 nm, and **(D - I)** 200 nm.

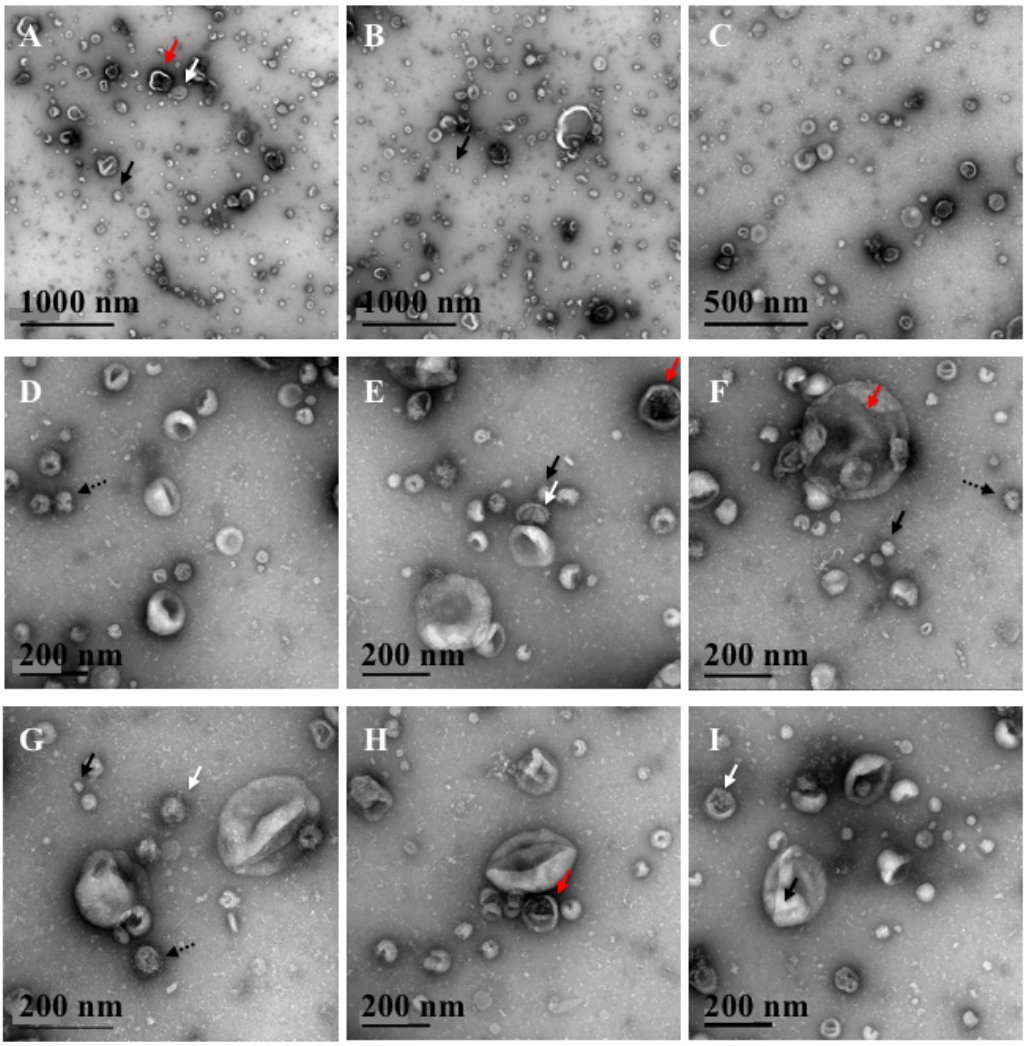


Fig 2.15 Electron microscopy of SF-EV preparation # 3.

Transmission electron microscopy images of SF-EV preparation # 3 with non-electron dense-single membrane SF-EVs (solid black arrows), electron dense-multiple membrane SF-EVs (solid red arrows), non-electron dense-multiple membrane SF-EVs (solid white arrows), and cauliflower-like SF-EVs (dotted black arrows). Scale bars represent **(A, B)** 1000 nm, **(C)** 500 nm, and **(D - I)** 200 nm.

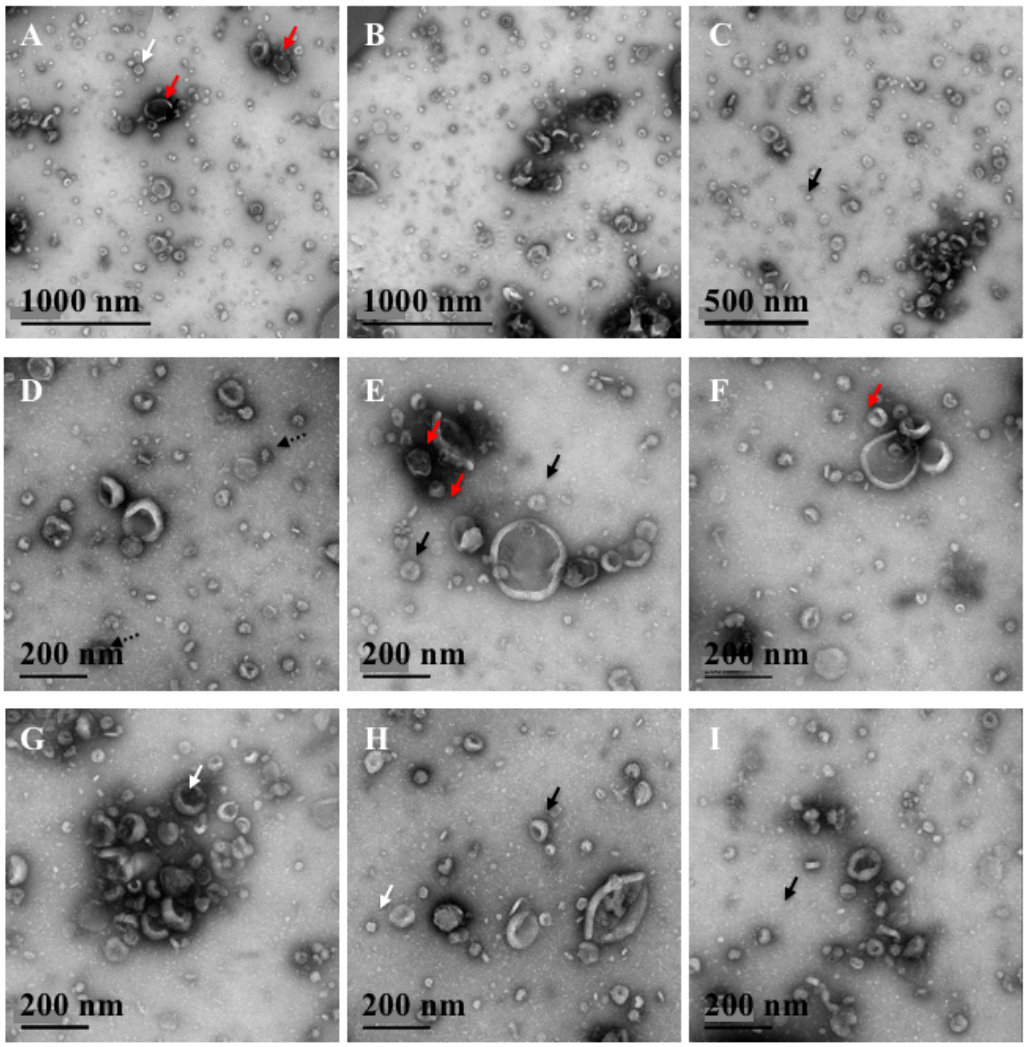


Fig 2.16 Electron microscopy of bio-maleimide labelled SF-EV preparation # 4. Transmission electron microscopy images of bio-maleimide labelled SF-EV preparation # 4 with non-electron dense-single membrane SF-EVs (solid black arrows), electron dense-multiple membrane SF-EVs (solid red arrows), non-electron dense-multiple membrane SF-EVs (solid white arrows) and cauliflower-like SF-EVs (dotted black arrows). Scale bars represent **(A, B)** 1000 nm, **(C)** 500 nm, and **(D - I)** 200 nm.

2.4.4.1.2 The majority of SF-EVs range from 20 to 80 nm

SF-EVs size distribution in SF-EV preparations # 1, # 2, and # 3 were determined analysing the electron microscopy images, the average mean size of all SF-EV preparations was 53.3 nm, and the average modal size was 32.7 nm (Table 2.4). The results were then compared to the NTA size distribution profiles of these SF-EV

preparations. Electron microscopy revealed an abundant population of SF-EVs at the edge of the range of detection of the NTA in SF-EV preparations # 1 (Fig 2.17 a), # 2 (Fig 2.17 b), and # 3 (2.17 c). Electron microscopy provided statistically lower SF-EV mean ($p = 0.0132$) and mode ($p = 0.0154$) sizes compared to NTA (Table 2.4). Based upon both these techniques, SF-EV sizes are found to range from 15 to 300 nm and minimal numbers of vesicles were detected from 300 to 500 nm. Importantly, the electron microscopy images showed the most abundant population of SF-EVs ranged from 15 to 80 nm, which were not detected by NTA. This population of SF-EVs constituted 84.90 %, 80.63 %, and 75 % of SF-EV preparations # 1, # 2, and # 3, respectively - they were also detected in bio-maleimide labelled SF-EV preparation # 4 by electron microscopy.

Table 2.4 SF-EV mean and mode size of SF-EV preparations # 1, # 2, and # 3 Nanoparticle Tracking Analysis (NTA) and Electron Microscopy (EM).

Non-treated purified pooled SF-EVs	**Mean size (nm)**		**Mode size (nm)**	
	NTA	**EM**	**NTA**	**EM**
1	204.9	36.4	155.7	18.2
2	182.8	56.6	137.2	41.8
3	183.6	66.8	135.0	38.2
Average	190.4	53.3	142.6	32.7
p value	p = 0.0132 *		p = 0.0154 *	

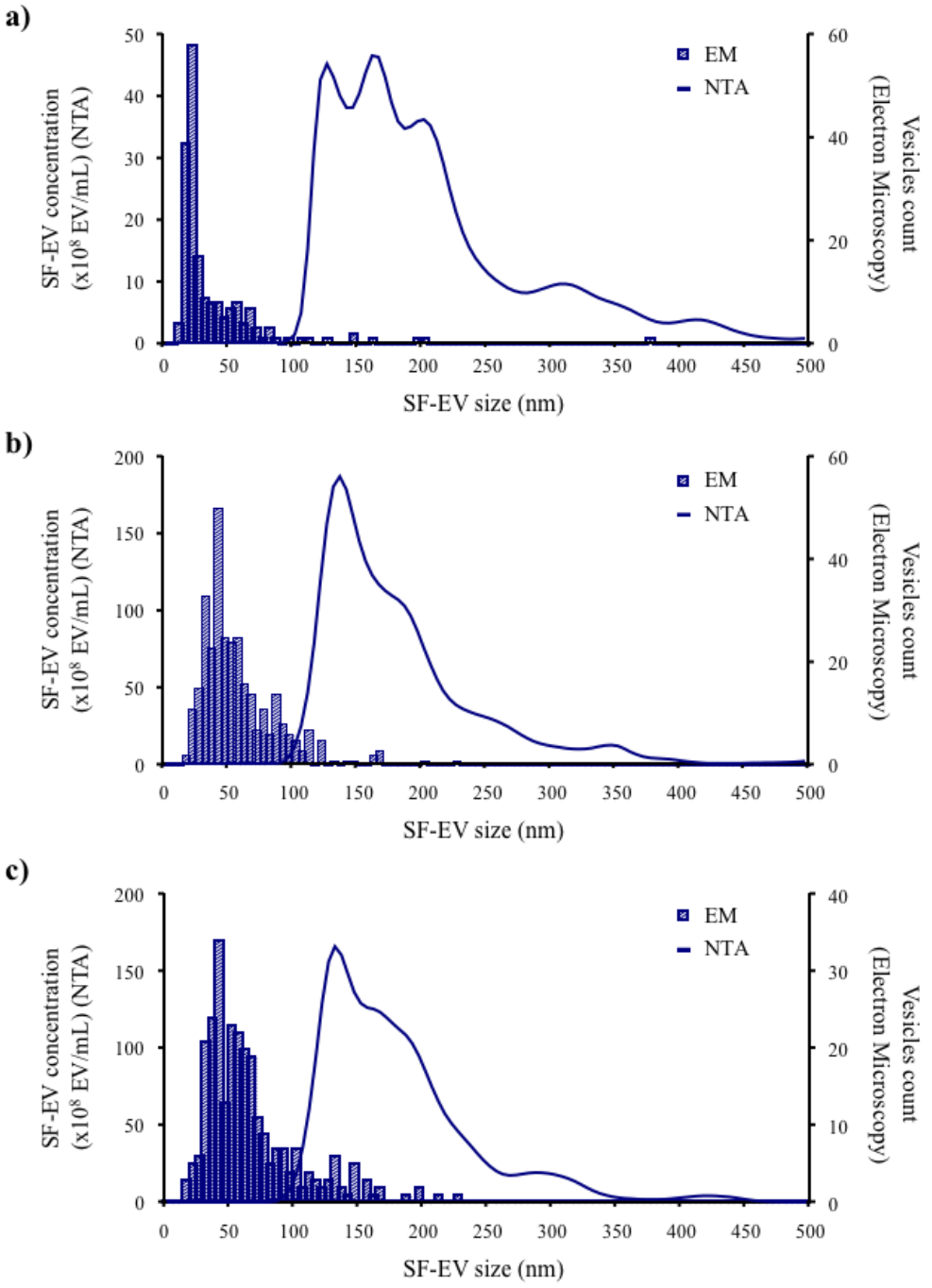


Fig 2.17 SF-EV size distribution determined by nanoparticle tracking analysis (NTA) and electron microscopy.

SF-EV preparations **(a)** # 1, **(b)** # 2, and **(c)** # 3 were analysed by NTA (solid blue line) or electron microscopy (EM) (striped blue bars). Transmission electron microscopy images were analysed by Image J. In total, 192, 320, and 280 SF-EVs were analysed in SF-EV preparations # 1, # 2, and # 3, respectively.

2.4.5 Purified pooled SF-EVs are similar to unprocessed seminal fluid SF-EVs (NanoView Biosciences Collaboration)

The ExoView can detect the size and concentration of EVs, as well as the expression of different EV proteins and determine if these proteins colocalize. This platform analyses EVs in a microarray captured by immunoglobulins, this has the advantage of being able to analyse EVs in biological fluids with no further processing by ultracentrifugation, column purification, or density gradient. Therefore, for my research SF-EVs could also be analysed in seminal fluid after sperm removal. In this axis, SF-EV preparations # 1, # 2 and # 3, as well as unprocessed seminal fluid samples # 37, and # 38 were analysed with the ExoView.

2.4.5.1 SF-EVs comprise three different $CD63^+$ populations of extracellular vesicles

ExoView data revealed 3 different populations of SF-EVs according to the expression of CD81 (green), CD63 (Blue) and CD9 (red). One SF-EV population was characterised as $CD63^+CD9^+CD81^-$, and another was characterised as $CD63^+CD9^+CD81^+$. These two populations were identified in all purified SF-EV preparations (Fig 2.18 a, b, c) and unprocessed seminal fluid samples (Fig 2.18 d, e). In addition, SF-EV preparation # 2 also contained $CD63^+CD9^-CD81^+$ SF-EVs (Fig 2.18 b) – $CD63^+CD9^-CD81^+$ SF-EV population constituted a small percentage of SF-EVs detected in unprocessed seminal fluid samples (2.18 d, e).

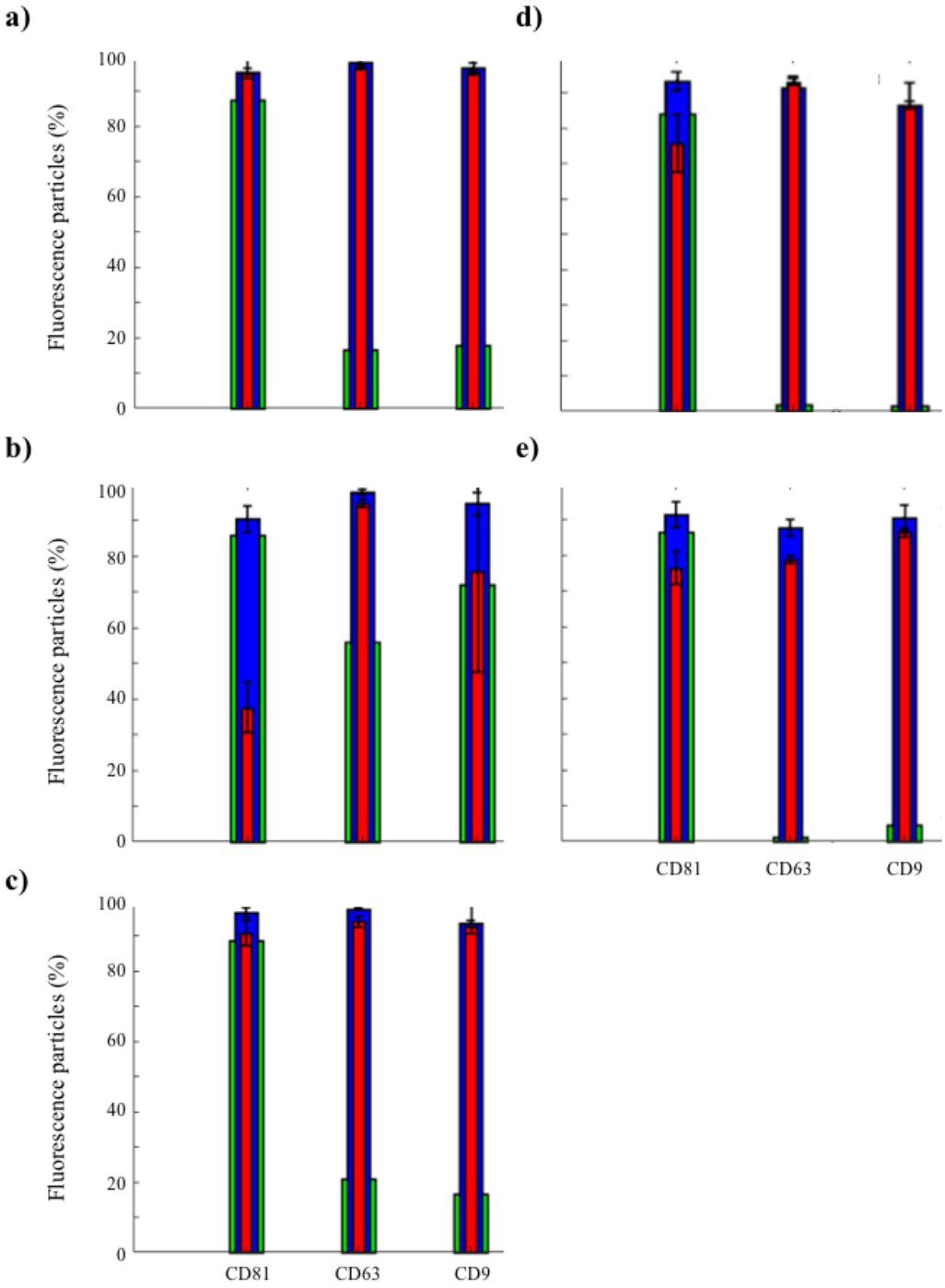


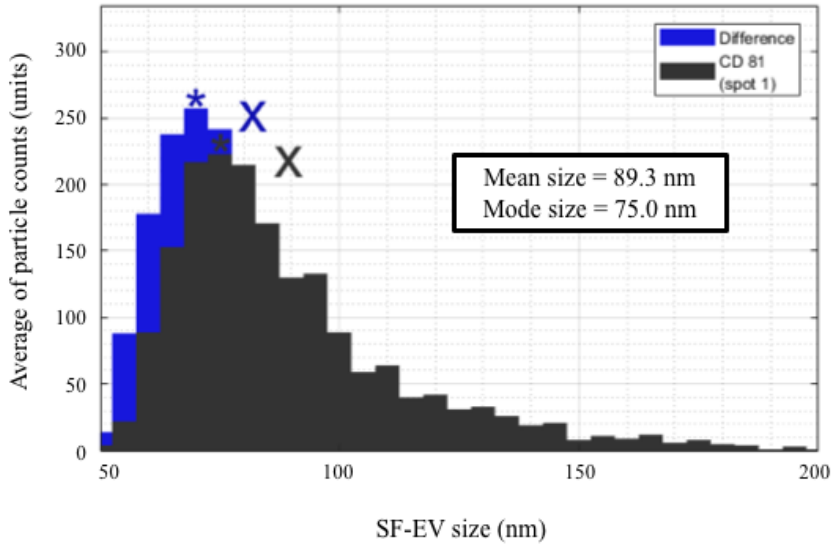
Fig 2.18 Co-localization of SF-EV exosomal markers CD81, CD63 and CD9: ExoView.

SF-EV preparations **(a)** # 1, **(b)** # 2, and **(c)** # 3, as well as unprocessed seminal fluid samples **(d)** 37 and **(e)** 38 were incubated on a NanoView microarray containing antibodies against CD81, CD63 and CD9. Afterwards fluorescence antibodies against these same tetraspanins, CD81 (green), CD63 (blue) and CD9 (red) were added, washed, and analysed using the ExoView.

2.4.5.2 The majority of SF-EVs range from 50 to 100 nm

The ExoView detected EVs from 50 to 200 nm in SF-EV preparation # 1 (Fig 2.19 a) and unprocessed seminal fluid sample # 38 (Fig 2.19 b). The majority of these SF-EVs ranged from 50 to 100 nm in both samples (Fig 2.19 a, b). This is previously observed by electron microscopy. The average modal size of SF-EV preparation # 1 was 70.0 nm and the average mean size was 82 nm (n = 3 spots in the microarray). The average modal size of the unprocessed seminal fluid sample # 38 was 65 nm and the average mean size was 77 nm (n = 4 spots in the microarray).

a)



b)

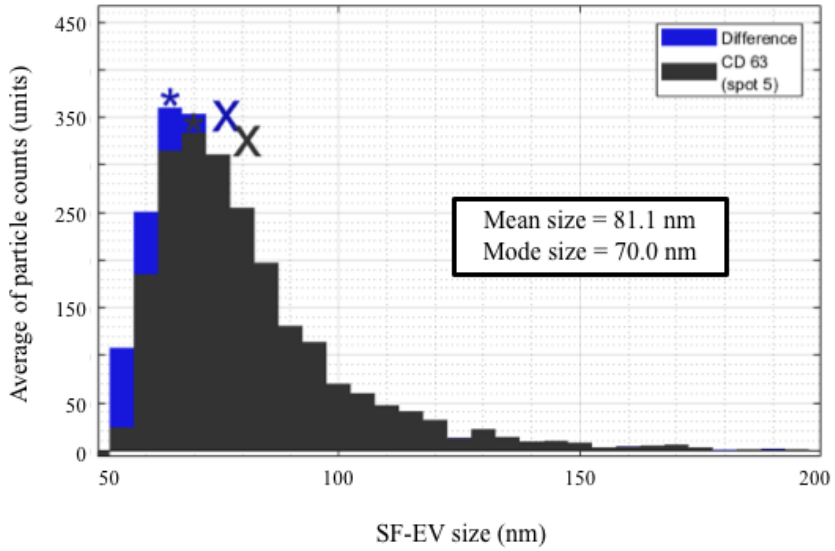


Fig 2.19 Representative images of SF-EV size distribution: ExoView.
(a) SF-EV preparation # 1, and **(b)** unprocessed seminal fluid sample # 38 were incubated on an ExoView microarray containing antibodies against CD81, CD63 and CD9. SF-EV size was then determined using the ExoView.

Importantly, the results obtained with the ExoView showed EVs from SF-EVs preparations and unprocessed seminal fluid samples were similar, which suggest the purification technique employed in this thesis is physiologically relevant and does preserve the sub 100 nm SF-EV population.

2.5 Discussion

2.5.1 SF-EV sizes range from 15 to 300 nm

In recent years NTA has become the gold standard technology for the enumeration and sizing of SF-EVs. In this chapter I used NTA, but also other techniques such as electron microscopy and ExoView. The results showed that SF-EV sizes range from 15 to 300 nm with the majority of SF-EVs being less than 100 nm, between approximately 15 to 80 nm.

NTA analysis of individual SF-EV samples with NanoSight NTA 2.3 software showed SF-EV size between 50 to 500 nm with an average modal size of 120 ± 9 nm and an average mean size of 148 ± 7 nm. This is consistent with previous NTA studies describing SF-EV sizes between 50 to 350 nm with mode size of 120 nm (Tannetta *et al.*, 2014), and mean size of 146 nm (Garcia-Rodriguez *et al.*, 2018). Interestingly, the electron microscopy analysis of SF-EV preparations revealed sizes ranged from 15 to 375 nm and the majority of the SF-EVs were between 15 to 80 nm. The average modal size (32.7 nm) obtained by electron microscopy was smaller than the average modal size (142.6 nm) obtained by NTA. NTA might not detect this abundant population of small SF-EVs because they are at the edge of the size limit of detection of the technique (van der Pol *et al.*, 2014). ExoView analysis of the SF-EV preparations confirmed that the main SF-EV population was smaller than 100 nm, with average modal size of 70 nm and average mean size of 80 nm. The results presented here are akin to a previous analysis of SF-EVs using DLS, that showed two populations of SF-EVs with different mean size; the smaller group had a mean size of 80 nm (Chiasserini *et al.*, 2015).

A recent study of SF-EVs using DLS indicated ultracentrifugation may result in EV loss when compared to isolation by polyethylene glycol (PEG) precipitation (Eswaran *et al.*,

2018). They observed SF-EVs isolated by ultracentrifugation were between 60 and 1,000 nm with an Z average size of 501.3 nm. On the contrary, the size of SF-EVs isolated by PEG precipitation range from 30 to 1,000 nm with an Z average size of 75.4 nm (Eswaran 2018). In the studies presented here I did use ultracentrifugation as part of the SF-EV purification strategy. However, the abundant population of SF-EVs from 20 to 80 nm were detected by electron microscopy, unlike previous electron microscopy studies which detected SF-EVs from 50 to 300 nm, mode size = 120 nm (Poliakov *et al.*, 2009, Hoog and Lotvall, 2015). This is likely due to differences in the protocols used to isolate SF-EVs between Poliakov *et al.*'s 2009 study and those used here. In this chapter I successfully optimised a new isolation protocol that consisted only of one ultracentrifugation step with later purification using size-exclusion chromatography (Exo-spin^{TM} columns). Poliakov *et al.*'s isolation of SF-EVs consisted of a first ultracentrifugation (100,00 x g, 2 hrs) step, sucrose gradient purification, and a second ultracentrifugation (75, 000 x g, 8 hrs). It seems likely small SF-EVs are lost during the sucrose gradient purification or the second ultracentrifugation step. Electron microscopy analysis of human ejaculates did detect particles between 20 to 300 nm, however, the authors considered the majority of the SF-EVs between 20 to 80 nm to be particles and not extracellular vesicles because they did not observe a clear trilamellar membrane (Hoog and Lotvall, 2015). In this chapter, a trilamellar membrane was observed on SF-EVs from 15 to 80 nm. In addition, the ExoView captured SF-EVs expressing CD9, CD63 and/or CD81 confirming this population of small SF-EVs expresses exosomal markers, therefore they are extracellular vesicles.

Overall, the protocol described here appears to include all the types of EV populations described and is therefore likely representative of total SF-EVs.

2.5.2 SF-EVs exhibit 4 different morphologies

Electron microscopy images revealed 4 morphologically different populations of SF-EVs, data are summarised in Fig 2.20 and compared to previous SF-EVs electron microscopy studies. This chapter provides the first evidence of non-electron dense-single vesicles in purified SF-EVs, they were previously described in human ejaculates (≥ 50 nm) (Hoog and Lotvall, 2015). These non-electron dense-single vesicles were the most abundant population of SF-EVs and included the majority of SF-EVs from 15 to 80 nm. In addition, non-electron dense multiple membrane and electron-dense multiple membrane SF-EVs were also observed. Both of the latter SF-EV populations were previously described, and as observed in other studies electron-dense multiple membrane SF-EVs showed asymmetric distribution of a dark substance and internal vesicle/s (Poliakov *et al.*, 2009, Hoog and Lotvall, 2015). Finally, non-electron dense cauliflower-like SF-EVs were found. This type of SF-EVs were previously described by Poliakov *et al*. 2009 but in this study they were less frequent. Interestingly, electron microscopy images of healthy prostate tissue showed electron-dense vesicles with a dark substance and secondary vesicles inside (Brody *et al.*, 1983, Sahlen *et al.*, 2002), suggesting electron-dense multiple membrane SF-EVs with dark substance are most likely to be prostasomes. Non-electron dense vesicles were also observed in healthy prostate tissue (Brody *et al.*, 1983, Sahlen *et al.*, 2002), therefore some of the non-electron dense SF-EVs might also originate in the prostate.

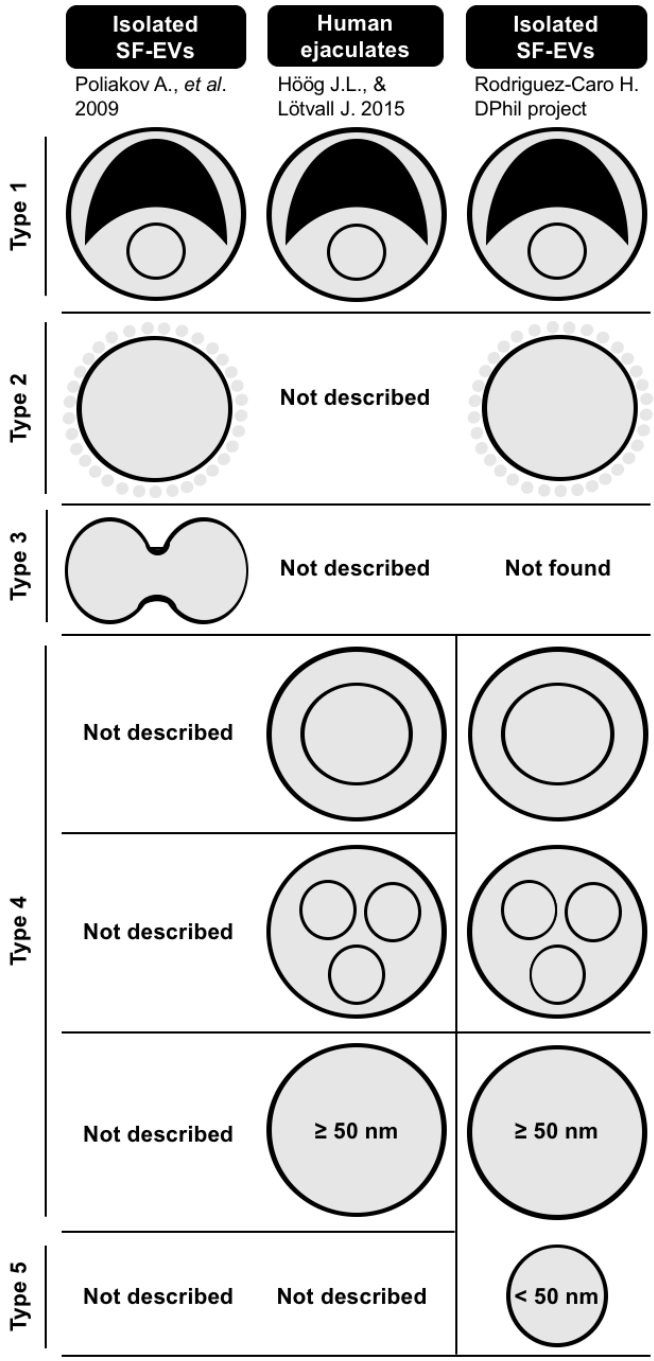


Fig 2.20 Morphology of SF-EVs: electron microscopy diagrams.
Types of SF-EVs described in previous electron microscopy studies (Poliakov *et al.*, 2009; Hoog and Lotvall, 2015) and in this chapter. **Type 1)** Round high-electron dense SF-EVs with asymmetric distribution of a dark substance and one or more secondary vesicles inside. **Type 2)** Round low-electron dense SF-EVs with cauliflower protrusions and sometime secondary vesicles inside. **Type 3)** Elongated or pear-shaped low-electron dense SF-EVs. **Type 4)** Round low-electron dense SF-EVs without or with 1 or more inside vesicles. **Type 5)** Round low electron dense single SF-EVs of less than 50 nm - described in this DPhil project.

2.5.3 SF-EVs populations and their biogenesis

As discussed in the introduction to this chapter SF-EVs are a heterogeneous group of EVs derived from different organs of the male reproductive tract. In addition, cells secrete multiple types of EVs with varying morphology and cargo. EV biogenesis mechanisms are involved in this heterogeneity since a cell can produce several EV populations using different pathways of biogenesis. In this chapter SF-EV's expression of exosomal markers involved in cargo-sorting and formation of intraluminal vesicles (ILV) of the multivesicular bodies were analysed by Western blotting, and ExoView. Correlation and co-localization studies were then performed to identify SF-EV populations based upon protein cargo and to elucidate the SF-EV biogenesis pathways involved (Fig 2.21). SF-EVs were shown to express ALIX, syntenin-1, and the tetraspanins CD9, CD81 and CD63.

2.5.3.1 Correlation study

SF-EV ALIX expression positively correlated with CD9 but not with syntenin-1. ALIX-CD9 correlation was true for less than half of the cases. The results of the correlation study suggest 4 potential SF-EV populations: $CD9^{+}ALIX^{+}Syntenin\text{-}1^{-}$, $CD9^{+}ALIX^{-}Syntenin\text{-}1^{-}$, $CD9^{-}ALIX^{+}Syntenin\text{-}1^{-}$ and $CD9^{-}ALIX^{-}Syntenin\text{-}1^{+}$ (Table 2.5).

Table 2.5 SF-EV populations based upon expression of CD9, ALIX and syntenin-1

SF-EV populations	CD9	ALIX	Syntenin-1
1	+	+	-
2	+	-	-
3	-	+	-
4	-	-	+

ALIX is an ESCRT-accessory protein that links ESCRT-I and ESCRT-III in the canonical exosome biogenesis pathway suggesting $CD9^{+}ALIX^{+}Syntenin\text{-}1^{-}$, and $CD9^{-}ALIX^{+}Syntenin\text{-}1^{-}$ SF-EVs are formed by the canonical ESCRT pathway (Fig 2.21). Interestingly, the lack of correlation between ALIX and syntenin-1 suggest that the ESCRT dependent ALIX/Syntenin/Syndecan pathway is not involved in SF-EV biogenesis. Briefly, heparan sulfate proteoglycan syndecan can recruit specific cargo and then binds to syntenin-1. Syntenin-1 interacts with ALIX that links the complex to ESCRT-III for ILVs formation (Baietti *et al.*, 2012, Friand *et al.*, 2015, Juan and Furthauer, 2018). $CD9^{-}ALIX^{-}Syntenin\text{-}1^{+}$ SF-EVs might be produced through a non-canonical ESCRT-independent exosome biogenesis pathway (Fig 2.21). A study showed that transfection of MCF-7 cells with syntenin-1 RNAi blocked exosomal accumulation of syndecan, including the intact core protein and the C-terminal fragment (CTF). On the contrary transfection of ALIX RNAi suppressed exosomal expression of syndecan CTF but not syntenin (Baietti *et al.*, 2012), supporting that an ESCRT-independent pathway might also regulate $Syntenin\text{-}1^{+}$ EVs. Exosomes can also be generated by the inward budding of ceramide subdomains in the MVB membrane – neutral type II sphingomyelinase forms these subdomains hydrolysing sphingomyelin to ceramide (Trajkovic *et al.*, 2008, Goni and Alonso, 2009, van Niel *et al.*, 2018). Inhibition of the neutral type II sphingomyelinase in MCF-7 decreased syntenin-1 in exosomes (Baietti *et*

al., 2012). Therefore, the Ceramide ESCRT-independent pathway might be involved in the generation of $CD9^-ALIX^-Syntenin\text{-}1^+$ SF-EVs (Fig 2.21).

To confirm the hypothesis presented here, future experiments could be to immunodeplete $CD9^+$ SF-EVs, and analyse ALIX, and syntenin-1 expression in these SF-EVs by Western blotting. Unfortunately, ALIX and Syntenin-1 SF-EVs cannot be immunodepleted because these proteins are inside the vesicles, and, to my knowledge, there are no technologies available to directly validate $CD9^-ALIX^+Syntenin\text{-}1^-$, and $CD9^-ALIX^-Syntenin\text{-}1^+$ SF-EVs. Indirectly, it would be possible to calculate the proportion of the latter SF-EV populations using Western blotting to identify ALIX and syntenin-1 expression in two samples: unprocessed SF-EVs and processed SF-EVs of the same patient in which $CD9^+$ SF-EVs are immunodepleted.

2.5.3.2 Co-localization study

In this chapter, the co-localization study with the Exo-View platform demonstrates for the first time the existence of 3 $CD63^+$ SF-EV populations: $CD63^+CD9^+CD81^+$. $CD63^+CD9^+CD81^-$, and $CD63^+CD9^-CD81^+$ (Table 2.6). Evidence suggest tetraspanins also regulate other non-canonical ESCRT-independent exosome biogenesis pathway (Hessvik and Llorente, 2018, van Niel *et al.*, 2018). CD63 mainly regulates endosomal sorting in ESCRT-independent manner, as observed in fibroblasts (Gauthier *et al.*, 2017), melanocytes (van Niel *et al.*, 2011), and melanoma cells (van Niel *et al.*, 2015). It is likely that some of the $CD63^+$ SF-EV populations arise from this non-canonical biogenesis pathway (Fig 2.25). In addition, CD63/CD9/CD81 complexes, as one of the SF-EV populations detected, had been previously shown in 2 different melanoma cell lines (Radford *et al.*, 1996).

Table 2.6 SF-EV populations based upon expression of CD63, CD9 and CD81

SF-EV populations	CD63	CD9	CD81
1	+	+	+
2	+	+	-
3	+	-	+

Interestingly, CD9 and CD81 have been shown to play an important role in reproduction. Oocyte CD9 and CD81 play a complementary role during pregnancy (Rubinstein *et al.*, 2006). Female $CD9^{-/-}$ and $CD81^{-/-}$ mice exhibit reduced pregnancy rates, and pregnancy is completely abolished in female $CD9^{-/-}CD81^{-/-}$ mice. Specifically, sperm cannot fuse with the oocyte from female $CD9^{-/-}CD81^{-/-}$ mice. Pregnancy rates are not altered when male $CD9^{-/-}CD81^{-/-}$ mice mate with wild type female mice (Rubinstein *et al.*, 2006), suggesting CD9 and CD81 do not affect sperm function in mice. Nevertheless, CD9 and CD81 have been shown to form complexes in human sperm but not in mice sperm (Frolikova *et al.*, 2018). In addition, in humans CD9 and CD81 co-localised in the apical acrosome of ejaculated and capacitated sperm; but after the acrosome reaction, CD9 remains in the equatorial segment but CD81 disappeared from this region, although CD81 is still detected in the post acrosomal region (Frolikova *et al.*, 2018). Importantly, CD9/CD81 complexes are re-localised after the acrosome reaction suggesting a role in sperm fertility. Potentially, $CD63^{+}CD9^{+}CD81^{+}$ might act as reservoirs of CD9/CD81 complexes to assist with the reproductive events listed above.

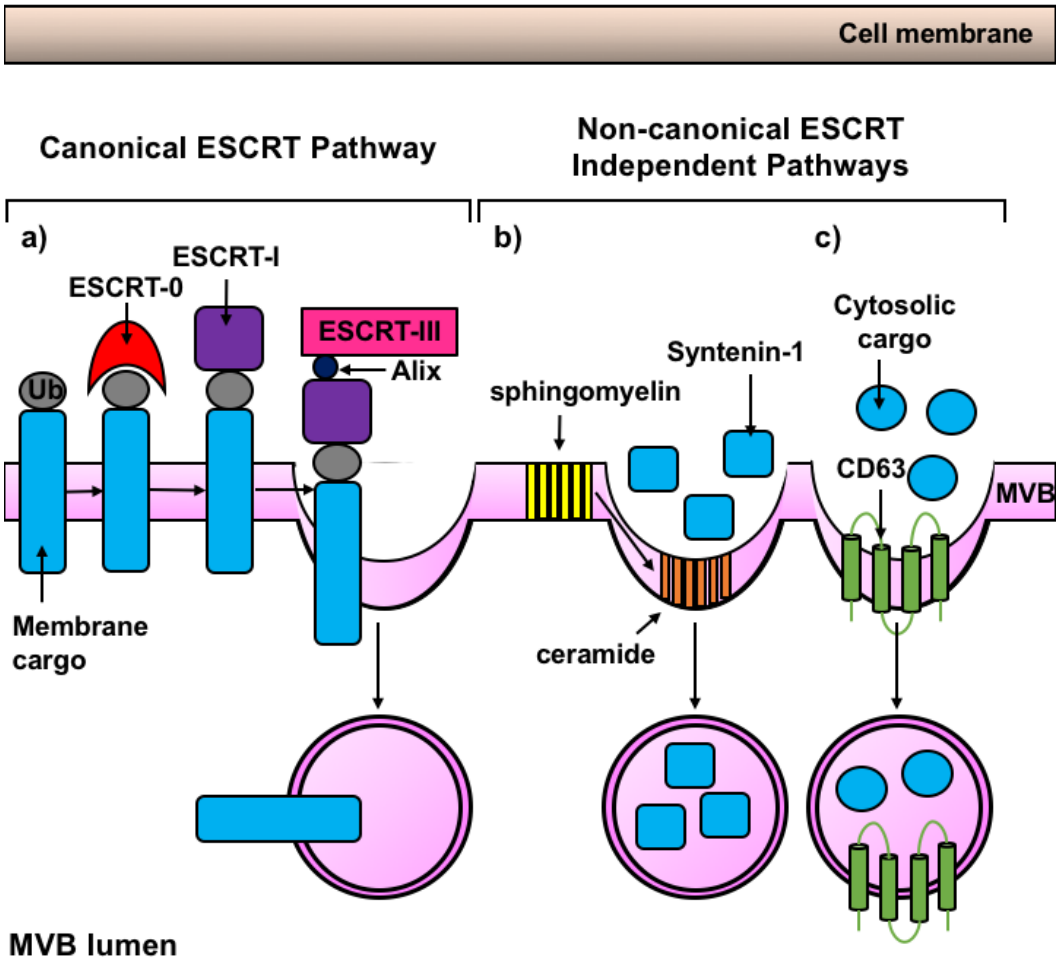


Fig 2.21 Potential SF-EV biogenesis pathways.
Evidence suggests SF-EVs might be produced by the canonical ESCRT Pathway and non-canonical ESCRT Independent Pathways. **(a)** ALIX^{+} SF-EVs populations are likely ESCRT dependent. The protein cargo is transferred to the multivesicular body (MVB) and ubiquitinated (Ub). It is then recognised by ESCRT-0, that then recruits ESCRT-I. ESCRT-I activates ESCRT-II and binds ALIX. ALIX links ESCRT-I to ESCRT-III inducing invagination of the membrane. Then all the protein complex is disassembled, and the membrane is divided forming the intraluminal vesicle (ILV). **(b)** Syntenin-1^{+} SF-EV populations might be synthesized in ceramide-rich regions of the MBV membrane. Membrane sphingomyelin is hydrolysed into ceramide that then buds inside the MBV forming an ILV with the cytosolic cargo originally near the membrane. **(c)** CD63^{+} is mainly involved in generating ILV through an ESCRT independent pathway. ESCRT: endosomal sorting complexes required for transport

2.5.4 SF-EVs' CD9 level positively correlates with sperm count

Recently, SF-EV characteristics have been shown to be associated to sperm quality. Here I analysed if SF-EV concentration, size, or expression of the exosomal markers ALIX,

CD9, and syntenin-1 correlated with patient's characteristics - age, sperm count and sperm progressive motility. No relationships were found between the patient's age or sperm progressive motility and SF-EV concentration, size, or expression of exosomal marker. A previous study did suggest a linear dependence between SF-EV size and patient's age (Chiasserini *et al.*, 2015). However, the authors were critical of the sample size (n = 10) and did state the data was not "unequivocally demonstrated". Here my data did not support this observation.

CD9 expression was found to positively correlate with sperm count. This correlation was true for less than half of the cases. No correlation was found between ALIX and sperm count. All these suggests that some $CD9^+$ SF-EVs are $ALIX^-$ and that specific population correlates with sperm count. A potential reason explaining the increase of $CD9^+ALIX^-$ SF-EVs with sperm might be that non $CD9^+ALIX^-$ SF-EVs may have bound to sperm; so, higher sperm counts lead to a reduction in these free SF-EVs.

2.5.5 Purified pooled SF-EVs are similar to unprocessed seminal fluid SF-EVs

As previously discussed, in this chapter I developed a protocol for further purification of centrifuged-isolated SF-EVs using size-exclusion chromatography to remove proteins not associated to SF-EVs. The average recovery yield was 61 %, and NTA and Western blotting confirmed SF-EV size and phenotype remained unaltered after purification.

Using ExoView and electron microscopy I have showed the purified SF-EVs are similar to unprocessed seminal fluid SF-EVs. This is also the first analysis specifically studying exosomal markers in EVs from unprocessed human seminal fluid in the literature. The

data revealed both unprocessed seminal fluid and SF-EV preparations contained the same three different $CD63^+$ populations in similar proportions: $CD63^+CD9^+CD81^-$, $CD63^+CD9^+CD81^+$, $CD63^+CD9^-CD81^+$. Only SF-EV preparation # 2 seemed to have a higher percentage of $CD63^+CD9^-CD81^+$ SF-EVs when compared to unprocessed seminal fluid SF-EVs and the other purified SF-EV preparations – this might be due to patient variability since this pool had a higher proportion of subfertile patients with oligozoospermia. In addition, the ExoView showed the size of both purified SF-EVs and SF-EVs from unprocessed seminal fluid ranged from 50 to 200 nm with an average modal size of 70 nm and 65 nm, respectively.

In conclusion, purified SF-EVs obtained using a single ultracentrifugation step and size-exclusion chromatography are a good representation of physiological SF-EVs. The preparation method retains vesicles which are lost in other preparation protocols (Poliakov *et al.*, 2009). These SF-EVs were used in forthcoming chapters.

3 The role of SF-EVs on luminal endometrial epithelial cell (EEC) receptivity to embryo implantation

3.1 Introduction

3.1.1 Development of luminal EEC receptivity to embryo implantation

After ovulation, the progesterone surge promotes differentiation of luminal and glandular EECs to become receptive to embryo implantation. Luminal EECs are the uppermost layer of the endometrium, therefore they are not only the first point of contact for embryos, but also the first layer of cells SF-EVs contact. Hence, in this chapter I focus specifically on luminal EECs.

Luminal EECs are simple columnar cells with non-adhesive plasma membranes that separate the endometrium from the uterine lumen. Receptivity to embryo implantation involves cellular differentiation whereby luminal EECs become more cuboidal and develop adhesive plasma membranes to facilitate embryo implantation – this involves formation of pinopodes, loss of apico-basal cell polarity, and complex molecular changes (Fig 3.1) (Glasser and Mulholland, 1993, Buck *et al.*, 2012, Hantak *et al.*, 2014, Aplin and Ruane, 2017, Rarani *et al.*, 2018).

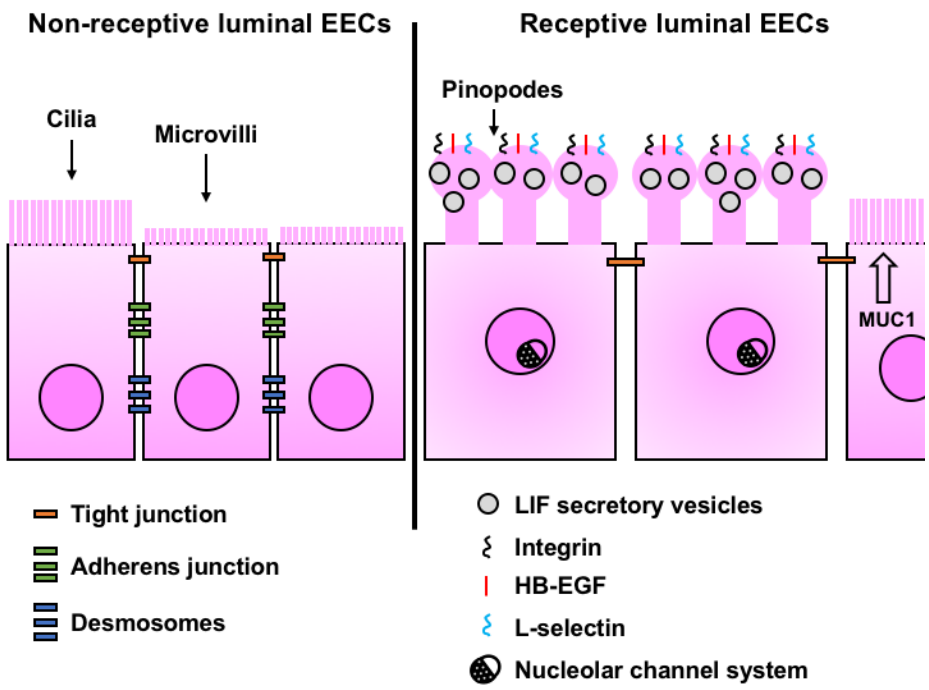


Fig 3.1 Development of receptivity to embryo implantation in luminal EECs.
Endometrial epithelium contains ciliated and microvillus cells. After the progesterone surge, EECs become receptive to embryo implantation which involves loss of cell polarity and pinopodes formation. This phenotypic differentiation also requires complex molecular changes such as increased expression of integrins, Heparin Binding Epidermal Growth Factor (HB-EGF), L-selectin, and Leukemia Inhibitory Factor (LIF) in pinopode-forming EECs and increased expression of mucin 1 (MUC1) in ciliated cells. In addition, luminal EECs receptive to embryo implantation present characteristic structures in the nuclei denominated nucleolar channel systems.

To date most scientific data pertaining to EEC receptivity to embryo implantation comes from animal studies, due to difficulties in performing human studies (human samples are not readily available and primary cultures are challenging) Results from animal studies must be considered carefully because early luminal EECs receptivity, embryo apposition, and attachment is species-specific (Lindenberg *et al.*, 1989). For instance, in mice the trophoblast sloughs the epithelium away and in rabbits the trophoblast fuses with the EECs (Larsen, 1962). In cows the trophoblasts do not penetrate but form a plate on the maternal epithelium (Wathes and Wooding, 1980, Guillomot and Guay, 1982), and in

humans trophoblast cells penetrate between the EECs forming a multilayer (Lindenberg *et al.*, 1986) – all these differences are also observed *in vitro* (Lindenberg et al., 1989).

Human EEC receptivity to embryo implantation research primarily relies on immunohistochemistry experiments and *in vitro* studies using cell lines or primary tissue cultures. Ishikawa cells are a commonly used line of EECs, established from an endometrial adenocarcinoma of a 39-year-old Japanese patient (Nishida, 2002). Ishikawa cells are polygonal cells with fine chromatin granules, small nucleoli and irregularly shaped nuclei. They also contain vacuoles, and express oestrogen and progesterone receptors (Nishida, 2002). In addition, under progesterone stimulation *in vitro* Ishikawa cells form domes, a structure similar to pinopodes, mimicking the endometrium at the implantation window (Fleming, 1995). Other cell lines available are RL95-2, HEC-1A, and AN3-CA. RL95-2 are luminal EECs from an adenosquamous carcinoma receptive to embryo implantation (Way *et al.*, 1983, Thie and Denker, 2002). HEC-1A (Kuramoto *et al.*, 1972, Thie and Denker, 2002) and AN3-CA (Ininns *et al.*, 1992)are luminal EECs from endometrial adenocarcinomas resistant to embryo implantation. Attempts to develop primary tissue cultures of human endometrial epithelial cells have been made, these protocols are challenging (Osteen *et al.*, 1989, White *et al.*, 1990, Bentin-Ley *et al.*, 1994, Zhang *et al.*, 2012, Chen and Roan, 2015, Chen *et al.*, 2016b). It is common place to study human EEC physiology combining at least two approaches such as animal models and cell lines (Rahnama *et al.*, 2009), or cell lines and primary cultures (Whitby *et al.*, 2018).

3.1.1.1 Loss of apico-basal cell polarity

The epithelial cells are polarised cells with asymmetric cytoplasmic distribution. Three cell surfaces are identified in an epithelial cell, the apical, lateral and basal membranes. The lateral and basal membranes express adhesion molecules for cell-cell and cell-matrix interactions. On the contrary, the apical membranes lack adhesive molecules acting as a barrier to the external lumen (Simons and Fuller, 1985, Rodriguez-Boulan and Nelson, 1989, Thie *et al.*, 1996). Embryo implantation is a biological cell paradox, because the initial interaction between the endometrium and the trophoblast epithelia involves their non-adherent apical membranes. However, the rise in progesterone after ovulation promotes a partial epithelium-to-mesenchyme transformation in the luminal epithelium receptive to embryo implantation that results in the loss of polarity (Fig 3.1) (Thie *et al.*, 1996, Whitby *et al.*, 2018). RL95-2 and HEC-1A cells are non-polarised and polarised luminal EEC cell lines, respectively. RL95-2 showed higher efficiency to attach to JAR spheroids (mimicking embryo in an implantation model) than HEC-1A, where spheroid attachment levels were as low as the control (human dermal fibroblasts) (Thie *et al.*, 1996). This illustrated that the loss of polarity in receptive EECs is essential for trophoblast attachment.

Cell to cell contacts establish and maintain cell polarity (Garcia *et al.*, 2018). Polarised EECs present three different types of intercellular junctions involved in maintaining this asymmetry: tight junctions, adherens junctions, and desmosomes (Farquhar and Palade, 1963), which are hormonally regulated (Fig 3.1) (Singh and Aplin, 2009, Grund and Grummer, 2018). Tight junctions divide the apical and lateral membranes, and regulate paracellular transport and epithelial cellular organization (Zihni *et al.*, 2016). Adherens junctions and desmosomes are in the lateral membrane and hold cells together (Campbell

et al., 2017). In the luminal endometrium at the time of implantation tight junctions are still present but they are deeper and extensive (Murphy *et al.*, 1982), while desmosomes and adherens junction are reduced (Potter *et al.*, 1996, Orchard *et al.*, 1999, Paria *et al.*, 1999, Sarani *et al.*, 1999, Illingworth *et al.*, 2000).

Establishment and maintenance of epithelial polarity is also dependent on assymetrical localization of polarity complexes such as Crumbs, atypical protein kinase C (PKC) and Stardust complexes found in the apical side, and Scribble complex found in the basolateral side (Fig 3.1) (Whitby *et al.*, 2018). Recently, it was shown that human luminal EECs at the implantation window downregulated atypical PKC, Crumbs, Sturdust and Scribble – while human glandular EECs did not show downregulation of these proteins. This is the first evidence of a physiological loss of epithelial cell polarity in luminal EECs in humans (Whitby *et al.*, 2018). In addition, the same group showed that treatment of the endometrial epithelial ECC-1 cell line with estrogen, progestin, and human chorionic gonadotropin downregulated Scribble, and knockout of Scribble in this cell line resulted in reduced trophoblast spheroid attachment (Whitby *et al.*, 2018).

3.1.1.2 Pinopodes formation

The luminal epithelium contains two types of EECs: ciliated and secretory epithelial cells – secretory EECs are the main population and they have microvilli (Dockery, 2008). After a rise in progesterone, secretory EECs form pinopodes that are cell protrusions on the EECs apical side (Fig 3.1) (Stavreus-Evers *et al.*, 2001). Human pinopodes are characterised for a mushroom-like shape and, unlike pinopodes in mice and rats (Parr and Parr, 1974, Lopata *et al.*, 2002), human pinopodes do not have large vacuoles. In addition, pinopode expressing cells contain rough endoplasmic reticulum, enlarged mitochondria,

well-developed Golgi complex, secretory vesicles and glycogen throughout the whole cell membrane (Wynn and Woolley, 1967, Adams *et al.*, 2002, Afami, 2015). Pinopodes are initially developed through swelling of the EECs and progressive fusion of the microvilli, termed progressive pinopodes. Pinopodes then increase in size becoming 'fully-developed pinopodes', and after 48 hrs EEC swelling decreases and the microvilli reappear, these are 'regressing pinopodes' (Oborna *et al.*, 2004). These pinopodes are a cycle dependent-structure, therefore pinopodes at different developmental stages can be found at the same time (Stavreus-Evers *et al.*, 2001, Da Broi *et al.*, 2017).

The exact role of pinopodes is not well understood, fully-developed pinopodes are specific to the implantation window suggesting they may be a good marker of endometrial receptivity (Nikas, 1999, Nikas and Makrigiannakis, 2003). Evidence suggest they are the preferential attachment site for the embryo (Bentin-Ley *et al.*, 1999), although there are contradictory results (Bentin-Ley *et al.*, 2000, Rarani *et al.*, 2018). In line with the hypothesis that they are a preferential attachment site for the embryo, pinopodes express proteins specific to the implantation window that are involved in embryo-maternal endometrium crosstalk such as integrins, L-selectin, and heparin binding epidermal growth factor that promote embryo apposition/attachment and development (Fig 3.1) (Stavreus-Evers *et al.*, 2002, Nikzad *et al.*, 2010, Nejatbakhsh *et al.*, 2012). They also secrete vesicles containing Leukemia Inhibitory Factor (LIF), involved in multiple implantation processes including embryo-endometrium crosstalk, endometrial stromal cell decidualisation, regulation of the endometrial immune environment and trophoblast invasion (Fig 3.1) (Kabir-Salmani *et al.*, 2005, Salleh and Giribabu, 2014, Rarani *et al.*, 2018). In addition pinopodes downregulate mucins of the glycocalyx, such as Mucin 16 and Mucin 1 (MUC1), that are involved in the anti-adhesiveness of the epithelium (Fig

3.1) (Meseguer *et al.*, 1998, Horne *et al.*, 2002, Horne *et al.*, 2005, Gipson *et al.*, 2008). Interestingly in human receptive endometrium MUC1 is expressed by ciliated luminal EECs but is suppressed in pinopodes (Horne *et al.*, 2002, Horne *et al.*, 2005, Gipson *et al.*, 2008).

3.1.1.3 Molecular changes

A series of complex molecular changes occur during acquisition of luminal EECs receptivity to embryo implantation, some of them discussed above. This complexity was exemplified on a proteome and secretome study of the luminal epithelial cell line, ECC1, under progesterone and oestrogen stimulation (Greening *et al.*, 2016). 157 proteins were found to be differentially expressed in the proteomic analysis, 68 were upregulated while 89 were downregulated. Similarly, the secretome analysis found 123 proteins differentially expressed, 36 were upregulated and 87 were downregulated (Greening *et al.*, 2016).

A characteristic feature of the molecular changes in EECs at the implantation window is the development nucleolar channel systems (NCS) (Fig 3.1) (Terzakis, 1965, Guffanti *et al.*, 2008, Nejat *et al.*, 2014). NCS are a 1 μm membranous structure consisting of a labyrinth of channels throughout an electron-dense matrix, and opaque particles regularly arranged around the total structure or the individual channel (Kohorn *et al.*, 1970, Kohorn *et al.*, 1972). They are in the periphery of the nucleolus and are stimulated by progesterone and progesterone analogues (Kohorn *et al.*, 1970, Kohorn *et al.*, 1972) NCS are exclusively of the time of implantation, they start appearing on day 2 after ovulation and disappear by day 12 after ovulation; because of their specific time-span indirect NCS

detection by immunofluorescence has been suggested to accurately determine the implantation window (Guffanti *et al.*, 2008, Nejat *et al.*, 2014).

3.1.2 Failed luminal EEC receptivity to embryo implantation and subfertility

Inadequate luminal EEC receptivity to embryo implantation is thought to be involved in subfertility. For instance, pinopode formation, as well as LIF and LIF receptor protein expressions in luminal EECs, were reduced in patients with unexplained infertility (Aghajanova *et al.*, 2009a). The role of defective EEC receptivity to embryo implantation in recurrent implantation failure (RIF) has also been studied. For instance, analysis of endometrial biopsies from fertile and RIF patients by transmission electron microscopy showed RIF patients had significantly lower numbers of pinopodes and higher numbers of ciliated and microvillus cells. Not all the pinopodes presented were fully-developed (Bahar *et al.*, 2015). In addition, MUC1 protein levels were significantly reduced in luminal and glandular EECs in RIF patients (Bastu *et al.*, 2015, Wu *et al.*, 2018). RIF patients also showed significantly less MUC1 protein levels than patients with idiopathic recurrent pregnancy loss (Wu *et al.*, 2018).

3.1.3 The role of seminal fluid on EEC receptivity to embryo implantation

Seminal fluid has been shown to modulate gene expression of human EECs. A study showed that *in vitro* exposure of primary EECs to seminal fluid activated cell pathways involved in cell viability, proliferation, growth and immune cell trafficking, and inhibited cell death (Chen *et al.*, 2014). This same study showed that seminal fluid induced upregulation of *IL-11*, *Fibroblast Growth Factor 2 (FGF2)* and *VEGF-A* mRNA –

VEGF-A, IL-8, and IL-6 protein levels also increased (Chen *et al.*, 2014). Another *in vitro* study also reported that seminal fluid induced EECs upregulation of *IL-6*, LIF and IL-1β (Gutsche *et al.*, 2003). To date, there has been no published research about SF-EV interactions with human EECs.

3.1.3.1 SF-EVs effect on Ishikawa cells

Data obtained during my MSc Clinical Embryology suggested SF-EVs induced molecular changes on progesterone treated Ishikawa cells (Rodriguez-Caro, MSc dissertation 2015). Ishikawa cells, treated with 8-Br-cAMP and progesterone for 7 days, were incubated with SF-EVs for 30 min ($5x10^{10}$ SF-EVs/10^6 cells) and lysed. A phospho-kinase array was then performed to look for cell activation – the array showed SF-EVs decreased cAMP response element binding (CREB) protein phosphorylation at S133 and total protein levels of total 60 kDa heat shock protein (HSP60) in day 7 progesterone treated Ishikawa cells (Fig 3.2 a). Western blotting analysis confirmed SF-EVs induced dephosphorylation of CREB at S133 by 30 % ($p < 0.05$) ($n = 3$) (Fig 3.2 b) (Rodriguez-Caro, MSc dissertation 2015).

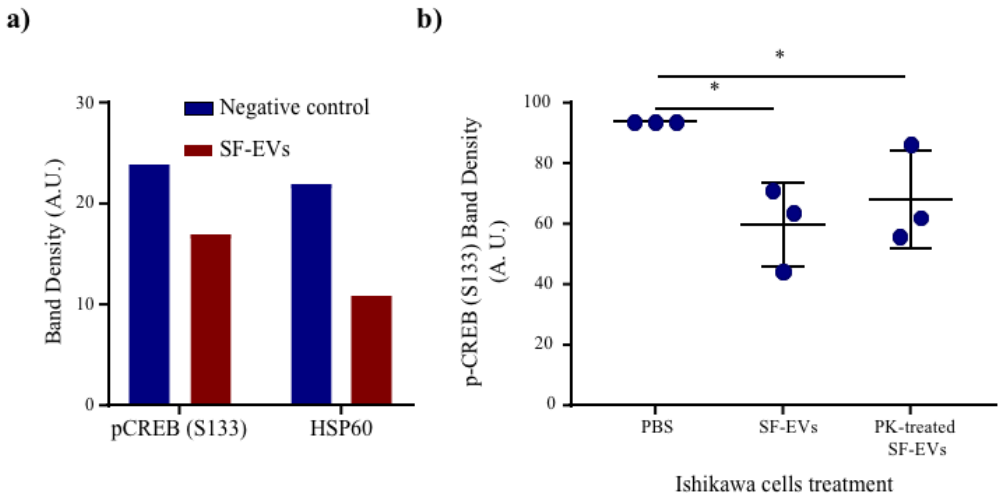


Fig 3.2 Protein expression of p-CREB (S133) and HSP60 in day 7 progesterone treated Ishikawa cells after SF-EV treatment.

(a) A human phospho-kinase array was performed on cell lysates of Ishikawa cells stimulated with 8-Br-cAMP and progesterone for 7 days and treated with PBS (negative control) (blue bars) or SF-EVs (red bars) for 30 min. **(b)** 8-Br-cAMP and progesterone treated Ishikawa cells were also stimulated with PBS, SF-EVs, or proteinase K (PK)-treated SF-EVs and analysed by Western blotting to detect CREB phosphorylation at S133. Bars represent mean ± SD.

This evidence for SF-EV induction of molecular changes to Ishikawa cells led the hypothesis that SF-EVs would also influence primary isolated human EECs. This chapter aims to further investigate SF-EV interactions with both the Ishikawa cell line and primary EECs.

3.2 Aims of the chapter

I hypothesize that SF-EVs assist the development of luminal EECs receptivity to embryo implantation. The aims of this chapter are:

1) To investigate if SF-EVs bind to Ishikawa cells
2) To determine if SF-EVs induce molecular changes in Ishikawa cells
3) To optimise a protocol for the isolation and *in vitro* culture of primary luminal EECs
4) To investigate if SF-EVs bind to primary luminal EECs

3.3 Methods

3.3.1 *In vitro* culture of Ishikawa cells

Ishikawa cells were obtained from Ms. Janet Carver (NDWRH, University of Oxford) and authenticated by the European Collection of Authenticated Cell Cultures (ECACC) in May 2017 – the short tandem repeat DNA profile of the Ishikawa cells matched 100 % with the ECACC Ishikawa cell profile.

The Ishikawa cells were cultured in Dulbecco's Modified Eagle's Medium/Nutrient Mixture F-12 Ham (DMEM-F12) (Sigma-Aldrich, USA), supplemented with 10 % fetal calf serum (FCS) (Sigma-Aldrich, USA), penicillin (100 IU/ml) (Sigma-Aldrich, USA), streptomycin (100 µg/ml) (Sigma-Aldrich, USA) and 2 mM L-glutamine (Sigma-Aldrich, USA). Cells were cultured at 37°C, 20 % O_2 and 5 % CO_2. Culture media was changed every 2 days and cell passage performed when ~ 80 % confluence was reached.

To mimic endometrial epithelial cells receptive to embryo implantation Ishikawa cells were grown in growth media supplemented with 0.5 mM dibutyryl cyclic-AMP sodium salt (Sigma-Aldrich, USA) and 1 µM progesterone (Sigma-Aldrich, USA). This media was changed every 2 days and the treatment lasted for 7 days. Cells were used on either day 3 or day 7 of progesterone treatment.

3.3.2 Subject Recruitment

Ethical approval for the collection of endometrial biopsies was obtained from the Oxford South Central Regional Ethics Committee - #08/H0606/94. All patients gave written informed consent. Endometrial biopsies were obtained from patients undergoing IVF at

Oxford Fertility, before embryo transfer (n = 47). Patients characteristics are described in appendix 2. These endometrial samples were collected using an Endocell disposable endometrial cell sampler (Wallach Surgical devices, USA).

3.3.3 Isolation and *in vitro* culture of primary luminal EECs

Endometrial biopsies were incubated overnight at 4°C before isolation of primary luminal EECs (diagram describing the processes show in Fig 3.3).

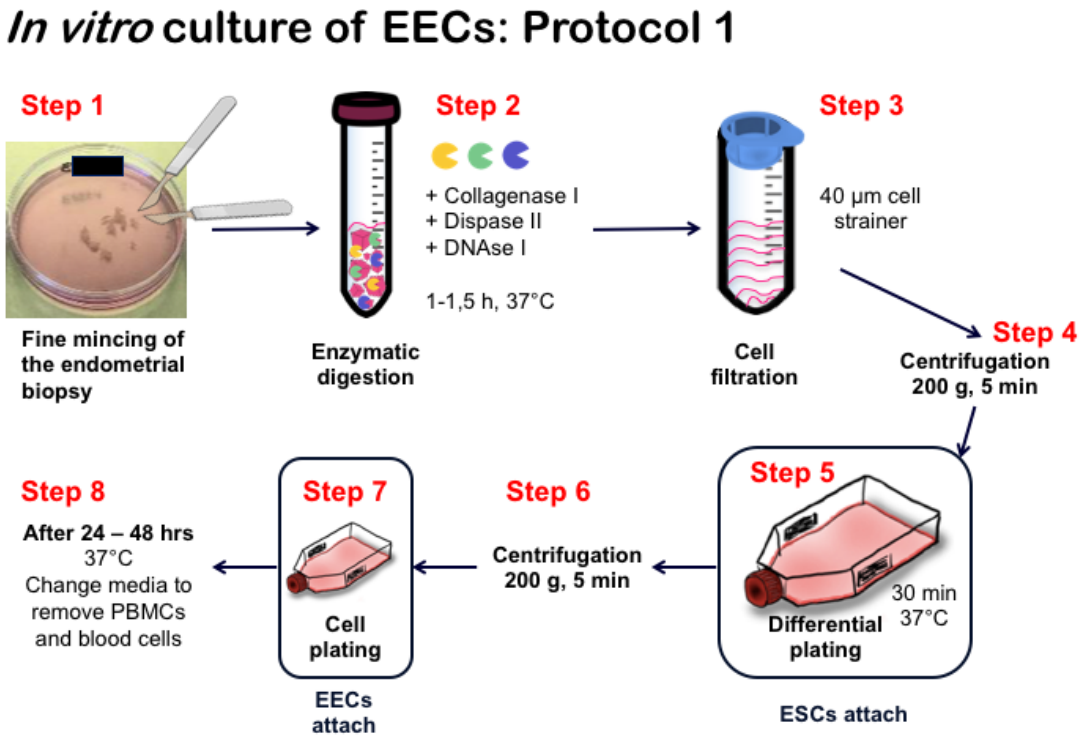


Fig 3.3 Isolation of primary EECs.
Diagram detailing the protocol stages for EEC generation. EECs were cultured in Keratinocyte Serum Free Medium supplemented with bovine pituitary extract, epidermal growth factor 1-53, penicillin (100 IU/ml), streptomycin (100 µg/ml), and amphotericin B (2.5 µg/ml).

Step 1 - the endometrial biopsies were transferred to a petri dish with digestion culture media (recipe below) and fine minced with 2 scalpel blades (Swann-Morton, England).

Step 2 - the biopsy fragments were enzymatically digested with Collagenase I (10 mg/biopsy) (Thermo Fisher, USA), Dispase II (5 mg/biopsy) (Thermo Fisher, USA) and DNAse I (800 IU/biopsy) (Sigma-Aldrich, USA) in 2 mL of digestion media for 1 – 1.5 hrs at 37 °C in a water bath with agitation.

Step 3 - the digested samples were passed through a 40 μm cell strainer (Corning, USA Corning, USA). The glandular EECs remained on the top of membrane and were discarded.

Step 4 - the eluate contained luminal endometrial cells and blood cells. This was centrifuged at 200 x g for 5 min at RT.

Step 5 - the pellets were resuspended in stromal cell culture media (recipe below) and plated on tissue culture 75 cm^2 flasks (Nunc) for 30 min at 37°C. After 30 min the stromal cells were attached and the culture media containing non-adhered cells was collected.

Step 6 – the cell suspension was centrifuged at 200 x g for 5 min at RT.

Step 7 - the pellets with the luminal EECs were then cultured in tissue culture 25 cm^2 flasks (Nunc) overnight at 37 °C in epithelial cells culture media (see below). After 24 hrs EECs attachment was confirmed using bright field microscopy, if only a few of the cells had attached they were incubated for another 24 hrs.

Step 8 - culture supernatant was collected to remove red blood cells and endometrial immune cells – for some samples the collected immune cells were used to established *in vitro* cultures of endometrial T regulatory cells (Chapter 5). EEC culture media was added to the adherent cells.

EECs were cultured at 37°C, 20 % O_2 and 5 % CO_2. Culture media was changed every 2 days and cell passage performed when structurally defined EECs were formed, after approximately 5 days of culture. In the original protocol (**Protocol 1**) cells were lifted

with Trypsin-EDTA (Sigma-Aldrich, USA). To improve cell yields after isolation and cell passage, in **Protocol 2** EECs were cultured on fibronectin (Sigma-Aldrich, USA)-coated tissue culture 25 cm^2 flasks (Nunc), and lifted with accutase (Sigma-Aldrich, USA). Finally, to continue improving EEC survival rates after cells passage, in **Protocol 3**, EECs were cultured in epithelial cell culture media containing 10 μM ROCK inhibitor Y-27632 Dihydrochloride (Sigma-Aldrich, USA) for 24 - 48 hrs after lifting. Afterwards epithelial cells culture media without ROCK inhibitor was added.

Collection/digestion culture media: Dulbecco's Modified Eagle's Medium (DMEM) - 4500 glucose (Sigma-Aldrich, USA), supplemented with penicillin (100 IU/ml), and streptomycin (100 μg/ml).

Stromal cells culture media: DMEM-F12, supplemented with 10 % FCS, penicillin (100 IU/ml), streptomycin (100 μg/ml) and 2 mM L-glutamine.

Epithelial cells culture media: Keratinocyte Serum Free Medium (Thermo Fisher, USA) supplemented with bovine pituitary extract (Thermo Fisher, USA), epidermal growth factor 1-53 (Thermo Fisher, USA), penicillin (100 IU/ml), streptomycin (100 μg/ml), and amphotericin B (2.5 μg/ml) (Gibco, UK).

3.3.3.1 Bright field microscopy

Bright Field Images of primary luminal EECs were captured using the Leitz Labovert FS inverted light microscope (Leitz,USA) with Micropublisher 3.3 camera (Q imaging, USA). Images were taken at 10x amplification using Q Capture Pro 7™ software (Q imaging, USA).

3.3.4 SF-EV isolation and purification

SF-EVs were isolated and purified as described in chapter 2.

3.3.5 Binding studies

As explained in chapter 2, fluorescent SF-EVs were generated by labelling EVs with bio-maleimide and the excess of dye was removed by size-exclusion chromatography. For negative controls in flow cytometry binding experiments bio-maleimide labelled PBS purified by size-exclusion chromatography was used to confirm removal of the excess of dye, and to determine cell autofluorescence. An equal volume to that used for SF-EVs treatment was used in the negative control group.

All samples were analysed using a BD LSRII flow cytometer and FlowJo software version 10.4.2 - mean fluorescence intensity was measured and the increase calculated by subtracting the mean fluorescence intensity of the negative control group to the SF-EV treated group. In addition, the percentage of cells binding SF-EVs was determined subtracting the negative control.

3.3.5.1 Flow cytometry of Ishikawa cells

Ishikawa cells were treated with bio-maleimide labelled SF-EV preparation # 1, the negative control or PBS at different incubation times ($5x10^{10}$ SF-EVs/10^6 cells) (n = 3), and different SF-EV/cell ratios (2 hrs incubation) (n = 3), at 37°C to determine optimal binding conditions. After 2 hrs incubation, cells were washed twice with PBS and detached with accutase. Cells were centrifuged for 5 sec at 13,000 x g and the pellets resuspended in 500 µl of 2 % FCS/PBS for flow cytometry analysis, a 1 % gate was used as the percentage of cells in the negative control. After optimal conditions were

established, untreated (day 0), and day 3 and day 7 progesterone treated Ishikawa cells were incubated with bio-maleimide labelled SF-EV preparation # 4, the negative control or PBS for 2 hrs at 37°C ($5x10^{10}$ SF-EVs/10^6 cells) (n = 3). Cells were again washed, detached from the flasks with accutase and analysed, a 5 % gate was used as the percentage of cells in the negative control.

3.3.5.2 Flow cytometry of primary EECs

Isolated luminal EECs on passage 0, or after *in vitro* culture with protocol 2, that were forming defined EECs colonies were treated with bio-maleimide labelled SF-EV preparation # 4, or the negative control for 2 hrs at 37°C ($5x10^{10}$ SF-EVs/10^6 cells) (n = 3). Non-treated wells were used to determine cell yield per well, so required SF-EV numbers could be calculated. After the incubation, cells were washed twice with PBS and detached with accutase. EECs were then centrifuged for 5 min at 300 x g. Pellets were resuspended in 100 µl of 2 % FCS/PBS and incubated with APC[15] anti-human CD326 (Epithelial cell adhesion molecule, EpCam) antibody (Table 3.1) for 20 min in the dark at RT. EECs were centrifuged again for 5 min at 300 x g, resuspended in 400 µl of 2 % FCS/PBS and analysed (Fig 3.4). A 5 % gate was used as the percentage of cells in the negative control. The average EECs purity yield was 54.53 ± 21.38 %.

[15] APC: allophycocyanin

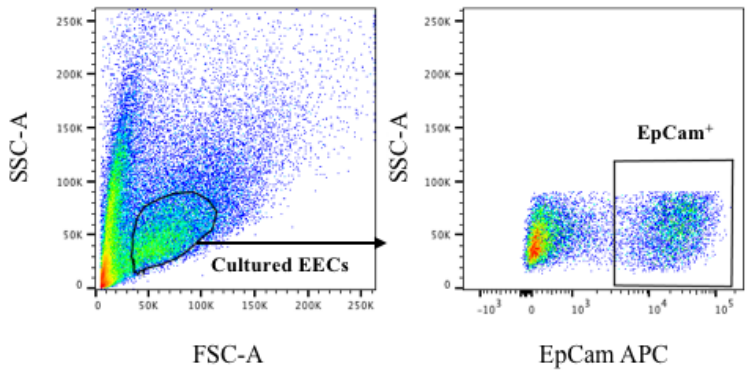


Fig 3.4 Flow cytometry identification of isolated primary luminal EECs on passage 0 or 2 (Protocol 2).
EEC were first identified on their FCS vs SSC parameters, then EpCAM expression was determined by staining with anti-human EpCAM APC antibodies.

Isolated luminal EECs cultured *in vitro* with the ROCK inhibitor were also treated with bio-maleimide labelled SF-EV preparation # 4, or the negative control for 2 hrs at 37°C ($5x10^{10}$ SF-EVs/10^6 cells, n = 1) ($1x10^{11}$ SF-EVs/10^6 cells, n = 3), 2 days after the removal of the ROCK inhibitor. As before, non-treated wells were used to determine cell yield per well. Then, cells were washed, detached with accutase, incubated with the viability dye - Zombie Aqua (Table 3.1) in PBS for 15 min in the dark at RT, and labelled with APC anti-human CD326 (EpCam) antibody (Table 3.1). Binding was then assessed (Fig 3.5). The average EECs purity yield was 91.95 ± 8.76 %

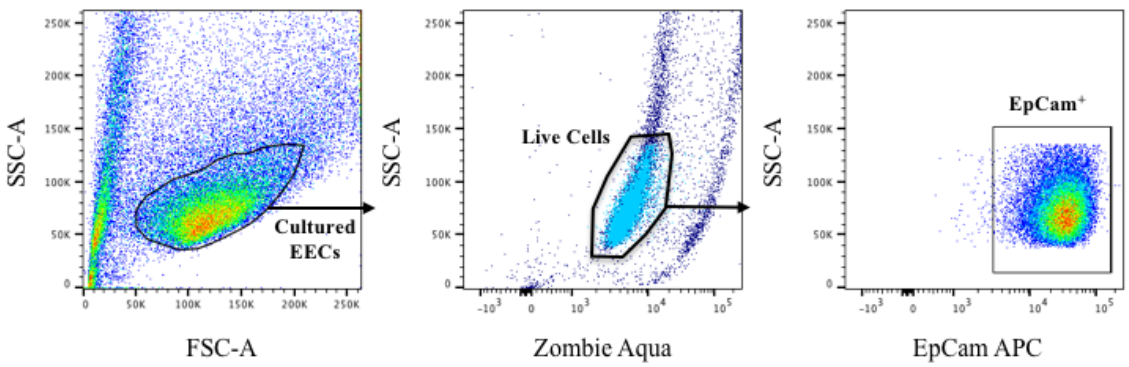


Fig 3.5 Flow cytometry identification of live primary luminal EECs isolated with protocol 3.

EEC were identified on their FCS vs SSC parameters, live cells were analysed using Zombie Aqua staining and EpCAM expression was determined by staining with anti-human EpCam APC.

3.3.5.3 Fluorescence microscopy of Ishikawa cells (IN Cell 1,000 Analyser)

Untreated Ishikawa cells were incubated with bio-maleimide labelled SF-EV preparation # 1 or PBS for 2 hrs at 37°C ($5x10^{10}$ SF-EVs/10^6 cells) (n = 1). Cells were then washed once with PBS, fixed with 100 % methanol (Sigma-Aldrich, USA) for 10 min at - 20°C, washed, and permeabilised with 0.5 % Triton X-100 (Sigma-Aldrich, USA) for 15 min at RT. Afterwards, cells were washed with PBS and incubated with antibodies towards LC3 (microtubule-associated protein) for 2 hrs at RT (Table 3.1) in permeabilization buffer containing FCS (Thermo Fisher, USA). Cells were washed with PBS and incubated with polyclonal antibodies recognising mouse IgG (Alexa Fluor® 594 nm) for 40 min at RT and with DAPI[16] for 5 min at RT (Table 3.1). 20x and 40x fluorescence images were captured using an IN Cell 1,000 analyser (GE Healthcare Life sciences, UK).

[16] DAPI: 4',6-Diamidino-2-Phenylindole, Dihydrochloride

3.3.5.4 *Fluorescence microscopy of Ishikawa cells (Nanoimager)*

Bio-maleimide labelled SF-EV preparation # 1 was incubated with 10 ng/mL fluorescence primary antibodies towards CD63 (Alexa Fluor® 647) (Table 3.1) for 30 min at RT in the dark. SF-EVs were then washed with PBS twice using Amicon Ultra Centrifugal filter units 100 KDa (Merck Millipore, Ireland) and SF-EV concentration determined by NTA. Untreated Ishikawa cells were then incubated with bio-maleimide, anti-human CD63 (Alexa Fluor® 647) labelled SF-EV preparation # 1 or PBS for 2 hrs at 37°C ($5x10^{10}$SF-EVs/10^6 cells) (n = 1). Cells were then washed twice with PBS, fixed with 100 % methanol (Sigma-Aldrich, USA) for 10 min at - 20°C, and incubated with Hoescht 33258 for 10 min at RT in the dark (Table 3.1). SF-EV binding was then visualised using the Nanoimager (Oxford Nanoimaging, UK) – a newly-designed super-resolution fluorescence microscope for extracellular vesicles analysis (https://www.oxfordni.com/product/the-nanoimager). Super-resolution is achieved using single-molecule localisation. In short, samples are labelled with fluorophores that can switch between on and off states. Then, consecutives images are taken at high intensity in specific conditions causing the fluorophores to blink between both states, only activated fluorophores are localised in each image. Finally, the super-resolved image is re-constructed by merging all localised points (Oxford Nanoimaging, UK).

Table 3.1 Fluorescence dye, primary and secondary antibodies used for flow cytometry and fluorescence microscopy studies.

Antibody/dye	Dilution/ Concentration	Antigen	Source	Clones	Company
Anti-human CD326/EpCam (APC)	1:20	EpCam	Mouse	9C4	Biolegend, USA
Zombie Aqua	1:1000	Live/Dead cells	-	-	Biolegend, USA
Anti-LC3 pAb	1:500	LC3	Rabbit	Polyclonal	MBL International, USA
Anti-Mouse IgG(Alexafluor® 594nm)	1:200	Mouse Ig	Donkey	Polyclonal	Molecular probes, USA
DAPI	1:1,000	Nuclei	-	-	Molecular probes, USA
Anti-human CD63 (Alexa Fluor® 647)	10 ng/mL	H5C6	Biolegend, USA		
Hoechst 33258	1:10,000	Nuclei	-	-	Molecular probes, USA

3.3.6 Molecular studies on Ishikawa cell activation

Untreated Ishikawa cells were incubated with either PK-non treated or PK-treated SF-EV preparations # 1, # 2, or # 3; or PBS for 30 min at 37°C ($5x10^{10}$ SF-EVs/10^6 cells) (n = 3). After incubation Ishikawa cells were lysed in 300 µl of lysis buffer (recipe below), samples were collected and stored at - 80°C until used. The protein concentration of the lysates was determined using a BCA assay kit and changes on the phosphorylation of CREB (S133), and total HSP60 levels were analysed by Western blotting.

Lysis buffer recipe: 50 mM HEPES[17] (Sigma-Aldrich, USA), 69 mM SDS[18] (Sigma-Aldrich, USA), 10 % v/v glycerol (Sigma-Aldrich, USA) and distilled H_20 in a total

[17] HEPES: 4-(2-hydroxyethyl)-1-piperazineethanesulfonic acid
[18] SDS: Sodium dodecyl sulfate

volume of 100 mL (pH 7.5). A protease inhibitor tablet (Roche, Germany) was added per 10 mL of lysis buffer before use.

3.3.6.1 Western blot

Western blotting was performed as previously described in chapter 2. The antibodies used in this chapter are described in table 3.2, all of them were diluted 1:1,000.

Table 3.2 Primary and secondary antibodies used for Western blot on Ishikawa cells.
Approx. MW = Approximate Molecular Weight

Antibody	Approx. MW	Source	+ Control	Clone	Company
Anti-CREB (S133)	43 KDa	Rabbit	HeLa	8763	Cell Signalling Technology, The Netherlands
Anti-β ACTIN	42 KDa	Mouse	Any cell type	AC-15	Abcam®, UK
Anti-HSP60	60 KDa	Mouse	HeLa	LK1	NeoMarkers, USA
Anti-Mouse IgG-HRP	-	Goat	-	Polyclonal	Dako, Denmark
Anti-Rabbit IgG-HRP	-	Goat	-	Polyclonal	Dako, Denmark

3.3.7 Statistical analysis

3.3.7.1 In vitro culture of primary EECs – survival rates

Statistical analysis was performed using GraphPad Prism 7.01 (GraphPad Software, USA). The percentage survival was determined, and the data was analysed using the Logrank. Differences were considered significant if $p < 0.05$.

3.3.7.2 Binding and Molecular studies

Statistical analysis was performed using GraphPad Prism 7.01 (GraphPad Software, USA). Shapiro-Wilk tests were used to confirm normality of the data. Parametric data was then analysed using paired Student's *t*-test or a repeated measures one-way ANOVA without Geisser-Greenhouse correction. Nonparametric data was analysed using the Friedman test. In the ANOVA and the Friedman test, experimental groups were always compared controlling the False Discovery Rate using the two-stage step-up method of Benjamini, Krieger and Yekutieli. Data were represented as mean ± SD or median ± IQR. Differences were considered significant if $p < 0.05$.

3.4 Results

3.4.1 SF-EVs bind to Ishikawa cells

Ishikawa cells were incubated with fluorescent bio-maleimide labelled SF-EVs, and SF-EV binding was demonstrated by flow cytometry and fluorescence microscopy.

A negative control (bio-maleimide labelled PBS) was used in flow cytometry experiments to confirm that there was no free bio-maleimide and to determine the autofluorescence of Ishikawa cells. To confirm that size-exclusion chromatography eluted free bio-maleimide in non-SF-EV fractions (see chapter 2), Ishikawa cells were treated with each fraction of the purified negative control for 30 min at 37°C and analysed by flow cytometry (n = 2). Representative fluorescence flow cytometry histograms of negative control and PBS treated Ishikawa cells fractions 1 to 30 are shown in appendix 3.

3.4.1.1 SF-EV binding to Ishikawa cells increases with longer incubation times

To determine the optimal incubation time for future experiments, Ishikawa cells were treated with SF-EVs for 0.5, 1, 2, and 3 hrs and analysed by flow cytometry (n = 3). A shift in bio-maleimide fluorescence can be observed after SF-EV treatment (Fig 3.6).

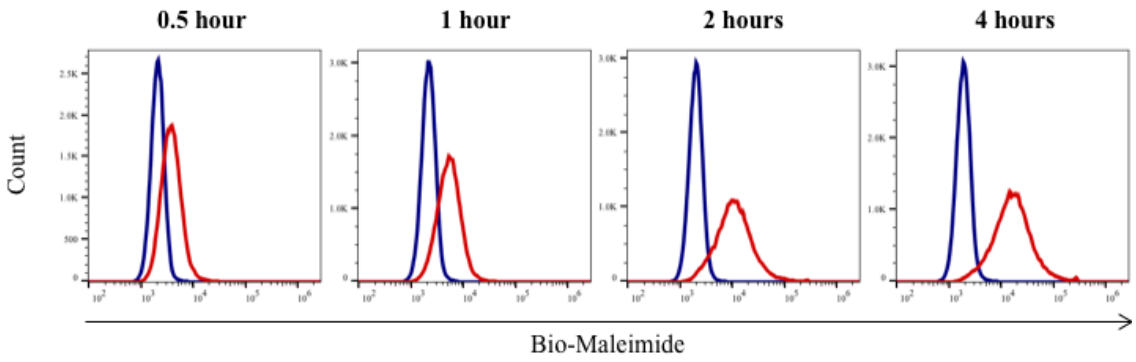


Fig 3.6 Representative flow cytometry histograms of SF-EV binding to Ishikawa cells: time-dependent experiment.
Ishikawa cells were treated with bio-maleimide labelled SF-EVs (red), or the negative control (blue) for 0.5, 1, 2, and 4 hrs ($5x10^{10}$ SF-EVs/10^6 cells). Afterwards, cells were washed and analysed by flow cytometry.

There was a significant increase in bio-maleimide mean fluorescence intensity (MFI) in SF-EV treated Ishikawa cells compared to the negative control at 0.5 hr ($p = 0.0071$), 1 hr ($p = 0.0162$), 2 hrs ($p = 0.0023$), and 4 hrs ($p = 0.0002$) (Fig 3.7). No differences were observed between the negative control and the PBS groups after 4 hrs of incubation (Fig 3.7 d). In addition, bio-maleimide MFI significantly increased with time ($F < 0.0001$), between 0.5 - 2 hrs ($p = 0.0002$), 0.5 – 4 hrs ($p < 0.0001$), 1 – 2 hrs ($p = 0.0008$), 1 – 4 hrs ($p < 0.0001$), and 2 – 4 hrs ($p = 0.0058$) (Fig 3.8 a). No significant changes were observed between 0.5 and 1 hr of incubation time (Fig 3.8 a). The percentage of cells binding SF-EVs was also determined, Ishikawa cells bound significantly more SF-EVs with increasing incubation times ($F = 0.0006$) – raising from an average of 57.36 ± 11.44 % of the cells after 0.5 of incubation to 93.18 ± 0.85 % after 4 hrs of incubation (Fig 3.8 b). As the percentage of Ishikawa cells binding SF-EVs did not change between 2 to 4 hrs (Fig 3.8 b), 2 hrs was established as the optimal incubation time for future experiments.

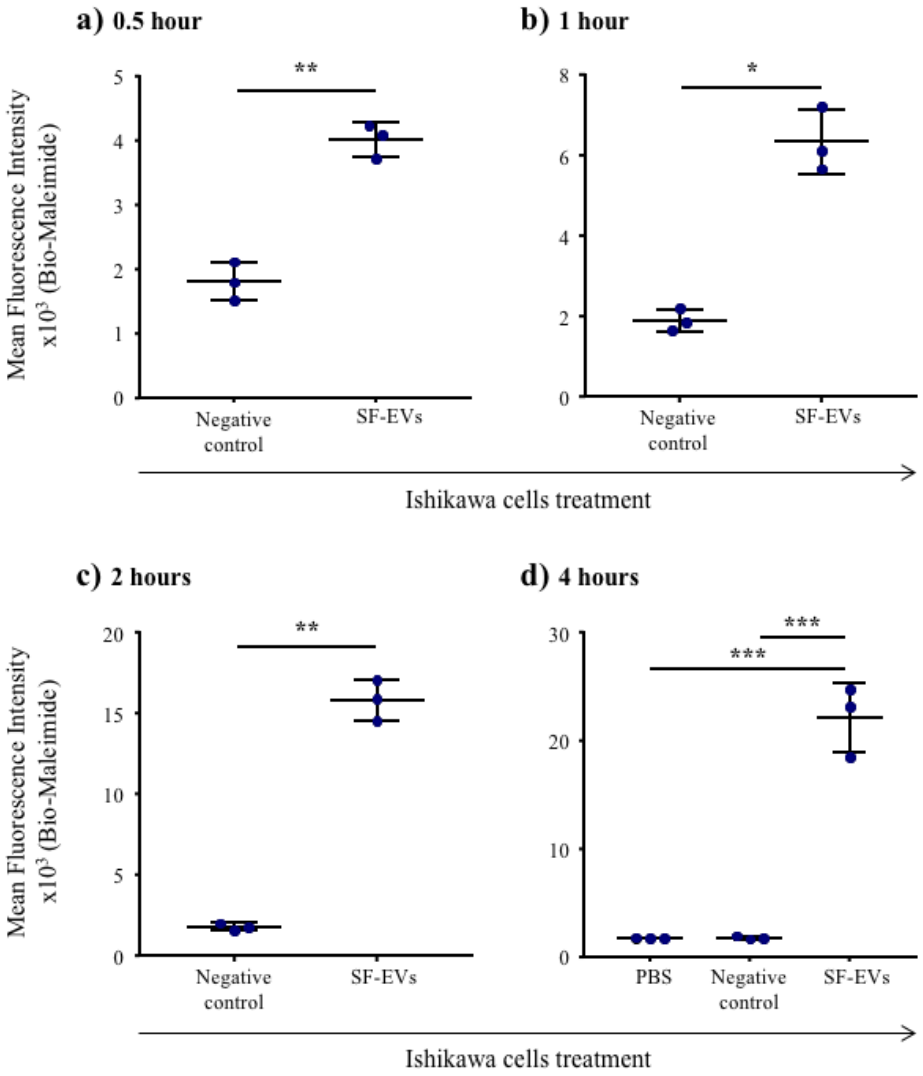


Fig 3.7 SF-EVs bind to Ishikawa cells at different incubation times: mean fluorescence intensity.

Ishikawa cells were treated with bio-maleimide labelled SF-EVs, or the negative control for **(a)** 0.5 h, **(b)**1 h, **(c)** 2 hrs, and **(d)** 4 hrs ($5x10^{10}$ SF-EVs/10^6 cells), or PBS only for 4 hrs. The mean fluorescence intensity of the cells was then analysed by flow cytometry (n = 3). Bars represent mean ± SD. * = $p < 0.05$, ** = $p < 0.01$, *** = $p < 0.001$.

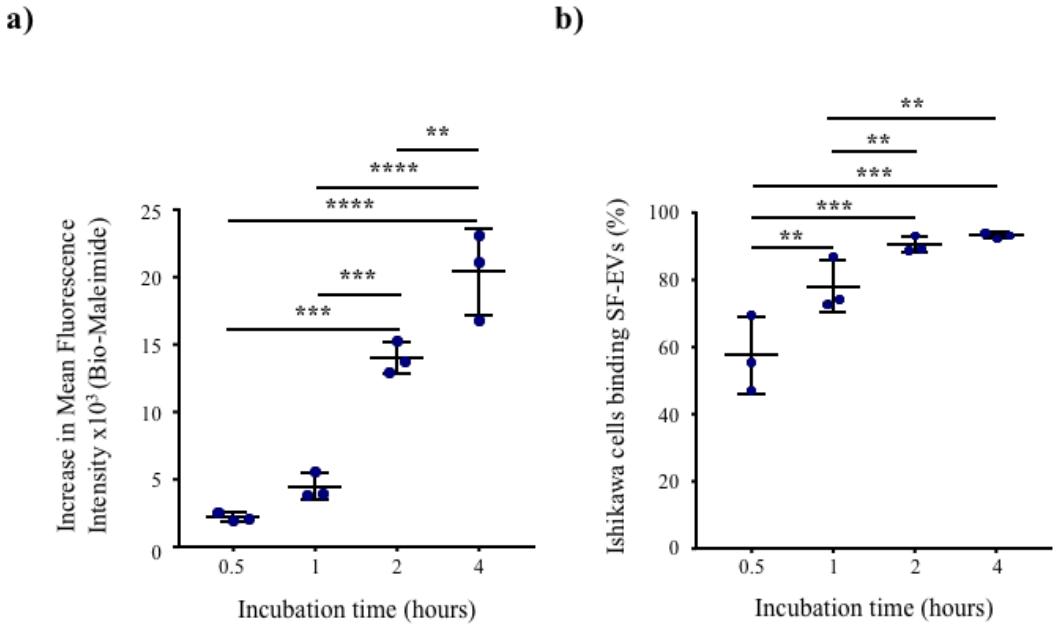


Fig 3.8 SF-EV binding to Ishikawa cells increases with longer incubation.
Ishikawa cells were treated with bio-maleimide labelled SF-EVs, or the negative control for 0.5, 1, 2, and 4 hrs ($5x10^{10}$ SF-EVs/10^6 cells). Cells were washed and analysed by flow cytometry (n = 3). **(a)** The increase in mean fluorescence intensity and **(b)** the percentage of Ishikawa cells binding bio-maleimide labelled SF-EVs were calculated to compare SF-EV binding at different incubation times. Bars represent mean ± SD. ** = $p < 0.01$, *** = $p < 0.001$, **** = $p < 0.0001$.

3.4.1.2 Ishikawa cells binding of SF-EVs increased with higher EV:cell ratios.

To determine the optimal SF-EV/cell ratio for future experiments, approximately 10^6 Ishikawa cells were incubated with either $2.5x10^{10}$, $5x10^{10}$, or $1x10^{11}$ SF-EVs for 2 hrs and analysed by flow cytometry (n = 3). A shift in bio-maleimide fluorescence was observed after SF-EV incubation (Fig 3.9).

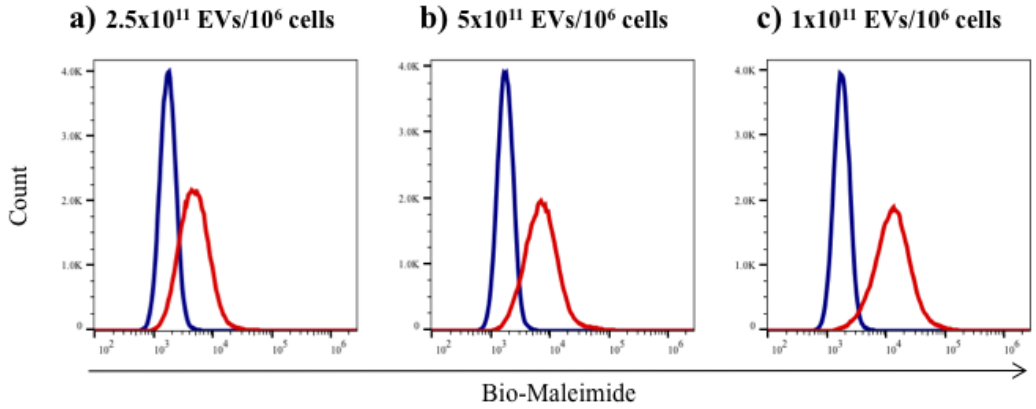


Fig 3.9 Representative flow cytometry histograms of SF-EV binding to Ishikawa cells: concentration-dependent experiment.
Ishikawa cells were treated with bio-maleimide labelled SF-EVs (red) or the negative control (blue) for 2 hrs at **(a)** $2.5x10^{10}$, **(b)** $5x10^{10}$, and **(c)** $1x10^{11}$ SF-EVs/10^6 cells. Afterwards, cells were washed and analysed by flow cytometry.

The amount of SF-EVs binding Ishikawa cells (as measured by MFI of the Ishikawa population) increased as numbers of EV raised: $2.5x10^{10}$ EVs/10^6 cells ($p = 0.0051$), $5x10^{10}$ EVs/10^6 cells ($p = 0.0027$), and $1x10^{11}$ EVs/10^6 cells ($p < 0.0001$) ratio (Fig 3.10). In addition, the negative control did not contain free dye as unchanged from a PBS control treatment (Fig 3.10 c). Bio-maleimide MFI significantly increased with increasing EV/cell ratio ($F = 0.0278$), and significantly higher MFI increased was detected after treating 10^6 Ishikawa cells with $5x10^{10}$ SF-EVs than $2.5x10^{10}$ ($p = 0.0143$) (Fig 3.11 a). The percentage of Ishikawa cells binding SF-EV was also greater with increasing EVs numbers per cells ($F = 0.0019$) – $2.5x10^{10}$ EVs/10^6 cells resulted in 78.92 ± 2.32 % of cells binding SF-EVs, and $1x10^{11}$ EVs/10^6 cells resulted in 92.42 ± 0.41 % of the cells (Fig 3.11 b). $5x10^{10}$ SF-EVs per 10^6 cells was chosen as the optimal EV/cell ratio for following experiments, unless stated.

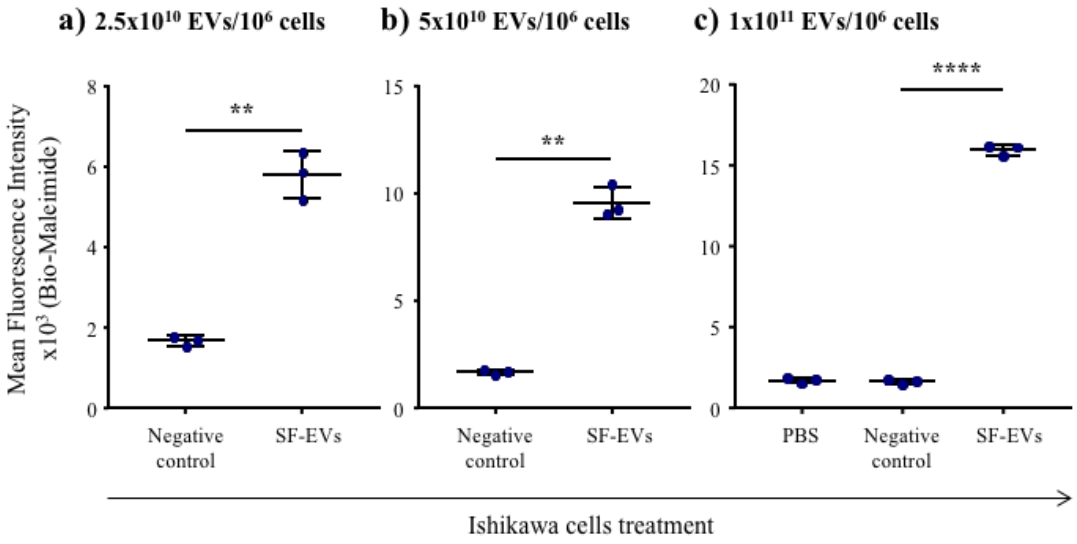


Fig 3.10 SF-EVs bind to Ishikawa cells at different ratios of EV:cell
Ishikawa cells were treated with bio-maleimide labelled SF-EVs, or the negative control for 2 hrs at **(a)** 2.5x10^{10} SF-EVs/10^{6} cells, **(b)** 5x10^{10} SF-EVs/10^{6} cells, and **(c)** 1x10^{11} SF-EVs/10^{6} cells ratio. At 1x10^{11} SF-EVs/10^{6} cells ratio Ishikawa cells were also treated with PBS. The mean fluorescence intensity was then analysed by flow cytometry (n = 3). Bars represent mean ± SD. ** = $p < 0.01$, **** = $p < 0.0001$.

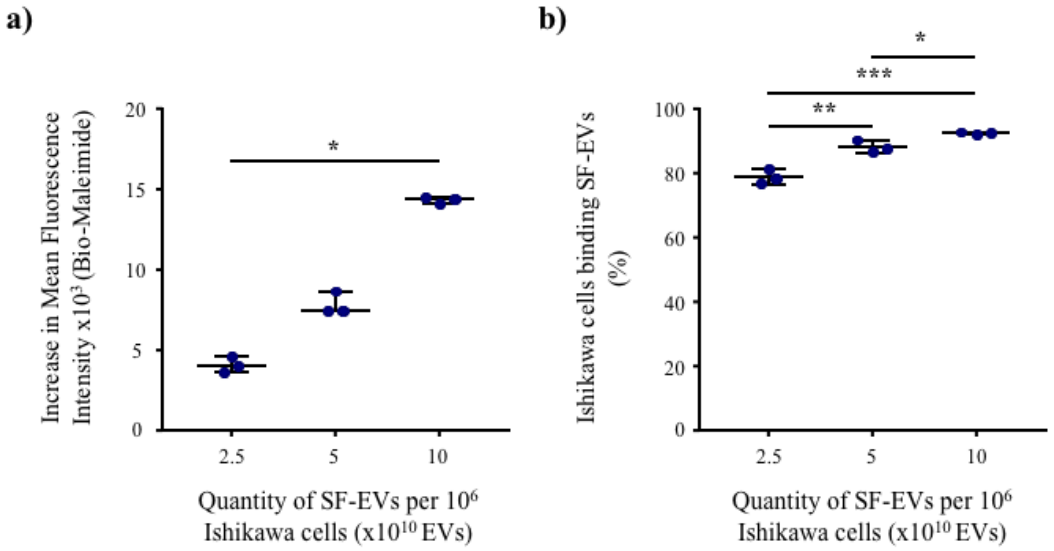


Fig 3.11 Increased SF-EV binding to Ishikawa cells with increasing EV:cell ratio.
Ishikawa cells were treated with bio-maleimide labelled SF-EVs or the negative control for 2 hrs at 2.5x10^{10}, 5x10^{10}, and 1x10^{11} SF-EVs/10^{6} cells ratio. Cells were washed and analysed by flow cytometry (n = 3). **(a)** The increase in mean fluorescence intensity and **(b)** the percentage of Ishikawa cells binding bio-maleimide labelled SF-EVs were calculated to compare SF-EV binding at different EVs/cell ratio. Bars represent **(a)** median ± IQR, or **(b)** mean ± SD. * = $p < 0.05$, ** = $p < 0.01$, *** = $p < 0.001$.

3.4.1.3 SF-EV binding to Ishikawa cells decreased with increasing exposure time to progesterone and cAMP.

To determine if SF-EVs have an altered ability to bind to EECs at different stages of the secretory phase Ishikawa cells were treated with progesterone (and cAMP). Progesterone induced the formation of domes, 3D-structures similar to pinopodes, resembling the morphological characteristics of *in vivo* endometrial epithelium receptive to embryo implantation (Fig 3.12). These cells were then used in SF-EV association studies

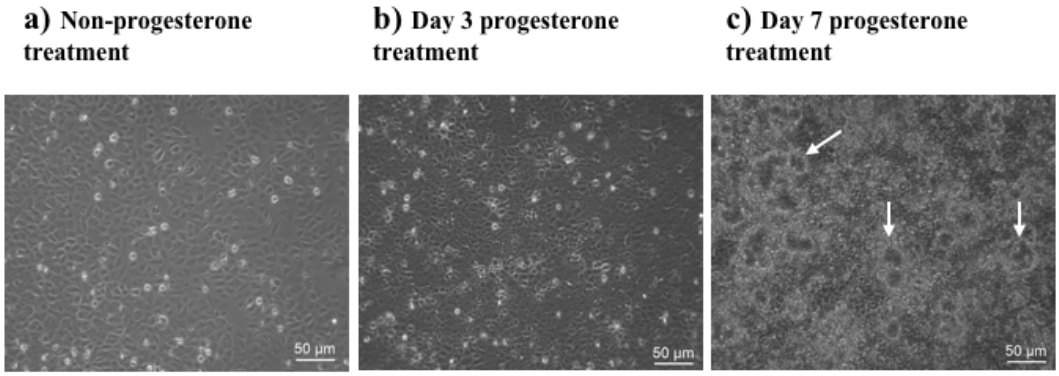


Fig 3.12 Morphology of Ishikawa cells under progesterone treatment.
Ishikawa cells were treated with **(a)** PBS, or progesterone and dibutyryl cAMP sodium salt for **(b)** 3 or **(c)** 7 days. Bright field images were then captured at 10x magnification. Scale bars = 50 µm. Arrows signal domes structures.

Untreated (day 0), and progesterone treated day 3 and day 7 Ishikawa cells were incubated with SF-EVs ($5x10^{10}$ EVs per 10^6 cells for 2 hrs) and binding was confirmed by flow cytometry (Fig 3.13). SF-EV binding (as determined by bio-maleimide MFI) was significantly increased in untreated ($p = 0.0035$), day 3 ($p = 0.0057$) and day 7 ($p = 0.0040$) progesterone treated Ishikawa cells compared to the negative control (Fig 3.14). However, the amount of binding decreased throughout treatment ($F = 0.0091$) (Fig 3.15 a). Significantly less SF-EVs bound on day 7 compared to day 0 ($p = 0.0038$), and day 3

to day 7 (p = 0.0151). While lower, no significant change was observed from day 0 to day 3 (Fig 3.15 a). In addition, the percentage of Ishikawa cells binding SF-EVs also dropped significantly during treatment (F = 0.0009), SF-EVs were approximately 85 % less able to associate to progesterone treated day 7 Ishikawa cells than native Ishikawa cells (Fig 3.15 b).

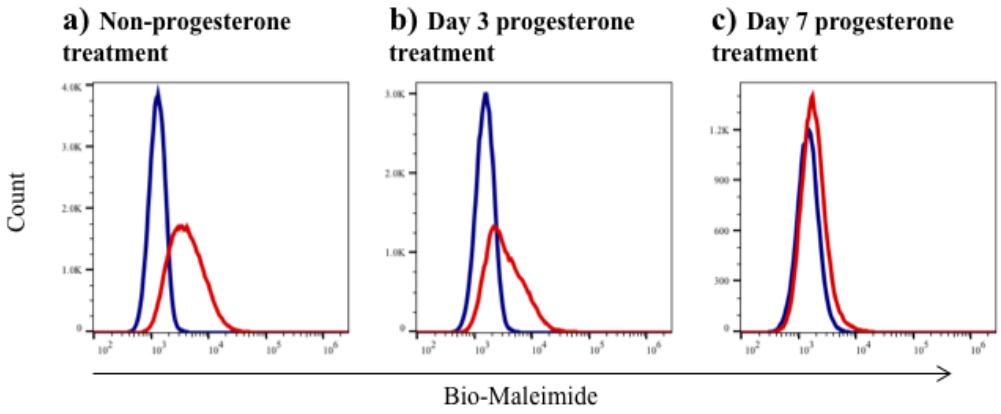


Fig 3.13 Representative flow cytometry histogram of SF-EV binding to Ishikawa cells at different days of progesterone treatment.
(a) untreated, **(b)** day 3 and **(c)** day 7 progesterone treated Ishikawa cells were incubated with bio-maleimide labelled SF-EVs (red) or the negative control (blue) for 2 hrs ($5x10^{10}$ SF-EVs/10^6 cells). Cells were then washed and analysed by flow cytometry.

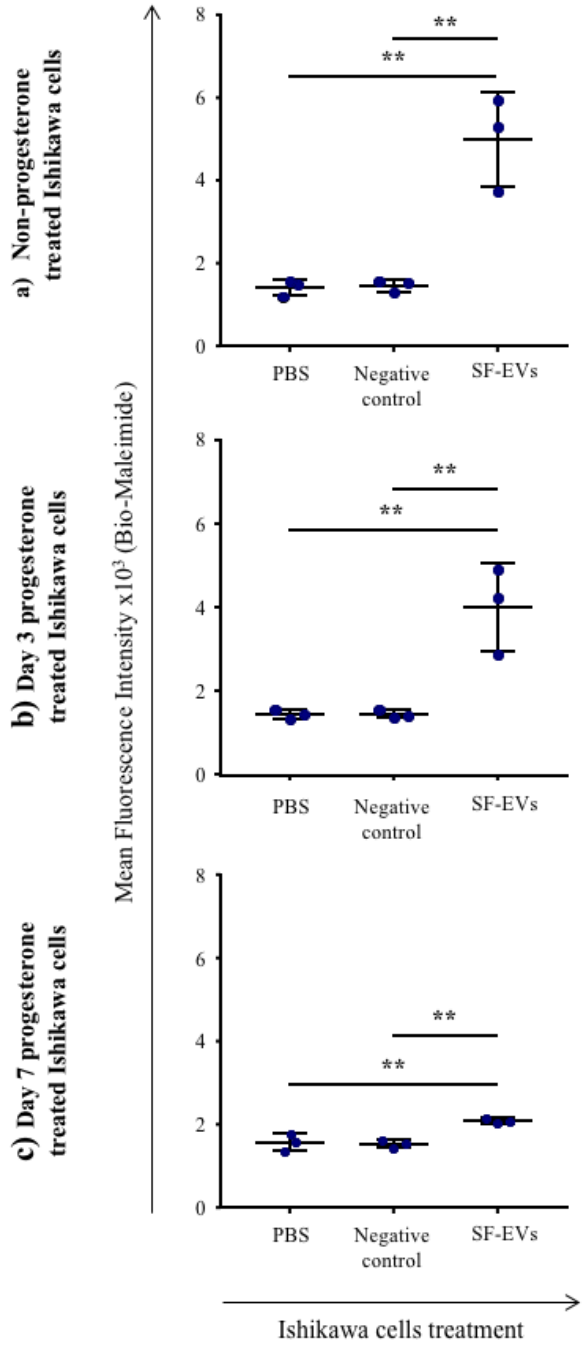


Fig 3.14 SF-EVs bind to Ishikawa cells at different days of progesterone treatment: mean fluorescence intensity.

(a) Untreated, **(b)** day 3 and **(c)** day 7 progesterone treated Ishikawa cells were incubated with bio-maleimide labelled SF-EVs ($5x10^{10}$ SF-EVs/10^6 cells), PBS or the negative control for 2 hrs. The mean fluorescence intensity was analysed by flow cytometry (n = 3). Bars represent mean ± SD. ** = $p < 0.01$.

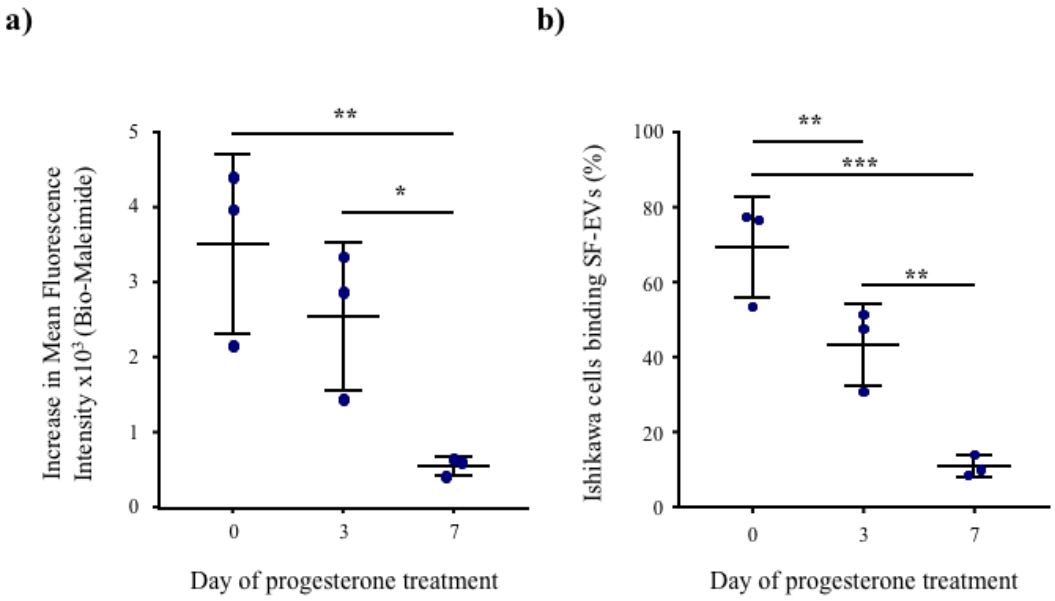
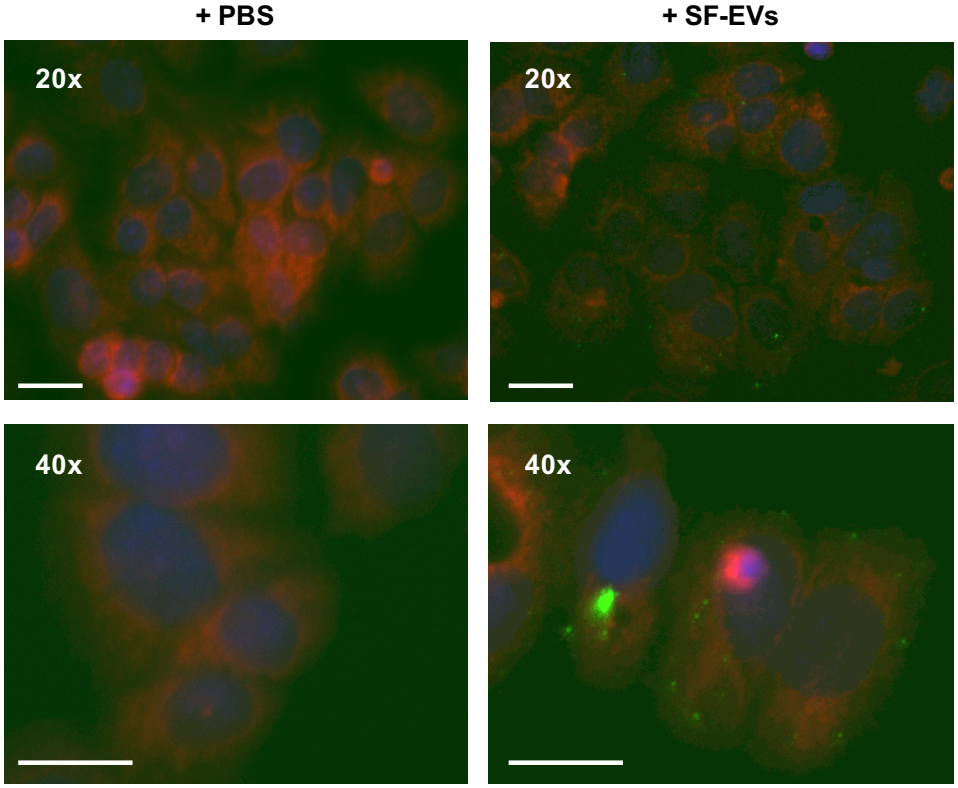


Fig 3.15 SF-EV binding to Ishikawa cells decreases when cells have been treated with progesterone.

Untreated, day 3 and day 7 progesterone treated Ishikawa cells were incubated with bio-maleimide labelled SF-EVs or the negative control for 2 hrs at $5x10^{10}$ SF-EVs/10^6 cells ratio. Cells were then washed and analysed by flow cytometry (n = 3). **(a)** The increase in mean fluorescence intensity and **(b)** the percentage of Ishikawa cells binding bio-maleimide labelled SF-EVs were calculated. Bars represent mean ± SD. * = $p < 0.05$, ** = $p < 0.01$, *** = $p < 0.001$.

SF-EV binding to untreated Ishikawa cells was confirmed by fluorescence microscopy (Fig 3.16). Images captured by the IN Cell Analyser depicted bio-maleimide labelled SF-EVs (green) bound to Ishikawa cells, and no green fluorescence signal was detected in the controls (PBS) (Fig 3.16 a). Accordingly, images taken using the Nanoimager, a super-resolution fluorescence microscope, also showed bio-maleimide (green) and CD63 Alexa 647 (red) labelled SF-EVs binding to Ishikawa cells – SF-EVs seemed to be localized around the nuclei (purple) (Fig 3.16 b), although further experiments are needed to confirm this observation.

a)



b)

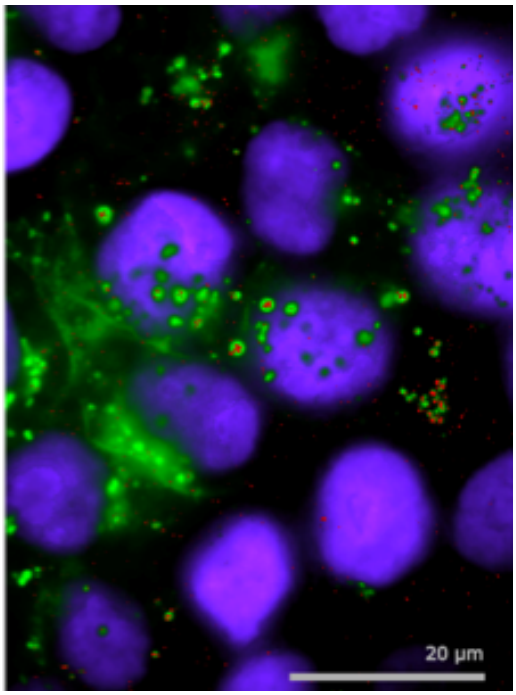


Fig 3.16 SF-EVs associated with Ishikawa cells: Fluorescence microscopy.
Ishikawa cells were incubated with bio-maleimide labelled SF-EVs or bio-maleimide and CD63 Alexa 647 labelled SF-EVs for 2 hrs ($5x10^{10}$ SF-EVs/10^6 cells). Fluorescence images were captured using **(a)** the IN Cell Analyser at 20x and 40x magnification (green = SF-EVs, red = beta actin, blue = nuclei) (n = 1), and **(b)** the Nanoimager (green = SF-EVs membrane, red = CD63 in SF-EVs, purple = nuclei) (n = 1). Scale bars = 20 µm.

3.4.2 Analysis of CREB phosphorylation at S133 and HSP60 expression in untreated Ishikawa cells upon SF-EV exposure

Previous work (Rodriguez-Caro, MSc dissertation 2015) indicated SF-EVs might decrease phosphorylation of serine 133 CREB protein and HSP60 levels in day 7 progesterone treated Ishikawa cells (see introduction 3.1.3.1). I investigated if these molecular changes were also induced by SF-EVs in untreated Ishikawa cells, which actually have higher SF-EV binding capacity. Untreated Ishikawa cells were incubated with non-treated or PK-treated SF-EV preparations # 1, # 2, and # 3; or PBS for 30 min ($5x10^{10}$SF-EVs/10^6 cells). Cells were then lysed, and CREB phosphorylation at S133 as well as HSP60 protein levels were investigated by Western blotting (n = 3).

Western blot images revealed phospho-CREB (S133), HSP60, and β-actin proteins at 43, 60, and 42 KDa, respectively (Fig 3.17 a). Protein expression levels were normalised to β-actin. Neither CREB phosphorylation at S133 (Fig 3.17 b) nor total HSP60 (Fig 3.17 c) protein levels changed after incubation with non-treated or PK-treated SF-EVs in Ishikawa cells that were not treated with progesterone.

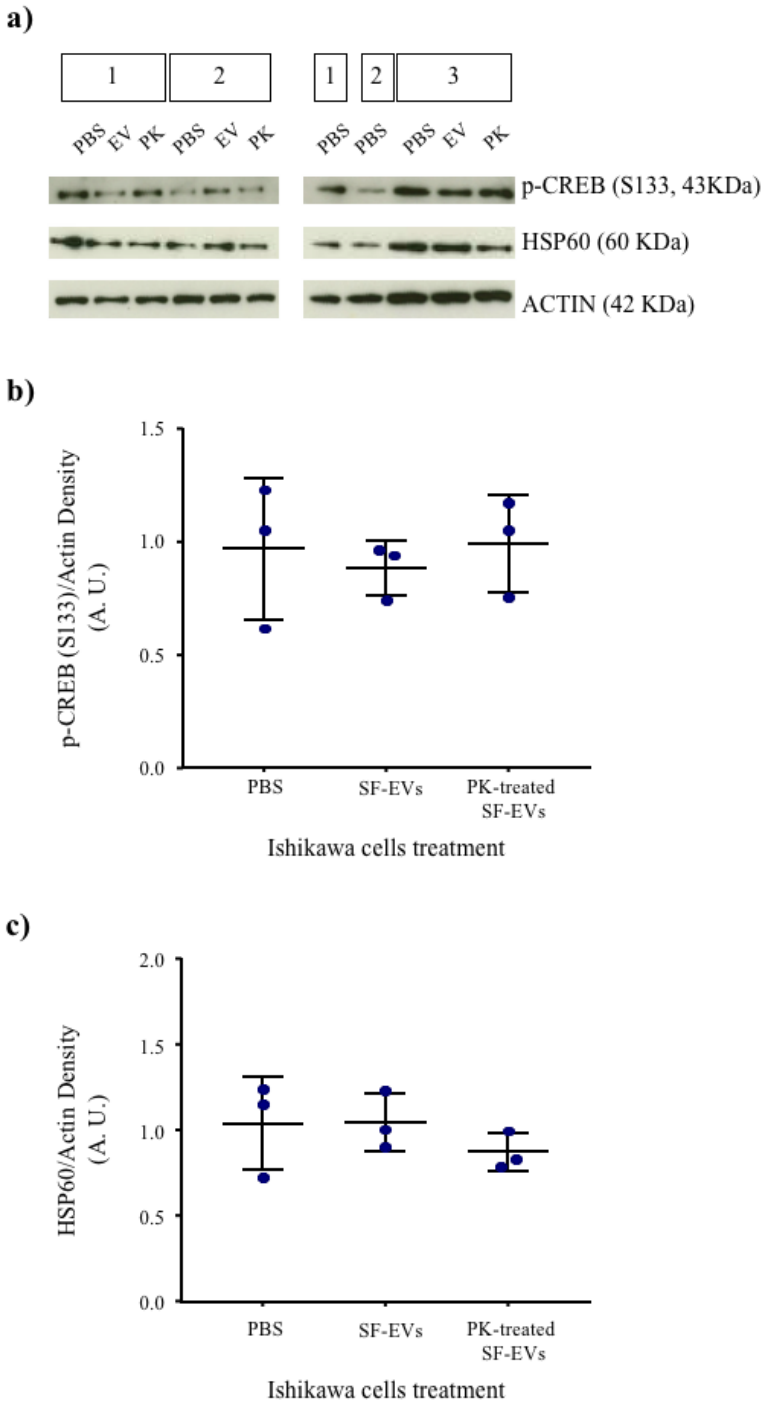
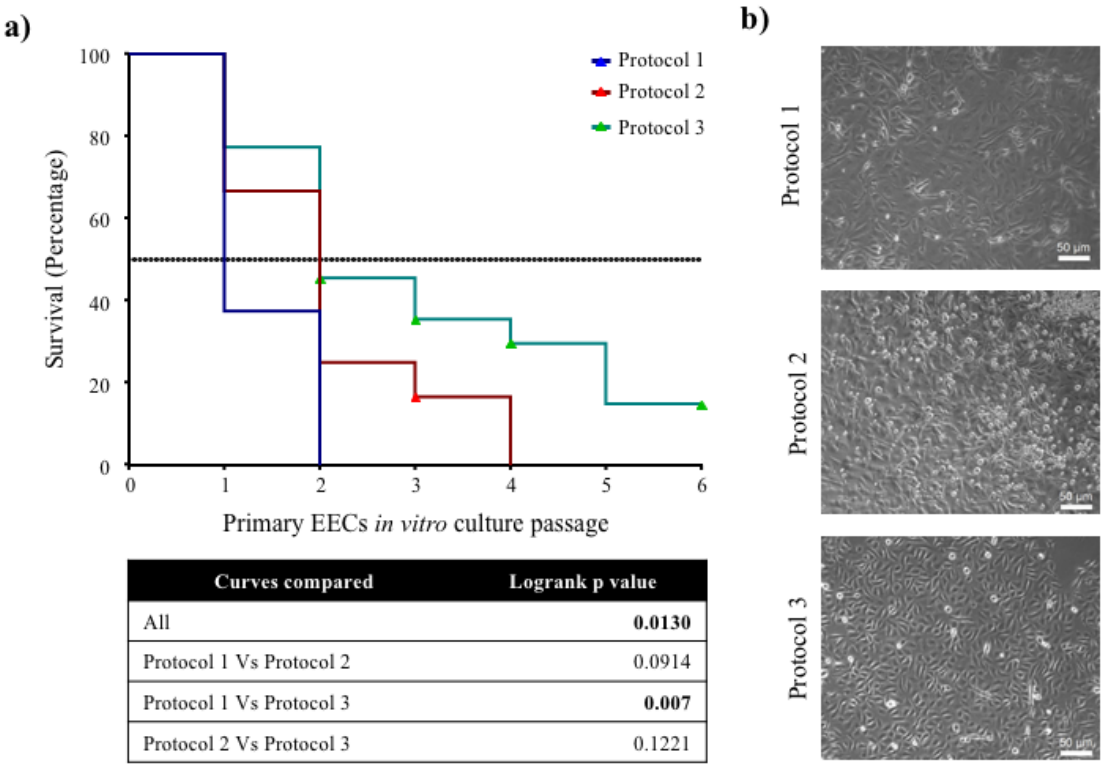


Fig 3.17 Western blotting analysis of CREB phosphorylation at S133 and HSP60 levels in untreated Ishikawa cells after SF-EV exposure.

Ishikawa cells were treated with SF-EV preparations # 1, # 2, and # 3 ($5x10^{10}$SF-EVs/10^6 cells); or PBS for 30 min, then lysed. 10 μg of protein was analysed by Western blotting, membranes were probed with antibodies towards phospho-CREB (S133), HSP60, and β-actin. Samples PBS 1 was run on both gels to allow comparison between membranes. Band density was measured by Image J. Phospho-CREB (S133) and HSP60 were normalised to β-actin. These figures show **(a)** Western blots membranes **(b)** phospho-CREB (S133) dot plot **(c)** HSP60 dot plot. Bars are mean ± SD.

3.4.3 Optimisation of isolation and *in vitro* culture of primary EECs

Having established Ishikawa cells bind SF-EVs, I hypothesized that primary luminal EECs would also bind SF-EVs. To investigate further I had to first optimize a methodology for i*n vitro* culture primary EECs, which was challenging with low survival rates, specifically after cell passage. Primary luminal EECs were isolated from endometrial biopsies following protocol 1, which was adapted from a protocol provided by Dr Karin Hellner (NDWRH, University of Oxford). Using 'protocol 1' less than 50 % of the cultures survived cell passage 1 (n = 9) (Fig 3.18 a). To improve EEC yield and survival after cell passages, two modifications were included in 'protocol 2': cells were plated on fibronectin-coated flasks and EECs were lifted with accutase. Using 'protocol 2' more than 50 % of the cultures survived cell passage 1 but survival rate fell to approximately 25 % of EECs cultures on passage 2 (n = 15) (Fig 3.18 a). EEC yields after cell passage were still low therefore to continue improving EECs culture conditions the ROCK inhibitor Y-27632 dihydrochloride was added for 24 - 48 hrs after cell passage was performed in 'protocol 3'. More than 50 % of the EECs cultured survived cell passages 1 and 2, some cultures even reached passage 5 or 6 (n = 22) (Fig 3.18 a). Statistical analysis of the survival rates achieved by the different protocols showed protocol 3 significantly increased EECs survival compared to protocol 1 ($p = 0.007$). In addition, protocol 2 tended to improved EECs survival rates when compared to protocol 1, although significance was not achieved ($p = 0.0914$) (Fig 3.18 a). Bright field microscopy showed that primary luminal EECs isolated by protocol 1, 2, and 3 exhibited epithelial-like morphology – defined as polygonal cells with regular dimensions growing in colonies – and looked healthy (Fig 3.18 b).



Curves compared	Logrank p value
All	**0.0130**
Protocol 1 Vs Protocol 2	0.0914
Protocol 1 Vs Protocol 3	**0.007**
Protocol 2 Vs Protocol 3	0.1221

Fig 3.18 Optimization of isolation and *in vitro* culture of primary luminal EECs. Primary luminal EECs were isolated from endometrial biopsies following 3 protocols. Endometrial biopsies were minced and enzymatically digested. The samples were then filtered, and EECs were obtained through differential plating. In protocol 1 EECs were lifted using trypsin (n = 9). In protocol 2 EECs were lifted using accutase and plated on fibronectin-coated flasks (n = 15). In protocol 3 EECs were treated as in protocol 2 and also incubated with a ROCK inhibitor for 24 - 48 hrs after cell passage was performed (n = 22). **(a)** Survival curve of primary luminal EECs cultured following protocol 1 (blue line), protocol 2 (red line), and protocol 3 (green line). **(b)** Representative bright field images of primary luminal EECs isolated with the different protocols. Scale bars = 50 µm.

3.4.4 Primary luminal EECs bind SF-EVs

SF-EV binding to primary luminal EECs was investigated by flow cytometry. As native Ishikawa cells bind more SF-EVs than progesterone treated cells, I decided to study SF-EV binding to the former primary luminal EECs in initial experiments.

Luminal EECs were treated with SF-EVs for 2 hrs ($5x10^{10}$ EVs/10^6 cells). Cells were then washed, lifted with accutase, labelled for the epithelial marker EpCam and analysed

by flow cytometry. A preliminary study with EECs at passage 2 (n = 1), obtained following protocol 2, showed EECs binding of SF-EVs (Fig 3.19 a). 52 % of these EECs bound SF-EVs. The low survival rates and EEC yield after cell passages of protocol 2 compromised repeating the above experiment. Therefore, SF-EV binding to primary luminal EECs was assessed on EECs on passage 0 (n = 3). These cells were plated after isolation and once the EECs were forming defined colonies, the binding experiment was performed. A shift in bio-maleimide fluorescence was also observed after SF-EVs treatment (Fig 3.19 b). Primary luminal EECs treated with SF-EVs tended to have higher bio-maleimide median fluorescence intensity (MeFI) than their negative control, although it did not reach significance ($p = 0.062$) (Fig 3.20 a). In addition, less than 10 % of the EECs bound SF-EVs (Fig 3.20 b), which was far lower than I had observed for Ishikawa cells.

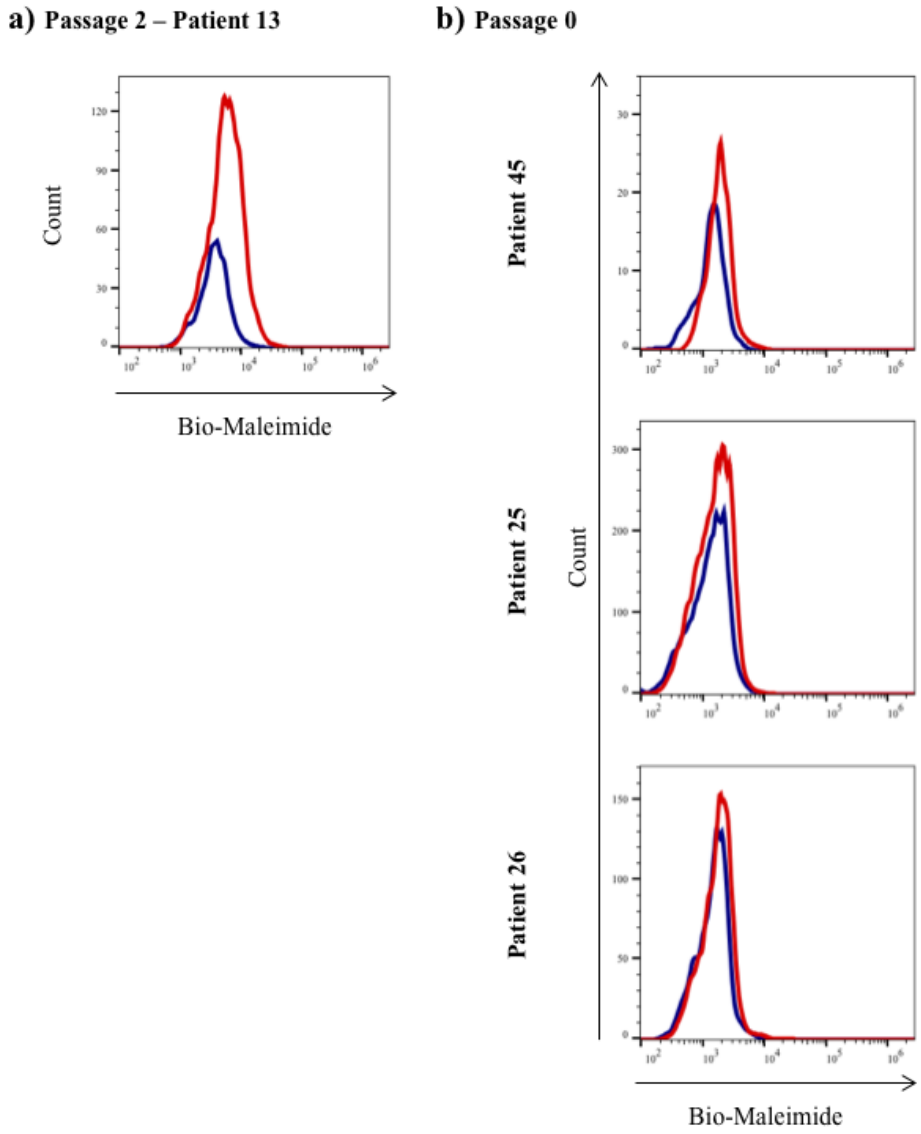


Fig 3.19 Flow cytometry histograms of SF-EV binding to primary luminal EECs isolated with protocol 2 ($5x10^{10}$ SF-EVs/10^6 cells).

Primary luminal EECs at **(a)** passage 2 (n = 1), and at **(b)** passage 0 (n = 3) were treated with bio-maleimide labelled SF-EVs (red), or the negative control (blue) for 2 hrs ($5x10^{10}$ SF-EVs/10^6 cells). Cells were then probed towards EpCam and analysed by flow cytometry (n = 3).

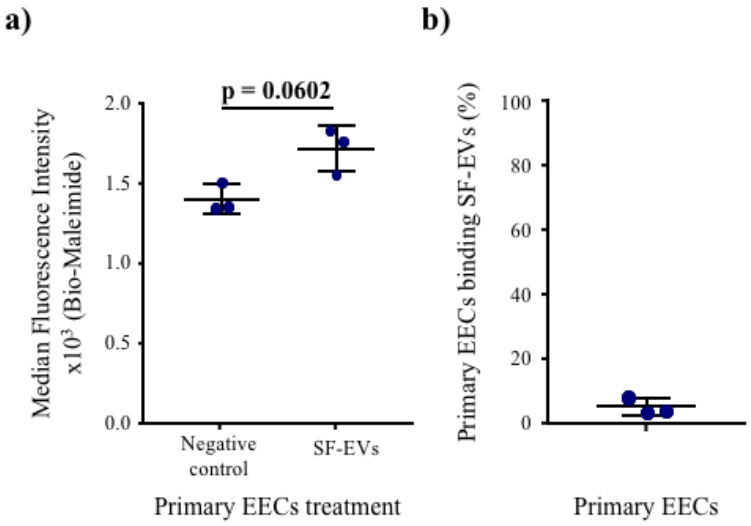


Fig 3.20 SF-EV binding to primary luminal EECs at passage 0 ($5x10^{10}$ SF-EVs/10^6 cells).

Primary luminal EECs were treated with bio-maleimide labelled SF-EVs, or the negative control for 2 hrs ($5x10^{10}$ SF-EVs/10^6 cells). Cells were then probed for EpCam expression and analysed by flow cytometry (n = 3). **(a)** Bio-maleimide median fluorescence intensity of SF-EVs, versus negative control. **(b)** Percentage of primary luminal EECs binding bio-maleimide labelled SF-EVs. Bars represent mean ± SD.

SF-EV binding to Ishikawa cells increased with increasing number of EVs per cells (see above). Therefore, a preliminary concentration-dependent study was performed to see if untreated primary luminal EECs incubated with $1x10^{11}$ EVs/10^6 cells exhibited more SF-EV binding. To perform this replicate experiment higher number of live EECs were needed (normally the yield of cells was only sufficient for control versus 1 treatment), this was achieved using protocol 3. This concentration titration was done using EECs at passage 5, which gave sufficient numbers. EECs bound more SF-EVs when incubated with $1x10^{11}$ EVs/10^6 cells ratio (91.03 %) than with $5x10^{10}$ EVs/10^6 cells ratio (75.36 %) (Fig 3.21 a). Consequently, SF-EV binding to EECs at a $1x10^{11}$ EVs/10^6 cells ratio was repeated on two additional patients. The amount of SF-EVs associated to Ishikawa cells after incubation were variable between patients (n = 3) (Fig 3.21 and 3.22 a). The percentage of primary luminal EECs binding SF-EVs was wide ranging from 0 to 91 %

(Fig 3.22 b). Analysis of this variability of SF-EV binding between samples also revealed that binding capacity tended to increase with increasing *in vitro* culture passage of primary luminal EECs (Fig 3.22 c), although the experiment data set was low. In all, SF-EVs were able to bind to primary luminal EECs, in two out of three EECs lines.

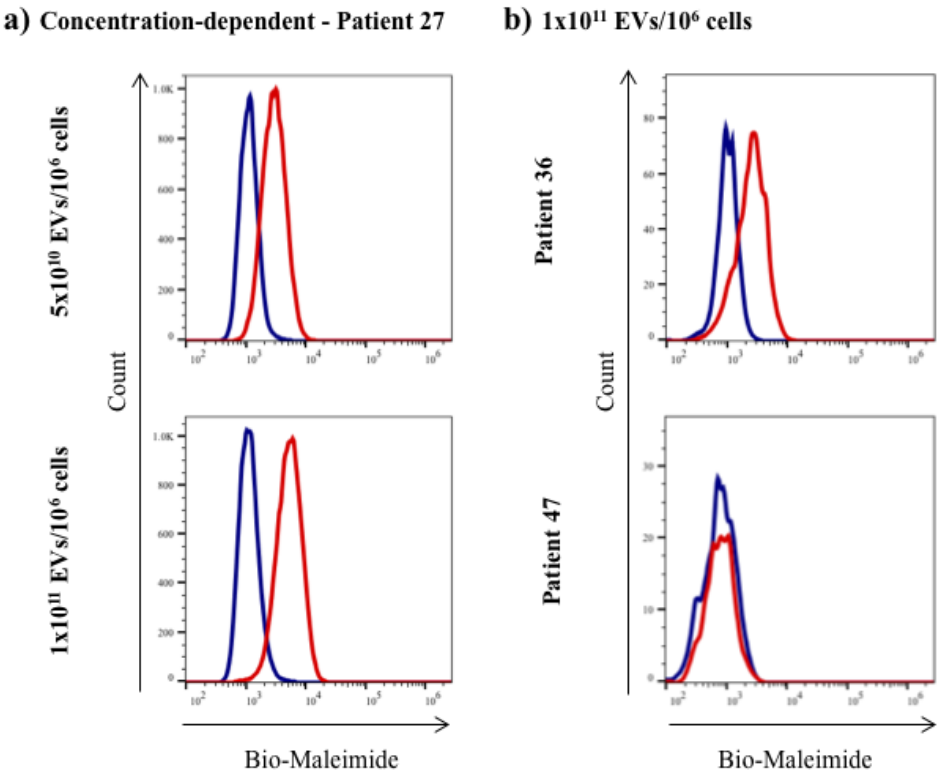


Fig 3.21 Flow cytometry histograms of SF-EV binding to primary luminal EECs isolated with protocol 3.

Primary luminal EECs were treated with bio-maleimide labelled SF-EVs (red), or the negative control (blue) for 2 hrs at $5x10^{10}$ SF-EVs/10^6 cells, or $1x10^{11}$ SF-EVs/10^6 cells ratio. Cells were then labelled with Zombie Aqua, probed towards EpCam and analysed by flow cytometry. **(a)** Concentration-dependent experiment (n = 1) **(b)** SF-EV binding to primary EECs at $1x10^{11}$ SF-EVs/10^6 cells ratio (n = 2).

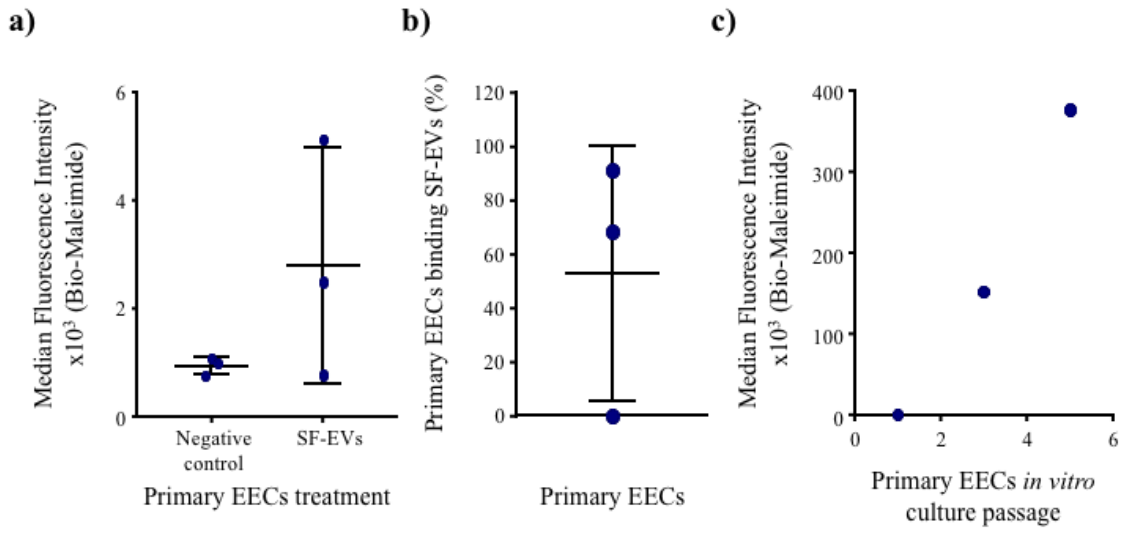


Fig 3.22 SF-EV binding to primary luminal EECs isolated with protocol 3 ($1x10^{11}$ SF-EVs/10^6 cells).

Primary luminal EECs were treated with bio-maleimide labelled SF-EVs ($1x10^{11}$ SF-EVs/10^6 cells), or the negative control for 2 hrs. Cells were then labelled with Zombie Aqua, probed towards EpCam and analysed by flow cytometry (n = 3). **(a)** Fluorescence of EECs after bio-maleimide labelled SF-EVs or negative control treatment. **(b)** Percentage of primary luminal EECs binding bio-maleimide labelled SF-EVs. **(c)** Bio-maleimide median fluorescence intensity of SF-EVs group according to the *in vitro* culture passage number of their primary EECs. Bars represent mean ± SD.

3.5 Discussion

3.5.1 EECs bind SF-EVs

In this chapter I have shown that SF-EVs bind to Ishikawa cells *in vitro* using both flow cytometry and fluorescence microscopy. Flow cytometry analysis showed Ishikawa cells bound SF-EVs within 0.5 hr of incubation, and SF-EV binding was greater with increasing incubation times and SF-EV:cell ratio. In addition, flow cytometry analysis of Ishikawa cells at different days of progesterone treatment incubated with bio-maleimide labelled SF-EVs (2 hrs; $5x10^{10}$ SF-EVs/10^6 cells) revealed that untreated Ishikawa cells had higher total SF-EV binding population of cells than day 3 and 7 progesterone treated Ishikawa cells. This suggest SF-EVs interact more with EECs before receptivity to embryo implantation is fully-achieved.

Isolated primary luminal EECs were treated with bio-maleimide labelled SF-EVs for 2 hrs to validate SF-EV binding to luminal EECs. SF-EV binding to luminal EECs on passage 2 at $5x10^{10}$ SF-EVs/10^6 cells ratio was detected by flow cytometry. Using the same conditions as before, luminal EECs on passage 0 also seemed to bind SF-EVs. In addition, a preliminary flow cytometry study showed higher SF-EV:cell ratio increased SF-EV binding to primary EECs isolated. However, no significant SF-EV binding to luminal EECs was detected after 2 hrs incubation with $1x10^{11}$ SF-EVs/10^6 cells when the sample size was increased. The latter was likely due to the dispersion of the data, in some samples the MeFI doubled, and more than 50 % of the cells bound SF-EVs. Increased SF-EV binding to luminal EECs seemed to be associated to increased time of *in vitro* culture, if this was because those luminal EECs were healthier, or because *in vitro* culture negatively affected EECs physiology remains to be elucidated.

In short, in this chapter I have shown for the first time that SF-EVs can bind to human luminal EECs – SF-EV binding to Ishikawa cells and to some primary luminal EECs was demonstrated. This is supported by a recent animal study that, to my knowledge, is the only paper in the literature studying SF-EVs effect on EECs. This group showed that EVs isolated from boar seminal fluid upregulated and downregulated 70 and 114 genes respectively, in primary isolated boar EECs (Bai *et al.*, 2018). These EVs downregulated genes involved in metabolic pathways and steroid biosynthesis, and upregulated genes related to chemokine signalling pathway, immune response, and inflammatory response in boar EECs (Bai *et al.*, 2018). In addition, previous studies have shown that EECs interact with other types of EVs. Giacomini *et al*. showed binding of Vybrant DiO carbocyanine labelled-embryo EVs to primary human EECs by fluorescence microscopy (Giacomini *et al.*, 2017). In addition, EVs from bovine uterine fluid during the implantation window were shown to upregulate mRNA levels in bovine isolated primary EECs (Kusama *et al.*, 2018).

3.5.2 Increased survival rates of *in vitro* culture primary luminal EECs

In this chapter, I optimised a protocol that achieved and maintained higher yields of primary luminal EECs *in vitro* to increase cell numbers for future functional experiments. In this protocol (protocol 3) luminal EECs were cultured on fibronectin-coated tissue culture flasks, lifted with accutase, and cultured in epithelial cell culture media with ROCK inhibitor for 24 - 48 hrs after passage. Although higher EECs yield were achieved after multiple cell passages, reproducibility was still erratic and the binding studies suggested cell physiology might be dramatically altered in long-term *in vitro* cultures, therefore it was unviable to use *in vitro* cultured EECs to assess the functional effect of SF-EVs on this cell type. Using high-sensitive techniques like RNA arrays to analyse the

effect of SF-EVs on luminal EECs was also unviable because isolated luminal EECs are not pure, they are mixed with remaining stromal cells and immune cells making impossible to define which cell type generates a specific response. Therefore, SF-EV functional effect on primary luminal EECs was not investigated.

In vitro passage of endometrial epithelial cells has been reported in other papers (Zhang *et al.*, 2012, Chen *et al.*, 2016b), but these EECs were retained on the strainer after filtration, which are mainly glandular EECs (K. Hellner, personal communication, April 2016). Nevertheless, another protocol suggested luminal EECs also remain on the strainer (Chen and Roan, 2015). Future work should determine in which fractions the luminal EECs are mainly secreted. Interestingly, in our lab we observed better preparations from glandular EECs fractions (retained on the filter) than from luminal EECs (eluted through filter as single cells). EECs from the luminal EECs fractions have lower yields than glandular preparations reducing cell-cell contacts that are strictly necessary for establishment of cell polarity and culture. In addition, trypsin was shown to induce depolarization of EECs in mice and a human EEC cell line (Ruan *et al.*, 2012, Sun *et al.*, 2014). It might be possible that *in vitro* culture is triggering excessive depolarization of primary luminal EECs, that are already primed to depolarise, leading to poor survival rates and variable cell fitness after cell passage. This feature might be observed in luminal but not in glandular EECs because loss of polarity seems to be specific of luminal EECs (Whitby et al., 2018). Future works should focus on developing reproducible protocols different for the generation of pure human luminal, and glandular EEC *in vitro* cultures.

3.5.3 SF-EVs induce differential changes in CREB phosphorylation at S133 in Ishikawa cells during the implantation window

Having established that SF-EVs bind to EECs, I next sought to investigate if they had any effect on Ishikawa cells. A pilot molecular study during my MSc showed SF-EVs induced dephosphorylation of CREB at S133 Ishikawa cells treated for 7 days with progesterone (see introduction 3.1.3.1; Rodriguez-Caro, MSc dissertation 2015). Interestingly, CREB phosphorylation at S133 remained unchanged after Ishikawa cells that had not been progesterone treated were incubated with SF-EVs despite higher binding capacity. This suggests SF-EVs only affect CREB activation on the luminal EECs receptive to embryo implantation.

CREB S133 phosphorylation results in dimerization of this transcription factor with the co-activator "CREB-binding protein" which enables binding to cAMP-responsive elements in gene sequences (Sassone-Corsi, 1998). CREB plays an important role during the implantation window and studies show it regulates EECs signalling (Ruan *et al.*, 2012, Sun *et al.*, 2014). For instance, CREB is known to bind to the cyclooxygenase-2 (COX2) promoter and upregulate COX2 expression in EECs (Tsatsanis *et al.*, 2006, Ruan *et al.*, 2012, Sun *et al.*, 2014). In detailed (Fig 3.23), murine studies and work in a human epithelial cell line demonstrated that activation epithelial Na^+ channel on EECs – which is upregulated on EECs at the implantation window in mice – have increased Ca^{2+} levels that induce phosphorylation of CREB at S133, which upregulates COX2 expression and downregulates miR-101 & miR-199-a-3p expression, which directly inhibit COX2 transcription (Ruan *et al.*, 2012, Sun *et al.*, 2014). CREB-induced COX2 synthesises prostaglandin E2 (PGE2), which is secreted to the stromal cells throughout the multi-drug resistance protein 4 in the basal membrane and also stimulates endometrial stromal cells

decidualisation (Frank *et al.*, 1994, Ruan *et al.*, 2012, Sun *et al.*, 2014, Chen *et al.*, 2017), a process essential for embryo implantation (see chapter 4). SF-EVs specific dephosphorylation of CREB S133 in day 7 progesterone treated Ishikawa cells but not in untreated ones suggests SF-EVs might assist to the optimal timing of the implantation window (Fig 3.23).

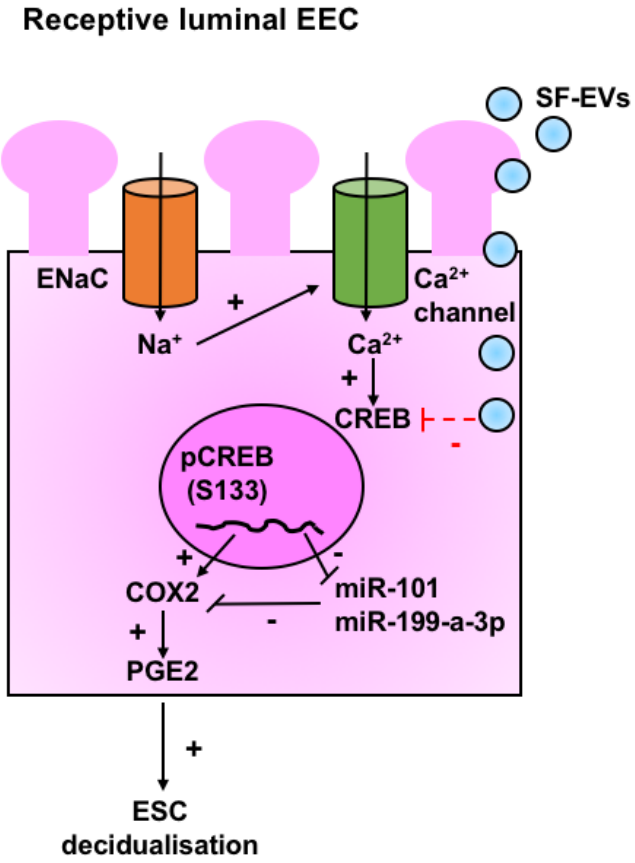


Fig 3.23 SF-EV regulation of CREB signalling in luminal EECs receptive to embryo implantation.
Activation of epithelial Na^+ channels (ENaC) during endometrial receptivity to embryo implantation increases intracellular $Ca2^+$ levels that phosphorylate cAMP response element binding (CREB) protein at S133. Active CREB translocates to the nucleus stimulating cyclooxygenase-2 (COX2) translation and inhibiting miR-101/miR-199-a-3p (COX2 inhibitors). COX2 then synthesises prostaglandin E2 (PGE2) that promotes endometrial stromal cell (ESC) decidualisation. SF-EVs inhibit CREB activation by S133 phosphorylation only in EECs receptive to embryo implantation.

4 The role of SF-EVs on endometrial stromal cell (ESC) decidualisation

4.1 Introduction

4.1.1 Decidualisation of ESCs

ESC decidualisation is a process by which cells are reprogrammed to be able to support implantation and embryo development (Dunn *et al.*, 2003, Gellersen *et al.*, 2007, Gellersen and Brosens, 2014, Zhu *et al.*, 2014, Vinketova *et al.*, 2016); in humans ESC decidualisation occurs in response to increased progesterone levels after ovulation. It is characterised by the differentiation of ESCs from fibroblast-like cells into enlarged round secretory cells. In addition, decidualised ESCs (dESCs) also show expanded Golgi complexes and rough endoplasmic reticulum, more ribosomes, lysosomes and mitochondria, and increased numbers of lipids and glycogen droplets in the cytoplasm (Wynn, 1974, Tabanelli *et al.*, 1992, Gellersen *et al.*, 2007, Kara *et al.*, 2007, Gellersen and Brosens, 2014, Zhu *et al.*, 2014).

During decidualisation ESCs change their genetic expression profile to promote diverse processes including extracellular matrix reorganisation, cytoskeleton rearrangement and differentiation (Zhu *et al.*, 2014). Moreover, dESCs are highly secretory and their secretory products are used as markers of decidualisation. Prolactin and Insulin like Growth Factor Binding Protein 1 (IGFBP-1) are widely used as biochemical markers of ESC decidualisation (Dunn *et al.*, 2003, Gellersen *et al.*, 2007, Gellersen and Brosens, 2014, Zhu *et al.*, 2014). Prolactin is synthesised by the endometrium at the beginning of decidualisation, and if implantation occurs levels continue to rise until 20 - 25 weeks of

pregnancy, afterwards they decrease toward term (Ben-Jonathan *et al.*, 1996). Similarly, the protein levels of IGFBP-1, previously known as placental protein 2, also increase after the onset of ESC decidualisation. After embryo implantation, IGFBP-1 levels rise until reaching a plateau from 12 weeks of gestation until term (Rutanen *et al.*, 1985, Wang *et al.*, 1991, Fowler *et al.*, 2000).

ESC decidualisation starts in proximity to the spiral arteries and the glands, then spreads throughout the endometrium (Wynn, 1974, Gellersen *et al.*, 2007). Progesterone alone is a weak inducer of decidualisation and no morphological changes in the superficial layer of the endometrium are observed until approximately 10 days after the ovulation induced surge in progesterone *in vivo* (de Ziegler *et al.*, 1998, Gellersen and Brosens, 2003, Gellersen *et al.*, 2007). Additional signals are required; *in vitro* studies showed that the cyclic adenosine monophosphate (cAMP) pathway (Fig 4.1) is the compulsory process to initiate decidualisation and cAMP sensitises ESCs to progesterone induced decidualisation – this is also mediated by cAMP (Tang *et al.*, 1993, Gellersen and Brosens, 2003, Gellersen *et al.*, 2007). Accordingly, endometrial biopsies from the secretory phase showed higher levels of adenylyl cyclase activity and cAMP than biopsies from the proliferative endometrium (Bergamini *et al.*, 1985, Tanaka *et al.*, 1993). In addition, *in vitro* treatment of ESCs with cAMP induces the expression of prolactin and IGFBP-1 within hours, although this phenotype cannot be maintained without progesterone or a progesterone analogue (Gellersen and Brosens, 2003, Gellersen *et al.*, 2007).

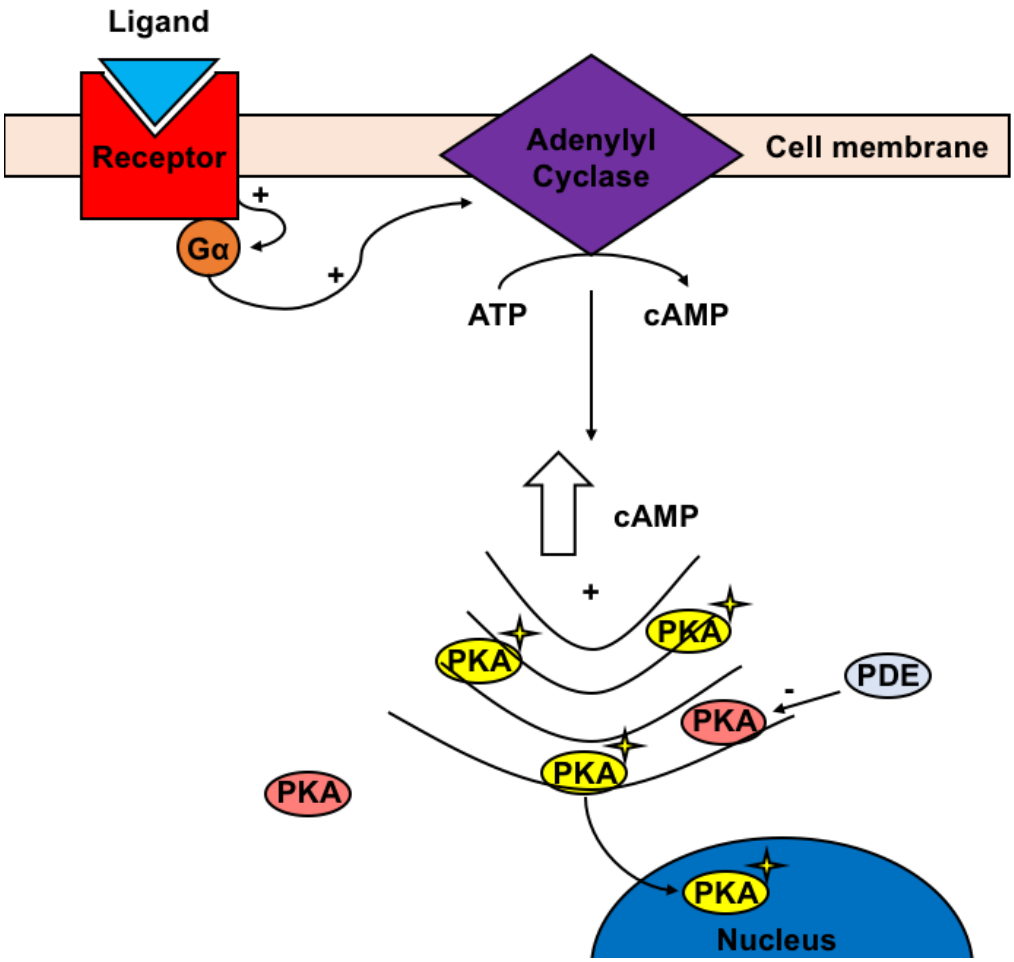


Fig 4.1 cAMP signalling pathway.
The ligand binds to the receptor activating the Gα subunit. Gα subunit stimulates adenylyl cyclase activity that transforms ATP into cyclic AMP (cAMP), increasing cAMP levels. This cAMP is produced in waves creating a concentration gradient. The cAMP binds and activate protein kinase A (PKA), which can phosphorylate and regulate the activity of multiple molecules in the cytoplasm or in the nucleus (e.g.: transcription factors). High levels of cAMP are required to stimulate PKA activity because each individual PKA needs 2 cAMP molecules to be activated. PKA activation is regulated by the concentration levels of cAMP and phosphodiesterases (PDE), which can hydrolase cAMP. Active PKA = yellow, inactive PKA = pink.

During the implantation window dESCs secrete factors that further alter the structure of the endometrium in preparation for implantation. dESCs regulate the remodelling of the extracellular matrix (ECM); for instance, they secrete tissue inhibitors of metalloproteases (TIMP), such as TIMP-1, TIMP-2, and TIMP-3, that inhibit ECM degradation by metalloproteases (MMPs) (Zhang and Salamonsen, 1997). They also

produce MMP-2 and MMP-9 to drive ECM remodelling (Rawdanowicz *et al.*, 1994, Chou *et al.*, 2003). In addition, dESCs secrete TGF-β which is involved in maternal tolerance (Sanjabi *et al.*, 2017) and control of trophoblast invasion (Graham *et al.*, 1992, Irving and Lala, 1995, Stoikos *et al.*, 2008), and decorin, a proteoglycan of the ECM that stores TGF-β and also regulates trophoblast invasion (Xu *et al.*, 2002). dESCs also contribute to remodelling of the uterine spiral arteries secreting VEGF and tissue factor (Zhu *et al.*, 2014).

4.1.1.1 The role of dESCs in endometrial immune modulation

dESCs also regulate immunity summarised in Fig 4.2 (Gellersen *et al.*, 2007, Gellersen and Brosens, 2014, Zhu *et al.*, 2014, Vinketova *et al.*, 2016). Uterine Natural Killer (uNK) cells ($CD16^{-}CD56^{bright}CD9^{+}CD103^{+}KIR^{+}$) have reduced cytotoxic activity and high secretory phenotype compared to the majority of circulating peripheral blood NK cells which tend to have a $CD56^{dim}$ phenotype. dESCs secrete TGFβ-1 that increases NK cell expression of CD9, CD103 and KIR[19], and downregulates NK cell expression of CD16 (Keskin *et al.*, 2007). In addition, dESCs secrete IL-15; a cytokine that stimulates proliferation of uterine $CD56^{bright}$ NK cells (Okada *et al.*, 2000, Verma *et al.*, 2000).

dESCs also regulate endometrial T cells and dendritic cells. For example, ESCs secrete galectin-1 that inhibits T cells proliferation and secretion of proinflammatory cytokines (von Wolff *et al.*, 2005). A study showed mice with galectin-1 deficiency had high rates of fetal loss in allogeneic matings (Blois *et al.*, 2007). Treatment of galectin-1 deficient mice with recombinant galectin-1 restored pregnancy rates inducing tolerogenic dendritic

[19] KIR: Killer-cell immunoglobulin-like receptor

cells and T regulatory cells (Blois *et al.*, 2007). In addition, dESCs express HLA[20]-DR through which they stimulate $CD4^+$ T cell cytokine secretion (Laguens *et al.*, 1990, Nagamatsu *et al.*, 2009). dESCs also express B7-H1[21] and B7-DC[22] which are co-stimulatory molecules typically expressed by antigen presenting cells (APCs), and regulates HLA-DR pathway. In fact, dESCs B7-H1 and B7-DC molecules suppress $CD4^+$ T cell secretion of Interferon γ (IFNγ), Tumor Necrosis Factor α (TNFα), Interleukin (IL)-2 and IL-10. Therefore, evidence suggests dESCs act as non-conventional APCs (Nagamatsu *et al.*, 2009). Expression of indoleamine 2,3-dioxygenase (IDO) has also been described in human dESCs (Ligam *et al.*, 2005). This is involved in immune tolerance as it regulates T cell responses (Mellor *et al.*, 2002), and IDO inhibition in mice leads to T cells induced rejection of semiallogenic fetuses (Munn *et al.*, 1998).

[20] HLA: Human Leukocyte Antigen
[21] B7-H1: Programmed death ligand 1
[22] B7-DC: Programmed death ligand 2

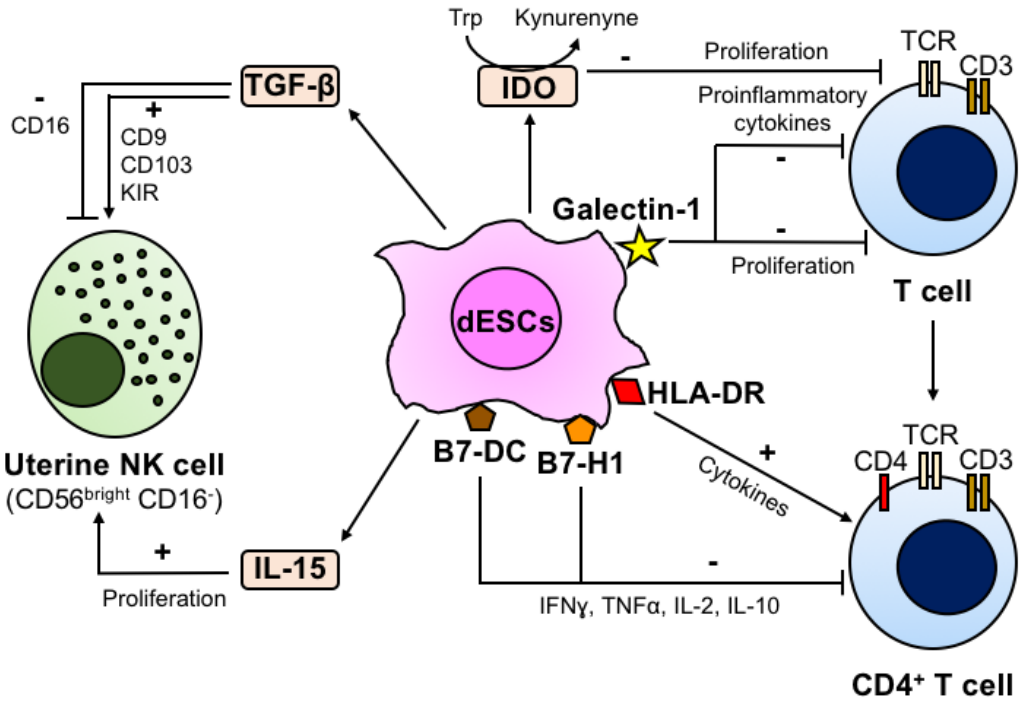


Fig 4.2 Immunoregulation by decidualised ESCs (dESCs).
dESCs regulate uterine natural killer (uNK) cells and endometrial T cells. dESCs secrete TGFβ-1 that supresses expression of CD16 by uNK cells and enhances CD9, CD103 and KIR expression by these same cells. In addition, dESCs secrete IL-15 promoting uNK cell proliferation. dESCs also produce indoleamine 2,3-dioxygenase (IDO) and galectin-1 that inhibit T cell proliferation, the latter also inhibits secretion of proinflammatory cytokines. IDO catabolyses tryptophan (Trp) producing kynurenine. dESCs express HLA-DR acting as non-conventional antigen presenting cells and stimulating cytokine secretion by endometrial $CD4^+$ T cells. In addition, they also express B7-DC and B7-H1 that inhibit IFNγ, TNFα, IL-2 and IL-10 secretion by endometrial $CD4^+$ T cells.

The immunomodulatory properties of dESCs were demonstrated in a human clinical trial for graft-versus-host disease (GVHD) (Ringden *et al.*, 2013). This pilot study showed that dESCs effectively suppress immune cell proliferation *in vitro*, as observed by mixed lymphocyte reactions, and that intravenous administration of dESCs could completely or partially prevent GVDH (Ringden *et al.*, 2013). Another trial in 2018 showed dESCs was a promising treatment against severe acute GVHD. They observed a one-year survival rate of 76 % and 73 % after dESCs treatment of severe acute GVHD and steroid-refractory acute GVHD patients respectively (Ringden *et al.*, 2018). The sample size on

these studies was small and there were no placebo groups, therefore more extensive studies need to be done to confirm these outcomes.

4.1.1.2 Defective ESC decidualisation and subfertility

Inadequate ESC decidualisation is thought to be involved in numerous reproductive pathologies associated with subfertility. For instance, defective ESC decidualisation, characterised by low prolactin and IGFBP-1 protein and mRNA levels, was observed in ESCs from patients with endometriosis (Klemmt *et al.*, 2006, Aghajanova *et al.*, 2009b). Attenuated prolactin mRNA was also observed in ESCs from patients with recurrent pregnancy loss (Salker *et al.*, 2010).

4.1.2 The role of seminal fluid on ESC decidualisation

Seminal fluid has been shown to enhance ESC decidualisation. Doyle *et al*. 2012 showed *in vitro* that extended exposure (27 days) of dESC to seminal fluid enhanced prolactin and IGFBP-1 mRNA and secreted protein levels (Doyle *et al.*, 2012). In addition, seminal fluid contains soluble proteins known to be involved in ESC decidualisation, such as TGF-β1 (Chang *et al.*, 2008), relaxin (Lane *et al.*, 1994), glycoprotein hormone-free α subunit (Moy *et al.*, 1996), and PGE2 (Frank *et al.*, 1994). Relaxin and PGE2 stimulate cAMP signalling (Dunn *et al.*, 2003). Moreover, ESC gene expression of CCL7[23], FGF2, IL-8, IL-6 and VEGF increased after *in vitro* treatment of ESCs with 1 % seminal fluid (Chen *et al.*, 2014).

To date there is no published literature regarding the role of SF-EVs in ESC decidualisation.

[23] CCL7: C-C Motif Chemokine Ligand 7

4.2 Aims of the chapter

I hypothesize that SF-EVs assist ESC decidualisation. The aims of this chapter are:

1) To investigate if SF-EVs bind to ESCs
2) To establish if SF-EVs induce ESC decidualisation
3) To investigate the molecular pathways involved in SF-EV induction of ESC decidualisation

4.3 Methods

4.3.1 Subject Recruitment

Ethical approval for the endometrial biopsies were obtained from the Oxford South Central Regional Ethics Committee - #08/H0606/94. All patients gave written informed consent. Endometrial biopsies were obtained from patients at Oxford Fertility (n = 2) and the John Radcliffe Hospital, Oxford (n = 3). Patients characteristics are described in appendix 4.

4.3.2 Isolation and culture of ESCs

Endometrial biopsies were cut into 1 mm^3 fragments and incubated with 1X liberase ^{TM} (Roche, UK) and 50,000 U/ml DNAse (Sigma-Aldrich, USA) for 30 min at 37°C. After incubation, the digest was passed through consecutive 70 μm and 40 μm filters (Corning, USA) to remove aggregates, and centrifuged at 300 x g for 3 min. ESCs were cultured in DMEM-F12, supplemented with 10 % FCS, penicillin (100 IU/ml), streptomycin (100 μg/ml) and 2 mM L-glutamine. Cells were cultured at 37°C, 20 % O_2 and 5 % CO_2. Culture media was changed every 2 days and cell passage performed when ~ 80 % confluence was reached.

ESC decidualisation was induced by supplementing the growth media with 0.5 mM dibutyryl cyclic-AMP sodium salt and 1 μM progesterone. Decidualisation media was changed every 2 days and the treatment lasted for 7 days.

4.3.3 SF-EV isolation and purification

SF-EVs were isolated and purified as described in chapter 2.

4.3.4 Binding studies

Fluorescent SF-EVs were generated by labelling EVs with bio-maleimide, as described in chapter 2. $2.5x10^5$ ESCs were plated per well in 12-wells plates (Nunc), one well was used for experiment to quantify the number of cells on different days of decidualisation. 16 hrs later ESCs were incubated with the bio-maleimide labelled SF-EVs, the negative control or PBS for 2 hrs at 37°C ($5x10^{10}$ SF-EVs/10^6 cells) The incubation conditions were decided upon using the previous optimisation of SF-EV binding to Ishikawa cells (chapter 3).

For the negative control, PBS and 2 μM of bio-maleimide were incubated and purified with Exo-spin™ columns to confirm removal of the excess of dye in binding experiments.

4.3.4.1 Flow cytometry

Non-decidualised (day 0), day 3 and day 7 decidualised ESCs were treated with bio-maleimide labelled SF-EV preparation # 1, the negative control or PBS (n = 3). After incubation, cells were washed twice with PBS and detached with accutase (Sigma-Aldrich, USA). Cells were centrifuged for 5 sec at 13,000 x g. Pellets were resuspended in 500 μl of 2 % FCS/PBS and analysed using a BD LSRII flow cytometer. The results were analysed using FlowJo software version 10.4.2. MFI was measured and the increase calculated subtracting the MFI of the negative control group to the SF-EVs group. In addition, the percentage of cells binding SF-EVs was determined subtracting a 5 % gate from the negative control.

4.3.4.2 Fluorescence microscopy

Non-decidualised and day 7 decidualised ESCs were treated with bio-maleimide labelled SF-EV preparation # 1 or PBS (n = 1). Cells were then washed once with PBS, fixed with 100 % methanol (Sigma-Aldrich, USA) for 10 min at - 20°C, washed, and permeabilised with 0.5 % Triton X-100 (Sigma-Aldrich, USA) for 15 min at RT. Afterwards, cells were washed with PBS and incubated with antibodies towards β-actin for 2 hrs at RT (Table 4.1) in permeabilization buffer containing FCS (Thermo Fisher, USA). Cells were washed with PBS and incubated with polyclonal antibodies towards mouse immunoglobulins (Alexa Fluor® 594 nm) for 40 min at RT and with DAPI for 5 min at RT (Table 4.1). 20x and 40x fluorescence images were captured using IN Cell 1,000 Analyser (GE Healthcare Life sciences, UK)

Table 4.1 Fluorescence dye, primary and secondary antibodies used for flow cytometry and fluorescence microscopy studies.

Antibody/dye	Concentration/ dilution	Target	Source antibody	Clone	Company
β ACTIN	1:500	β actin	Mouse	AC-15	Abcam®, UK
anti-Mouse (Alexa Fluor® 594nm)	1:200	Mouse Ig	Donkey	Polyclonal	Molecular probes, USA
DAPI	1:1,000	Nuclei			Molecular probes, USA

4.3.5 Functional studies

$2.5x10^5$ ESCs were plated per well in 12-wells plates (Nunc). After 16 hrs cells were treated with PBS (control group) or SF-EV preparation # 1 (single and multiple SF-EV exposure groups) for 2 hrs at 37°C ($5x10^{10}$ SF-EVs/10^6 cells). After incubation, cells were washed with PBS and decidualisation media was added. On day 3 cells were treated again

with PBS (control and single SF-EV exposure groups) or SF-EV preparation # 1 (multiple SF-EV exposure group) for 2 hrs at 37°C ($5x10^{10}$ SF-EVs/10^6 cells). Non-treated wells were used to determine the number of cells present and calculate the amount of SF-EVs to add. After incubation, cells were washed again with PBS and incubated with new decidualisation media.

4.3.5.1 Prolactin and IGFBP-1 ELISAs

Cell supernatants were collected for 7 days and the concentrations of prolactin and IGFBP-1 were determined by human prolactin ELISA and human IGFBP-1 ELISA kits (R&D systems, UK) following the manufacturer's instructions. Briefly, a 96-well microplate (Nunc) was coated with the capture antibody in PBS overnight at RT. The following day the plate was washed with PBS-T three times and blocked with 1 % bovine serum albumin (BSA) in PBS for a minimum of 1 hr at RT. The plate was then washed again three times with PBS-T and the samples and standards added for a 2 hrs incubation at RT. After the incubation the plate was washed with PBS-T as before and incubated with the detection antibody for 2 hrs at RT. After washing with PBS-T three times, the plates were then incubated for 20 min with Streptavidin-HRP at RT in the dark. Afterwards, the plate was washed again, and 3,3',5,5'-Tetramethylbenzidine substrate (Biolegend, USA) was added for 20 min in the dark at RT to develop the color, then 2 N H_2SO_4 was added to stop the reaction and the optical density of each well was measured at 450 nm using the FLUOstar OPTIMA microplate reader (BMG LABTECH, UK). Prolactin and IGFBP-1 measures were performed in triplicate and duplicate respectively. The results were normalised between plates.

4.3.5.2 Bright field microscopy

Bright Field Images of ESCs at 10x amplification were captured as described in chapter 3. Non-decidualised and decidualised ESCs were then counted in triplicate on day 7 of decidualisation using Image J software version 1.43v (National Institutes of Health, USA), and the percentages of dESCs were calculated.

4.3.6 Molecular studies on ESC activation

4.3.6.1 Human phospho-kinase array

10^6 ESCs were treated with $5x10^{10}$ SF-EVs or PBS for 30 min (day 0 of decidualisation) or for 2 hrs (day 0 of decidualisation) and 30 min (day 3 of decidualisation) at 37°C. ESCs were then washed with PBS and incubated with lysis buffer for 30 min at 4°C. Samples were centrifuged at 14,000 x g for 5 min and supernatants transferred into clean tubes. Supernatant protein concentrations were determined using a BCA protein assay (Thermo Scientific, USA). Afterwards, a human phospho-kinase array (Proteome Profiler™, R&D systems, USA) was performed following the manufacturer's instructions.

Briefly, the array membranes were incubated with a blocking buffer for 1 hr at RT, then 300 µg of cell lysate in a total volume of 2 mL was added to each membrane and incubated overnight at 4°C. Next day the membranes were washed 3 times for 10 min at RT and incubated with the detection antibody cocktails for 2 hrs at RT. The membranes were then washed 3 times for 10 min at RT and incubated in 1 mL of 1:2000 diluted Streptavidin-HRP for 30 min at RT. Membrane were washed 3 times for 10 min at RT and then the arrays were developed using Chemi Reagent Mix (Proteome Profiler™, R&D systems, USA) and Amersham Hyperfilm™ ECL (GE Healthcare, UK), a high performance chemiluminiscence film. All incubations were done on a rocking platform.

Results were analysed using Image J software version 1.43v (National Institute of Health, USA) and fold increases calculated.

4.3.6.2 Western blot validation

$2.5x10^5$ ESCs were plated per well in 12-well plates (Nunc) and treated with SF-EVs ($5x10^{10}$ SF-EVs/10^6 cells) for 30 min on day 0 or day 3 of decidualisation at 37°C. Non-treated wells were used to determine cell yield per well to enable SF-EV to cell ratio to be standarised and maintained. After incubation ESCs were lysed in 300 µl of lysis buffer, samples were collected and stored at - 80°C until used. The protein concentration of the lysates was determined using a BCA assay kit and changes on the phosphorylation of Hematopoietic cell kinase (HCK) (Y411) and mammalian Target of Rapamycin (mTOR) (S2448), and total HSP60 levels were validated by Western blotting following the protocol previously described in chapter 2. The antibodies used in this chapter are described in table 4.2.

Table 4.2 Primary and secondary antibodies used for Western blot validation of phospho-kinase array on ESCs.
Conc. = concentration, Approx. MW = Approximate Molecular Weight

Antibody	Conc./ dilution	Approx. MW	Source antibody	+ Control	Clone	Company
pHCK (Y411)	1:500	59 KDa	Rabbit	Jurkats	Polyclonal	Biorbyt, UK
HCK	1:500	58 KDa	Rabbit	Jurkats	Polyclonal	Biorbyt, UK
Human phopho-mTOR (S2448)	1 µg/mL	250 KDa	Rat	HeLa	834115	R&D systems, USA
β ACTIN	1:500	42 KDa	Mouse	Any cell type	AC-15	Abcam®, UK
anti-HSP60	1:1,000	60 KDa	Mouse	HeLa	LK1	NeoMarkers, USA
anti-Mouse IgG-HRP	1:1,000	-	Goat	-	Polyclonal	Dako, Denmark
anti-Rabbit IgG-HRP	1:1,000	-	Goat	-	Polyclonal	Dako, Denmark
Anti-Rat IgG-HRP	1:1,000	-		-	Polyclonal	Cell signalling, USA

4.3.7 Statistical analysis

4.3.7.1 Binding studies

Statistical analysis was performed using GraphPad Prism 7.01 (GraphPad Software, USA). Shapiro-Wilk tests were used to confirm normality of the data. Parametric data was then analysed using a repeated measures one-way ANOVA without Geisser-Greenhouse correction. Nonparametric data was analysed using the Friedman test. Experimental groups were always compared controlling the False Discovery Rate using the Two-stage step-up method of Benjamini, Krieger and Yekutieli. Data were

represented as mean ± SD or median ± IQR. Differences were considered significant if $p < 0.05$.

4.3.7.2 Functional studies

Statistical analysis of the functional studies was carried out using R3.3.2 (R Core Team, R Foundation for Statistical Computing, Austria) under the guidance of Dr. Daniel Lunn, Department of Statistics, University of Oxford. Prolactin and IGFBP-1 concentrations were modelled using the following logistic function, characterised by Asym, xmid and φ.

$$\sqrt[3]{Response} = \frac{Asym + a_1 z_1 + a_2 z_2}{1 + \exp\left(\frac{xmid - Day}{\varphi}\right)}$$

Asym represents the maximum asymptote of the curve, xmid is the position of the point of inflexion and φ is the scale parameter. The reference level was taken to be Control and z1 and z2 were indicator variables identifying the two treatments; thus the parameters a1 and a2 provide estimates of the contrasts in maximum asymptote due to Treatment and can be formally tested for significance. For the model to be valid it was necessary to ensure that the residuals were normally distributed and homoscedastic; this was achieved by taking the cube-root of the response variable for both Prolactin and IGFBP-1. With this transformation both normal Q-Q plots and formal Shapiro-Wilk tests confirmed normality and plots of residuals against fitted values showed no indication of heteroscedasticity.

The data were multilevel in structure in that repeated measurements over time were recorded for each subject, so that it was necessary to take account of within-subject correlation in the statistical analysis. Therefore multilevel non-linear models were fitted

using the R-library nlme (Pinheiro, 2000) with subject ID as level 1. Random effects were included across the parameters Asym, xmid and φ. When IGFBP-1 was the response a likelihood-ratio test showed that reducing the parameterisation by dropping the random effect on φ had no effect on the quality of fit of the model (p-value = 0.9714).

4.3.7.3 Molecular studies

Statistical significance was analysed using GraphPad Prism 7.01. As before Shapiro-Wilk tests were used to confirm normality of the data. Parametric data was assessed using paired Student's *t*-test, and nonparametric data was analysed using Wilcoxon test. Data were represented as mean ± SD or median ± IQR. Differences were considered significant if $p < 0.05$.

4.4 Results

4.4.1 SF-EVs bind to ESCs

ESCs were incubated with fluorescent bio-maleimide labelled SF-EVs at a concentration of $5x10^{10}$ SF-EVs/10^6 ESCs (n = 3) for 2 hrs and analysed by fluorescence microscopy and flow cytometry to detect binding. To determine if SF-EV binding depended on the stage of decidualisation, non-decidualised (day 0), day 3 and day 7 decidualised ESCs were used for these experiments.

Flow cytometry demonstrated binding of SF-EVs to ESCs (n = 3) – increased bio-maleimide fluorescence on ESCs after incubation was observed in non-decidualised, day 3, and day 7 decidualised ESCs (Fig 4.3 a, b, c).

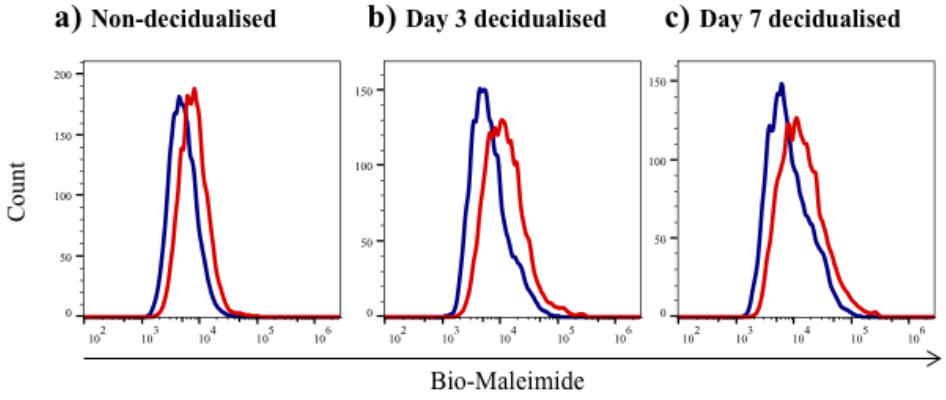


Fig 4.3 Representative flow cytometry histogram of SF-EV binding to primary ESCs ($5x10^{10}$ SF-EVs/10^6 cells).
(a) Non-decidualised, **(b)** day 3 and **(c)** day 7 decidualised ESCs were treated with bio-maleimide labelled SF-EVs or the negative control for 2 hrs; and analysed by flow cytometry. The figure depicts histograms with the SF-EV group fluorescence intensity in red and the negative control group fluorescence intensity in blue.

SF-EVs significantly bound to non-decidualised ESCs ($p = 0.0126$) day 3 ($p = 0.0236$) and day 7 ($p = 0.0241$) decidualised ESCs compared to their negative control (Fig 4.4). No differences were observed between the negative control and the PBS groups at any stage of decidualisation (Fig 4.4). In addition, no changes in MFI increase were observed between SF-EV treated ESCs at different decidualisation stages (Fig 4.5 a). The percentage of cells binding bio-maleimide labelled SF-EVs was also analysed, SF-EVs bound to significantly more non-decidualised ESCs than day 3 ($p = 0.0014$) and day 7 ($p = 0.0002$) decidualised ESCs (Fig 4.5 b). In addition, ESCs decidualised for 3 days bound more SF-EVs than those decidualising for 7 days ($p = 0.0088$).

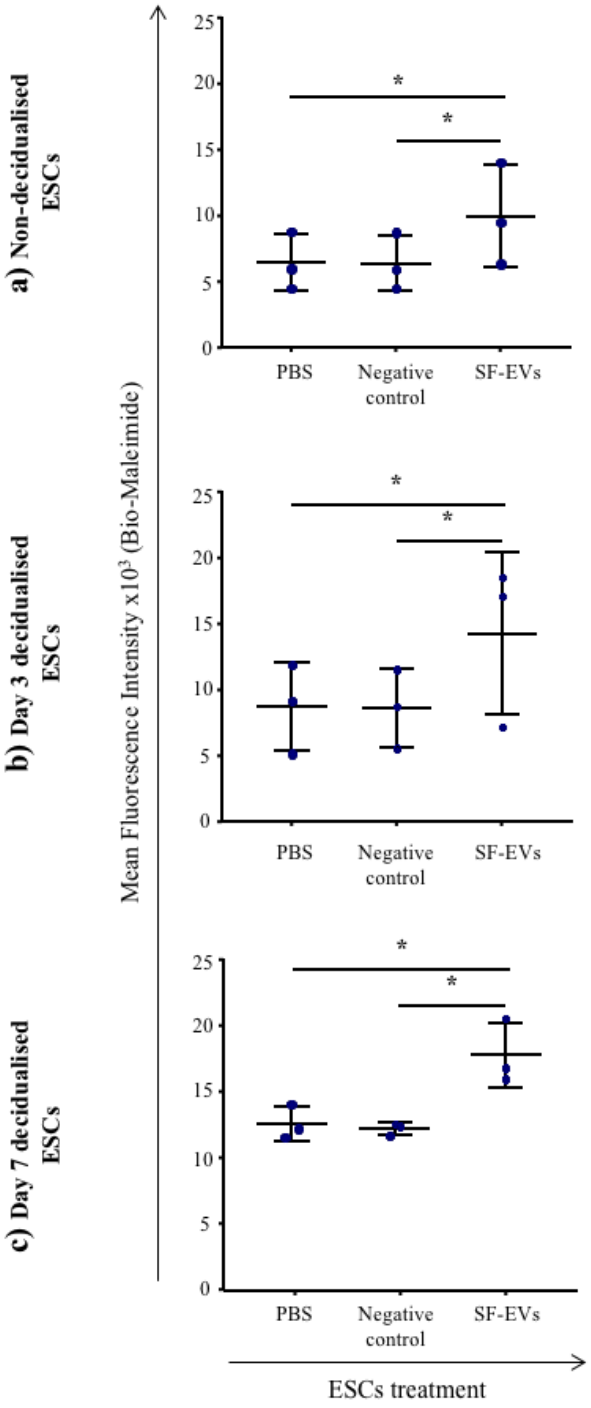


Fig 4.4 SF-EVs bind to primary ESCs: Mean fluorescence intensity.
ESCs were treated with bio-maleimide labelled SF-EV preparation # 1, PBS or the negative control for 2 hrs ($5x10^{10}$ SF-EVs/10^6 cells). The mean fluorescence intensity was then analysed by flow cytometry in **(a)** non-decidualised, **(b)** day 3 and **(c)** day 7 decidualised ESCs. Bars represent mean ± SD. * = $p < 0.05$

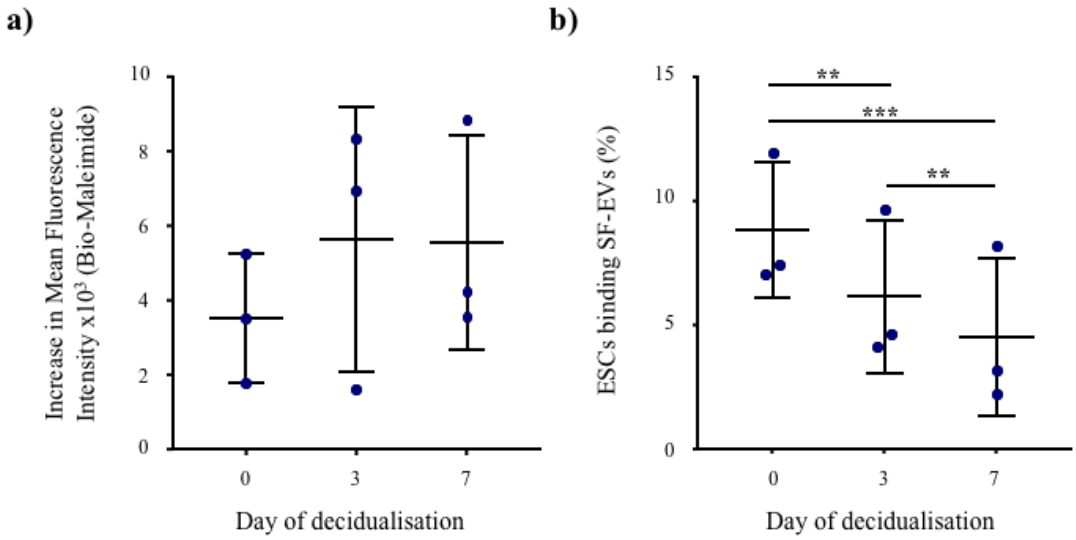


Fig 4.5 SF-EVs bind to primary ESCs at different days of decidualisation.
ESCs were treated with bio-maleimide labelled SF-EV preparation # 1 or the negative control for 2 hrs ($5x10^{10}$ SF-EVs/10^6 cells) and SF-EV binding was analysed by flow cytometry. **(a)** The increase in mean fluorescence intensity and **(b)** the percentage of ESCs binding bio-maleimide labelled SF-EVs were calculated to compare SF-EV binding on different days of decidualisation. Bars represent mean ± S.D. ** = $p < 0.01$, *** = $p < 0.001$.

Fluorescence images confirmed that bio-maleimide labelled SF-EVs (green) bound to non-decidualised (Fig 4.6 a) and day 7 decidualised (Fig 4.6 b) ESCs. No fluorescent (green) signal was detected in the controls (PBS).

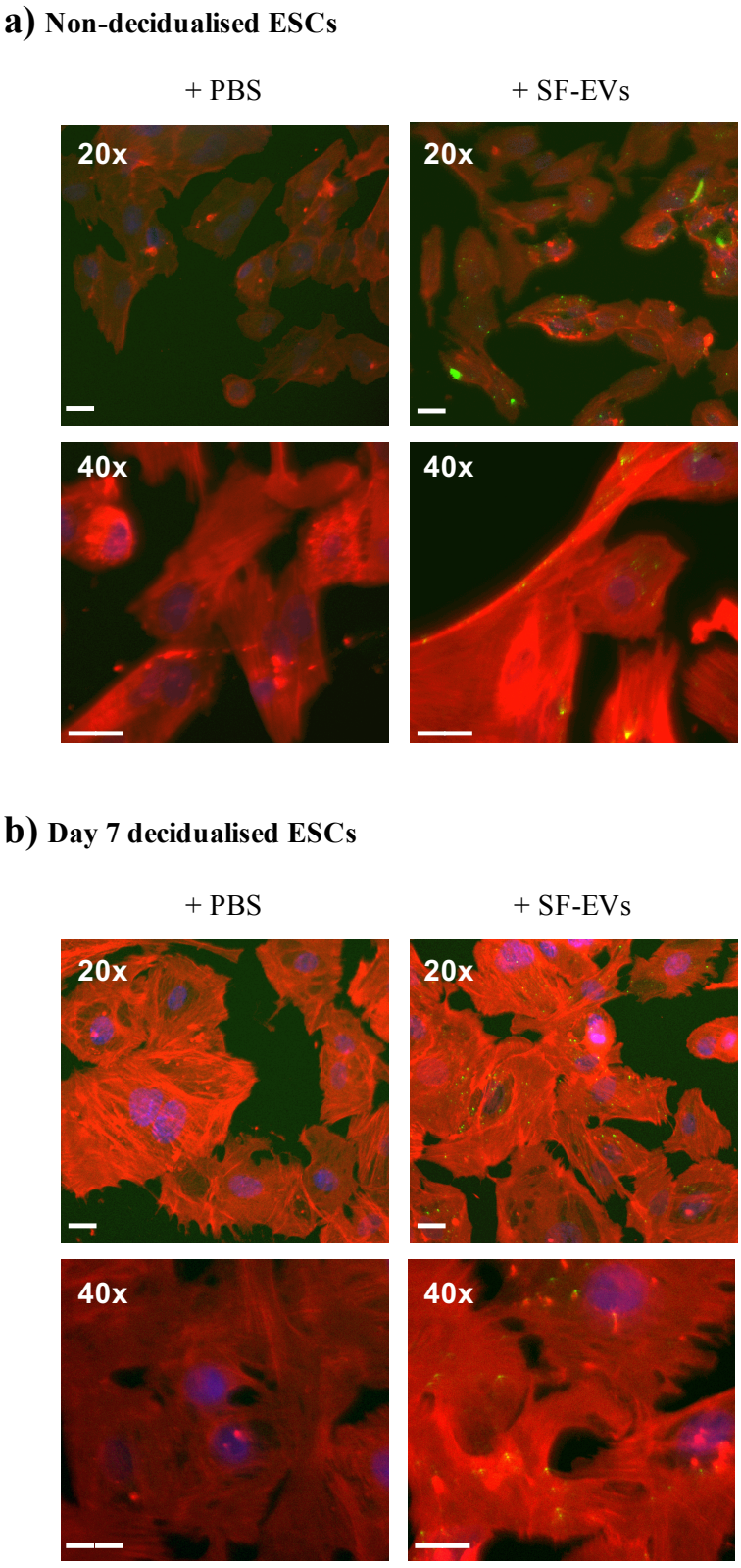


Fig 4.6 SF-EVs bind to primary ESCs: Fluorescence microscopy.

(a) Non-decidualised and **(b)** day 7 decidualised ESCs (n = 1) were incubated with bio-maleimide labelled SF-EVs for 2 hrs ($5x10^{10}$ SF-EVs/10^6 cells) and fluorescence images were captured at 20x and 40x magnification; green = SF-EVs, red = β-actin, blue = nuclei. Scale bars = 20 μm.

4.4.2 ESC decidualisation is enhanced after SF-EV exposure

Having demonstrated that ESCs bind SF-EVs, I hypothesized SF-EVs might enhance decidualisation. ESCs were decidualised for seven days and treated with SF-EVs once (day 0) or twice (day 0 and 3) ($5x10^{10}$ SF-EVs/10^6 cells). The latter experiment tested if multiple exposure to SF-EVs could further enhance decidualisation. Bright field images and cell culture supernatants were collected every day for later analysis.

4.4.2.1 ESCs morphological differentiation into round-secretory cells is not affected by SF-EV treatment

ESCs differentiated from fibroblast-like cells into round secretory cells during the 7 days of decidualisation (Fig 4.7). No obvious morphological differences were observed between PBS, single or multiple SF-EV exposure groups. The number of non-decidualised (fibroblast-like) and decidualised (round) cells on day 7 were counted manually using Image J (n = 3) – sample images were analysed blind to treatment condition. Percentage of decidualised cells were calculated, no differences in the percentage of decidualised ESCs on day 7 were detected after PBS, single or multiple SF-EV treatment (Fig 4.8). Approximately 80 % of ESCs had acquired decidualised morphology by day 7 of decidualisation (Fig 4.8).

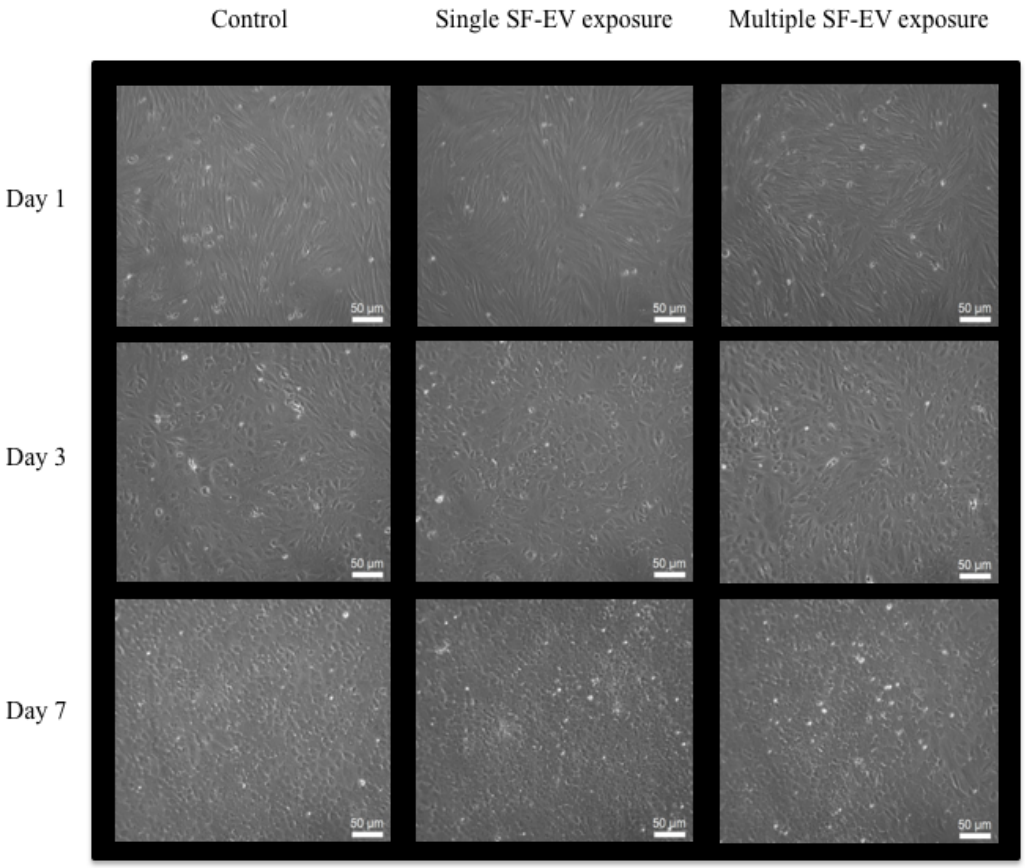


Fig 4.7 Morphological ESCs differentiation into round secretory cells after single or multiple SF-EV exposure.

Primary ESCs (n = 5) were treated with SF-EVs ($5x10^{10}$ SF-EVs/10^6 cells) once (day 0 of decidualisation) or twice (day 0 and 3 of decidualisation). PBS was used as control. Bright field images were then captured at 10x magnification. Scale bars = 50 µm.

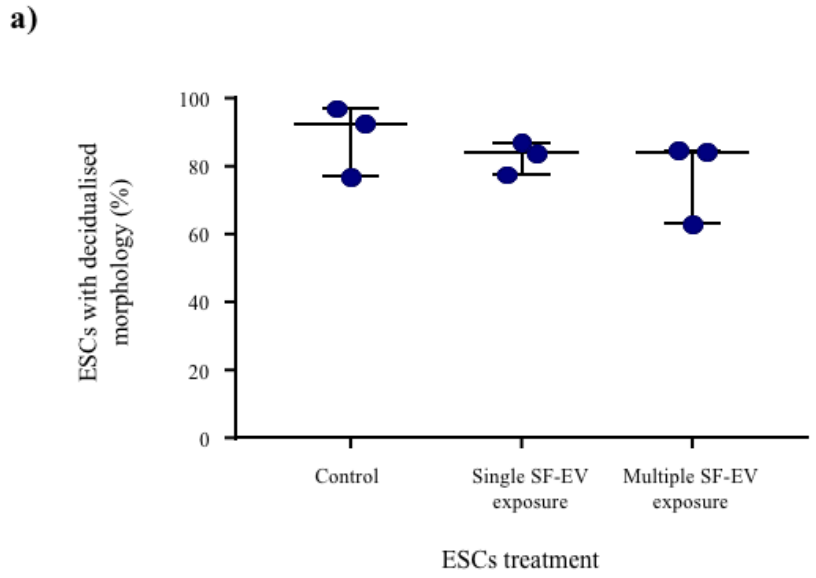


Fig 4.8 Percentage of decidualised ESCs at day 7 of decidualisation induction after SF-EV exposure.

Primary ESCs (n = 3) were treated with SF-EVs ($5x10^{10}$ SF-EVs/10^6 cells) once (day 0 of decidualisation) or twice (day 0 and 3 of decidualisation). PBS was used as a control. Bright field images were then captured in triplicate at 10x magnification and the numbers of fibroblast-like cells (non-decidualised ESCs) and enlarged round cells (decidualised ESCs) were counted using Image J. Data is depicted as percentages of decidualised ESCs. Bars represent median ± IQR.

4.4.2.2 ESC prolactin secretion increases after SF-EV treatment

Prolactin concentrations were measured in cell culture supernatants using ELISAs (n = 5). ESC prolactin production was significantly increased after single (p = 0.0044) and multiple (p = 0.0021) SF-EV treatment throughout the days of decidualisation (Fig 4.9). Higher prolactin levels were observed from day 3 decidualisation after SF-EV exposure. No significant differences in prolactin secretion were observed between single and multiple SF-EV exposures (p = 0.8128) (Fig. 4.9).

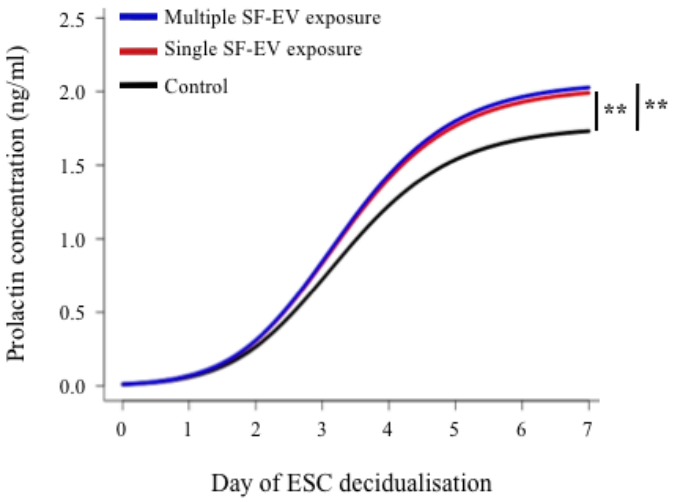


Fig 4.9 Concentration of ESCs supernatant prolactin after single or multiple SF-EV exposure.
Primary ESCs (n = 5) were treated with SF-EVs ($5x10^{10}$ SF-EVs/10^6 cells) once (day 0 of decidualisation, red line) or twice (day 0 and 3 of decidualisation, blue line). PBS was used as a control (black line). Cell supernatants were collected daily and prolactin concentration measured by ELISA. ** = $p < 0.01$.

4.4.2.3 ESCs IGFBP-1 secretion does not change after SF-EV treatment

Having demonstrated enhanced ESCs prolactin secretion after SF-EV exposure, I investigated if SF-EVs also affected the production of IGFBP-1. IGFBP-1 concentration in cell supernatants were measured using ELISAs (n = 5). SF-EV treatment did not significantly change IGFBP-1 secretion by ESCs (Fig 4.10).

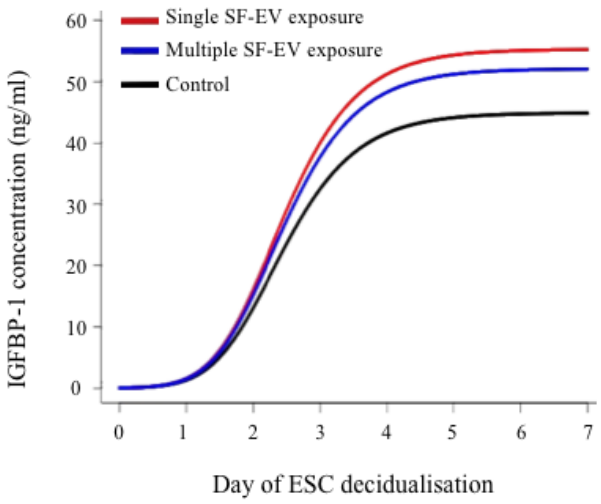


Fig 4.10 Concentration of ESCs supernatant IGFBP-1 after single or multiple SF-EV exposure.
Primary ESCs (n = 5) were treated with SF-EVs ($5x10^{10}$ SF-EVs/10^6 cells) once (day 0 of decidualisation, red line) or twice (day 0 and 3 of decidualisation, blue line). PBS was used as a control (black line). Cell supernatants were collected daily and IGFBP-1 concentration measured using ELISAs.

4.4.3 Analysis of signalling pathways in ESCs upon SF-EV exposure

A human phospho-kinase array (R&D systems, USA) was performed to identify changes in cell activation induced by SF-EV exposure (n = 1). 10^6 ESCs had been previously treated with $5x10^{10}$ SF-EVs or PBS for 30 min (non-decidualisation) (Fig 4.11 a) or for 2 hrs (non-decidualisation) and 30 min (day 3 of decidualisation) (Fig 4.11 b). Results of the SF-EV treated groups were normalised to their respective controls (PBS) and the fold increases calculated. None of the 45 different proteins in the array exhibited a 1-fold increase or more. However, HCK phosphorylation at tyrosine 411, showed almost 0.5-fold increase after 30 min of SF-EV treatment of non-decidualised cells (Fig 4.11 c). After SF-EV exposure for 2 hrs (day 0) and 30 min (day 3), HCK phosphorylation at Tyr411 showed an increase of more than 0.30-fold (Fig 4.11 d). In addition, mTOR phosphorylation at S2448 increased by approximately 0.30-fold after SF-EV treatment for 30 min (Fig 4.11 c) and, 2 hrs and 30 min (Fig 4.11 d). None of the proteins analysed

demonstrated a decrease of 0.15-fold or more. Total levels of HSP60 decreased by 0.10-fold after both SF-EV treatments (Fig 4.11 c, d). Although, the array showed no difference in HSP60 levels, Western blots were undertaken because previous experiments on day 7 progesterone-treated Ishikawa cells suggested a decrease in HSP60 after 30 min.

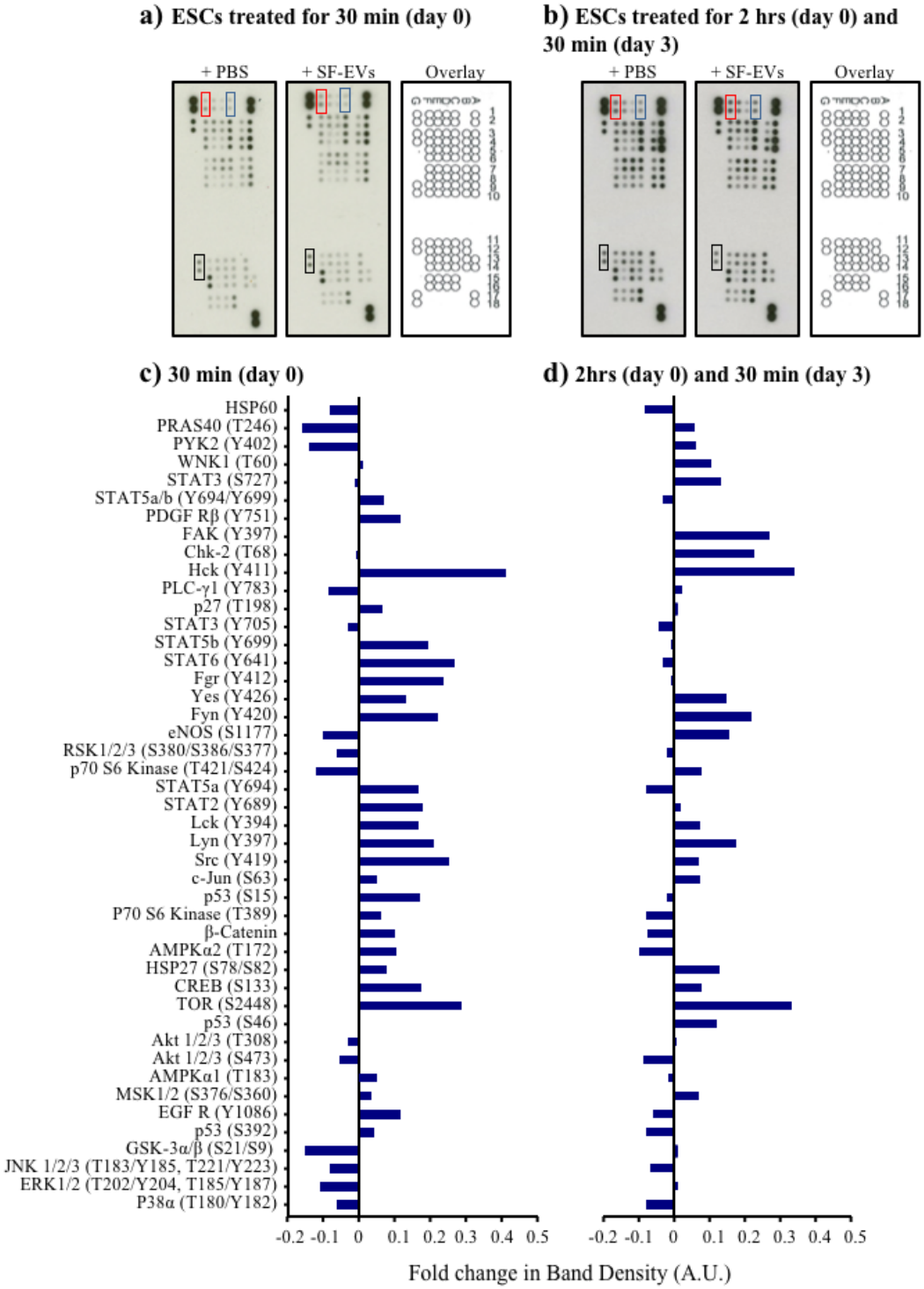


Fig 4.11 Phosphorylation profiles of ESCs after SF-EV exposure.

10^6 ESCs were treated with $5x10^{10}$ SF-EVs for **(a)** 30 min (non-decidualised) or **(b)** 2 hrs (non-decidualised) and 30 min (day 3 of decidualisation). Cells were then lysed and a human phospho-kinase array was performed. Protein levels were compared with the transparency overlay to identify the coordinates and the target phosphorylation in the Human Phospho-Kinase array coordinates table. Fold changes were calculated for **(c)** 30 min, and **(d)** 2 hrs and 30 min stimulations. The red rectangles surround HCK

phosphorylation at tyrosine 411. The blue rectangles surround mTOR phosphorylation at S2448. The black rectangles surround HSP60.

The increases in phospho-HCK (Y411) and phospho-mTOR (S2448) as well as the decrease in total HSP60 were next validated by Western blotting (n = 5). Non-decidualised and day 3 decidualised ESCs were treated with SF-EVs for 30 min ($5x10^{10}$ SF-EVs/10^6 cells) and cells lysed to extract cell proteins, Western blots were then performed.

4.4.3.1 Total HCK Tyr411 phosphorylation in ESCs augments after SF-EV treatment

Western blot images of phospho-HCK (Y411) showed bands at 61 KDa and 59 KDa, 2 known isoforms of HCK, in non-decidualised (Fig 4.12 a) and day 3 decidualised (Fig 4.12 b) ESCs. The phospho-kinase array performed detected total HCK phosphorylation at tyrosine 411. Western blot densitometry analysis of both phospho-HCK isoforms confirmed a significant increase of total phospho-HCK (Y411) after SF-EV treatment of non-decidualised ESCs ($p = 0.0103$) (Fig 4.13 a). No significant difference was observed at day 3 of decidualisation (Fig 4.13 b). Analyses of the 61 KDa and 59 KDa HCK isoforms separately demonstrated no significant increase in non-decidualised ESCs HCK phosphorylation at 61 KDa (Fig 4.13 c) or 59 KDa (Fig 4.13 e). Although, the trend to increase by the 61 KDa isoform was observed ($p = 0.0929$) (Fig 4.13 c), suggesting the overall significant increase was mainly contributed by this isoform. No tendency to an increase on 61 KDa phospho-HCK (Y411) after SF-EV exposure was observed on day 3 decidualised ESCs (Fig 4.13 d). A trend to increase was observed in Tyr411 phosphorylation of the 59 KDa HCK isoform after SF-EV treatment of day 3 decidualised, but significance was not achieved ($p = 0.0906$) (Fig 4.13 f). The concentration of HCK was also normalised to actin to confirm that the changes observed

were due to different phosphorylation levels and not changes in HCK concentration. Total, 61 KDa, and 59 KDa HCK normalised concentrations did not vary significantly after SF-EV treatment on non-decidualised (Fig 4.14 a, b, c) or day 3 decidualised ESCs (Fig 4.14 d, e, f)

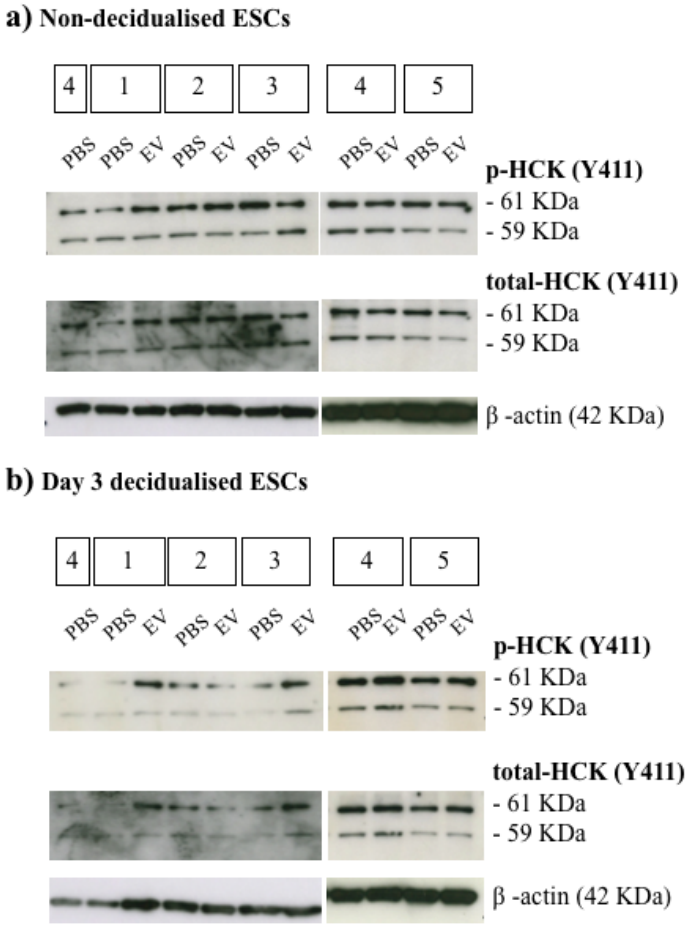


Fig 4.12 Expression of HCK phosphorylation at Tyr411 in primary ESCs after SF-EV exposure: Western blots.
(a) Non-decidualised and **(b)** day 3 decidualised primary ESCs (n = 5) were treated with SF-EVs ($5x10^{10}$ SF-EVs/10^6 cells) or PBS (control) for 30 min and then lysed - 10 μg of protein was analysed by Western blotting.

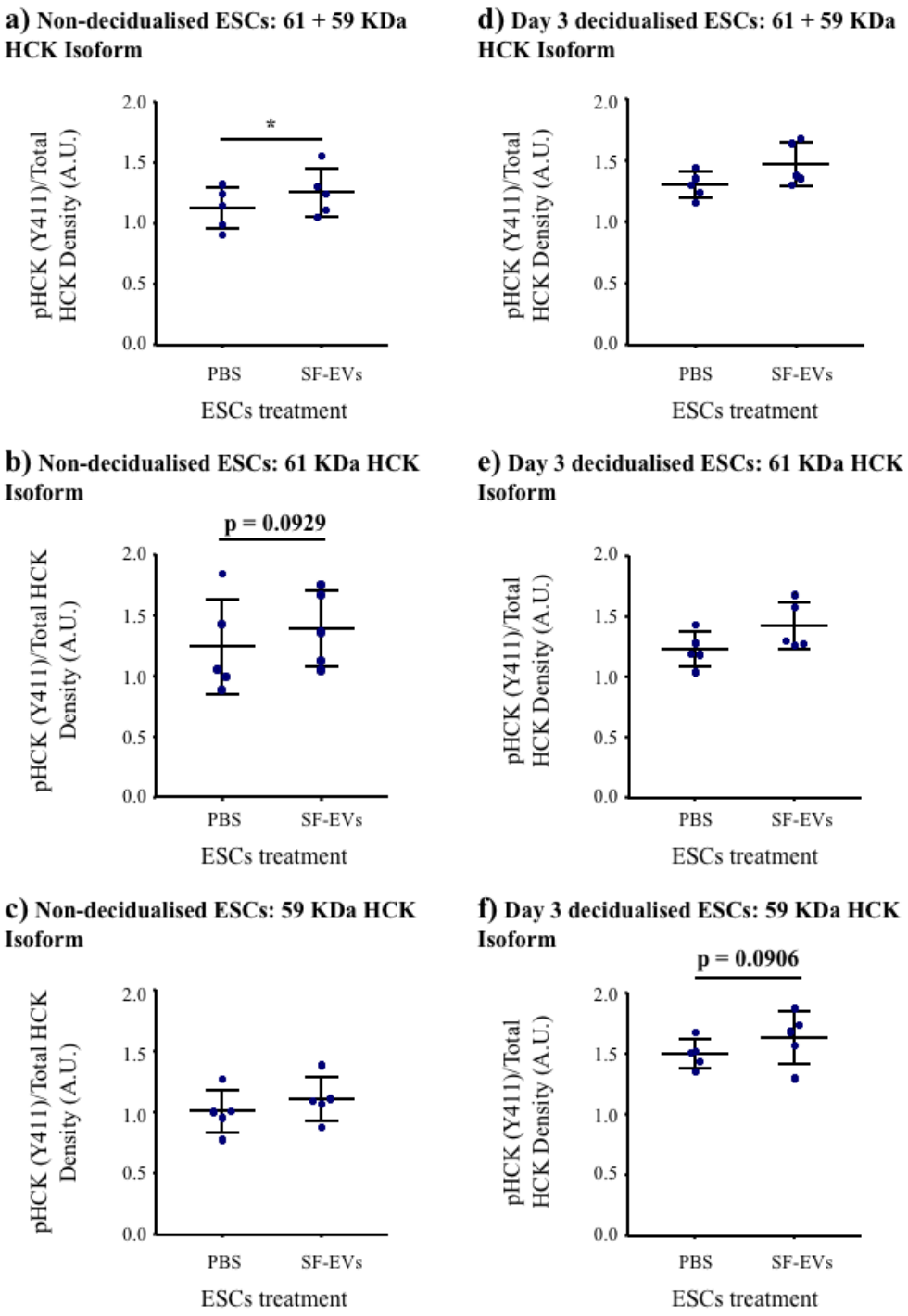


Fig 4.13 Expression of HCK phosphorylation at Tyr411 in primary ESCs after SF-EV exposure: dot plots.

(a, b, c) Non-decidualised and **(d, e, f)** day 3 decidualised primary ESCs (n = 5) were treated with SF-EVs ($5x10^{10}$ SF-EVs/10^6 cells) or PBS (control) for 30 min and then lysed - 10 μg of proteins was analysed by Western blotting. Band density was measured by Image J. Phospho-HCK (Y411) was normalised to total HCK. This figure shows **(a, d)** total phospho-HCK (Y411) **(b, e)** 61 KDa phospho-HCK (Y411), and **(c, f)** 59 KDa phospho-HCK (Y411) in ESCs. Bars represent mean ± SD. * = $p < 0.05$.

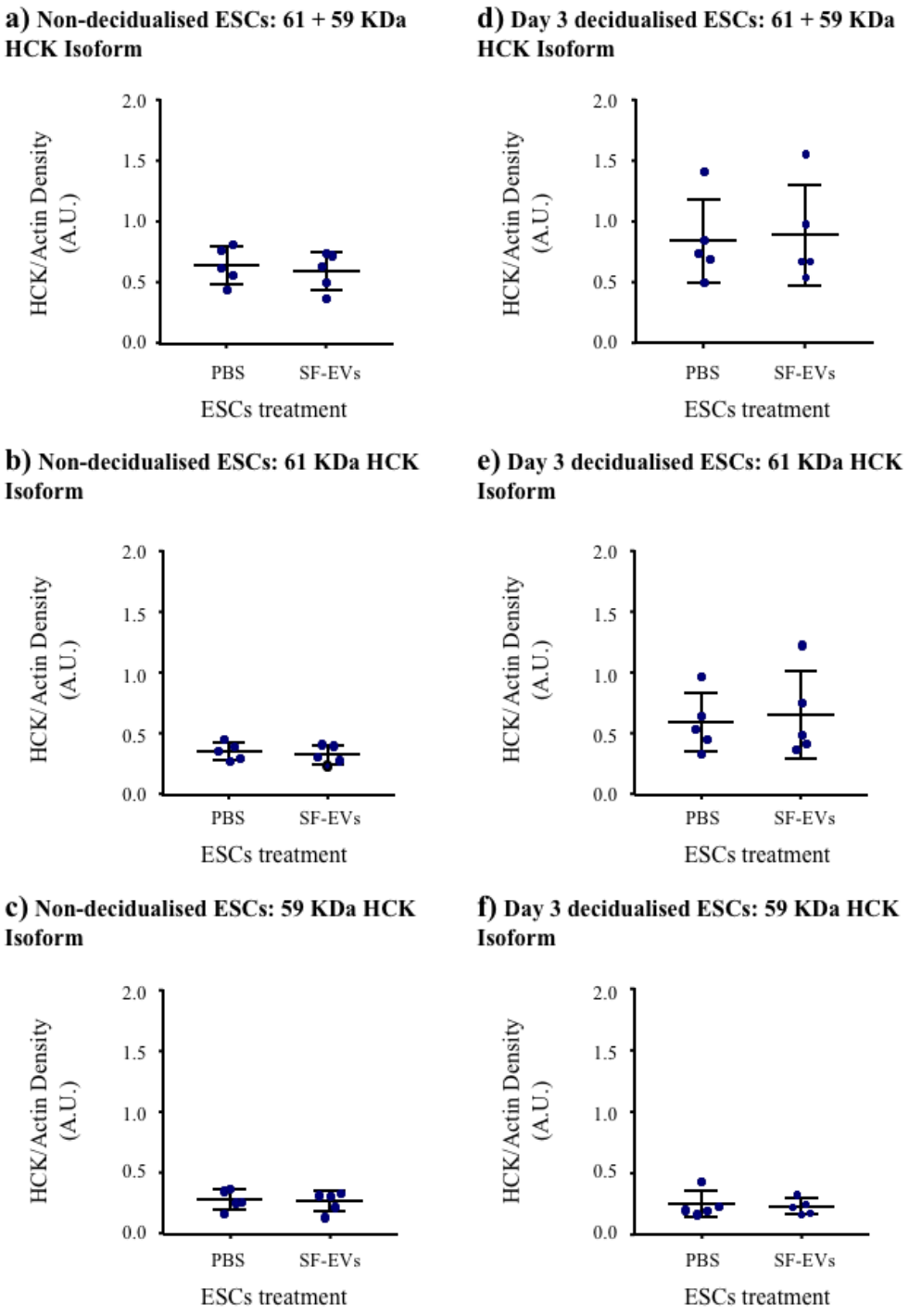


Fig 4.14 Expression of HCK in primary ESCs after SF-EV exposure: dot plots.
(a, b, c) Non-decidualised and **(d, e, f)** day 3 decidualised primary ESCs (n = 5) were treated with SF-EVs ($5x10^{10}$ SF-EVs/10^6 cells) or PBS (control) for 30 min and then lysed - 10 μg of proteins was analysed by Western blotting. Band density was measured by Image J. HCK was normalised to actin. This figure shows **(a, d)** total HCK **(b, e)** 61 KDa HCK, and **(c, f)** 59 KDa HCK in ESCs. Bars represent mean ± SD.

4.4.3.2 SF-EV treatment of ESC does not affect S2448 mTOR phosphorylation

Western blotting revealed a band at 250 KDa on non-decidualised (Fig 4.15 a) and day 3 decidualised (Fig 4.15 b) ESCs (n = 5) coinciding with the expected size for the phospho-mTOR (S2448) protein. Protein expression levels were normalised to β-actin. No significant increase in phospho-mTOR (S2448) was observed on non-decidualised (Fig 4.15 c) nor day 3 decidualised (Fig 4.15 d) ESCs (n = 5).

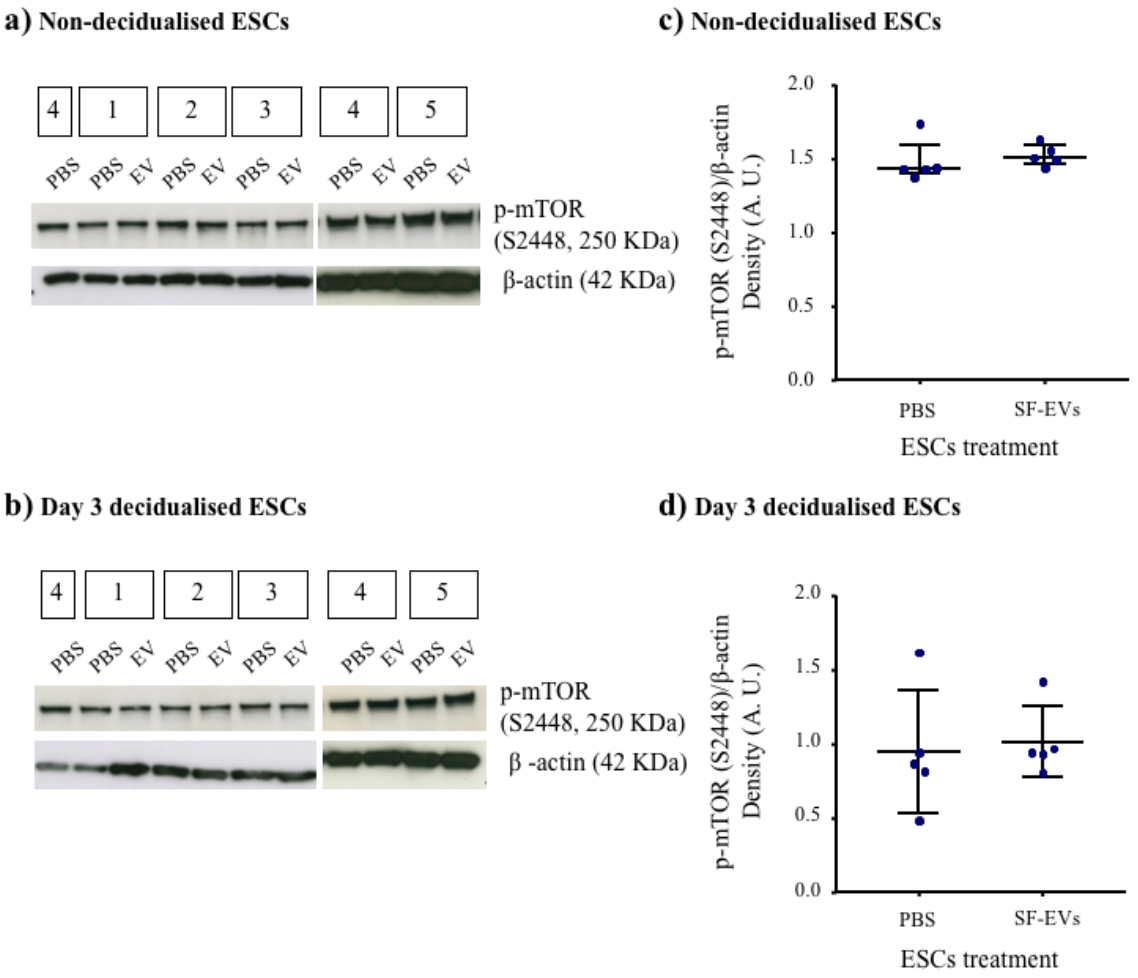


Fig 4.15 Western blotting and densitometry analysis of mTOR phosphorylation at S2448 in primary ESCs after SF-EV exposure.

(a, c) Non-decidualised and **(b, d)** day 3 decidualised primary ESCs (n = 5) were treated with SF-EVs ($5x10^{10}$ SF-EVs/10^6 cells) or PBS (control) for 30 min and then lysed - 10 μg of protein was analysed by Western blotting. Membranes were probed with antibodies towards phospho-mTOR (S2448) and β-actin. Experiments 1 to 5 were run on separate gels and sample PBS 4 was run on both gels to allow comparison between membranes. Band density was measured by Image J. Phospho-mTOR (S2448) was normalised to β-actin and compared to the control (PBS). These figures show **(a)** non-decidualised and **(b)** day 3 decidualised phospho-mTOR (S2448) Western blots, and **(c)** non-decidualised and **(d)** day 3 decidualised phospho-mTOR (S2448) dot plots. Bars represent **(c)** median ± IQR, or **(d)** mean ± SD.

4.4.3.3 HSP60 expression in ESCs does not change after SF-EV treatment

Western blot images of HSP60 showed a band at 60 KDa on non-decidualised (Fig 4.16 a) and day 3 decidualised (Fig 4.16 b) ESCs (n = 5). Protein expression levels were

normalised to β-actin. No significant change in HSP60 expression was observed in either non-decidualised (Fig 4.16 c) or day 3 decidualised (Fig 4.16 d) ESCs (n = 5).

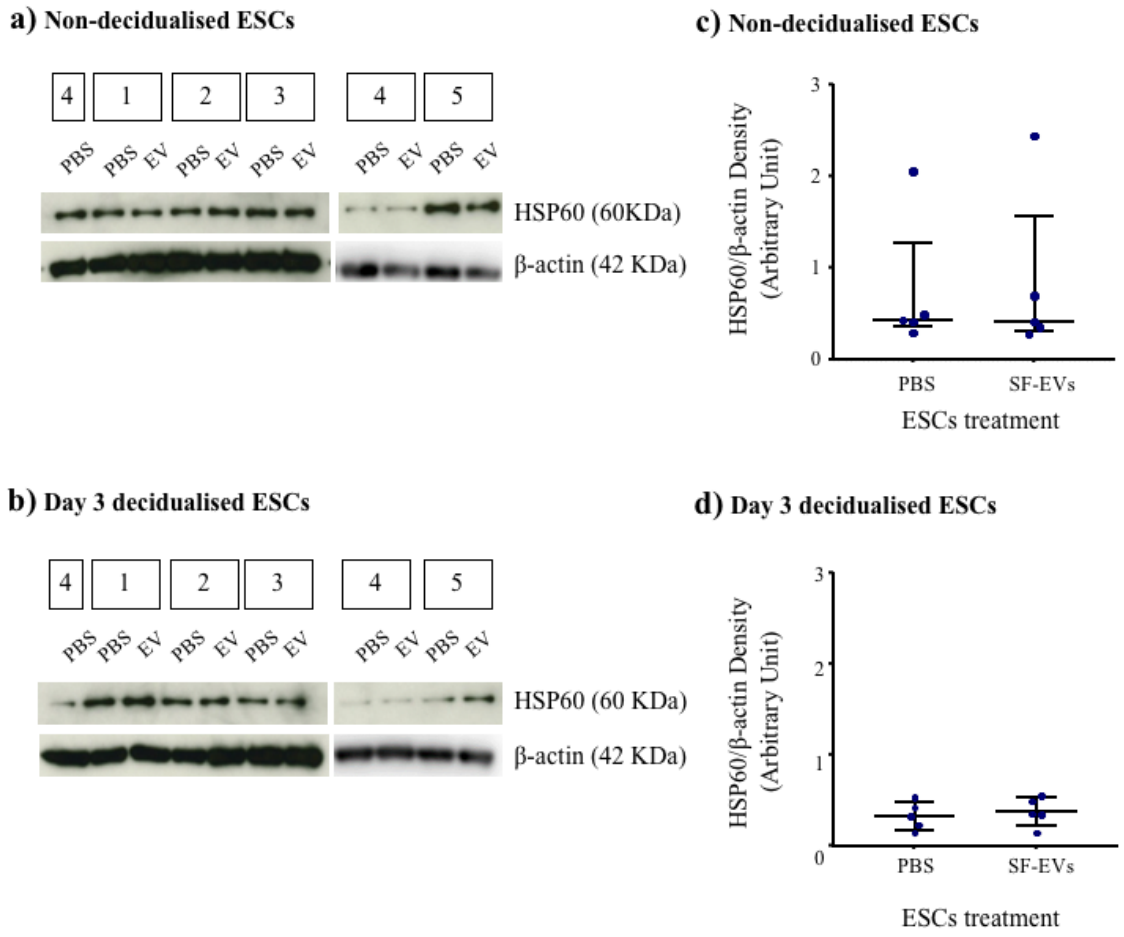


Fig 4.16 Expression of HSP60 in primary ESCs after SF-EV exposure.
(a, c) Non-decidualised and **(b, d)** day 3 decidualised primary ESCs (n = 5) were treated with SF-EVs ($5x10^{10}$ SF-EVs/10^6 cells) or PBS (control) for 30 min and then lysed - 10 μg of protein was analysed by Western blotting. Membranes were probed with antibodies towards HSP60 and β-actin. Experiments 1 to 5 were run on separate gels and sample PBS 4 was run on both gels to allow comparison between membranes. Band density was measured by Image J. HSP60 was normalised to β-actin and compared to the control (PBS). These figures show **(a)** non-decidualised and **(b)** day 3 decidualised HSP60 Western blots, and **(c)** non-decidualised and **(d)** day 3 decidualised HSP60 dot plots. Bars represent **(c)** median ± IQR, or **(d)** mean ± SD.

In summary SF-EVs induced an increase in HCK phosphorylation at Y411 when added to non-decidualised ESCs.

4.5 Discussion

4.5.1 SF-EVs bind to ESC

In this chapter I have shown that SF-EVs bind to primary human ESCs *in vitro* using both flow cytometry and fluorescence microscopy. It is also known ESCs bind EVs from other sources, such as Ishikawa cells and human embryos. CD63-GFP^{+} exosomes, isolated from CD63-GFP-expressing Ishikawa cells adhere to primary human ESCs (Flow cytometry and microscopy) (Maida *et al.*, 2016). In addition, Vybrant DiO carbocyanine labelled-embryo EVs bind to primary human ESCs (fluorescence microscopy) (Giacomini *et al.*, 2017).

No differences in SF-EV binding, as determined by MFI, were observed between non-decidualised, day 3 or day 7 decidualised ESCs suggesting that they can interact with the ESCs at similar intensity throughout the menstrual cycle. Interestingly, ESC binding of bio-maleimide labelled SF-EVs decreased significantly through the days of decidualisation, although no differences in bio-maleimide fluorescence intensity were observed (as described above). This might suggest a different binding pattern of SF-EVs to non-decidualised and decidualised ESCs. Fewer dESCs might bind more bio-maleimide labelled SF-EVs than non-decidualised ESCs. It is not surprising that ESCs have different SF-EV binding patterns depending on the stage of decidualisation since SF-EV functional effect might vary.

4.5.2 ESC decidualisation is enhanced after SF-EV exposure

After demonstrating SF-EV binding to ESCs, I investigated if SF-EVs assist ESC decidualisation. Primary human ESCs were decidualised for seven days and treated with SF-EVs once or twice to mimic single or multiple ESCs exposure to paternal SF-EVs.

Bright field microscopy confirmed that after 7 days incubation with dibutyryl cyclic-AMP sodium salt and progesterone there was no morphological differences observed when SF-EVs were present - the majority of the treated and control ESCs exhibited decidualised morphology.

The analysis of factors released by decidualising ESCs showed SF-EVs induced prolactin secretion but not IGFBP-1. Single and multiple SF-EV treatments increased ESCs secretion of prolactin throughout the seven days of decidualisation compared with the control. By day 3 of decidualisation the differences in prolactin concentration were apparent and this difference increased over time. No significant differences in prolactin concentration were observed between single and multiple SF-EV exposures. The latter suggests SF-EVs induce ESCs' prolactin on non-decidualised cells and once this stimulation is triggered, additional exposure does not further enhance prolactin release.

Prolactin plays an essential role in embryo implantation and pregnancy. Homozygous prolactin receptor knockout (*PRLR*$^{-/-}$) female mice are sterile because the maternal endometrium is refractive to embryo implantation (Bole-Feysot *et al.*, 1998). Prolactin increases progesterone receptors and enhances progesterone effects promoting progesterone-induced ESC decidualisation in rabbits (Daniel *et al.*, 1984, Chilton and Daniel, 1987). In addition, prolactin decreases myometrial contractions in rabbits to facilitate attachment of the conceptus (Mati *et al.*, 1974). Prolactin also regulates endometrial epithelial (Franchi *et al.*, 2011) and immune cells (Ain *et al.*, 2004). For instance, in humans, prolactin increases endometrial epithelial cell secretion of milk fat globule epidermal growth factor 8, also known as lactadherin (Franchi *et al.*, 2011). In

mice prolactin interacts with uNK cells and lack of prolactin leads to poor uNK cells responsiveness to hypoxia, hindering placental growth (Ain *et al.*, 2004). In humans prolactin also interact with uNK cells (Gubbay *et al.*, 2002). In addition, prolactin interacts with the placenta promoting human trophoblast migration and invasion (Stefanoska *et al.*, 2013).

IGFBP-1 mainly controls placentation through the regulation of insulin-like growth factor I and II, during implantation it prevents excessive placental invasion (Fowler *et al.*, 2000). The significant increase of the decidualisation marker prolactin, but not IGFBP-1, suggests SF-EVs may stimulate implantation processes regulated by prolactin, but not by IGFBP-1. As mentioned in the introduction (chapter 1) seminal fluid promotes a pro-inflammatory environment in the endometrium known to assist pregnancy (Robertson and Sharkey, 2016). SF-EVs might promote this pro-inflammatory environment through the enhancement of ESC prolactin secretion. Prolactin's role in the regulation of the immune system has been extensively reviewed, and this regulation is dose-dependent, in other words, prolactin can stimulate or suppress the same immune response in a dose-dependent manner (Costanza *et al.*, 2015, Pereira Suarez *et al.*, 2015). For example, in humans lymphocyte proliferation is suppressed by high prolactin concentrations while low prolactin concentration stimulates this lymphocyte proliferation (Matera *et al.*, 1992). Importantly, elevated prolactin concentrations also suppress uNK cell cytotoxicity in humans (Gerli *et al.*, 1986).

Doyle *et al*. 2012 studied the effect of seminal fluid on ESC prolactin and IGFBP-1 secretion (Doyle *et al.*, 2012). They observed that 27 days incubation of decidualised ESCs with seminal plasma increased significantly the concentration of prolactin mRNA

and protein (Doyle *et al.*, 2012), similar to the data in this chapter. Therefore, SF-EVs might be partially responsible for the increase in ESCs prolactin secretion described by Doyle *et al*. 2012. Unlike in this chapter, they showed increased IGFBP-1 mRNA and protein levels (Doyle *et al.*, 2012). This difference in outcome might be due to the longer incubation time (27 versus 7 days of incubation) or to the presence of soluble proteins in the seminal fluid that can induce ESC decidualisation.

4.5.3 ESCs protein phosphorylations vary after SF-EV exposure

Having established that SF-EVs bind to ESCs and induce enhanced prolactin secretion during the decidualisation process, I next sought to investigate the molecular signalling pathways involved. I performed a protein phosphokinase array of the 45 proteins analysed. Several were found to be moderately increased.

Only the increase in total HCK phosphorylation at tyrosine 41 in non-decidualised ESCs after SF-EV exposure was confirmed by Western blotting, no changes were observed on day 3 decidualised ESCs. The later suggests SF-EVs affects the pathway around pHCK-Tyr411 before decidualisation has begun. HCK is a member of the Src family kinase (Guiet *et al.*, 2008, Poh *et al.*, 2015). The SRC family kinases (SFK) are non-receptor tyrosine kinases and includes Src, Fyn, Yes, Lyn, Fgr, Hck, Lck, and Blk. These kinases regulate multiple signalling pathways including activation of signal transducer and activator of transcription (STAT) proteins through phosphorylation (Fig 4.17). Interestingly, the array performed in this study detected moderate increased phosphorylation levels of many SFK: Src (Y419), Fyn (Y420), Yes (Y426), Lyn (Y397), Fgr (Y412), and Lck (Y394), although not as high as HCK phosphorylation (Y411). Blk was not present in the membrane. Of this SFK, Src, Fyn, and Yes are expressed

ubiquitously, while the expression of the others, including Hck, are tissue-specific (Guiet *et al.*, 2008).The optimal active form of SFKs are induced by the phosphorylation of the tyrosine residue in the activation loop located at the SH1 domain (Guiet *et al.*, 2008, Poh *et al.*, 2015). Specifically, HCK is activated by phosphorylation of tyrosine 411, the residue analysed in this study, which suggests SF-EVs promoted HCK enzymatic activity in ESCs, HCK was expressed in 2 isoforms: p61 HCK and p59 HCK (Lock *et al.*, 1991, Mohn *et al.*, 1995, Robbins *et al.*, 1995, Carreno *et al.*, 2000, Astarie-Dequeker *et al.*, 2002).

HCK is an SFK whose expression was thought to be exclusive of myeloid and B cells lineages. In 2006 Lalancette *et al*. 2006 demonstrated the expression of Hck in bull testis and spermatozoa by RT-PCR and northern blotting (Lalancette *et al.*, 2006) – this was the first evidence of a potential role of HCK in reproduction. To our knowledge, the expression of HCK in female reproductive tract remains unclear. The Human Protein Atlas[24] project found that HCK mRNA was expressed on endometrial smooth muscle and stromal cells – from higher to less mRNA expression levels. However, ESC HCK protein expression was not detected by immunohistochemistry. In this chapter I have shown that non-decidualised and day 3 decidualised ESCs express both p61 HCK and p59 HCK protein *in vitro*.

The role of HCK in female reproduction is unknown. However, some studies have shown a role of Src kinase, another member of the SFK in ESCs decidualisation. Homozygous Src kinase knockout (*Src*$^{-/-}$) female mice showed impaired ESC decidualisation (Shimizu *et al.*, 2005). After decidualisation induction, histological analysis of the *Src*$^{-/-}$ mice

[24] https://www.proteinatlas.org

endometrium did not show morphological differentiation of ESCs into enlarged round dESCs (Shimizu *et al.*, 2005). In addition, Src kinase activity increases after *in vitro* decidualisation of human ESCs (Maruyama *et al.*, 1999). Moreover, inhibition of Src kinase activity in human ESCs – introducing dominant-negative Src mutants- suppressed upregulation of prolactin and IGFBP-1 secretion after decidualisation induction. Interestingly, the inhibition of Src kinase activity was associated with reduced phosphorylation of STAT5 (Fig 4.17) (Nagashima *et al.*, 2008, Featherstone *et al.*, 2012).

The role of Src in ESC decidualisation is relevant because the members of the SFK can overlap functionally, therefore HCK might overlap functionally with Src kinase and also regulate ESC decidualisation. An example of Src and Hck functional overlap was observed on osteoclasts. $Src^{-/-}$ mice osteoclasts were osteopetrotic and their bone-resorptive capacity was defective – these mice had increased Hck expression. $Src^{-/-}Hck^{-/-}$ double mutant presented impaired haematopoiesis in the bone marrow and were sorely osteopetrotic. In addition, the birth rate of the double mutant was also decreased (Lowell *et al.*, 1996, Miyazaki *et al.*, 2006).

Although there are no studies investigating Hck phosphorylation of STATs in ESCs, Hck has been shown to phosphorylate STAT3 in rat fibroblasts (Schreiner *et al.*, 2002) and STAT5 in murine myeloid leukemia cells (Klejman *et al.*, 2002). In addition, the dominant-negative Src dESCs mutant experiments, described above, showed Src regulates STAT5 phosphorylation in dESCs - STAT5 regulates transcription of the decidual prolactin gene (Nagashima *et al.*, 2008, Featherstone *et al.*, 2012). This evidence suggests SF-EVs might enhance dESCs prolactin secretion by activating Hck which would lead to STAT5 phosphorylation and subsequent prolactin transcription (Fig 4.17).

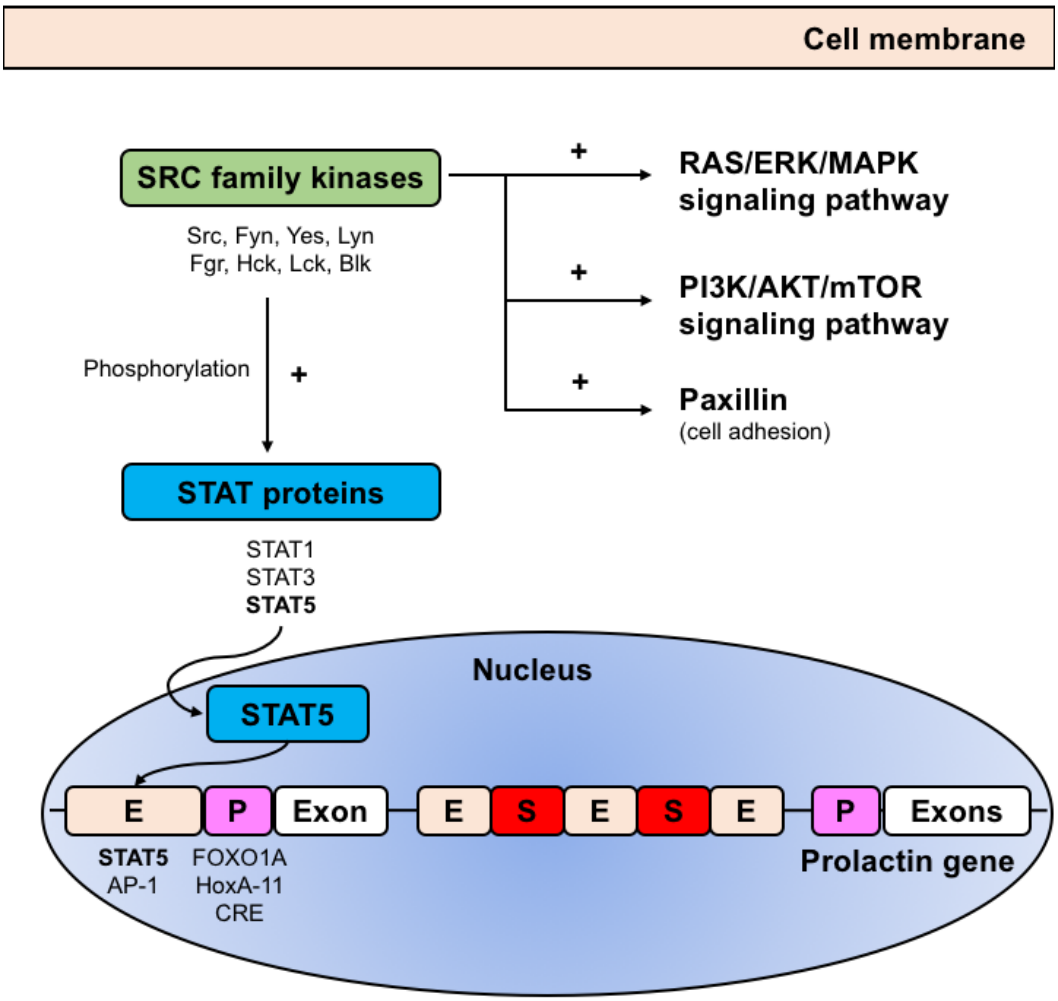


Fig 4.17 SRC family kinases signalling pathway and its relationship with dESCs prolactin gene.

SRC family kinases (SFKs) are non-receptor tyrosine kinases and includes Src, Fyn, Yes, Lyn, Fgr, Hck, Lck, and Blk. These kinases regulate multiple downstream signalling pathways, such as RAS/ERL/MAPK and PI3K/AKT/mTOR; and cell adhesion through paxillin. In addition, SFKs are involved in the non-canonical phosphorylation of signal transducer and activator of transcription (STAT) proteins, including STAT1, STAT3, STAT5. This phosphorylation activates the STAT proteins that then translocate to the nucleus to regulate gene expression. The prolactin gene contains 4 enhancer sequences (E), 2 promoters (P) and 2 silencers sequences (S). Phosphorylated STAT5 binds to the enhancer sequence near the distal promoter, which is essential for the transcription of decidual prolactin.

Interestingly, HCK is also known to play an important role in immune regulation (Guiet *et al.*, 2008, Poh *et al.*, 2015). In mice *hck*$^{-/-}$ single mutant exhibited impaired phagocytic

activity of macrophages (Lowell *et al.*, 1994), *hck*$^{-/-}$ and *fgr*$^{-/-}$ double mutant showed impaired neutrophil degranulation (Mocsai *et al.*, 1999), and *hck*$^{-/-}$*fgr*$^{-/-}$*lyn*$^{-/-}$ triple mutant depicted impaired migration and phagocytosis of immune cells (Fitzer-Attas *et al.*, 2000). In humans HCK regulates gene expression in immune cells, e.g.: HCK induces 15-lipoxygenase gene expression after IL-13 stimulation in human's monocytes (Bhattacharjee *et al.*, 2011). Based upon previous evidence, HCK might also be involved on ESCs regulation of the inflammatory environment in the endometrium during implantation.

5 The role of SF-EVs on maternal tolerance during the implantation window

5.1 Introduction

Embryo implantation and the subsequent pregnancy constitute an immunological paradox since the conceptus which contains half of the genetic material from the mother and half from the father, and is therefore semi-allogeneic to the maternal immune system, is not rejected (Munoz-Suano *et al.*, 2011, Sargent, 2013). During the menstrual cycle the endometrial immune repertoire is modulated to protect against infection and prepare the woman for a potential pregnancy. A successful pregnancy requires a complex regulation of both pro-inflammatory and anti-inflammatory responses (Wilczynski, 2005, Munoz-Suano *et al.*, 2011). For example, evidence suggests endometrial receptivity and embryo implantation are characterised by a pro-inflammatory environment in humans that promotes recruitment of immune cells, tissue remodelling (e.g.: remodelling of the spiral arteries) and embryo signalling. At the same time a tolerogenic environment is developed to prevent rejection of the embryo (Wilczynski, 2005, Ledee *et al.*, 2008, Granot *et al.*, 2012, Robertson and Moldenhauer, 2014). Accordingly, in humans, both over suppression or activation of pro-inflammatory responses in the endometrium lead to RIF (Ledee-Bataille *et al.*, 2004, Saito *et al.*, 2010).

The changes in the endometrial immunity are regulated by the cytokine and chemokine environment (Table 5.1). These cytokines and chemokines are secreted by endometrial cells under hormonal regulation, and by the trophoblast cells of the embryo (Robertson and Moldenhauer, 2014). For example, during the menstrual cycle, both oestrogen and

progesterone increase RNA levels of CXCL10[25] and CXCL11[26] in human endometrium, with higher protein levels of CXCL10 in the secretory phase, these chemokines are involved in uNK cell recruitment (Table 5.1) (Sentman *et al.*, 2004). In mice oestrogen also stimulates endometrial epithelial cell secretion of granulocyte-macrophage colony-stimulating factor (GM-CSF), while progesterone, which is secreted from the corpus luteum and the blastocyst, inhibits endometrial epithelial secretion of GM-CSF (Robertson *et al.*, 1996). In humans progesterone stimulates endometrial epithelial expression of IL-8 and monocyte chemoattractant protein 1 (MCP-1), the blastocyst also enhances IL-8 but not MCP-1 expression in these epithelial cells (Caballero-Campo *et al.*, 2002). This variation in the cytokine/chemokine profiles is associated with changes in the proportion of endometrial immune cells through the cycle (Lee *et al.*, 2015, Wira *et al.*, 2015). In humans, total endometrial immune cell ($CD45^+$) numbers increase during the secretory phase (Flynn *et al.*, 2000). From the proliferative to the secretory phase the percentage of T ($CD3^+$) cells decreases from approximately 60 % to 40 - 50 % of the leukocytes; the percentages of macrophages and uNK cells ($CD56^{bright}CD16^-$) increase from approximately 10 - 20 %, and 30 % to over 20 % and 50 % of the EICs respectively (Flynn *et al.*, 2000, Mselle *et al.*, 2007, Lee *et al.*, 2015, Wira *et al.*, 2015, Southcombe *et al.*, 2017). In early pregnancy T cells are reduced to around 10 % of the EICs while uNK cells increase to around 70 % of the EICs (Flynn *et al.*, 2000, Sargent, 2013).

[25] CXCL10: C-X-C motif chemokine ligand 10
[26] CXCL11: C-X-C motif chemokine ligand 11

Table 5.1 Examples of cytokines and chemokines involved in the immune environment

Role	Cytokines/ Chemokines	References
T cell recruitment	CCL20[27], CCL4[28], CCR5[29]	(van Mourik *et al.*, 2009, Dobaczewski *et al.*, 2010, Liu *et al.*, 2015)
uNK cell recruitment and activity	CCL3[30], IL-11, CXCL10, CXCL11, TGF-β1, IL-12, IL15	(Drake *et al.*, 2001, Eriksson *et al.*, 2004, van Mourik *et al.*, 2009)
Macrophage recruitment	CCL2[31], CCL5[32], CXCL2[33], CXCL3[34], CXCL8[35]	(Huang *et al.*, 2006, van Mourik *et al.*, 2009)

The mechanisms underlying maternal immune tolerance to the semi-allogenic fetus is one of the major questions in reproductive immunology. Importantly, the maternal immune system does not directly interact with the fetus, instead it is in contact with the placenta that develops from the trophectoderm of the blastocyst (Sargent, 2013). The trophectoderm of the implanting embryo and later the extravillous cytotrophoblast (EVT) of the placenta form the first interface contacting both individuals (Sargent, 2013). The EVT invades the endometrium anchoring the embryo to the decidua and breaking the endothelium of the spiral arteries to convert them into low-resistance high-flow arteries increasing blood flow to sustain the fetus (Sargent, 2013). uNK cells, which are characterised as $CD56^{high}CD16^{-}$ and also express CD9 and CD69 (Mselle *et al.*, 2007, Zhang *et al.*, 2016), play an important role in the remodelling of the spiral arteries (Zhang *et al.*, 2016). These uNK cells gather around the spiral arteries and assist remodelling by

[27] CCL20: C-C Motif Chemokine Ligand 20
[28] CCL4: C-C Motif Chemokine Ligand 4
[29] CCR5: Chemokine (C-C Motif) Receptor 5
[30] CCL3: C-C Motif Chemokine Ligand 3
[31] CCL2: C-C Motif Chemokine Ligand 2
[32] CCL5: C-C Motif Chemokine Ligand 5
[33] CXCL2: C-X-C motif chemokine ligand 2
[34] CXCL3: C-X-C motif chemokine ligand 3
[35] CXCL8: C-X-C motif chemokine ligand 8

direct interactions with endothelial or vascular smooth muscle cells, or by secreting metalloproteinases and angiogenic factors such as VEGF, and interferon gamma-induced protein 10 (Zhang *et al.*, 2016). By the end of the first trimester of pregnancy the syncytiotrophoblast (STB) of the placenta also contacts with the maternal blood for nutrient and gases exchange establishing a second interface between the individuals (Sargent, 2013). This second interface extends to the maternal circulation because placental cells and extracellular vesicles, as well as leaked fetal red blood cells and leucocytes enter the maternal blood system exposing embryo antigens to the immune system (Redman and Sargent, 2008, Munoz-Suano *et al.*, 2011, Sargent, 2013). To prevent fetal rejection in the endometrium neither the EVT nor STB express major histocompatibility complex (MHC) class II, the molecules which present self or non-self peptides to T helper cells for T Cell Receptor (TCR) recognition (Sargent, 2013). In addition, the STB does not express class I MHC antigens. Human EVT expresses a unique pattern of class I MHC, it lacks Human Leukocyte Antigen (HLA)-A and HLA-B, which are highly polymorphic and the contributing factor for immune rejection of tissue transplantation. On the contrary, EVT expresses HLA-C with is polymorphic, and HLA-E and HLA-G, which have low polymorphism and are pregnancy specific (Fernandez *et al.*, 1999, Hunt *et al.*, 2003, Munoz-Suano *et al.*, 2011, Sargent, 2013). The latter HLA modulate uNK cell activity, HLA-E and HLA-G inhibit uNK cytotoxicity (Ishitani *et al.*, 2006, Sargent, 2013). In addition, HLA-G and HLA-C interact with KIR receptors in uNK cells to stimulate secretion of cytokines, chemokines and angiogenic factors like VEGF (Hanna *et al.*, 2006, Sargent, 2013). HLA can also interact with T cells, and T-cell-mediated rejection seems to be prevented by regulatory T cells (see below) (Sargent, 2013). Finally, later in pregnancy placental cytokines (e.g.: IL-10 and IL-4) promote T helper 2 (Th2) cells that stimulate humoral immunity, and placental progesterone inhibits

T helper 1 (Th1) cells that suppress cell-mediated cytotoxic immunity (Wilczynski, 2005, Sargent, 2013). Clinically, we see evidence of a systemic Th1/Th2 shift in pregnancy with changes in the presentation of Th1/Th2 inflammatory or autoimmune diseases. For example rheumatoid arthritis, a Th1-driven disease, often remits during pregnancy (Ostensen and Husby, 1983, Barrett *et al.*, 1999, Ostensen and Villiger, 2007), while systemic lupus erythematosus, a Th2-driven disease, worsens during pregnancy (Doria *et al.*, 2004, Iaccarino *et al.*, 2012).

5.1.1 Endometrial T cells

T cells are $CD3^+CD45^+$ lymphocytes involved in cell-mediated adaptive immune response. There are different subtypes of T cells, including but not limited to cytotoxic T cells, Th1, Th2, T helper 17 (Th17), and regulatory T (Treg) cells (Erlebacher, 2013) – table 5.2 describes the phenotype and functional characteristics of several T cell subtypes. Data from endometrial biopsies showed $CD4^+$ T cells and $CD8^+$ T cells have similar percentages at the implantation window, approximately 20 % each of the total $CD45^+$ immune cells in the endometrium (Southcombe *et al.*, 2017). Data from human first-trimester decidua showed Treg cells constituted approximately 5 % of $CD4^+$ T cell population in early pregnancy (Mjosberg *et al.*, 2010) – to my knowledge there is no published data on the proportion of endometrial Treg cells in the implantation window. In addition, in human first-trimester decidua Th1 cells ranged from 5 - 45 % of this population while Th2 and Th17 were less than 5 % of the $CD4^+$ T cell population (Mjosberg *et al.*, 2010, Erlebacher, 2013).

Table 5.2 Main characteristics of T cell subtypes.
(Drake *et al.*, 2001, Eriksson *et al.*, 2004, van Mourik *et al.*, 2009, Kenneth Murphy, 2017)

Type of T cell	General Phenotype	Function	Secretion
Cytotoxic T cells	$CD3^+CD8^+CD4^-$	To kill cells infected with intracellular pathogens	Perforin, Granzymes, Granulysin
Th1 T cells	$CD3^+CD4^+CD8^-$ $T\text{-}bet^+$	To promote cellular immunity and rejection	IL-2, IFNγ, TNF-β
Th2 T cells	$CD3^+CD4^+CD8^-$ $GATA\text{-}3^+$	To promote humoral immunity	IL-4, IL-5, IL-13
Th17 T cells	$CD3^+CD4^+CD8^-$ ROR C2/ROR-α^+	To promote inflammation	IL-17
CD4+ Regulatory T cells	$CD3^+CD4^+FoxP3^+CD25^+CD127^-$	To promote immune regulation and tolerance	IL-10 TGF-β

In the stromal and epithelial layers of the proliferative endometrium $CD8^+$ T cells are scattered and form small aggregates (Yeaman *et al.*, 1997). In the late secretory phase $CD8^+$ cytotoxic T cells condensate into lymphoid aggregates (Yeaman *et al.*, 1997). The lymphoid aggregates are immune structures in the stratums basalis of the endometrium formed by a core of B cells (minor population of EICs), surrounded by a $CD8^+$ rich T cell population, and limited by macrophages (Yeaman *et al.*, 1997). Interestingly, the cytotoxic activity of $CD8^+$ T cells was shown to be specifically suppressed in the secretory endometrium while maintained in the lower tract of the female reproductive system in humans (White *et al.*, 1997).

Endometrial receptivity to embryo implantation and successful pregnancy are characterised for a Th1/Th2/Th17/Treg cells paradigm (Saito *et al.*, 2010). As mention

previously, Th1 pathways are required in the peri-implantation period while a shift to Th2 pathways is essential later in pregnancy. In addition, endometrial receptivity and early pregnancy requires high Treg/Th17 cell ratio, (Saito *et al.*, 2010). Progenitor cells develop into Treg/Th17 intermediate cells that depending on the environment result into Treg cells or Th17. For examples, dendritic cells present antigens to Treg/Th17 intermediate cells and secrete IL-6, IL-1, or TGF-β. High levels of TGF-β induce development of Treg cells and inhibit Th17 differentiation, Th17 differentiation requires low TGF-β levels and IL-6, as well as IL-1. In addition, Treg and Th17 cells show high plasticity and differentiated Treg cells can transform into Th17 and vice versa to adapt to the environment (Peck and Mellins, 2010). Consequently, environmental insults during the implantation window, infections, and other pathologies can modify the fine tuning of Treg/Th17 cell balance hindering maternal tolerance, embryo implantation or pregnancy.

5.1.1.1 Regulatory T cells

Treg cells are regulators of the immune response with high immunosuppressive capability (Mills, 2004, Saito *et al.*, 2013, Robertson and Moldenhauer, 2014). They suppress inflammation, cell-meditated immunity - including $CD8^+$ T cells, Th1 and Th17 responses, B cells, NK cells, and monocytes (Piccirillo and Shevach, 2001, Ghiringhelli *et al.*, 2005, Lim *et al.*, 2005, Taams *et al.*, 2005). Treg cells prevent excessive immune activation that would damage the organism, indeed defective Treg cell-mediated immunity can lead to autoimmunity (Paterson *et al.*, 2015, Yang *et al.*, 2018). The Forkhead Box P3 (FoxP3) transcription factor is the master regulator of Treg cells, Treg cells also express high levels of the IL-2 receptor, CD25, and the suppressive function of Treg inversely correlates with CD127 (Fontenot *et al.*, 2003, Hori *et al.*, 2003, Liu *et al.*,

2006, Dimova *et al.*, 2011). Therefore, these cells are often characterised as $CD3^{+}CD4^{+}CD25^{high}FoxP3^{+}CD127^{-}$.

The role of Treg cells in endometrial receptivity and pregnancy has been demonstrated by various publications (Aluvihare *et al.*, 2004, Kahn and Baltimore, 2010, Shima *et al.*, 2010, Zhang *et al.*, 2012, Saito *et al.*, 2013, Robertson and Moldenhauer, 2014, Schumacher and Zenclussen, 2014). Adoptive transfer of Treg depleted T cells to T cell deficient mice allowed progression of syngenic pregnancies (identical MHC phenotypes between parents) but allogenic fetuses were rejected (Aluvihare *et al.*, 2004). Depletion of Treg cells using denileukin diftitox (IL-2 coupled with diphtheria toxin) in syngenic pregnancies also resulted in less live males and male birth weight in mice (Kahn and Baltimore, 2010). Evidence suggest Treg cells are more important at the peri-implantation period than later in pregnancy. In mice depletion of Treg cells 2.5 days after coitum leads to implantation failure, while depletion of these cells after implantation on day 4.5 or 7.5 after coitum had a less severe phenotype but increased miscarriage rate; depletion in mid or late gestation did not have any adverse effect (Shima *et al.*, 2010).

Treg cells regulate the immune system through multiple mechanisms (Fig 5.1), including: 1) interaction with APC blocking activation of T cell signalling, 2) membrane expression of CD25 sequestering environmental IL-2, which is required for effector T cell proliferation and activation, 3) IL-10 secretion that inhibits APC activation of the immune response and production of pro-inflammatory cytokines, and 4) membrane and soluble expression of TGF-β that inhibits T cell proliferation (Kenneth Murphy, 2017). TGF-β is expressed in its inactive form associated with the latency-associated peptide (LAP) (Fig 5.1) (Khalil, 1999). The mechanisms by which endometrial Treg cells induce maternal

tolerance in implantation and pregnancy remain unclear. Human endometrial Treg cells express CTLA-4[36], a high affinity inhibitory receptor that interact with B7 ligand on APC inhibiting their co-stimulatory capability and increasing APC IDO secretion (Miwa *et al.*, 2005, Jin *et al.*, 2009). In addition, a murine study suggested endometrial Treg cellular immunosuppression might be dependent on IL-10, with less dependency on TGF-β; neutralizing TGF-β only partially suppressed the abortion preventing effect of endometrial Treg cells (Schumacher *et al.*, 2007).

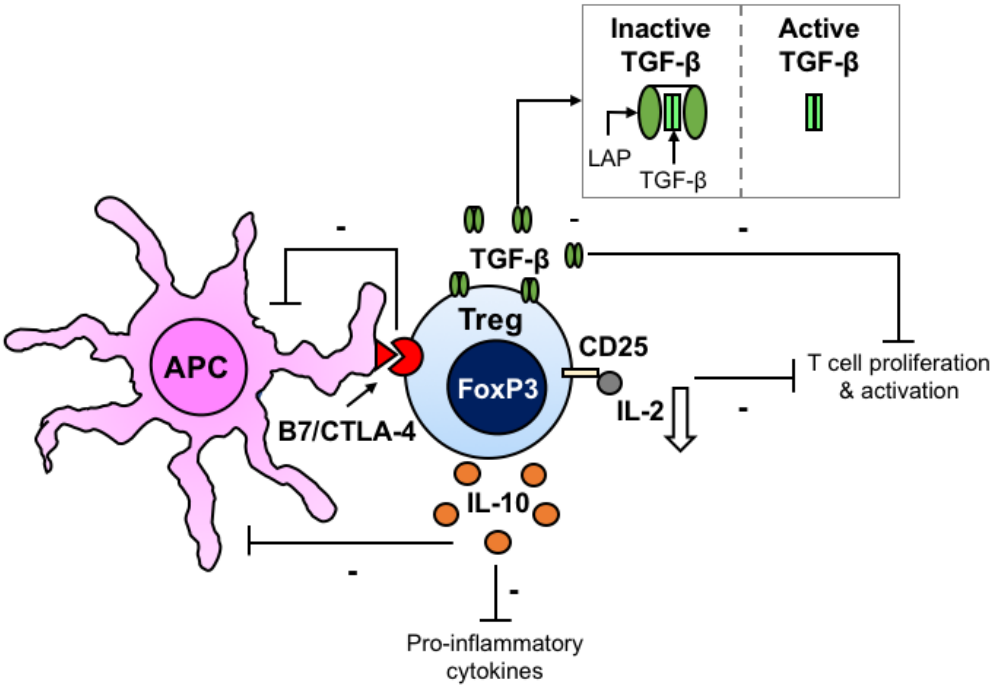


Fig 5.1 Regulatory T cells (Treg) mechanisms of immune suppression.
Treg cells block antigen presenting cells (APC) through CTLA-4/B7 interaction and secretion of IL-10, the latter also inhibits secretion of pro-inflammatory cytokines. Treg cells also express membrane CD25 to sequester extracellular IL-2, and membrane and soluble TGF-β - these inhibit T cells proliferation and activation. TGF-β is produced inactive associated with the latency-associated peptide (LAP).

[36] CTLA-4: Cytotoxic T-Lymphocyte Associated Protein 4

5.1.2 Endometrial regulatory T cells in reproductive pathologies

An altered endometrial immune Treg cell environment has been described in several human reproductive pathologies. Women with primary unexplained infertility have reduced FoxP3 mRNA levels in mid-secretory endometrium (Jasper *et al.*, 2006). In addition, immunohistochemistry studies showed women with RIF and recurrent pregnancy loss (RPL) had significantly less $FoxP3^+$ Treg cells in the mid-secretory endometrium than healthy controls (Galgani *et al.*, 2015, Diao *et al.*, 2017). RPL has been widely associated with lower numbers of Treg cells. For instance, $FoxP3^+$ Treg cells were significantly reduced in the decidua of miscarriage patients with normal but not abnormal embryos in samples analysed by both immunohistochemistry and flow cytometry (Inada *et al.*, 2013). Other flow cytometry studies also showed a decrease in decidual Treg cells in spontaneous abortion and RPL (Sasaki *et al.*, 2004, Yang *et al.*, 2008, Bao *et al.*, 2011). It must be mentioned, that another immunohistochemically study showed increased numbers of $FoxP3^+$ Treg cells in the decidua of spontaneous abortion and RPL patients (Freier *et al.*, 2015). Interestingly, women with spontaneous miscarriage also exhibited reduced peripheral Treg cells (Jin *et al.*, 2009), suggesting that measurement of peripheral $CD4^+CD25^+FoxP3^+$ Treg levels could be a marker of miscarriage risk in newly pregnant women (Winger and Reed, 2011). Pre-eclampsia, a major complication in pregnancy with associated systemic inflammation and defects in early placentation events (Redman and Sargent, 2010), is also associated with reduced Treg cells in the endometrium. For example, Sasaki *et al*. 2007 showed decreased proportions of Treg cells in the placenta of women with pre-eclampsia (Sasaki *et al.*, 2007). In addition, women with pre-eclampsia have reduced FoxP3 mRNA levels in the placenta (Liu *et al.*, 2011).

5.1.3 Seminal fluid effect on maternal tolerance

Evidence suggests seminal fluid primes the endometrium to tolerate pregnancy; epidemiological studies show that regular unprotected intercourse with the father prior conception reduced the incidence of pre-eclampsia (Marti and Herrmann, 1977, Robillard *et al.*, 1994, Robertson *et al.*, 2003, Kho *et al.*, 2009). On the other hand, multiple sexual partners is associated with an increased risk of this inflammatory pathology of pregnancy (Need, 1975, Feeney and Scott, 1980). Murine studies demonstrate seminal fluid promotes EICs immunomodulation (Robertson *et al.*, 2013, Robertson and Moldenhauer, 2014, Robertson and Sharkey, 2016, Nederlof *et al.*, 2017); maternal exposure to seminal fluid enhances EICs recruitment and promotes endometrial Treg cell expansion (Robertson *et al.*, 2009). In humans, unprotected intercourse before ovulation increases uNK cells in the mid-secretory endometrium (Kimura *et al.*, 2009). *In vitro* human studies also showed that seminal fluid promotes a tolerogenic phenotype in dendritic cells and increases IL-10, and CD25 expression in peripheral T cells (Remes Lenicov *et al.*, 2012, Meuleman *et al.*, 2015).

5.1.3.1 Immunoregulatory roles of SF-EVs

There have been previous reports that SF-EVs have immunoregulatory capability (Ronquist and Nilsson, 2004, Aalberts *et al.*, 2014, Saez and Sullivan, 2016). SF-EVs bind to blood lymphocytes -T and B cells-, polymorphonuclear cells and monocytes (Skibinski *et al.*, 1992). In addition, SF-EVs immunosuppress lymphocyte proliferation (Kelly *et al.*, 1991). An *in vitro* study also demonstrated polymorphonuclear cells and monocytes internalized SF-EVs, which induced inhibition of latex particles phagocytosis but not of opsonized bacteria (Skibinski *et al.*, 1992). SF-EVs also suppress the NADPH[37]

[37] NADPH: Nicotinamide adenine dinucleotide phosphate

oxidase activity and the subsequent production of reactive oxygen species by blood and seminal neutrophils (Saez *et al.*, 1998, 2000). Moreover, SF-EVs carry CD48 which interacts with the CD244, the activating receptor of NK cells - they induce downregulation of this receptor in a dose-dependent manner in blood NK cells (Tarazona *et al.*, 2011). SF-EVs also carry CD59, an inhibitory protein of the membrane attack complex of the complement system (Rooney *et al.*, 1993). To the date there are no studies in the literature on SF-EVs effect on endometrial immune cells (EICs).

Pilot data in Dr. Granne's research group showed SF-EVs carry HLA-antigens, which could stimulate endometrial Treg cells via the canonical TCR/CD3 complex-dependent pathway (Fig 5.2). The TCR/CD3 complex-dependent pathway involves antigen stimulation of the TCR, whose C domains associate with CD3. CD3 contains immunoreceptor tyrosine-based activation motifs (ITAMs) that are then phosphorylated by tyrosine kinases recruited by the co-receptors CD4 or CD8. Phosphorylated ITAMs recruit other intermediate proteins, such as ZAP-70[38] in T $CD4^+$ cells, that trigger multiple signalling pathways involved in immune function, such as increased expression of CD25 (Malissen and Bongrand, 2015, Kenneth Murphy, 2017). Apart from CD4 and CD8, other membrane co-stimulatory receptors, such as CD2 and CD28, enhance TCR/CD3 complex-dependent T cell activation. I hypothesize that SF-EVs might promote endometrial Treg tolerance interacting with the TCR/CD3 complex.

[38] ZAP-70: Zeta Chain Of T Cell Receptor Associated Protein Kinase 70

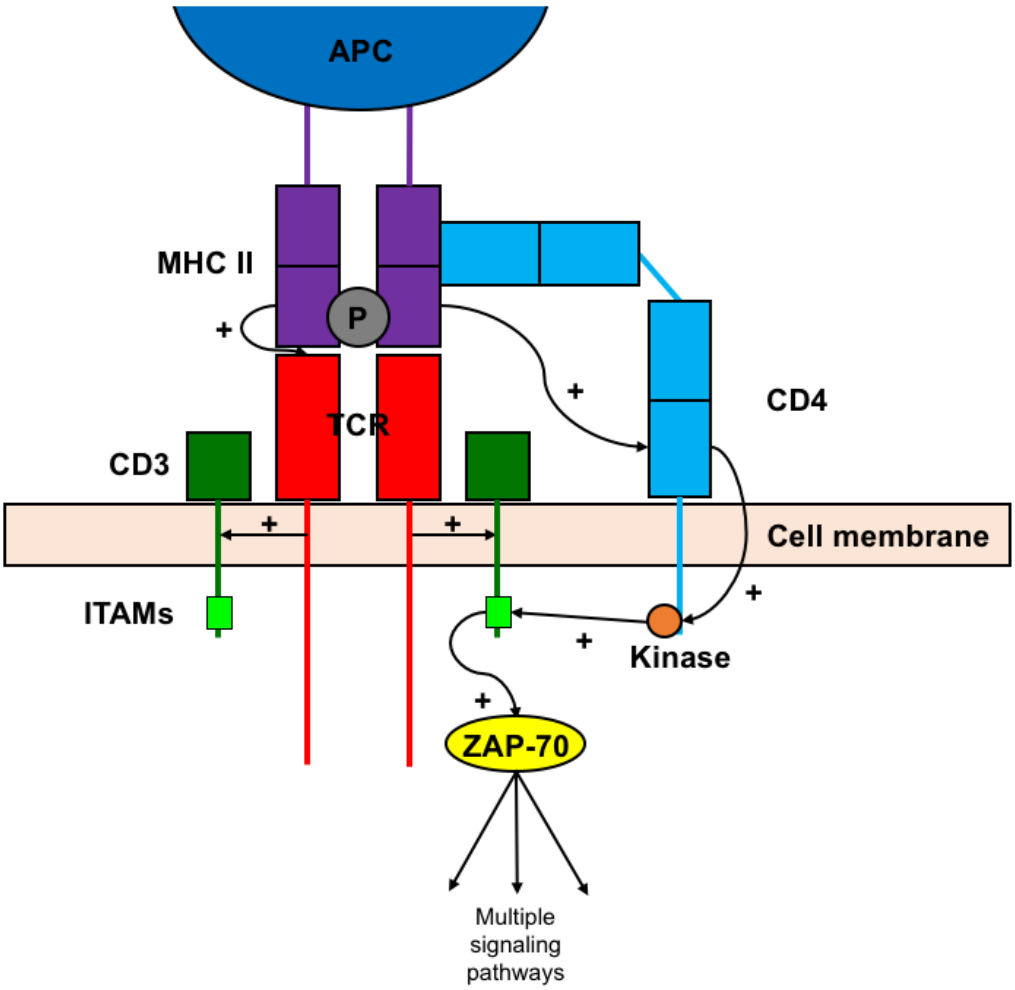


Fig 5.2 TCR/CD3 complex-dependent pathway in CD4$^+$ T cells.
An antigen presenting cell (APC) presents antigenic peptide on the major histocompatibility class II complex (MHC II), this is recognised by a specific T cell receptor (TCR) and CD3 becomes then activated after ITAMs phosphorylation by a CD4 activated kinase such as Lck. CD3 then recruits ZAP-70 initiating multiple signalling pathways and downstream effector functions. P = peptide, ITAMs = immunoreceptor tyrosine-based activation motifs

5.2 Aims of the chapter

1) To investigate if SF-EVs bind to EICs
2) To determine if SF-EVs can induce maternal tolerance
3) To characterise endometrial regulatory T cells

5.3 Methods

5.3.1 *In vitro* culture of JY cells

JY cell line, a B cell line immortalised by an Epstein-Barr virus, were obtained from Dr. Kalle Soderstrom (The Botnar Research Centre, University of Oxford). JY cells were cultured in Iscove's Modified Dulbecoo's Medium (Sigma-Aldrich, USA), supplemented with 10 % FCS, penicillin (100 IU/ml), streptomycin (100 µg/ml), and 2 mM L-glutamine. Cells were cultured at 37°C, 20 % O_2 and 5 % CO_2. Culture media was added every 2 days and cell passage performed when ~ 80 % of confluence was reached.

5.3.2 Subject Recruitment

As previously described endometrial biopsies were obtained from patients attending IVF at Oxford Fertility (n = 14). Patients characteristics are described in appendix 5.

Ethical approval for the peripheral blood mononuclear cells (PBMCs) were obtained from the Oxford South Central Regional Ethics Committee - #08/H0606/94. PBMCs were isolated from blood samples collected from two healthy female donors that were not taking hormonal contraception.

5.3.3 Isolation of primary endometrial immune cells

EICs were isolated from endometrial biopsies. Briefly, endometrial biopsies were transferred to a petri dish with PBS and fine minced with 2 scalpel blades, size 11. The minced biopsies were then enzymatically digested with 1X Liberase (10 mg/biopsy) (Roche, Germany), and DNAse I (500 IU/biopsy) (Sigma-Aldrich, USA) in 2 mL of immune cell culture media (see below) for 30 min at 37 °C in a shaking water bath. The digested samples were then resuspended in 10 mL of immune cell culture media and

passed through a 70 µm cell strainer. The eluates were then passed through a 40 µm cell strainer (Corning, USA) and centrifuged at 300 x g for 3 min. The pellets contained primary EICs. Samples were resuspended in immune cell culture media for binding studies or frozen in 10 % dimethyl sulfoxide (ROMIL Ltd, UK)/FCS for later functional studies.

Immune cells culture media: RPMI [39] -1640 medium (Sigma-Aldrich, USA), supplemented with 10 % FCS, penicillin (100 IU/ml), streptomycin (100 µg/ml), 2 mM L-glutamine, amphotericin B (2.5 µg/ml), and 2 % human serum (Sera Laboratories International Ltd, UK).

5.3.4 Isolation of Peripheral Blood Mononuclear Cells (PBMCs)

Venous blood was collected and coagulation prevented with sodium heparin (10 IU/mL) (Wockhardt, Wrexham, UK). Blood samples were diluted 1:1 with PBS and layered onto 5 ml Lymphoprep™ (Axis-Shield, Norway). Samples were then centrifuged at 300 x g for 30 min at RT without the brake separating the PBMCs by density gradient centrifugation. Afterwards, the PBMC layer was collected and the cells were washed with PBS twice, first at 400 x g for 10 min, and secondly at 100 x g for 10 min. The pellets containing the PBMCs were resuspended in immune cell culture media for following experiments.

5.3.5 Isolation and *in vitro* culture of expanded endometrial Treg cells

In vitro cultures of expanded endometrial Treg cells were obtained from endometrial biopsies using the EICs isolated at the same time as EECs in chapter 3. EICs were cultured

[39] RPMI: Roswell Park Memorial Institute

with immune cell media supplemented with IL-15 (10 ng/mL) (PeproTech EC Ltd, UK) and TGF- β (10 ng/mL) (PeproTech EC Ltd, UK) for 1 week. After a week $CD4^+$ EICs were isolated using CD4 MicroBeads (Milteny Biotec, UK). Briefly, cells were counted and centrifuged at 300 x g for 10 min at RT. Pellets were then resuspended in 80 µl of isolation buffer (see below) and 10 µl of CD4 MicroBeads were added. The solutions were mixed thoroughly and incubated for 15 min at 4°C. Afterwards, cells were washed in isolation buffer at 300 x g for 10 min at RT. $CD4^+$ EICs were then separated using MS columns (Milteny Biotec, UK). MS columns were initially placed within the magnet (Milteny Biotec, UK) and equilibrated with 500 µl of isolation buffer. EICs solution was then applied into the column. $CD4^+$ EICs remained in the column attached to the magnetic field while unlabelled $CD4^-$ EICs passed through the column. $CD4^-$ EICs were washed adding 500 µl of isolation buffer three times. To extract $CD4^+$ EICs the columns were removed from the magnetic field and the $CD4^+$ T cells were eluted in 1 mL of isolation buffer by pushing a plunger into the column.

The Treg population in the isolated $CD4^+$ T cells was then expanded stimulating cell proliferation with a feeder mixture containing $1x10^6$ irradiated PBMCs (7,500 RAD) and $1x10^5$ irradiated JY cells (7,500 RAD) per $2.5x10^5$ $CD4^+$ T cells with 0.1 µg/mL phytohaemagglutinin (Sigma-Aldrich, USA) in immune cell culture media supplemented with IL-15 (10 ng/mL) and TGF-β (10 ng/mL). IL-15 and TGF-β in the culture media promoted Treg cell proliferation.

Cells were cultured at 37°C, 20 % O_2 and 5 % CO_2. New immune cell media supplemented with IL-15 (10 ng/mL) and TGF-β (10 ng/mL) was added every 2 days and cells passage performed when ~ 80% of confluence was reached.

Isolation buffer: 0.5 % BSA + 2 mM EDTA in PBS.

5.3.5.1 Bright field microscopy

Bright field microscopy was performed as described in chapter 3.

5.3.6 SF-EV isolation and purification

SF-EVs were isolated and purified as described in chapter 2.

5.3.7 Flow cytometry binding studies

All flow cytometry experiments were analysed using a BD LSRII flow cytometer and results were assessed using FlowJo software version 10.4.2. Compensation matrix were generated using BD Biosciences compensation beads. MeFI were measured and the increase calculated by subtracting the MeFI of the control group to the SF-EV treated group. In addition, the percentage of cells were determined subtracting 1 % gate on the negative control.

SF-EV binding to EICs was assessed by flow cytometry as previously described in chapter 2 with some modifications. Freshly isolated endometrial digests were further enriched for non-adherent EIC by incubation of cells on Nunc tissue culture plates to which ESC and EEC adhere with overnight incubation at 37°C. The live immune cells were further purified using Lymphoprep^{TM} as described above for PBMCs isolation. Then, EICs were counted and the samples were divided in two and treated with bio-maleimide labelled SF-EV preparation # 4 or the negative control for 2 hrs at 37°C ($5x10^{10}$SF-EVs/10^6 cells). After incubation, EICs were divided in two and washed in 2

% FCS/PBS at 300 x g for 5 min. Different types of EICs were then identified by 5-colour flow cytometry. Table 5.3 shows the two panels of 5 antibodies used to identify each cell type. Panel 1 identified uNK cells, $CD4^+$ T cells, and $CD8^+$ T cytotoxic cells. Panel 2 identified non-Treg $CD4^+$ T cells and Treg cells. Initially cell membrane proteins were labelled in both panels. Afterwards, in panel 2 the nuclear transcription factor FoxP3 was labelled following manufacturer's instructors. The staining protocols are described below.

Table 5.3 Antibody-fluorochrome combinations used to identify (Panel 1) uNK cells, $CD4^+$ T cells, $CD8^+$ T cells, and (Panel 2) non-Treg $CD4^+$ T cells and Treg cells.

	Antibodies					
Fluorochromes	PerCP[40] Cy5.5	APC Cy7	PE Cy7	PE[41]	APC	Alexa Fluor® 647
Panel 1	CD3	CD16	CD56	CD8	CD4	-
Panel 2	CD3	CD4	CD25	CD127	-	FoxP3

5.3.7.1 Cell membrane staining

Cell pellets were resuspended in 100 µl of 2 % FCS/PBS and incubated with fluorescence antibodies against membrane proteins (Table 5.4) for 20 min in the dark in ice. After incubation, EICs were washed with 2 % FCS/PBS at 300 x g for 5 min and pellets were resuspended in 400 µl of 2 % FCS/PBS for flow cytometry analysis.

5.3.7.2 Intracellular staining for nuclear proteins

After cell membrane staining intranuclear staining of FoxP3 was performed using True-Nuclear™ Transcription Factor Buffer Set (BioLegend, USA). EICs for panel 2 were treated with the Transcription Factor 1X Fix solution (BioLegend, USA) for 45 min in

[40] PerCP: Peridinin chlorphyll protein
[41] PE: R-phycoerythrin

the dark at RT. Transcription Factor 1X Perm Buffer (PB) (BioLegend, USA) was then added and the samples were centrifuged at 300 x g for 5 min at RT. Supernatants were discarded and the pellets were resuspended in PB and centrifuged as before. Cells were then resuspended in 100 µl PB and incubated with antibodies towards FoxP3 conjugated to Alexa Fluor® 647 (Table 5.4) for 30 min in the dark at RT. Afterwards, the cells were washed in PB at 300 x g for 5 min at RT and resuspended in 400 µl of 2 % FCS/PBS for flow cytometry analysis.

Table 5.4 Fluorescence conjugated antibodies used for flow cytometry.
All antibodies were purchased from BioLegend (USA).

Antibody	Concentration	Source	Clones
Membrane proteins			
Anti-human CD3 (PerCP Cy5.5)	Panel 1 – 10 µg/ml Panel 2 – 5 µg/ml	Mouse	OKT3
Anti-human CD16 (APC Cy7)	6 µg/ml	Mouse	3G8
Anti-human CD56 (PE Cy7)	5 µg/ml	Mouse	5.1H11
Anti-human CD8 (PE)	0.3 µg/ml	Mouse	HIT8a
Anti-human CD4 (APC)	1.5 µg/ml	Mouse	OKT4
CD4 (APC Cy7)	1.5 µg/ml	Mouse	OKT4
Anti-human CD127 (IL-7Rα) (PE)	5 µg/ml	Mouse	A019D5
Anti-human CD25 (PE Cy7)	5 µg/ml	Mouse	BC96
Nuclear proteins			
Anti-human FoxP3 (Alexa Fluor® 647)	6 µg/ml	Mouse	259D

5.3.7.3 Identification of endometrial uNK cells, $CD4^+$ T cells, and $CD8^+$ T cytotoxic cells

CD3 is a signalling complex associated with the TCR required for cell-surface TCR signal transduction. T cells were identified within the $CD3^+$ lymphocyte population. T cells are divided into different populations, including non-Treg $CD4^+$ T cells and Treg cells - both of which express CD4 a co-receptor for MHC class II. On the contrary CD8 is a co-receptor for MHC class I, which is expressed by cytotoxic T cells. Therefore, non-Treg $CD4^+$ T cells and Treg cells were detected together within the $CD4^+$ T cell population while cytotoxic T cells were identified within the $CD8^+$ T cell population (Fig 5.3). uNK cells were within the $CD3^-$ lymphocyte population, in addition, uNK cells are characterised by high levels of expression of the adhesion molecule CD56 and lack of CD16, a signalling complex involved in NK cells cytotoxicity (Zhang *et al.*, 2016). Therefore, endometrial NK cells were identified within the $CD3^-CD56^{bright}CD16^-$ lymphocyte population (Fig 5.3).

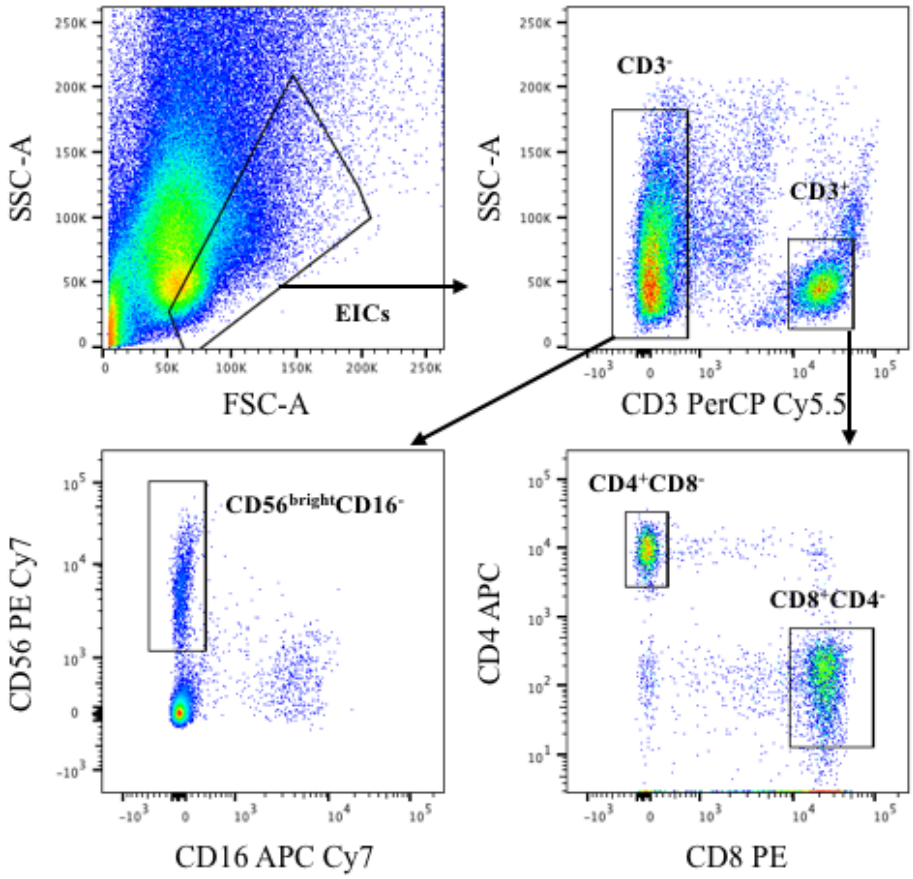


Fig 5.3 Flow cytometry identification of primary endometrial $CD4^+$ and $CD8^+$ T cells, and NK cells.

Endometrial biopsies were digested and single cell suspensions stained with the antibodies CD3 PerCP Cy5.5, CD4 APC, CD8 PE, CD56 PE Cy7, and CD16 APC Cy7 for flow cytometry acquisition and cell type identification. EIC gating on FSC-A vs SSC-A plots was identified by back gating from $CD3^+$ and $CD56^+$ events. $CD4^+$ T cells = $CD3^+CD4^+CD8^-$. $CD8^+$ T cells = $CD3^+CD8^+CD4^-$. NK cells = $CD3^-CD56^{bright}CD16^-$.

5.3.7.4 Identification of endometrial non-Treg $CD4^+$ T cells and Treg cells

As mentioned above, non-Treg $CD4^+$ T cells and Treg cells were detected within the $CD3^+CD4^+$ lymphocyte population. FoxP3 is a transcription factor essential for Treg development and function. Therefore, non-Treg $CD4^+$ T cells were detected as $FoxP3^-$ within the population of $CD3^+$ $CD4^+$ T cells (Fig 5.4). Treg cells are also characterised by the expression of CD25, IL-2 receptor, and the lack of CD127, IL-7 receptor (Fontenot *et al.*, 2003, Hori *et al.*, 2003, Liu *et al.*, 2006, Dimova *et al.*, 2011). Consequently, Treg

cells were identified as FoxP3^{+}CD25^{high}CD127^{-} within the population CD3^{+}CD4^{+} T cells (Fig 5.4).

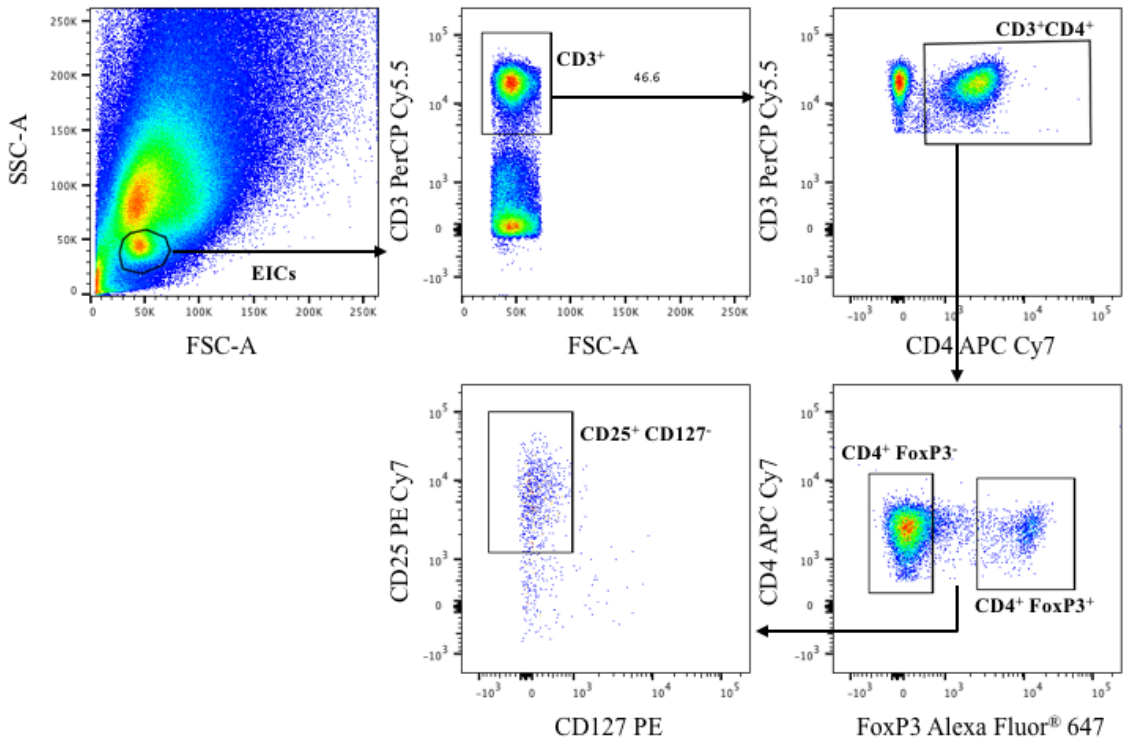


Fig 5.4 Flow cytometry identification of primary endometrial non-Treg CD4^{+} T cells and T regulatory cells.
Endometrial biopsies were digested and single cell suspensions stained with the antibodies CD3 PerCP Cy5.5, CD4 APC Cy7, FoxP3 Alexa Fluor® 647, CD25 PE Cy7, and CD127 PE for flow cytometry acquisition and cell type identification. Non-Treg CD4^{+} T cells = CD3^{+}CD4^{+}FoxP3^{-}. T regulatory cells = CD3^{+}CD4^{+}FoxP3^{+}CD25^{bright}CD127^{-}.

5.3.8 Flow cytometry functional studies

5.3.8.1 Endometrial CD4^{+} T cells

Frozen endometrial tissue digests were defrosted, resuspended in immune cell culture media supplemented with IL-15 (10 ng/mL), and plated overnight on a six well culture plate (Nunc) at 37°C. EICs were then further purified using Lymphoprep™ as previously described. EICs were counted and the samples were divided in three, and treated with

PBS (non-stimulated), CD3/CD28 beads (Thermo Fisher, USA) (positive control, 1:1 bead-to-cell ratio), or SF-EV preparation # 3 ($5x10^{10}$ SF-EVs/10^6 cells) for 24 hrs at 37°C. 5 hrs before the end of the incubation time 1X Brefeldin A (Thermo Fisher, USA) was added. After incubation, EICs were washed in PBS by centrifugation at 300 x g for 5 mins and labelled with the viability dye Zombie Aqua (Table 5.6) in PBS for 15 min in the dark at RT. Cells were then washed in 2 % FCS/PBS at 300 x g for 5 min. T cell activation and immunosuppressive capability were then investigated by 6-colour flow cytometry - table 5.5 shows the panels of 6 antibodies used. Cell membrane staining was performed as described above – the antibodies used are described in table 5.6, then intracellular cytokine staining was performed following manufacturer's instructions - the protocol is described below.

Table 5.5 Antibody-fluorochrome combinations used to identify membrane CD3 and CD25, and intracellular TGF-β1 expression in $CD4^+$ T cells

	Antibodies					
Fluorochromes	BV650	APC fire	PE Cy7	BV711	PE Dazzle 594	FITC
Panel 1	CD45	CD3	CD4	CD8	CD25	LAP (TGF-β1) / Isotype

5.3.8.1.1 Intracellular cytokine staining

EIC pellets were fixed with 500 µl of FluoroFix™ Buffer (BioLegend, USA) for 20 min in the dark at RT. Cells were then centrifuged at 300 x g for 5 min and resuspended in 500 µl 1X intracellular staining perm wash buffer (IPB) (BioLegend, USA) diluted in deionized water. EICs were then centrifuged at 300 x g for 10 min. The pellets were resuspended in 600 µl of IPB, divided in two and centrifuged at 300 x g for 5 min. Afterwards, the cells were resuspended in 100 µl of IPB and incubated with the target-antibodies toward LAP (TGF-β1) and the isotype control (Table 5.6) for 20 min in the

dark at RT. After incubation, the samples were washed twice with 1 mL of IPB at 300 x g for 5 min and resuspended in 400 µl of 2 % FCS / PBS for flow cytometry analysis.

Table 5.6 Fluorescence conjugated antibodies used for flow cytometry.
All antibodies were purchased from BioLegend (USA).

Antibody	Dilution / Concentration	Source	Clones
Zombie Aqua (BV510[42])	1:1000	-	-
Membrane proteins			
Anti-human CD45 (BV650[43])	0.5 µg/ml	Mouse	HI30
Anti-human CD3 (APC/Fire™)	6 µg/ml	Mouse	UCHT1
Anti-human CD4 (PE Cy7)	4.5 µg/ml	Mouse	OKT4
Anti-human CD8a (BV711[44])	0.4 µg/ml	Mouse	RPA-T8
Anti-human CD25 (PE Dazzle™ 594)	3 µg/ml	Mouse	M-A251
Cytoplasmic cytokines			
Anti-human LAP (TGF-β1) (FITC[45])	6 µg/ml	Mouse	TW4-2F8
Mouse IgG1, k Isotype Ctrl (FITC)	6 µg/ml	Mouse	MOPC-21

5.3.8.1.2 Identification of $CD4^+$ T cells

Live leukocytes were identified as Zombie $Aqua^{low}$ and $CD45^+$ population. Endometrial $CD4^+$ T cells were then detected together within the $CD4^+$ population of $CD45^+$ EICs (Fig 5.5). Afterwards, membrane CD3 and CD25 protein expression and intracellular

[42] BV510: Brilliant™ Violet 510
[43] BV650: Brilliant™ Violet 650
[44] BV711: Brilliant™ Violet 711
[45] FITC: Fluorescein isothiocyanate

expression of the cytokine TGF-β1 in non-stimulated, CD3/CD28 stimulated and SF-EV treated $CD4^+$ T cells were determined.

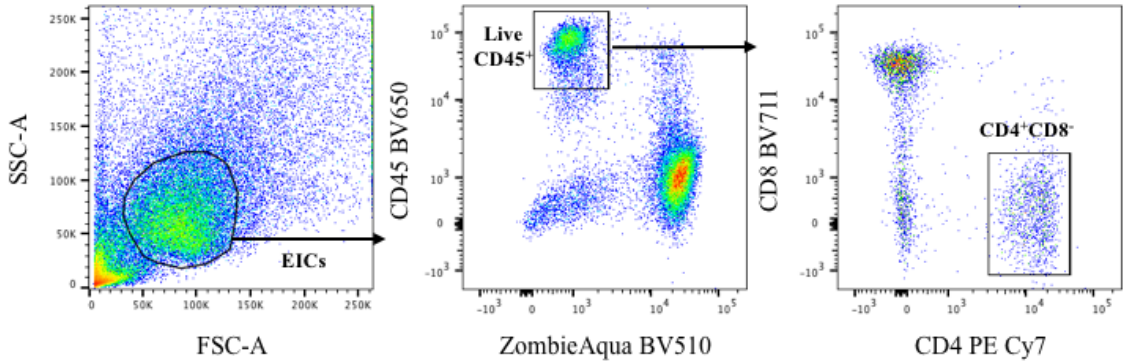


Fig 5.5 Flow cytometry identification of live primary endometrial $CD4^+$ T cells. Endometrial biopsies were digested and single cell suspensions stained with Zombie Aqua viability dye and antibodies CD45 BV650, CD4 PE and CD8 BV711 for flow cytometry acquisition and cell type identification.

5.3.8.2 In vitro expanded Treg cells

In vitro expanded Treg cells were cultured in immune cell culture media supplemented with IL-15 (10 ng/mL) alone for 24 hrs. Treg cells were then counted and divided in three groups to be treated with PBS (non-stimulated), CD3/CD28 beads (positive control, 1:1 bead-to-cell ratio), or SF-EV preparation # 1 ($5x10^{10}$SF-EVs/10^6 cells) for 24 hrs at 37°C. After incubation Treg cells were divided in two and washed in 2 % FCS/PBS at 300 x g for 5 min. Treg cell activation and immunosuppressive capability were then investigated by flow cytometry - table 5.7 shows the panel of 4 antibodies used. Cell membrane staining was performed as described above, an isotype IgG1 control of LAP (TGF-β1) was used. Afterwards, FoxP3 was labelled following the protocol for intracellular staining for nuclear proteins described above. CD3 and FoxP3 antibodies are described in table 5.4. CD4, LAP (TGF-β1) antibody, and the isotype are described in table 5.6, for these experiments 10 µg/ml LAP (TGF-β1) antibody or isotype IgG1 control were used.

Table 5.7 Antibody-fluorochrome combinations used to identify CD3 and CD25 expression in Treg cells.

	Antibodies			
Fluorochromes	PerCP Cy5.5	PE Cy7	Alexa Fluor® 647	FITC
Panel 1	CD3	CD4	FoxP3	LAP (TGF-β1) / Isotype

5.3.8.2.1 Identification of Treg cells

Endometrial Treg cells were identified within the $CD3^+CD4^+FoxP3^+$ lymphocyte population (Fig 5.6). Membrane expression of CD3 and LAP (TGF-β1) was analysed in untreated, CD3/CD28 treated and SF-EV treated cells.

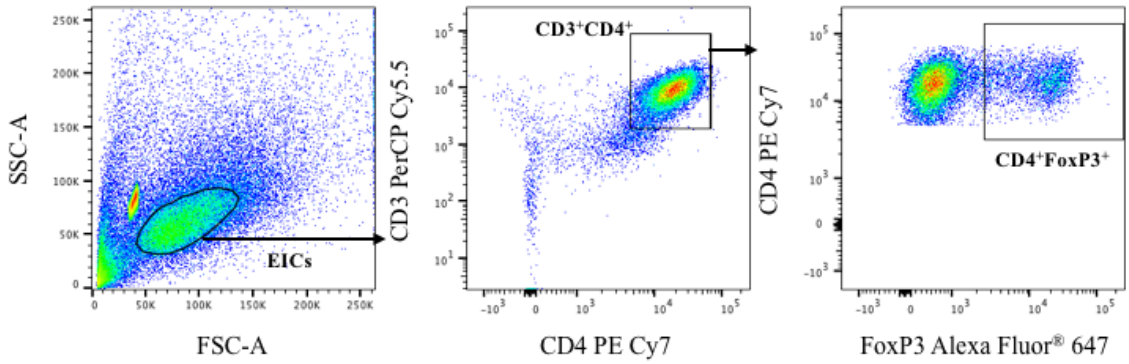


Fig 5.6 Flow cytometry identification of *in vitro* expanded endometrial T regulatory cells.
Endometrial biopsies were digested and single cell suspensions stained with antibodies CD3 PerCP Cy5.5, CD4 PE Cy7 and FoxP3 Alexa Fluor® 647 for flow cytometry acquisition and cell type identification.

5.3.9 Statistical analysis

5.3.9.1 Binding and Functional studies

Statistical analysis was performed using GraphPad Prism 7.01 (GraphPad Software, USA). Shapiro-Wilk tests were used to confirm normality of the data. Parametric data was then analysed using paired Students' *t*-test or a repeated measures one-way ANOVA without Geisser-Greenhouse correction. Non-parametric data was analysed using

Wilcoxon matched-pairs signed rank test. In the ANOVA, experimental groups were compared controlling the False Discovery Rate using the Two-stage step-up method of Benjamini, Krieger and Yekutieli. Data were represented as mean ± SD or median ± IQR. Differences were considered significant if $p < 0.05$.

5.4 Results

5.4.1 EICs bind SF-EVs

10^6 EICs were treated with $5x10^{10}$ bio-maleimide labelled SF-EVs for 2 hrs *ex vivo*, and binding to different types of EICs was then assessed by flow cytometry (n = 6) (Fig 5.8) – immune cell types were identified as described in Fig 5.3. Bio-maleimide labelled SF-EVs bound to endometrial $CD4^+$ T cells (p = 0.0007), $CD8^+$ T cells (p = 0.0004) and uNK cells (p = 0.0312) (Fig 5.7). In addition, the increase in bio-maleimide MeFI was significantly higher in $CD4^+$ (p = 0.0001) and $CD8^+$ (p = 0.0001) T cells when compared to uNK cells, (Fig 5.8 a). The percentage of cells binding bio-maleimide labelled SF-EVs was also determined by flow cytometry. Endometrial $CD4^+$ and $CD8^+$ T cells bound significantly more bio-maleimide labelled SF-EVs than uNK cells (p = 0.0002, p = 0.0002) (Fig 5.8 b) - mean values 88.71 ± 5.0 % for $CD4^+$ T cells, 87.72 ± 4.5 % for $CD8^+$ T cells and 60.31 ± 18.04 % for uNK cells.

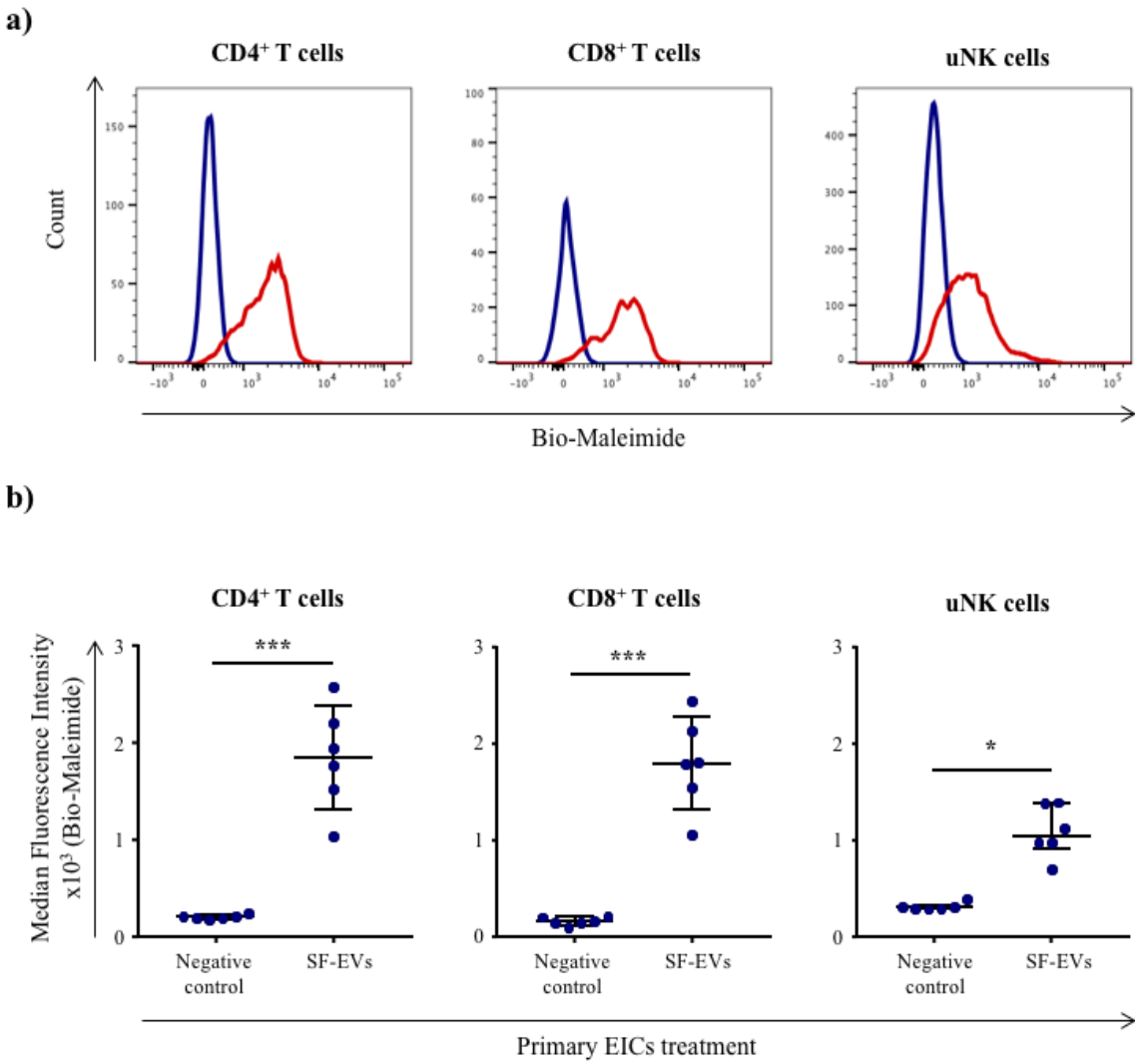


Fig 5.7 SF-EVs bind to primary EICs.

EICs were treated with bio-maleimide labelled SF-EVs or the negative control for 2 hrs ($5x10^{10}$ SF-EVs/10^6 cells). SF-EV binding to $CD4^+$ T cells ($CD3^+CD4^+CD8^-$), $CD8^+$ T cells ($CD3^+CD4^-CD8^+$), and uNK cells ($CD3^-CD56^{bright}$ $CD16^-$), was then analysed by flow cytometry. **(a)** Representative flow cytometry histogram of bio-maleimide fluorescence intensity after treatment with SF-EVs (red line) or negative control (blue line) **(b)** Median fluorescence intensity values of $CD4^+$ T cells, $CD8^+$ T cells and uNK cells when treated with negative control or bio-maleimide SF-EVs (n = 6). Bars represent **($CD4^+$ T cells, $CD8^+$ T cells)** mean ± SD, or **(uNK cells)** median ± IQR. * = $p < 0.05$, *** = $p < 0.001$

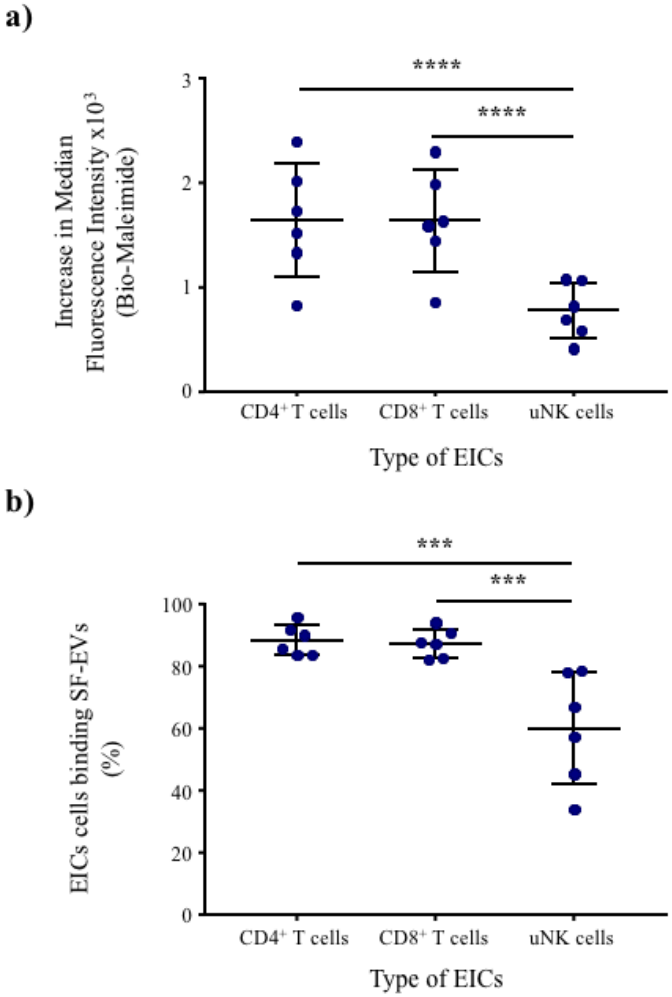


Fig 5.8 SF-EVs bind more to endometrial T cells than uNK cells.
EICs were treated with bio-maleimide labelled SF-EVs or the negative control for 2 hrs ($5x10^{10}$ SF-EVs/10^6 cells). SF-EV binding to $CD4^+$ T cells ($CD3^+CD4^+CD8^-$), $CD8^+$ T cells ($CD3^+CD4^-CD8^+$), and uNK cells ($CD3^-CD56^{bright}CD16^-$), was then analysed by flow cytometry (n = 6). **(a)** Increase in median fluorescence intensity **(b)** Percentage of EICs binding SF-EVs. Bars represent mean ± SD. *** = $p < 0.001$, **** = $p < 0.0001$

The preferential binding of SF-EVs to T cells over NK cells led me to focus further studies on the T cell population, specifically the CD4 positive subset. $CD4^+$ T cells are comprised of both non-Treg $CD4^+$ T and Treg cells, involved in assisting immune responses and immunosuppression respectively. Immune cell types were identified as described in Fig 5.4. SF-EVs bound to non-Treg $CD4^+$ T cells ($p = 0.0098$) and Treg cells ($p = 0.0312$) (n = 6) (Fig 5.9). In addition, the increase in bio-maleimide MeFI was higher in Treg cells

than non-Treg CD4$^+$ T cells (p = 0.0510) (Fig 5.10 a), and Treg cells bound significantly more SF-EVs than non-Treg CD4$^+$ T cells (p = 0.0109) (Fig 5.10 b).

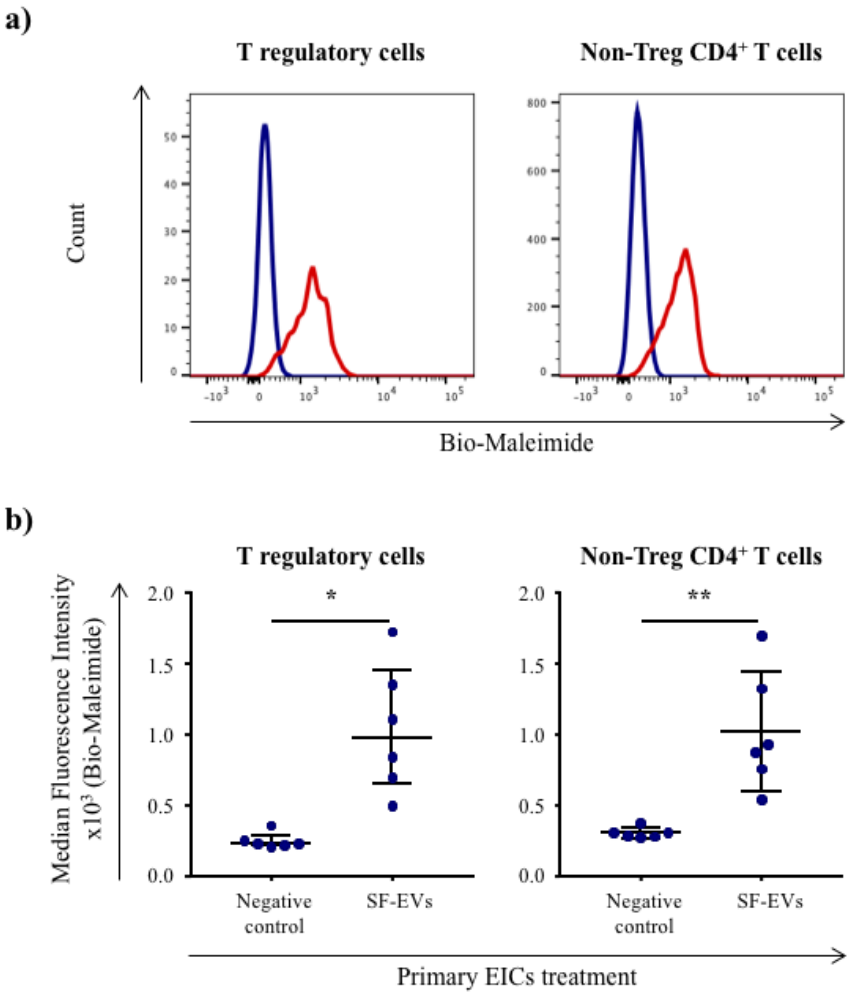


Fig 5.9 SF-EVs bind to endometrial CD4$^+$ T cells.
EICs were treated with bio-maleimide labelled SF-EVs or the negative control for 2 hrs ($5x10^{10}$ SF-EVs/10^6 cells). SF-EV binding to T regulatory cells ($CD3^+CD4^+FoxP3^+CD25^+CD127^-$) and non-Treg CD4$^+$ T cells ($CD3^+CD4^+FoxP3^-$) was then analysed by flow cytometry. **(a)** Representative flow cytometry histogram of bio-maleimide fluorescence intensity after treatment with SF-EVs (red line) or negative control (blue line) **(b)** Median fluorescence intensity values of T regulatory cells and non-Treg CD4$^+$ T cells when treated with negative control or bio-maleimide SF-EVs (n = 6). Bars represent **(T regulatory cells)** median ± IQR, or **(Non-Treg CD4$^+$ T cells)** mean ± SD. * = $p < 0.05$, ** = $p < 0.01$

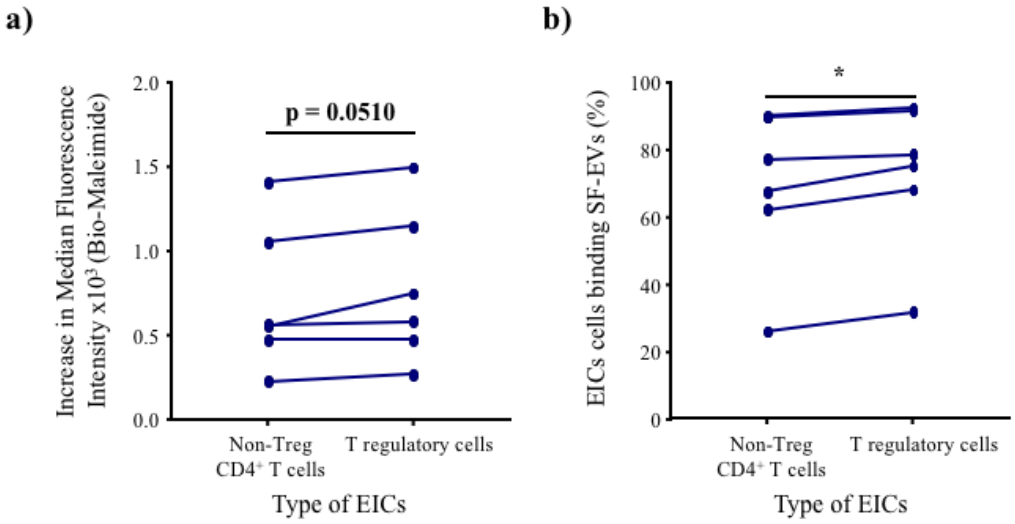


Fig 5.10 SF-EVs bind more to endometrial T regulatory cells than non-Treg CD4$^+$ T cells.
EICs were treated with bio-maleimide labelled SF-EVs or the negative control for 2 hrs ($5x10^{10}$ SF-EVs/10^6 cells). SF-EV binding to non-Treg CD4$^+$ T cells ($CD3^+CD4^+FoxP3^-$) and T regulatory cells ($CD3^+CD4^+FoxP3^+CD25^+CD127^-$) was then analysed by flow cytometry (n = 6). **(a)** Increase in median fluorescence intensity **(b)** Percentage of EICs binding SF-EVs. Bars represent mean ± SD. * = $p < 0.05$

5.4.2 Endometrial CD4$^+$ T cell activation is not stimulated by SF-EVs.

Having established endometrial CD4$^+$ T cells bind SF-EVs, I hypothesized SF-EVs would activate the cells to promote maternal tolerance and I investigated T cell activation via the canonical TCR/CD3 complex-dependent pathway.

5.4.2.1 SF-EVs do not affect membrane CD3 and CD25 expression in endometrial CD4$^+$ T cells

EICs were treated with PBS (non-stimulated), CD3/CD28 beads (positive control), or SF-EVs for 24 hrs and the expression of cell surface CD3 and CD25 was assessed by flow cytometry (n = 3). Endometrial CD4$^+$ T cells were identified as described in Fig 5.5.

Surface CD3 expression was downregulated on endometrial $CD4^+$ T cells stimulated with CD3/CD28 ($p = 0.0023$) beads but not on SF-EV treated $CD4^+$ T cells ($n = 3$) (Fig 5.11). CD25 expression was upregulated in endometrial $CD4^+$ T cells stimulated with CD3/CD28 beads ($p = 0.0002$) but not in SF-EV treated $CD4^+$ T cells ($n = 3$) (Fig 5.12).

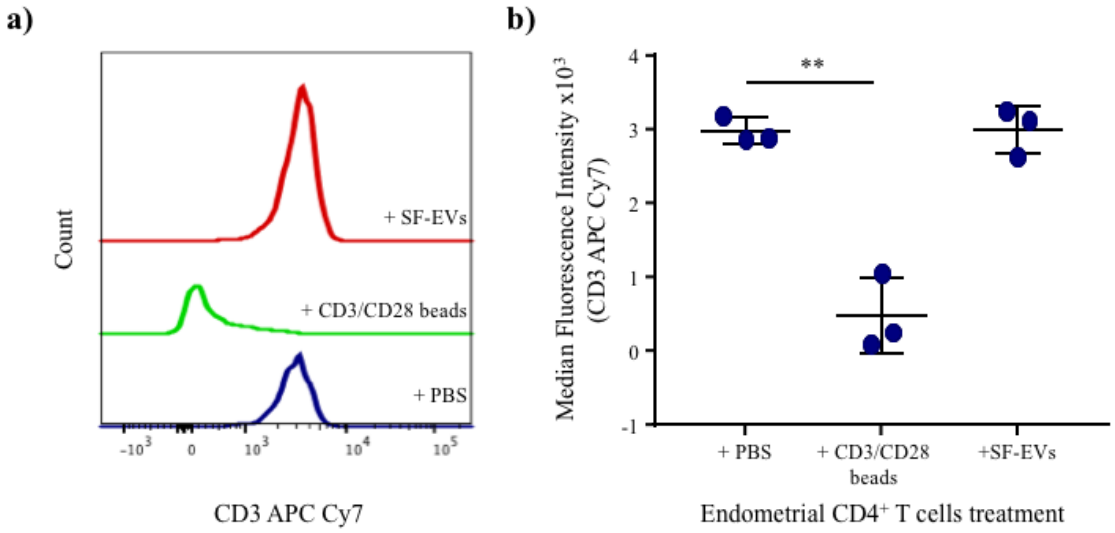


Fig 5.11 SF-EVs effect on endometrial $CD4^+$ T cells expression of membrane CD3. EICs were treated with PBS, CD3/CD28 beads or SF-EVs for 24 hrs ($5x10^{10}$ SF-EVs/10^6 cells). Brefeldin A was added 5 hrs before the end of the incubation time. Membrane CD3 expression on live $CD45^+CD4^+$ T cells was then analysed by flow cytometry. **(a)** Representative flow cytometry histogram of CD3 APC Cy7 fluorescence after treatment with PBS (blue line), CD3/CD28 beads (green line) or SF-EVs (red line) **(b)** CD3 APC-Cy7 median fluorescence intensity ($n = 3$). Bars represent mean ± SD. ** = $p < 0.01$

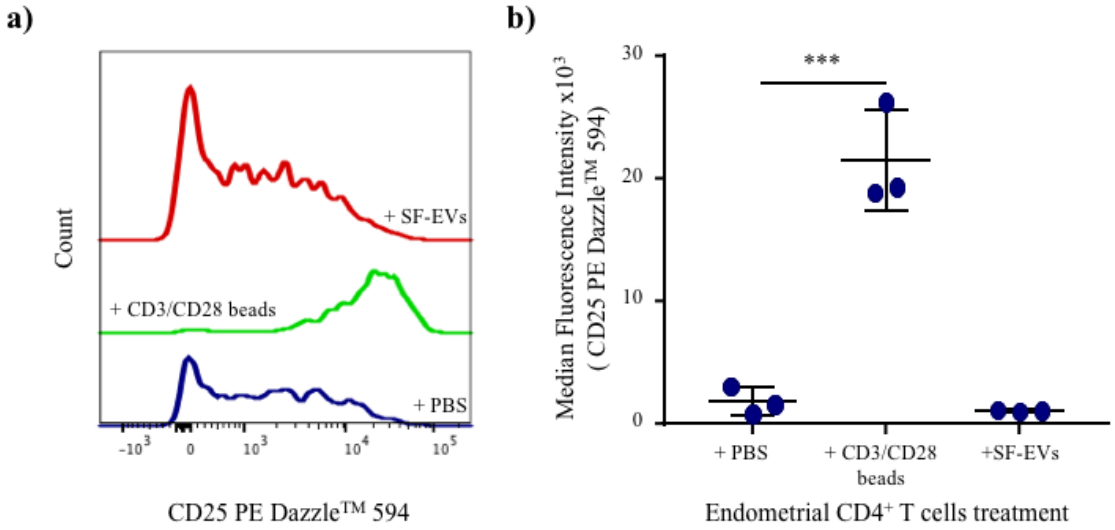


Fig 5.12 SF-EVs effect on endometrial CD4$^+$ T cells expression of membrane CD25. EICs were treated with PBS, CD3/CD28 beads, or SF-EVs for 24 hrs (5x10^{10} SF-EVs/10^6 cells). Brefeldin A was added 5 hrs before the end of the incubation time. Membrane CD25 expression in live CD45$^+$CD4$^+$ T cells was then analysed by flow cytometry. **(a)** Representative flow cytometry histogram of CD25 PE Dazzle™ 594 fluorescence after treatment with PBS (blue line), CD3/CD28 beads (green line) or SF-EVs (red line) **(b)** Dot plots of CD25 PE Dazzle™ 594 median fluorescence intensity (n = 3). Bars represent mean ± SD. *** = $p < 0.001$

In conclusion, when isolated endometrial T cells are incubated with CD3/CD28 to stimulate the TCR, CD3 expression is downregulated and CD25 expression is upregulated, however SF-EVs are unable to induce these phenotypic changes.

5.4.2.2 SF-EVs do not affect membrane CD3 expression in endometrial T regulatory cells

To further assess SF-EVs effect on endometrial Treg cells *in vitro* expanded endometrial Treg cells were treated with PBS (non-stimulated), CD3/CD28 beads (positive control), and SF-EVs for 24 hrs and the expression of CD3 analysed by flow cytometry (n = 3). *In vitro* expanded endometrial Treg cells were identified as described in Fig 5.6. CD25$^+$ was not identified this time, because it is upregulated on *in vitro* expanded/activated T cells.

As observed with $CD4^+$ T cells, CD3 expression was downregulated in endometrial Treg cells stimulated with CD3/CD28 beads ($p = 0.0247$) but not in SF-EV treated Treg cells ($n = 3$) (Fig 5.13).

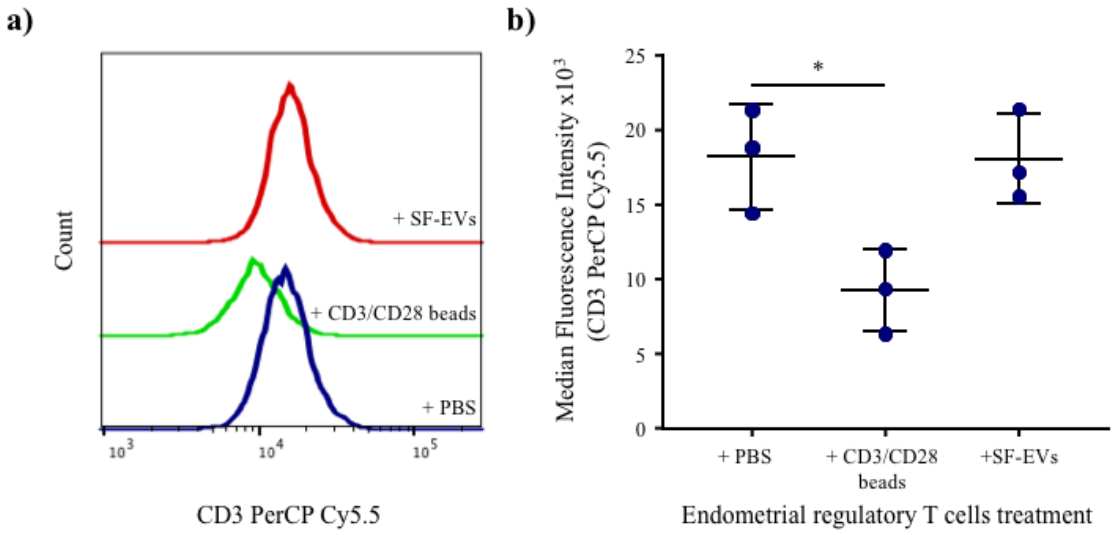


Fig 5.13 SF-EVs effect on endometrial T regulatory cells expression of membrane CD3.
In vitro expanded endometrial T regulatory cells were treated with PBS, CD3/CD28 beads, or SF-EVs for 24 hrs ($5x10^{10}$ SF-EVs/10^6 cells). Cell surface CD3 expression on $CD3^+CD4^+FoxP3^+$ T cells was then analysed by flow cytometry. **(a)** Representative flow cytometry histogram of CD3 PerCP Cy5.5 fluorescence after treatment with PBS (blue line), CD3/CD28 beads (green line) or SF-EVs (red line) **(b)** Dot plots of CD3 PerCP Cy5.5 median fluorescence intensity ($n = 3$). Bars represent mean ± SD. * = $p < 0.05$

5.4.3 Endometrial TGF-β1 secretion by $CD4^+$ T cells does not increase after stimulation

Neither endometrial $CD4^+$ T cells nor *in vitro* expanded Treg cells displayed changes to cell surface CD3 (or CD25 for $CD4^+$ T cells) expression in response to SF-EV incubation, however SF-EVs could still promote maternal tolerance through a non-canonical pathway that does not involve these markers. One of the mechanisms by which Treg cells regulate

the immune reaction is secreting TGF-β, therefore I investigated If SF-EVs could enhance TGF-β1 secretion by endometrial $CD4^+$ T cells through a non-canonical pathway. A preliminary result showed that SF-EVs did not seem to enhance endometrial or blood $CD4^+$ T cells intracellular expression of TGF-β1 after 24 hrs treatment (n = 1) – histograms displaying TGF-β1 expression are shown in Fig 5.14. Interestingly, 24 hrs simulation with CD3/CD28 beads minimally increased endometrial $CD4^+$ T cells MeFI, unlike a higher increase in blood $CD4^+$ T cells. In addition, the percentage of endometrial $CD4^+$ T cells expressing TGF-β1 remained unchanged before and after CD3/CD28 beads stimulation, 15.43 % and 15.35 %, respectively. On the contrary the percentage of blood $CD4^+$ T cells expressing TGF-β1 changed from 25.90 % to 72.78 % after 24 hrs CD3/CD28 beads stimulation. This suggested endometrial $CD4^+$ T cells, including Treg cells, might regulate immunosuppression differently than blood Treg. Therefore, I decided to characterise endometrial $CD4^+$ T cells, specifically Treg cells, expression of TGF-β1.

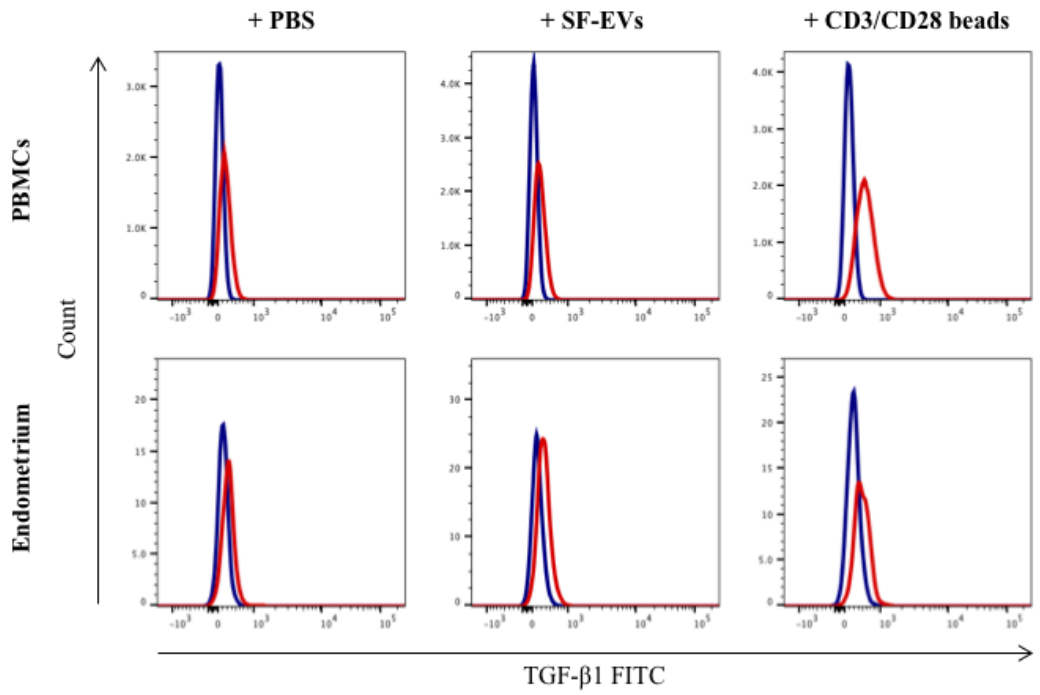


Fig 5.14 SF-EVs effect on intracellular TGF-β1 expression in endometrial CD4$^+$ T cells.
EICs and PBMCs were treated with PBS, SF-EVs, or CD3/CD28 beads for 24 hrs (5x10^{10} SF-EVs/10^6 cells). Brefeldin A was added 5 hrs before the end of the incubation time. Intracellular TGF-β1 in live CD45$^+$CD4$^+$ T cells was then analysed by flow cytometry (n = 1). This figure depicts a representative flow cytometry histogram of TGF-β1 FITC fluorescence after treatment with TGF-β1 antibody (red line) or the isotype control (blue line).

5.4.3.1 Intracellular expression of TGF-β1 in endometrial CD4$^+$ T cells

EICs were defrosted and treated with PBS (non-stimulated) or CD3/CD28 beads (stimulated) for 24 hrs, TGF-β1 expression was then labelled by intracellular cytokine staining and analysed by flow cytometry (n = 3). Endometrial CD4$^+$ T cells were identified as described in Fig 5.5.

Flow cytometry confirmed that both non-stimulated (p = 0.0172) and CD3/CD28 bead stimulated (p = 0.0223) endometrial CD4$^+$ T cells produce TGF-β1 when compared with the isotype control (n = 3) (Fig 5.15 a, b). Nevertheless, the increase in FITC MeFI was

similar between non-stimulated and CD3/CD28 bead stimulated endometrial $CD4^+$ T cells (Fig 5.15 c). In addition, the percentage of $CD4^+$ T cells expressing TGF-β1 was also similar between non-stimulated and CD3/CD28 bead stimulated cells (Fig 5.15 d) – 21.60 ± 6.77 % and 27.16 ± 10.73 %, respectively. This suggest CD3/CD28 stimulation does not increase endometrial $CD4^+$ T cells expression of TGF-β1.

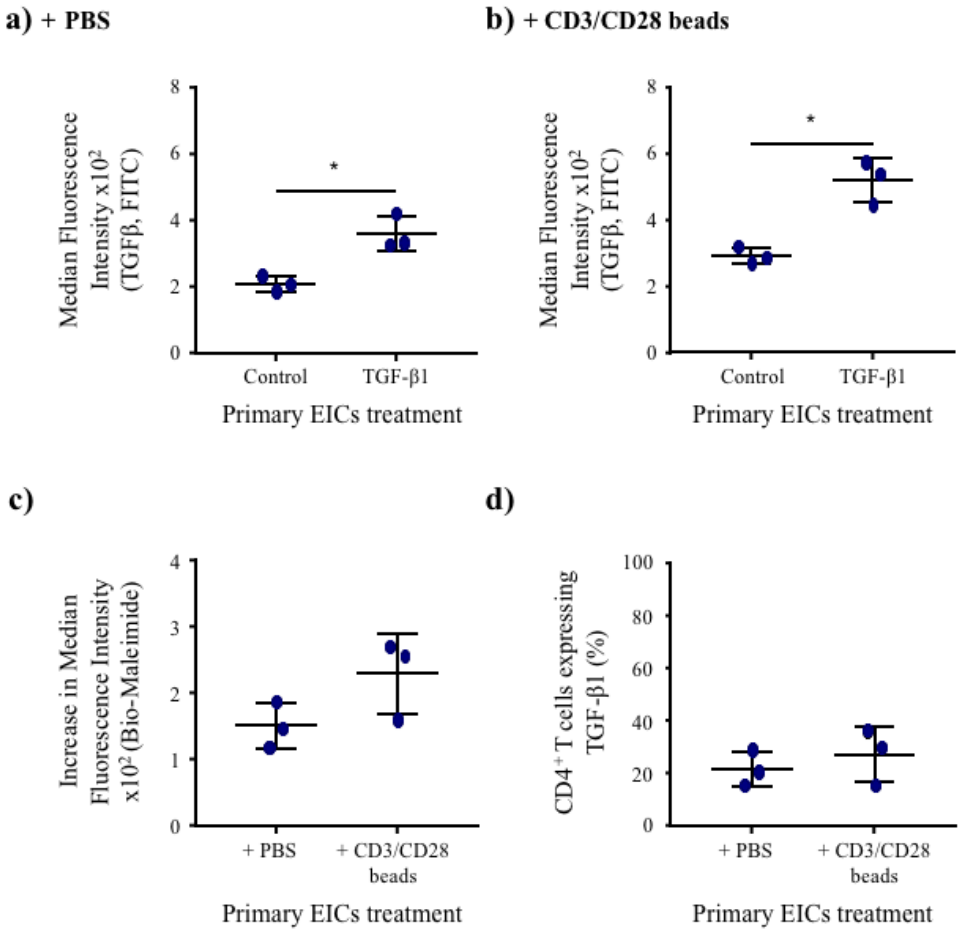


Fig 5.15 Intracellular TGF-β1 expression in endometrial $CD4^+$ T cells.
EICs were treated with PBS, or CD3/CD28 beads for 24 hrs. Brefeldin A was added 5 hrs before the end of the incubation time. Intracellular TGF-β1 in live $CD45^+CD4^+$ T cells was then analysed by flow cytometry (n = 3). TGF-β1 FITC median fluorescence intensity in **(a)** non-stimulated (PBS) and **(b)** CD3/CD28 beads stimulated $CD4^+$ T cells. **(c)** Increase in median fluorescence intensity **(d)** Percentage of $CD4^+$ T cells expressing TGF-β1. Bars represent mean ± SD. * = $p < 0.05$

5.4.3.2 Membrane expression of TGF-β1 in endometrial Treg cells

To specifically elucidate the expression pattern of TGF-β1 in endometrial Treg cells, membrane TGF-β1 levels were determined in non-stimulated (PBS) or CD3/CD28 beads stimulated *in vitro* expanded Treg cells (24 hrs) by flow cytometry (n = 3) – the Treg cells were identified as described in Fig 5.6. Blood Treg cells were analysed as a positive control for the experiment (n = 1).

Blood Treg cells expressed membrane TGF-β1 after 24 hrs stimulation with CD3/CD28 beads unlike endometrial Treg cells (Fig 5.16). The percentage of blood Treg cells expressing TGF-β1 after stimulation was 15.77 %. On the contrary, no significant differences in MeFI were found when non-stimulated (Fig 5.17 a) or CD3/CD28 beads stimulated (Fig 5.17 b) endometrial Treg cells labelled with TGF-β1 antibody when compared with the isotype control. This suggest that neither non-stimulated nor stimulated endometrial Treg cells expressed membrane TGF-β1.

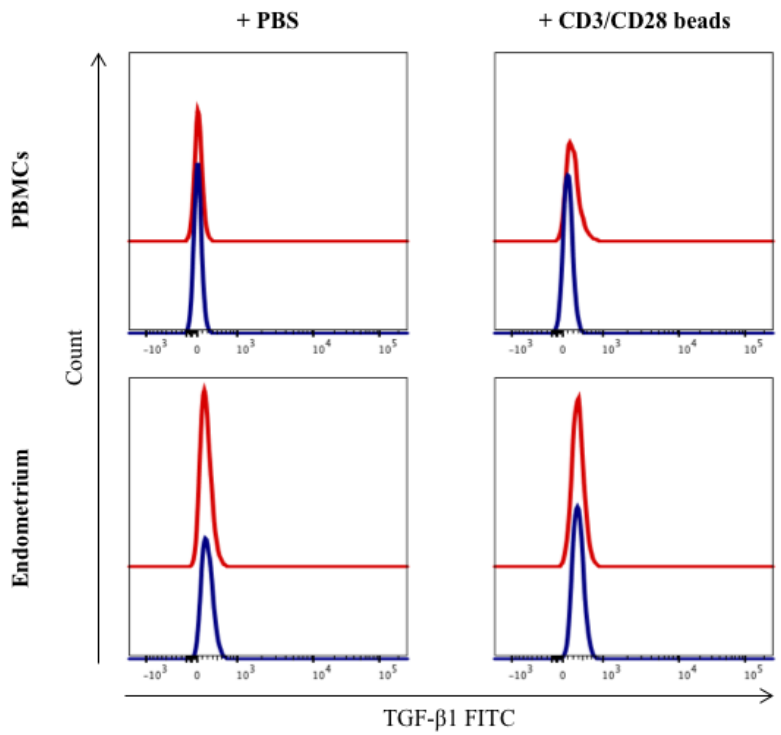


Fig 5.16 Representative image of TGF-β1 expression in endometrial and blood T regulatory cells.

In vitro expanded endometrial T regulatory cells and T regulatory cells from PBMCs were treated with PBS or CD3/CD28 beads for 24 hrs. Membrane TGF-β1 in $CD3^{+}CD4^{+}FoxP3^{+}$ T cells was then analysed by flow cytometry. This figure depicts a representative flow cytometry histogram of TGF-β1 FITC fluorescence after treatment with TGF-β1 antibody (red line) or the isotype control (blue line).

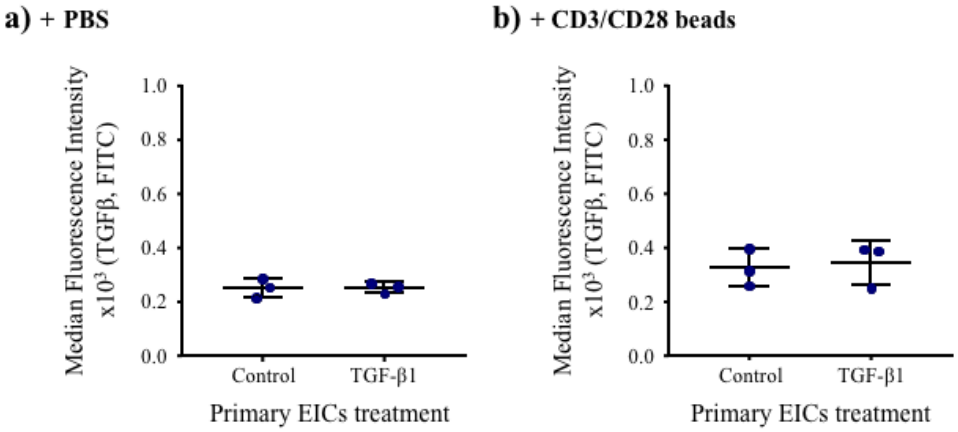


Fig 5.17 Membrane TGF-β1 expression in endometrial T regulatory cells.

In vitro expanded endometrial T regulatory cells were treated with PBS or CD3/CD28 beads for 24 hrs. Membrane TGF-β1 in $CD3^{+}CD4^{+}FoxP3^{+}$ T cells was then analysed by flow cytometry (n = 3). TGF-β1 FITC median fluorescence intensity in **(a)** non-stimulated (PBS) and **(b)** CD3/CD28 beads stimulated endometrial T regulatory cells. Bars represent mean ± SD.

5.5 Discussion

5.5.1 SF-EVs bind to EICs

In this chapter I have shown for the first time that SF-EVs bind to primary human EICs *in vitro* by flow cytometry. To my knowledge this is the first evidence of SF-EV binding to immune cells derived from the endometrium in the literature.

Flow cytometry analysis revealed SF-EV binding to endometrial $CD4^+$ and $CD8^+$ T cells, as well as uNK cells after 2 hrs incubation at a ratio of $5x10^{10}$ SF-EVs per 10^6 cells (optimized binding conditions). $CD4^+$ and $CD8^+$ T cells had higher capacity to bind SF-EV and more of these cells bound SF-EVs than uNK cells. This indicates SF-EV have differential binding potential to EIC, with a preference to T cells over uNK cells – this suggest binding is not random, if it were uNK cells would be expected to bind more SF-EVs because they have a bigger surface area.

Specific SF-EV binding to endometrial Treg cells and non-Treg $CD4^+$ T cells was also confirmed by flow cytometry. Interestingly, a higher proportion of Treg cells ($CD3^+CD4^+FoxP3^+CD25^{high}CD127^-$) bound SF-EVs than non-Treg $CD4^+$ T cells. This suggest SF-EVs might promote endometrial Treg function in the endometrium and may play a role in seminal fluid enhancement of maternal tolerance (see section 5.1.3).

5.5.2 SF-EVs do not activate endometrial Treg cells through the canonical TCR/CD3 complex-dependent pathway

After showing SF-EV binding to endometrial Treg cells, I investigated if SF-EVs enhance Treg activation. Primary human EICs and *in vitro* expanded endometrial Treg cells were treated with PBS, SF-EVs or CD3/CD28 beads (positive control) for 24 hrs. CD3 and

CD25 expression was then analysed by flow cytometry. T cell activation through the canonical TCR/CD3 complex-dependent pathway results in the downregulation of membrane CD3 and the upregulation of CD25 (Reinherz *et al.*, 1982, Zanders *et al.*, 1983, Cantrell *et al.*, 1988, Alberola-Ila *et al.*, 1991, Valitutti *et al.*, 1995, Trickett and Kwan, 2003). SF-EVs did not induce downregulation of CD3 or upregulation of CD25 in primary human endometrial $CD4^+$ T cells. In addition, CD3 expression also remained unchanged in endometrial Treg cells after SF-EV stimulation. Evidence therefore suggests SF-EVs cannot activate endometrial Treg function through the canonical TCR/CD3 complex-dependent pathway. The positive controls showed CD3 downregulation and CD25 upregulation confirming that endometrial Treg cells could be activated throughout this canonical pathway.

It might be possible that SF-EVs activate endometrial Treg cells through a TCR/CD3 complex – independent pathway. Interestingly, the co-receptors CD2 and CD28 have also been proposed to also activate T cells in a TCR/CD3 complex - independent manner (Gupta, 1989, Kabelitz, 1990). For example, CD2 – known as the sheep erythrocyte receptor- induce IL-2 receptors in $CD3^-$ T cells of the thymus (Fox *et al.*, 1985). Besides, CD2 stimulation triggers calcium signalling in NK cells ($CD2^+CD3^-$) in the absence of CD3 (O'Flynn *et al.*, 1986). CD28 can also activate T cells through the non-canonical CD28/VAV [46] /SLP-76 [47] pathway (Rudd and Raab, 2003). Research showed co-expression of VAV and SLP-76 in Jurkat cells and purified human T cells, followed by CD80 stimulation of CD28 in the cells, promoted IL-2 secretion (Raab *et al.*, 2001, Rudd and Raab, 2003). In addition, Bacchetta *et al* 2002 showed that IL-15 enhanced proliferation of T regulatory type 1 cells in the absence of TCR/CD3 complex activation

[46] VAV: Guanine Nucleotide Exchange Factor 1
[47] SLP-76: Lymphocyte cytosolic protein 2

– the latter inhibited proliferation and induced IL-10 and TGF-β secretion (Bacchetta *et al.*, 2002). Another study showed that in mice the alarmin IL-33 and the inflammatory cytokine IL-18 interact with their receptors, ST2L and IL-18R, in lung Treg cells in a TCR/CD3 complex – independent manner to promote amphiregulin expression (Arpaia *et al.*, 2015). This non-canonical activation of amphiregulin is involved in the tissue repair role of Treg cells (Arpaia *et al.*, 2015). Future work should look into these alternative activation pathways. In addition, as explained throughout this thesis, the endometrial immune environment involves a complex network of EECs, ESCs, and EICs. SF-EVs might act as adjuvants and assist endometrial Treg function in the presence of other stimuli, such as progesterone, or ESCs signalling. For instance, co-treatment of blood T cells, and Treg cells with ESCs from endometriotic lesions plus U937 (human monocytic cell line) resulted in a greater increase in Treg differentiation and IL-10 secretion than ESCs alone (Li *et al.*, 2014).

5.5.3 Endometrial Treg cell activation does not increase TGF-β1 expression

In this chapter, I have characterised the immunomodulatory function of endometrial Treg cells through TGF-β expression in humans. As explained in the introduction, TGF-β is a cytokine always secreted in an inactive form due to the non-covalent attachment of the mature TGF-β to LAP (Fig 5.2) (Khalil, 1999, Travis and Sheppard, 2014). The interaction can be dissociated through multiple mechanisms (for example serine proteases, plasmin, changes in pH) allowing the mature TGF-β to interact with its receptor – this process is important for physiological regulation of the bioactive form, and the cytokine functionality (Khalil, 1999). TGF-β plays an important role in immunoregulation (Li *et al.*, 2006, Travis and Sheppard, 2014). For instance, TGF-β1

knockout mice die due to multiorgan inflammation (Shull *et al.*, 1992, Kulkarni *et al.*, 1993). TGF-β is a strong inhibitor of T cell proliferation suppressing IL-2 synthesis and increasing cyclin-dependent kinase inhibitors (Kehrl *et al.*, 1986, McKarns and Schwartz, 2005) – it was also shown that this cytokine can enhance T cell survival (Cerwenka *et al.*, 1996). In addition, TGF-β inhibits Th1 differentiation blocking the expression of the transcription factor T-bet (Gorelik *et al.*, 2002), and suppressing NK release of IFNγ (Laouar *et al.*, 2005). TGF-β also supresses $CD8^+$ T cells cytotoxicity by inhibiting perforin (Smyth *et al.*, 1991). Importantly, activated Treg cells may exert their immunoregulatory role expressing soluble and/or membrane TGF-β, (Nakamura *et al.*, 2001, Green *et al.*, 2003, Yi *et al.*, 2006, Savage *et al.*, 2008, Kenneth Murphy, 2017).

To characterise TGF-β1 secretion by endometrial Treg cells in the endometrium, primary human EICs and *in vitro* expanded endometrial Treg cells were treated with PBS or CD3/CD28 beads for 24 hrs. LAP (TGF-β1) intracellular expression in primary EICs, and membrane expression in endometrial Treg cells was then analysed by flow cytometry. Primary human endometrial $CD4^+$ T cells produced TGF-β1, as shown by increase FITC MeFI after incubation with the antibody towards LAP (TGF-β1). However, no differences in the percentage increase in MeFI, or the percentage of cells expressing TGF-β1 were observed between before and after stimulation of endometrial $CD4^+$ T cells. Therefore, unlike observed in PBMCs, TCR/CD3 complex-dependent activation does not promote endometrial $CD4^+$ T cells synthesis of TGF-β1. In addition, FITC MeFI was not increased in *in vitro* expanded endometrial Treg cells after incubation with the antibody towards LAP (TGF-β1). Hence, unlike Treg cells circulating in the peripheral blood, TCR/CD3 complex-dependent activation does not stimulate endometrial Treg cells expression of membrane TGF-β1. This data suggest endometrial Treg cells might have unique

functional properties to regulate the maternal immune system for embryo implantation and pregnancy, differing from their mechanisms in other tissues.

Schumacher *et al*., 2007 showed that endometrial Treg tolerance required exposure to male-antigens in mice - only the transfer of Treg cells obtained from antigen-exposed pregnant mice could prevent fetal rejection in abortion-prone mice while Treg cells from virgin females did not (Schumacher *et al.*, 2007). In addition, mating of female mice with vasectomized male mice increased the number of Treg cells in the blood and lymph node, while generating pseudopregnancy through mechanical stimulation did not. This suggest that the male antigen-presentation is performed by factors in the seminal fluid but not the sperm (Schumacher *et al.*, 2007). Interestingly, this same group showed that the abortion-protective effect of transferring Treg cells was completely abrogated when IL-10 neutralizing antibodies were inserted peritoneally, and partially abrogated when using TGF-β neutralizing antibodies (Schumacher *et al.*, 2007). This data indicated that endometrial Treg cells can enhance IL-10 and TGF-β secretion for maternal tolerance in mice. However, our data suggest that endometrial Treg cells do not enhance TGF-β expression after TCR/CD3 complex-dependent stimulation in human. A major difference between the studies is that in this DPhil project there is no exposure to seminal fluid, therefore, it might be possible that endometrial Treg activation requires both TCR/CD3 complex-dependent stimulation and antigen-presentation by the seminal fluid at the same time. In the future it would be interesting to stimulate endometrial Treg cells with CD3/CD28 beads alone, CD3/CD28 beads + seminal fluid, and CD3/CD28 beads + SF-EVs; to assess if combined CD3 activation and seminal fluid presentation of male antigens activates endometrial Treg cells and if SF-EVs might mediate it. In addition, this difference may also reflect differences between species, or that TGF-β expression by

endometrial Treg cells is stimulated through a non-canonical activation pathway initiated by seminal factors but not in the presence of CD3/CD28 beads alone. This chapter highlights the lack of information on the physiology of endometrial Treg cells and the urgency of researching these cells as they are essential in maternal immune tolerance.

6 Final Discussion

In this thesis I hypothesised SF-EVs regulate maternal endometrial receptivity to facilitate embryo implantation and the overall aim was to investigate the role of SF-EVs on human endometrial receptivity, which is an essential-requirement for successful implantation. To fulfil this goal this thesis aims: 1) to characterise SF-EVs isolated from sperm samples obtained at Oxford Fertility before and after purification, 2) to evaluate the effect of SF-EVs on the receptivity of endometrial epithelium and stroma to embryo implantation, 3) to investigate the effect of SF-EVs on maternal tolerance. For aims 2 and 3 the effect of SF-EVs on endometrial epithelial, stromal, and immune cells was initially analysed *in vitro* by flow cytometry and fluorescence microscopy. Thereafter, SF-EVs effect on ESC decidualisation, the molecular activation of EECs and ESCs, as well as activation of endometrial $CD4^+$ T cells (especially Treg cells) was determined. Interestingly, the study of SF-EV effect on EICs (aim 3) led us to investigate TGF-β1 expression in Treg cells of the endometrium. This study is the first of its kind to investigate SF-EVs effect on the maternal endometrium and has led to novel data which also lead to interesting future projects.

6.1 Comprehensive characterisation of human SF-EVs (aim 1)

Chapter 2 of this thesis shows that SF-EVs range from 15 to 300 nm. Electron microscopy and ExoView analysis demonstrated that the majority of these EVs are between 15 to 80 nm in both purified SF-EV samples and unprocessed seminal fluid samples. This main population of SF-EVs has also been recently described using DLS (Chiasserini *et al.*, 2015, Eswaran *et al.*, 2018), but has not been found in ours nor other NTA studies (Garcia-Rodriguez *et al.*, 2018). This shows than NTA is not the best technique to determine total range of SF-EV sizes and concentrations, and other techniques such as

DLS, or the new ExoView are more accurate. Importantly, this is the first study showing the presence of this big population of SF-EVs from 15 to 80 nm in unprocessed seminal fluid samples.

Chapter 2 also provides a novel description in the literature of SF-EV populations based upon combined expression of exosomal markers - ExoView analysis showed $CD63^+CD9^+CD81^+$, $CD63^+CD9^+CD81^-$, and $CD63^+CD9^-CD81^+$ populations of SF-EVs. In addition, correlation studies of Western blotting suggested three potential different combinations of SF-EV populations based on the tetraspanin CD9 and the intravesicular exosomal markers, ALIX and syntenin-1; and electron microscopy revealed 4 different SF-EV morphologies. This novel data illustrates the high complexity of SF-EVs comprising phenotypically, more likely functionally, different EVs from multiple sources of the male reproductive tract.

6.1.1 SF-EVs alterations as markers of pathological conditions

Alterations in the heterogeneous population of SF-EVs might be useful as a diagnostic marker of different types of male infertility. For instance, different SF-EV cargoes were described between non-normoozospermic and normoozospermic patients (Garcia-Rodriguez *et al.*, 2018), and SF-EV miRNA profiles were shown to be able to distinguish between obstructive azoospermia and spermatogenic failure (Barcelo *et al.*, 2018). Only one of these studies investigated SF-EV sizes and concentrations, and no differences were found between non-normoozospermic and normoozospermic. However, this study used NTA to measure the aforementioned parameters, and here I have shown that NTA analysis is very limited in the detection of the main population of SF-EVs less of than 100 nm diameter.

SF-EVs may be altered in subfertile patients, with characteristics that permit differentiation between spermatogenic or epididymal failure, obstructive azoospermia, and subfertility due to external factors, such as non-prescribed drugs, alcohol, or environmental chemicals. Interestingly, recent studies suggest paternal factors in pregnancy might program offspring to non-communicable diseases (NCDs). NCDs are non-genetic non-infectious medical conditions, such as cancer and cardiovascular diseases (Rodriguez-Caro and Williams, 2018). For instance, in mice paternal malnutrition increased the risk of mammary cancer in female offspring (da Cruz *et al.*, 2018), while paternal overnutrition led to impaired insulin homeostasis in male offspring (Ornellas *et al.*, 2018). SF-EVs might act as delivery vehicle of these deleterious effects of paternal negative stimuli, therefore, SF-EVs alterations might be able to predict negative *in utero* programming with views to later pregnancy and postnatal management to prevent the development of NCDs in the offspring.

Future work should characterise SF-EVs from fertile and subfertile males to determine changes in SF-EV sizes and concentrations, and the proportion of SF-EV subpopulations. In addition, protein profiles of these subpopulations could be determined to trace the origin of the EVs, as well as any organ-specific alterations in the subfertile patients. It would also be interesting to analyse the aforementioned parameters in fertile fathers-to-be to determine the effect of paternal life styles (e.g: obesity, malnutrition, stress, exercise) on SF-EVs and use this information to predict the risk of NCDs development in future offspring. To determine if SF-EVs can indeed program deleterious *in utero* programming of NCDs, for example by negatively affecting endometrial receptivity (suppressing or expanding it) causing a ripple effect, mice studies could be performed.

For example, healthy female mice inseminated via intracytoplasmic sperm injection and IVF with the sperm of healthy male, could be exposed to SF-EVs from healthy or unhealthy male mice and the effect on pregnancy and the health of the offspring subsequently analysed.

6.2 Integrative model of SF-EVs role in human endometrial receptivity (aim 2 & aim 3)

This DPhil thesis describes for the first time a role of SF-EVs on the regulation of human endometrial receptivity. Based upon the results and available literature the following model is proposed (Fig 6.1):

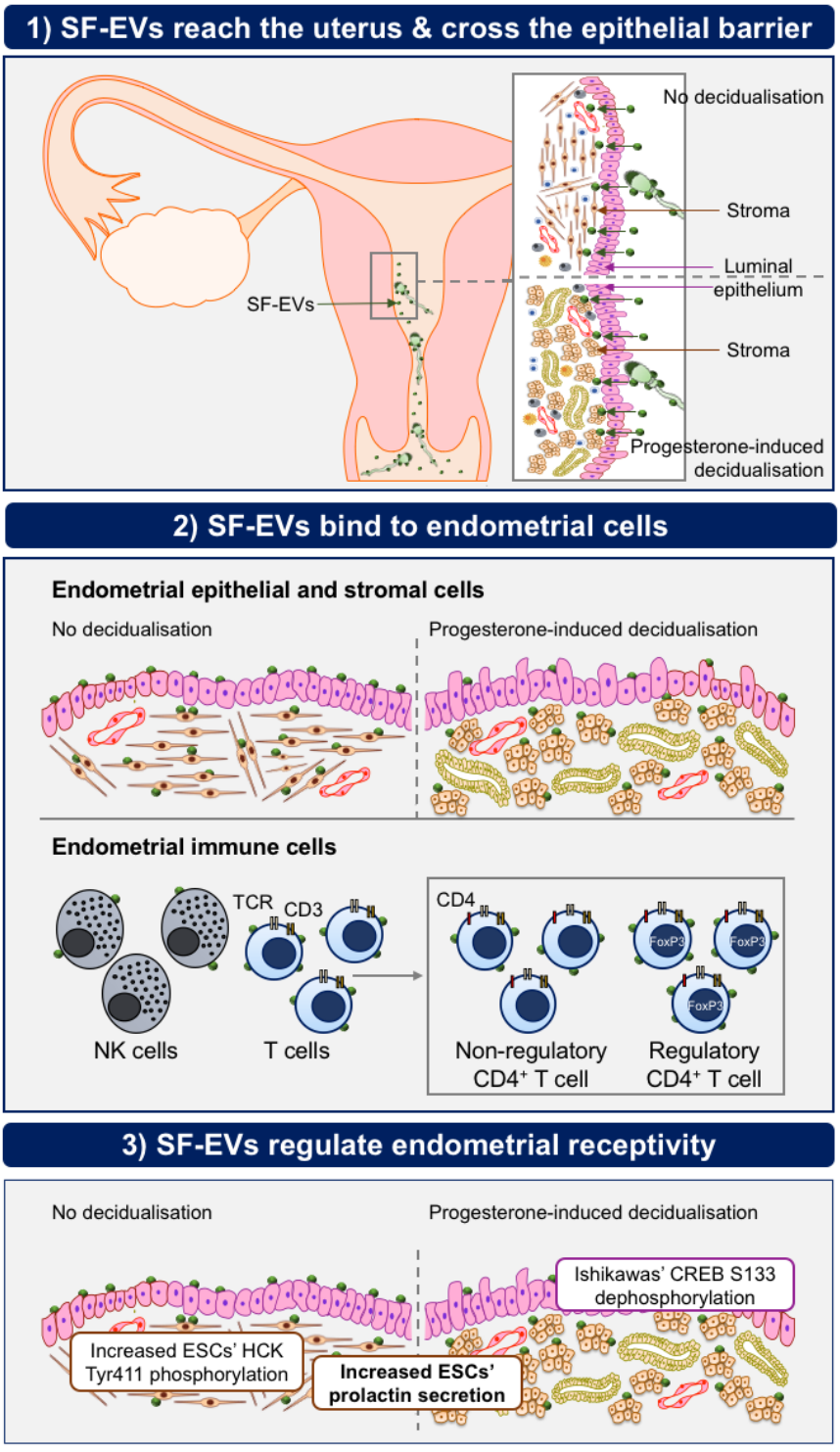


Fig 6.1 Integrative model of SF-EVs role in human endometrial receptivity

1) Seminal Fluid Extracellular Vesicles (SF-EVs) must first reach the uterine cavity and cross the mucosal endometrium to reach all endometrial cells. **2)** SF-EVs then bind to endometrial epithelial, stromal and immune cells in a cell-specific manner and might be affected by progesterone-induced decidualisation. TCR: T cell receptor. **3)** Finally, SF-EVs assist endometrial receptivity by enhancing ESCs' prolactin secretion, and by regulating cell activation; for instance, they modulate HCK Tyr411 and CREB S133 phosphorylation in stromal and epithelial cells, respectively.

First, during intercourse, SF-EVs reach the uterine cavity and travel near the endometrium reaching endometrial epithelial, stromal and immune cells. In this thesis all studies are performed *in vitro* using 2D cultures, therefore, SF-EVs access to the uterine cavity and crossing of the mucosal epithelium is assumed, it has not been shown. Nevertheless, other studies in the literature support that SF-EVs can reach the uterus. For instance, in humans Zervomanolakis *et al*. 2007 demonstrated that immotile-labelled particles inserted in the vagina were lifted into the uterus and oviducts, this was more likely drived by peristaltic movements (Zervomanolakis *et al.*, 2007). Furthermore, sperm cells bind SF-EVs at slighly alkaline or neutral pH, and they fuse with them at acidic pH (Aalberts *et al.*, 2014). This suggest that sperm cells could transport SF-EVs upwards into the uterus on fertile days of the cycle. As mentioned above, after reaching the uterus, SF-EVs would have to cross through the mucosal epithelium to reach ESCs, and EICs. Although EV transport through endometrial epithelium barrier has not been investigated, some studies support the theory of EVs crossing the epithelial barriers. Vashisht *et al.* 2017 demonstrated exosomes can cross the human intestinal epithelium (Vashisht *et al.*, 2017). In addition, Chen *et al*. 2016 showed that exosomes can cross the blood-brain barrier by transcytosis, as well as, clathrin-dependent and caveolae-dependent transcytosis (Chen *et al.*, 2016a).

Secondly, SF-EVs bind to the EECs, ESCs, and EICs. This novel binding is cell-specific and different binding patterns are described in this thesis. Untreated EECs bind more SF-EVs than progesterone treated ones. On the contrary, SF-EVs interact with non-decidualised and decidualised ESCs similarly throughout the menstrual cycle. The reason of this difference in binding patterns at the implantation window remains to be elucidated. It might be possible that throughout the development of endometrial receptivity EECs

become more permeable to SF-EVs to allow for higher transit of SF-EVs to the stromal cell layer, which will play an essential role on implantation and the ongoing pregnancy. EICs also differentially bind SF-EVs. More T cells bind SF-EVs than uNK cells. In addition, within the $CD4^+$ T cell population SF-EVs have preference for endometrial Treg cells.

Finally, SF-EV interaction with endometrial cells regulates maternal endometrial receptivity. Importantly, this thesis shows for the first time that SF-EVs enhance ESC decidualisation by promoting secretion of prolactin, a hormone essential in embryo implantation. As discussed in chapter 3, prolactin regulates EECs (Franchi *et al.*, 2011), ESCs (Daniel *et al.*, 1984), and EICs (Ain *et al.*, 2004) signalling; and prolactin receptor knockout female mice exhibit implantation failure (Bole-Feysot *et al.*, 1998). In addition, SF-EVs modulate activation of EECs, and ESCs. SF-EVs increase phosphorylation of HCK at Tyr411 in non-decidualised ESCs. Interestingly, in chapter 3, SF-EVs did not induce dephosphorylation of CREB S133 in untreated Ishikawa cells, while preliminary data had shown SF-EVs induced dephosphorylation of CREB S133 in day 7 progesterone treated Ishikawa cells. The reason of this underlying difference in SF-EVs effect on the endometrium at different stages of the implantation window unknown. SF-EVs may act as control point regulating the time-span of endometrial receptivity to prevent late implantation and its associated deleterious consequences (Coulam, 2016, Fleming *et al.*, 2018, Rodriguez-Caro and Williams, 2018)

6.2.1 SF-EVs as potential adjuvants to assist embryo implantation in IVF

SF-EV enhancement of human endometrial receptivity suggests SF-EVs might assist human embryo implantation and could be used as IVF adjuvants to improve implantation rates. Currently, there are some treatments available in clinic to improve implantation rates. From the embryo side the treatments available include embryo glue and assisted hatching, which might enhance embryo adhesion to the endometrial epithelium; and preimplantation genetic screening and embryonic mitochondrial load, which select the embryos most likely to implant (Harper *et al.*, 2017). From the maternal side some treatments are aspirin, immunoglobulins or intralipids which are used to modulate maternal immunity to increase endometrial receptivity (Hviid and Macklon, 2017). To improve endometrial receptivity it is also possible to perform whole uterus transplantation (Favre-Inhofer *et al.*, 2018). However, the data supporting the efficiency of the above-mentioned treatments/therapies to increase implantation rates is limited or controversial. In addition, some of these options are highly expensive, intrusive, and might have potential adverse effects. Insemination of SF-EVs would be a great alternative for two main reasons: 1) they would be safe to use because they physiologically play a role in reproduction, 2) they would be low-cost since SF-EVs are easily isolated and could be obtained from the partners' seminal fluid or a donor.

Future work should investigate the effect of SF-EVs on embryo implantation. For example, SF-EVs effect on an *in vitro* 3D embryo attachment model (Wang *et al.*, 2012) could be assessed using trophoblast spheroids, and endometrial cells isolated from healthy and subfertile (E.g.: RIF, RPL, endometriosis, pre-clampsia) patients. It would be interesting to analyse both the adhesion and invasion of the trophoblast spheroids in the

latter study. Another option would be to do a pilot clinical trial in which IVF women are treated with SF-EVs at the time of egg retrieval and then the implantation and live birth rates of those patients are evaluated – multiple factors should be considered in these cases like the underlaying cause of subfertility.

6.3 Physiology of endometrial regulatory T cells (aim 3 derived research)

The study of SF-EV effect on EICs (aim 3) directed us to characterise TGF-β1 expression in Treg cells of the endometrium. Chapter 5 shows that endometrial Treg cells do not behave as peripheral blood Treg cells – unlike the latter, endometrial Treg cells do not increase TGF-β1 expression after CD3/CD28 stimulation or express membrane TGF-β1. This novel evidence highlights the need for future research on the physiology of endometrial Treg cells to elucidate how they modulate the maternal immune response in the endometrium.

Future work should initially determine how endometrial Treg cells are activated. For example, endometrial Treg cells could be stimulated with CD3/CD28 beads alone, CD3/CD28 beads + seminal fluid, or trophoblast spheroids. Then TGF-β1 and IL-10 could be measured by intracellular cytokine staining and ELISAs to determine expression and secretion of these cytokines. In addition, endometrial Treg cell proliferation after simulation could be analysed using a CFSE[48]-proliferation assay. After determining how these Treg cells are stimulated, endometrial Treg cells could be incubated with other EICs, and activated to determine their inhibitory effect, e.g.: the proliferation of other

[48] CFSE: Carboxyfluorescein succinimidyl ester

EICs after stimulation could be assessed. Further characterisation could be achieved by analysing the transcriptome profile of endometrial Treg cells before and after stimulation with RNA sequencing. This technique would not only determine the effect of stimulation on the endometrial Treg cell transcriptome but would also allow to differentiate between Treg cell populations.

7 Final Discussion

In short, in this DPhil thesis I have provided the most comprehensive characterisation of SF-EVs to date and I have shown for the first time in the literature that SF-EVs play a role in human endometrial receptivity. In addition, my work on endometrial Treg cells highlights the lack of information on the physiology of these cells in the peri-implantation endometrium and the need for future research to elucidate how they modulate the maternal immunotolerance.

SF-EV characterisation showed the complexity of these SF-EVs that include phenotypically, and likely functionally, different populations of EVs. This thesis demonstrates that the majority of SF-EVs are between 15 to 80 nm and shows 4 different SF-EV morphologies by electron microscopy. Importantly, it provides a novel classification of SF-EV populations based upon combined expression of the exosomal markers: CD63, CD9, CD81, ALIX, and Syntenin-1. Alterations in this heterogeneous SF-EV population might be a useful marker for different types of male subfertility or other pathological conditions and these alterations could be involved in paternal programming of NCDs in the offspring. Routine assessment of SF-EV populations in fertility clinics as part of male evaluation could provide an insight into any association between particular SF-EV populations and to male subfertility.

Interestingly, this DPhil thesis reports for the first time that SF-EVs interact with endometrial cells and regulate human endometrial receptivity. Based upon the results and the information in the literature an integrative model of SF-EVs' role in human endometrial receptivity is proposed (Fig 6.1). First, SF-EVs reach the uterus, transported by sperm or lifted up likely by the peristaltic movements, and cross the epithelial barrier.

Secondly, SF-EVs bind to endometrial epithelial, stromal and immune cells in a cell & time-specific manner. Finally, SF-EVs facilitates optimal endometrial receptivity stimulating prolactin secretion by ESCs and regulating EECs as well as ESCs cell signalling. These results suggest SF-EV might be used as adjuvants to assist human embryo implantation in IVF. Practically, SF-EVs could first be isolated from the partner's seminal fluid or a donor and, then, these SF-EVs could be transferred into the women endometrium at the time of oocyte retrieval. Using SF-EV as adjuvants offers two advantages: 1) SF-EVs are safe to use because they physiologically play a role in reproduction, 2) this treatment would be low-cost since SF-EVs are easily isolated from semen samples, which are widely available. Nevertheless, safety and ethical considerations should be taken into account and further studies would be necessary to understand the functional effects of different subpopulations before considering assessing their use in the context of a clinical trial. For example, to date there is no data to demonstrate whether paternal or donor SF-EVs would be most beneficial for therapeutic use. In addition, care should be taken with the use of donor SF-EVs as the full genetic content and modulatory capacity of SF-EVs are not fully elucidated, and it would need to be established whether donor SF-EVs could directly influence the long-term development of the embryo, for example modifying the epigenome.

8 Appendices

8.1 Appendix 1

Table 8.1 Clinical characteristics of patients recruited for sperm samples.
Normal sperm count > 15 M/mL. Normal sperm progressive motility > 32%. N/A = not available

Patient	Age	Sperm count (M/mL)	Sperm Progressive motility (%)	Fertility
1	N/A	N/A	N/A	N/A
2	N/A	N/A	N/A	N/A
3	N/A	N/A	N/A	N/A
4	34	47	80	Normal
5	29	9.1	51	Oligozoospermia
6	44	36	64	Normal
7	31	41	61	Normal
8	36	20.5	56	Normal
9	N/A	N/A	N/A	N/A
10	37	70.2	61	Normal
11	37	24	63	Normal
12	28	45	74	Normal
13	33	47.5	48	Normal
14	N/A	N/A	N/A	N/A
15	N/A	N/A	N/A	N/A
16	35	93	59	Normal
17	32	51	60	Normal
18	40	121	64	Normal
19	47	106	56	Normal
20	35	97	74	Normal
21	36	61	59	Normal
22	38	56.3	58	Normal
23	N/A	N/A	N/A	N/A
24	36	17.5	57	Normal
25	33	0.8	37	Oligozoospermia
26	32	100	61	Normal
27	31	18	53	Normal
28	45	6	42	Oligozoospermia
29	33	2.4	41	Oligozoospermia
30	34	8.5	50	Oligozoospermia
31	32	0.1	27	Oligozoospermia and low sperm motility
32	32	11.7	81	Oligozoospermia
33	41	13.2	51	Oligozoospermia
34	33	66	69	Normal
35	38	5.8	48	Oligozoospermia

36	37	34	66	Normal
37	38	1.3	57	Oligozoospermia
38	26	7.1	48	Oligozoospermia

8.2 Appendix 2

Table 8.2 Clinical characteristics of patients recruited for EEC isolation.

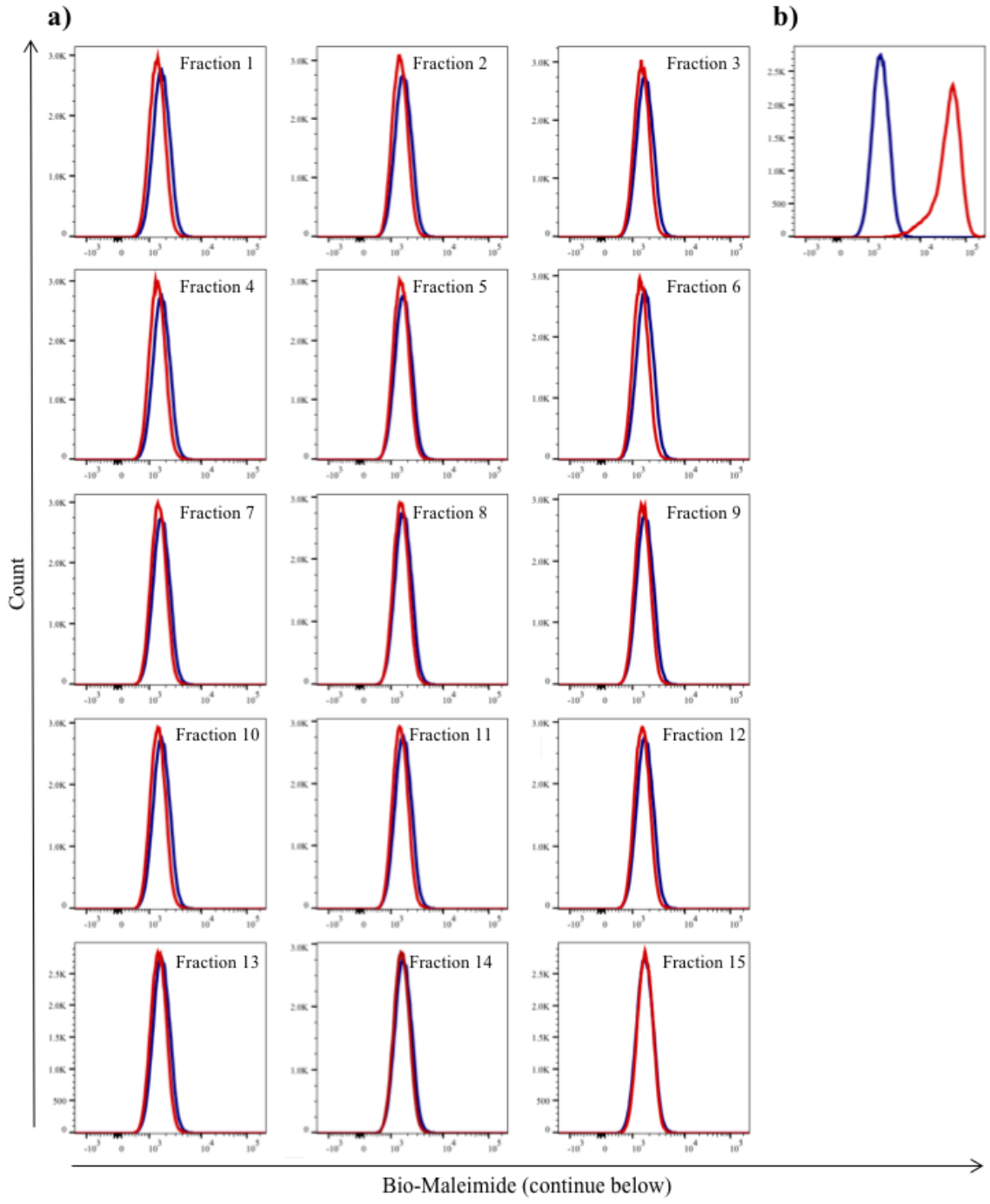
Pregnancy is defined as intrauterine implantation confirmed by ultrasound. Ectopic pregnancies are excluded. LOR = low ovarian reserve. Tubal = damage in the fallopian tube. POF = Premature ovarian failure. BSO = bilateral salpingectomy. ORS = Oophorectomy. LSO = left salpingectomy. PCOS = polycystic ovarian syndrome. * = same patients. N/A = not available

Patient	Age	Day of the cycle	Pregnancies	Livebirths	Fertility
1	34	N/A	N/A	N/A	N/A
2	39	29	0	0	Subfertile (fibroids)
3	38	23	0	0	Subfertile (LOR)
4	40	18	2	1	Subfertile (Tubal)
5	36	23	0	0	Subfertile (POF)
6	37	24	1	0	male factor
7	36	N/A	2	0	N/A
8	33	N/A	N/A	N/A	Subfertile (unexplained)
9	36	N/A	0	0	Subfertile (BSO & 1 ORS)
10	33	N/A	2	0	Subfertile (unexplained)
11	30	N/A	1	0	male factor
12*[1]	36	19	2	1	N/A
13	31	23	1	1	male factor
14	37	22	3	1	Subfertile (unexplained)
15	31	20	0	0	Subfertile (unexplained)
16	36	N/A	2	1	male factor
17	35	20	2	1	Subfertile (unexplained)
18	35	22	1	0	Subfertile (unexplained)
19	40	19	1	0	Subfertile (age)
20	35	25	0	0	Subfertile (unexplained)

21	28	22	0	0	same sex couple
22	36	20	0	0	male factor
23	32	18	1	0	male factor
24	32	N/A	0	0	male factor
25	42	22	0	0	Subfertile (unexplained)
26*[1]	37	17	2	1	Subfertile (unexplained)
27	38	19	2	1	Subfertile (LOR)
28*[2]	31	20	0	0	male factor
29	44	N/A	N/A	N/A	Subfertile (age)
30	29	N/A	2	0	Subfertile (LSO & male factor)
31	40	N/A	5	1	Subfertile (PCOS)
32	39	19	2	0	Subfertile (endometriosis)
33	43	20	0	0	Subfertile (age)
34	33	21	1	0	Subfertile (genetic)
35	29	20	1	0	male factor
36*[3]	34	18	1	0	male factor
37	35	19	1	0	Subfertile (Tubal)
38	45	22	1	0	Subfertile (Age, LOR, & male factor)
39	31	N/A	0	0	Subfertile (anovulation)
40	34	21	5	0	Subfertile (PCOS)
41	38	N/A	1	0	Subfertile (PCOS)
42*[3]	33	N/A	0	0	male factor

43	32	22	0	0	male factor
44	33	20	1	0	Subfertile (combined factors)
45	38	23	0	0	Subfertile (LOR & endometriosis)
46	44	22	4	1	Subfertile (age)
47*[2]	32	21	0	0	male factor

8.3 Appendix 3



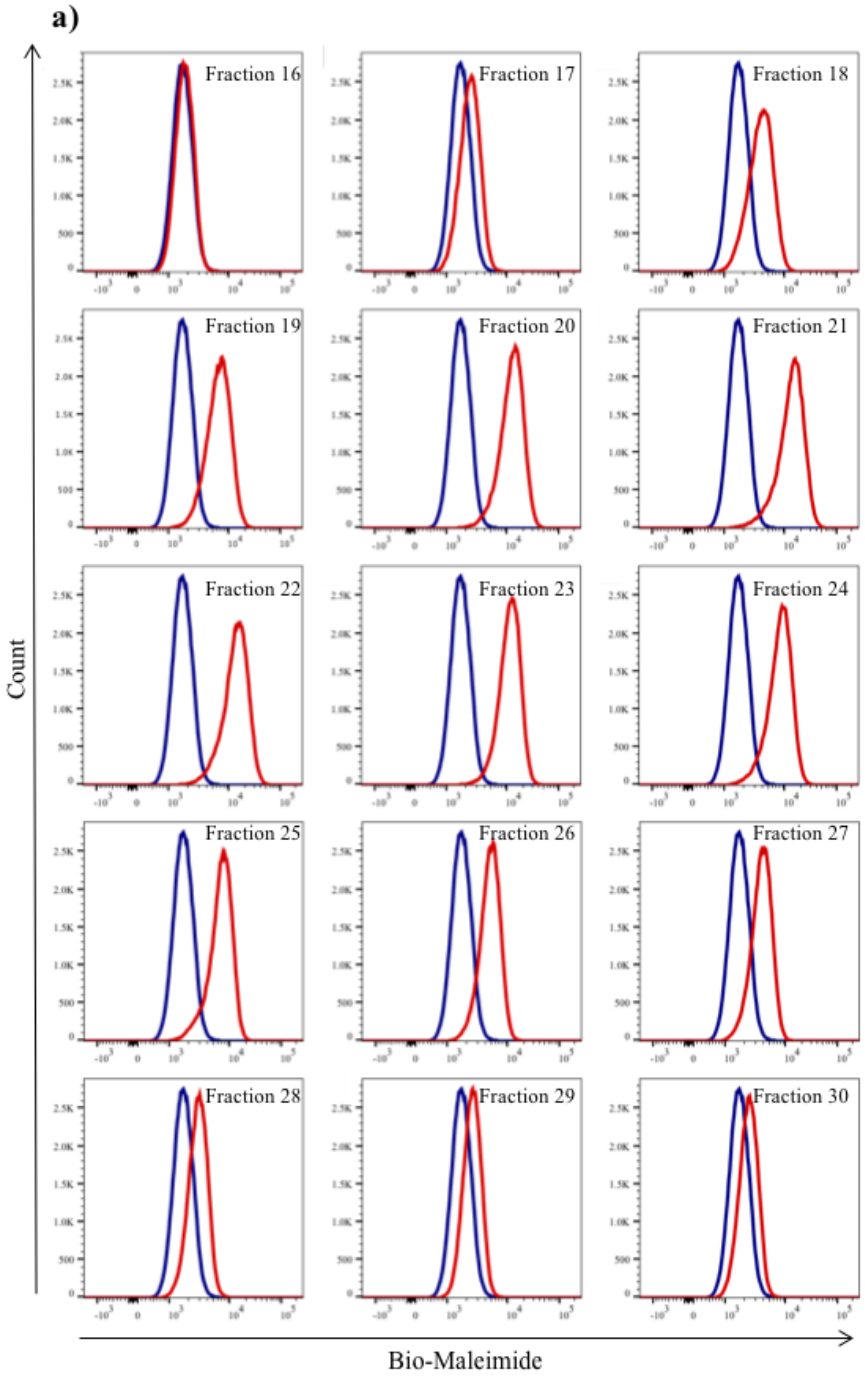


Fig 8.1 Representative flow cytometry histograms of Ishikawa cells treated with purified bio-maleimide labelled PBS (Negative control).

Ishikawa cells were treated with 100 µL of each fraction of bio-maleimide labelled PBS (negative control, red) or PBS (blue) for 30 min; and analysed by flow cytometry. This figure depicts histograms with the bio-maleimide fluorescence intensity of negative control **(a)** purified fractions 1 to 30 and **(b)** non-purified fraction.

8.4 Appendix 4

Table 8.3 Clinical characteristics of patients recruited for ESC isolation.

Patient	Age	Medical Procedure	Day of the cycle	Pregnancies	Fertility
1	35	Laparoscopic sterilisation	21	3	Normal
2	37	Laparoscopic sterilisation	23	2	Normal
3	33	Laparoscopic sterilisation	13	2	Normal
4	39	*In Vitro* Fertilization	Unknown	Unknown	Subfertile (Unknown cause)
5	47	*In Vitro* Fertilization	21	Unknown	Subfertile (female age)

8.5 Appendix 5

Table 8.4 Clinical characteristics of patients recruited for EIC isolation.
Pregnancy is defined as implantation happening in the utero, albeit ectopic pregnancies are precluded. PCOS = polycystic ovarian syndrome. LSO = left salpingectomy.

Patient	Age	Day of the cycle	Pregnancies	Livebirths	Fertility
1	33	20	0	0	male factor
2	35	N/A	1	0	N/A
3	37	N/A	2	0	Subfertile (PCOS)
4	39	N/A	1	0	Subfertile (unexplained)
5	29	N/A	0	0	Subfertile (endometriosis)
6	32	N/A	0	0	male factor
7	33	19	0	0	Subfertile (endometriosis)
8	35	21	0	0	male factor
9	29	N/A	2	0	Subfertile (LSO & male infertility)
10	31	21	1	0	Subfertile (unexplained)
11	42	21	2	1	Subfertile (unexplained, fibroid removed)
12	31	23	1	1	male factor
13	32	18	1	0	male factor
14	32	23	0	0	Subfertile (unexplained)

References

Aalberts M, Stout TA, Stoorvogel W. Prostasomes: extracellular vesicles from the prostate. *Reproduction* 2014;**147**:R1-14.

Aalberts M, van Dissel-Emiliani FM, van Adrichem NP, van Wijnen M, Wauben MH, Stout TA, Stoorvogel W. Identification of distinct populations of prostasomes that differentially express prostate stem cell antigen, annexin A1, and GLIPR2 in humans. *Biol Reprod* 2012;**86**:82.

Adams SM, Gayer N, Hosie MJ, Murphy CR. Human uterodomes (pinopods) do not display pinocytotic function. *Hum Reprod* 2002;**17**:1980-1986.

Afami M, Martin, F., Fullwood N. Identify and characterise stem cell population of the human endometrium. 2015. Lancaster University.

Aghajanova L, Altmae S, Bjuresten K, Hovatta O, Landgren BM, Stavreus-Evers A. Disturbances in the LIF pathway in the endometrium among women with unexplained infertility. *Fertil Steril* 2009a;**91**:2602-2610.

Aghajanova L, Hamilton A, Kwintkiewicz J, Vo KC, Giudice LC. Steroidogenic enzyme and key decidualization marker dysregulation in endometrial stromal cells from women with versus without endometriosis. *Biol Reprod* 2009b;**80**:105-114.

Ain R, Dai G, Dunmore JH, Godwin AR, Soares MJ. A prolactin family paralog regulates reproductive adaptations to a physiological stressor. *Proc Natl Acad Sci U S A* 2004;**101**:16543-16548.

Alberola-Ila J, Places L, de la Calle O, Romero M, Yague J, Gallart T, Vives J, Lozano F. Stimulation through the TCR/CD3 complex up-regulates the CD2 surface expression on human T lymphocytes. *J Immunol* 1991;**146**:1085-1092.

Aluvihare VR, Kallikourdis M, Betz AG. Regulatory T cells mediate maternal tolerance to the fetus. *Nat Immunol* 2004;**5**:266-271.

Aplin JD, Ruane PT. Embryo-epithelium interactions during implantation at a glance. *J Cell Sci* 2017;**130**:15-22.

Arienti G, Carlini E, Palmerini CA. Fusion of human sperm to prostasomes at acidic pH. *J Membr Biol* 1997;**155**:89-94.

Arpaia N, Green JA, Moltedo B, Arvey A, Hemmers S, Yuan S, Treuting PM, Rudensky AY. A Distinct Function of Regulatory T Cells in Tissue Protection. *Cell* 2015;**162**:1078-1089.

Asea A, Jean-Pierre C, Kaur P, Rao P, Linhares IM, Skupski D, Witkin SS. Heat shock protein-containing exosomes in mid-trimester amniotic fluids. *J Reprod Immunol* 2008;**79**:12-17.

Astarie-Dequeker C, Carreno S, Cougoule C, Maridonneau-Parini I. The protein tyrosine kinase Hck is located on lysosomal vesicles that are physically and functionally distinct from CD63-positive lysosomes in human macrophages. *J Cell Sci* 2002;**115**:81-89.

Ata B, Abou-Setta AM, Seyhan A, Buckett W. Application of seminal plasma to female genital tract prior to embryo transfer in assisted reproductive technology cycles (IVF, ICSI and frozen embryo transfer). *Cochrane Database Syst Rev* 2018;**2**:CD011809.

Bacchetta R, Sartirana C, Levings MK, Bordignon C, Narula S, Roncarolo MG. Growth and expansion of human T regulatory type 1 cells are independent from TCR activation but require exogenous cytokines. *Eur J Immunol* 2002;**32**:2237-2245.

Bahar L, Kahraman S, Eras N, Pirkevi C. Comparison of endometrial biopsies of fertile women and women with repeated implantation failure at the ultrastructural level. *Turk J Med Sci* 2015;**45**:706-713.

Bai R, Latifi Z, Kusama K, Nakamura K, Shimada M, Imakawa K. Induction of immune-related gene expression by seminal exosomes in the porcine endometrium. *Biochem Biophys Res Commun* 2018;**495**:1094-1101.
Baietti MF, Zhang Z, Mortier E, Melchior A, Degeest G, Geeraerts A, Ivarsson Y, Depoortere F, Coomans C, Vermeiren E *et al.* Syndecan-syntenin-ALIX regulates the biogenesis of exosomes. *Nat Cell Biol* 2012;**14**:677-685.
Bao SH, Wang XP, De Lin Q, Wang WJ, Yin GJ, Qiu LH. Decidual CD4+CD25+CD127dim/- regulatory T cells in patients with unexplained recurrent spontaneous miscarriage. *Eur J Obstet Gynecol Reprod Biol* 2011;**155**:94-98.
Barcelo M, Mata A, Bassas L, Larriba S. Exosomal microRNAs in seminal plasma are markers of the origin of azoospermia and can predict the presence of sperm in testicular tissue. *Hum Reprod* 2018;**33**:1087-1098.
Barrett JH, Brennan P, Fiddler M, Silman AJ. Does rheumatoid arthritis remit during pregnancy and relapse postpartum? Results from a nationwide study in the United Kingdom performed prospectively from late pregnancy. *Arthritis Rheum* 1999;**42**:1219-1227.
Bastu E, Mutlu MF, Yasa C, Dural O, Nehir Aytan A, Celik C, Buyru F, Yeh J. Role of Mucin 1 and Glycodelin A in recurrent implantation failure. *Fertil Steril* 2015;**103**:1059-1064 e1052.
Bechoua S, Rieu I, Sion B, Grizard G. Prostasomes as potential modulators of tyrosine phosphorylation in human spermatozoa. *Syst Biol Reprod Med* 2011;**57**:139-148.
Bellinge BS, Copeland CM, Thomas TD, Mazzucchelli RE, O'Neil G, Cohen MJ. The influence of patient insemination on the implantation rate in an in vitro fertilization and embryo transfer program. *Fertil Steril* 1986;**46**:252-256.
Ben-Jonathan N, Mershon JL, Allen DL, Steinmetz RW. Extrapituitary prolactin: distribution, regulation, functions, and clinical aspects. *Endocr Rev* 1996;**17**:639-669.
Bentin-Ley U, Horn T, Sjogren A, Sorensen S, Falck Larsen J, Hamberger L. Ultrastructure of human blastocyst-endometrial interactions in vitro. *J Reprod Fertil* 2000;**120**:337-350.
Bentin-Ley U, Pedersen B, Lindenberg S, Larsen JF, Hamberger L, Horn T. Isolation and culture of human endometrial cells in a three-dimensional culture system. *J Reprod Fertil* 1994;**101**:327-332.
Bentin-Ley U, Sjogren A, Nilsson L, Hamberger L, Larsen JF, Horn T. Presence of uterine pinopodes at the embryo-endometrial interface during human implantation in vitro. *Hum Reprod* 1999;**14**:515-520.
Bergamini CM, Pansini F, Bettocchi S, Jr., Segala V, Dallocchio F, Bagni B, Mollica G. Hormonal sensitivity of adenylate cyclase from human endometrium: modulation by estradiol. *J Steroid Biochem* 1985;**22**:299-303.
Bhattacharjee A, Pal S, Feldman GM, Cathcart MK. Hck is a key regulator of gene expression in alternatively activated human monocytes. *J Biol Chem* 2011;**286**:36709-36723.
Biggs CN, Siddiqui KM, Al-Zahrani AA, Pardhan S, Brett SI, Guo QQ, Yang J, Wolf P, Power NE, Durfee PN *et al.* Prostate extracellular vesicles in patient plasma as a liquid biopsy platform for prostate cancer using nanoscale flow cytometry. *Oncotarget* 2016;**7**:8839-8849.
Blois SM, Ilarregui JM, Tometten M, Garcia M, Orsal AS, Cordo-Russo R, Toscano MA, Bianco GA, Kobelt P, Handjiski B *et al.* A pivotal role for galectin-1 in fetomaternal tolerance. *Nat Med* 2007;**13**:1450-1457.

Bole-Feysot C, Goffin V, Edery M, Binart N, Kelly PA. Prolactin (PRL) and its receptor: actions, signal transduction pathways and phenotypes observed in PRL receptor knockout mice. *Endocr Rev* 1998;**19**:225-268.
Brody I, Ronquist G, Gottfries A. Ultrastructural localization of the prostasome - an organelle in human seminal plasma. *Ups J Med Sci* 1983;**88**:63-80.
Brouwers JF, Aalberts M, Jansen JW, van Niel G, Wauben MH, Stout TA, Helms JB, Stoorvogel W. Distinct lipid compositions of two types of human prostasomes. *Proteomics* 2013;**13**:1660-1666.
Buck VU, Windoffer R, Leube RE, Classen-Linke I. Redistribution of adhering junctions in human endometrial epithelial cells during the implantation window of the menstrual cycle. *Histochem Cell Biol* 2012;**137**:777-790.
Byrn RA, Zhang D, Eyre R, McGowan K, Kiessling AA. HIV-1 in semen: an isolated virus reservoir. *Lancet* 1997;**350**:1141.
Caballero-Campo P, Dominguez F, Coloma J, Meseguer M, Remohi J, Pellicer A, Simon C. Hormonal and embryonic regulation of chemokines IL-8, MCP-1 and RANTES in the human endometrium during the window of implantation. *Mol Hum Reprod* 2002;**8**:375-384.
Caby MP, Lankar D, Vincendeau-Scherrer C, Raposo G, Bonnerot C. Exosomal-like vesicles are present in human blood plasma. *Int Immunol* 2005;**17**:879-887.
Campbell HK, Maiers JL, DeMali KA. Interplay between tight junctions & adherens junctions. *Exp Cell Res* 2017;**358**:39-44.
Cantrell DA, Collins MK, Crumpton MJ. Autocrine regulation of T-lymphocyte proliferation: differential induction of IL-2 and IL-2 receptor. *Immunology* 1988;**65**:343-349.
Carlini E, Palmerini CA, Cosmi EV, Arienti G. Fusion of sperm with prostasomes: effects on membrane fluidity. *Arch Biochem Biophys* 1997;**343**:6-12.
Carlsson L, Nilsson O, Larsson A, Stridsberg M, Sahlen G, Ronquist G. Characteristics of human prostasomes isolated from three different sources. *Prostate* 2003;**54**:322-330.
Carreno S, Gouze ME, Schaak S, Emorine LJ, Maridonneau-Parini I. Lack of palmitoylation redirects p59Hck from the plasma membrane to p61Hck-positive lysosomes. *J Biol Chem* 2000;**275**:36223-36229.
Cerwenka A, Kovar H, Majdic O, Holter W. Fas- and activation-induced apoptosis are reduced in human T cells preactivated in the presence of TGF-beta 1. *J Immunol* 1996;**156**:459-464.
Cha J, Sun X, Dey SK. Mechanisms of implantation: strategies for successful pregnancy. *Nat Med* 2012;**18**:1754-1767.
Chachamovich JR, Chachamovich E, Ezer H, Fleck MP, Knauth D, Passos EP. Investigating quality of life and health-related quality of life in infertility: a systematic review. *J Psychosom Obstet Gynaecol* 2010;**31**:101-110.
Chang HJ, Lee JH, Hwang KJ, Kim MR, Chang KH, Park DW, Min CK. Transforming growth factor (TGF)-beta1-induced human endometrial stromal cell decidualization through extracellular signal-regulated kinase and Smad activation in vitro: peroxisome proliferator-activated receptor gamma acts as a negative regulator of TGF-beta1. *Fertil Steril* 2008;**90**:1357-1365.
Chargaff E, West R. The biological significance of the thromboplastic protein of blood. *J Biol Chem* 1946;**166**:189-197.
Chemes EH, Rawe YV. Sperm pathology: a step beyond descriptive morphology. Origin, characterization and fertility potential of abnormal sperm phenotypes in infertile men. *Hum Reprod Update* 2003;**9**:405-428.

Chen CC, Liu L, Ma F, Wong CW, Guo XE, Chacko JV, Farhoodi HP, Zhang SX, Zimak J, Segaliny A *et al.* Elucidation of Exosome Migration across the Blood-Brain Barrier Model In Vitro. *Cell Mol Bioeng* 2016a;**9**:509-529.
Chen CD, Chen SU, Chou CH, Chen MJ, Wen WF, Wu SY, Yang YS, Yang JH. High Estradiol Concentrations Induce Heat Shock Protein 70 Expression and Suppress Nuclear Factor Kappa B Activation in Human Endometrial Epithelial Cells. *Biol Reprod* 2016b;**95**:87.
Chen JC, Johnson BA, Erikson DW, Piltonen TT, Barragan F, Chu S, Kohgadai N, Irwin JC, Greene WC, Giudice LC *et al.* Seminal plasma induces global transcriptomic changes associated with cell migration, proliferation and viability in endometrial epithelial cells and stromal fibroblasts. *Hum Reprod* 2014;**29**:1255-1270.
Chen JC, Roan NR. Isolation and Culture of Human Endometrial Epithelial Cells and Stromal Fibroblasts. *Bio Protoc* 2015;**5**.
Chen JJ, Wang Y, Meng X, Ruan YC, Zou F, Chan HC. MRP4 regulates ENaC-dependent CREB/COX-2/PGE2 signaling during embryo implantation. *Oncotarget* 2017;**8**:78520-78529.
Chiasserini D, Mazzoni M, Bordi F, Sennato S, Susta F, Orvietani PL, Binaglia L, Palmerini CA. Identification and Partial Characterization of Two Populations of Prostasomes by a Combination of Dynamic Light Scattering and Proteomic Analysis. *J Membr Biol* 2015;**248**:991-1004.
Chicea R, Ispasoiu F, Focsa M. Seminal plasma insemination during ovum-pickup--a method to increase pregnancy rate in IVF/ICSI procedure. A pilot randomized trial. *J Assist Reprod Genet* 2013;**30**:569-574.
Child T. Causes and investigations of male and female infertility. In Kevin Coward DW (ed) *Textbook of Clinical Embryology*. 2013. Cambridge University Press, Spain.
Chilton BS, Daniel JC, Jr. Differences in the rabbit uterine response to progesterone as influenced by growth hormone or prolactin. *J Reprod Fertil* 1987;**79**:581-587.
Chou CS, Tai CJ, MacCalman CD, Leung PC. Dose-dependent effects of gonadotropin releasing hormone on matrix metalloproteinase (MMP)-2, and MMP-9 and tissue specific inhibitor of metalloproteinases-1 messenger ribonucleic acid levels in human decidual Stromal cells in vitro. *J Clin Endocrinol Metab* 2003;**88**:680-688.
Costanza M, Binart N, Steinman L, Pedotti R. Prolactin: a versatile regulator of inflammation and autoimmune pathology. *Autoimmun Rev* 2015;**14**:223-230.
Coulam C. What about superfertility, decidualization, and natural selection? *J Assist Reprod Genet* 2016;**33**:577-580.
Crawford G, Ray A, Gudi A, Shah A, Homburg R. The role of seminal plasma for improved outcomes during in vitro fertilization treatment: review of the literature and meta-analysis. *Hum Reprod Update* 2015;**21**:275-284.
D'Souza-Schorey C, Schorey JS. Regulation and mechanisms of extracellular vesicle biogenesis and secretion. *Essays Biochem* 2018;**62**:125-133.
Da Broi MG, Rocha CV, Jr., Carvalho FM, Martins WP, Ferriani RA, Navarro PA. Ultrastructural Evaluation of Eutopic Endometrium of Infertile Women With and Without Endometriosis During the Window of Implantation: A Pilot Study. *Reprod Sci* 2017;**24**:1469-1475.
da Cruz RS, Carney EJ, Clarke J, Cao H, Cruz MI, Benitez C, Jin L, Fu Y, Cheng Z, Wang Y *et al.* Paternal malnutrition programs breast cancer risk and tumor metabolism in offspring. *Breast Cancer Res* 2018;**20**:99.
Daniel JC, Jr., Jetton AE, Chilton BS. Prolactin as a factor in the uterine response to progesterone in rabbits. *J Reprod Fertil* 1984;**72**:443-452.

de Ziegler D, Fanchin R, de Moustier B, Bulletti C. The hormonal control of endometrial receptivity: estrogen (E-2) and progesterone. *Journal of Reproductive Immunology* 1998;**39**:149-166.
Diao LH, Li GG, Zhu YC, Tu WW, Huang CY, Lian RC, Chen X, Li YY, Zhang T, Huang Y *et al.* Human chorionic gonadotropin potentially affects pregnancy outcome in women with recurrent implantation failure by regulating the homing preference of regulatory T cells. *Am J Reprod Immunol* 2017;**77**.
Dimova T, Nagaeva O, Stenqvist AC, Hedlund M, Kjellberg L, Strand M, Dehlin E, Mincheva-Nilsson L. Maternal Foxp3 expressing CD4+ CD25+ and CD4+ CD25- regulatory T-cell populations are enriched in human early normal pregnancy decidua: a phenotypic study of paired decidual and peripheral blood samples. *Am J Reprod Immunol* 2011;**66 Suppl 1**:44-56.
Dobaczewski M, Xia Y, Bujak M, Gonzalez-Quesada C, Frangogiannis NG. CCR5 signaling suppresses inflammation and reduces adverse remodeling of the infarcted heart, mediating recruitment of regulatory T cells. *Am J Pathol* 2010;**176**:2177-2187.
Dockery PaB, M. *The fine structure of the mature human endometrium*. 2008. Informa Healthcare, London, UK.
Doria A, Ghirardello A, Iaccarino L, Zampieri S, Punzi L, Tarricone E, Ruffatti A, Sulli A, Sarzi-Puttini PC, Gambari PF *et al.* Pregnancy, cytokines, and disease activity in systemic lupus erythematosus. *Arthritis Rheum* 2004;**51**:989-995.
Doyle U, Sampson N, Zenzmaier C, Schwarzler P, Berger P. Seminal plasma enhances and accelerates progesterone-induced decidualisation of human endometrial stromal cells. *Reprod Fertil Dev* 2012;**24**:517-522.
Drabovich AP, Saraon P, Jarvi K, Diamandis EP. Seminal plasma as a diagnostic fluid for male reproductive system disorders. *Nat Rev Urol* 2014;**11**:278-288.
Dragovic RA, Southcombe JH, Tannetta DS, Redman CW, Sargent IL. Multicolor flow cytometry and nanoparticle tracking analysis of extracellular vesicles in the plasma of normal pregnant and pre-eclamptic women. *Biol Reprod* 2013;**89**:151.
Drake PM, Gunn MD, Charo IF, Tsou CL, Zhou Y, Huang L, Fisher SJ. Human placental cytotrophoblasts attract monocytes and CD56(bright) natural killer cells via the actions of monocyte inflammatory protein 1alpha. *J Exp Med* 2001;**193**:1199-1212.
Druart X, de Graaf S. Seminal plasma proteomes and sperm fertility. *Anim Reprod Sci* 2018;**194**:33-40.
Dunn CL, Kelly RW, Critchley HO. Decidualization of the human endometrial stromal cell: an enigmatic transformation. *Reprod Biomed Online* 2003;**7**:151-161.
Eriksson M, Meadows SK, Wira CR, Sentman CL. Unique phenotype of human uterine NK cells and their regulation by endogenous TGF-beta. *J Leukoc Biol* 2004;**76**:667-675.
Erlebacher A. Immunology of the maternal-fetal interface. *Annu Rev Immunol* 2013;**31**:387-411.
Eswaran N, Agaram Sundaram V, Rao KA, Thalaivarisai Balasundaram S. Simple isolation and characterization of seminal plasma extracellular vesicle and its total RNA in an academic lab. *3 Biotech* 2018;**8**:139.
Farquhar MG, Palade GE. Junctional complexes in various epithelia. *J Cell Biol* 1963;**17**:375-412.
Favre-Inhofer A, Rafii A, Carbonnel M, Revaux A, Ayoubi JM. Uterine transplantation: Review in human research. *J Gynecol Obstet Hum Reprod* 2018;**47**:213-221.
Fazleabas AT, Strakova Z. Endometrial function: cell specific changes in the uterine environment. *Mol Cell Endocrinol* 2002;**186**:143-147.

Featherstone K, White MR, Davis JR. The prolactin gene: a paradigm of tissue-specific gene regulation with complex temporal transcription dynamics. *J Neuroendocrinol* 2012;**24**:977-990.
Feeney JG, Scott JS. Pre-eclampsia and changed paternity. *Eur J Obstet Gynecol Reprod Biol* 1980;**11**:35-38.
Ferlay J, Parkin DM, Steliarova-Foucher E. Estimates of cancer incidence and mortality in Europe in 2008. *Eur J Cancer* 2010;**46**:765-781.
Fernandez N, Cooper J, Sprinks M, AbdElrahman M, Fiszer D, Kurpisz M, Dealtry G. A critical review of the role of the major histocompatibility complex in fertilization, preimplantation development and feto-maternal interactions. *Hum Reprod Update* 1999;**5**:234-248.
Fitzer-Attas CJ, Lowry M, Crowley MT, Finn AJ, Meng F, DeFranco AL, Lowell CA. Fcgamma receptor-mediated phagocytosis in macrophages lacking the Src family tyrosine kinases Hck, Fgr, and Lyn. *J Exp Med* 2000;**191**:669-682.
Fleming H. Differentiation in human endometrial cells in monolayer culture: dependence on a factor in fetal bovine serum. *J Cell Biochem* 1995;**57**:262-270.
Fleming TP, Watkins AJ, Velazquez MA, Mathers JC, Prentice AM, Stephenson J, Barker M, Saffery R, Yajnik CS, Eckert JJ *et al.* Origins of lifetime health around the time of conception: causes and consequences. *Lancet* 2018;**391**:1842-1852.
Flynn L, Byrne B, Carton J, Kelehan P, O'Herlihy C, O'Farrelly C. Menstrual cycle dependent fluctuations in NK and T-lymphocyte subsets from non-pregnant human endometrium. *Am J Reprod Immunol* 2000;**43**:209-217.
Fontenot JD, Gavin MA, Rudensky AY. Foxp3 programs the development and function of CD4+CD25+ regulatory T cells. *Nat Immunol* 2003;**4**:330-336.
Fowler DJ, Nicolaides KH, Miell JP. Insulin-like growth factor binding protein-1 (IGFBP-1): a multifunctional role in the human female reproductive tract. *Hum Reprod Update* 2000;**6**:495-504.
Fox DA, Hussey RE, Fitzgerald KA, Bensussan A, Daley JF, Schlossman SF, Reinherz EL. Activation of human thymocytes via the 50KD T11 sheep erythrocyte binding protein induces the expression of interleukin 2 receptors on both T3+ and T3- populations. *J Immunol* 1985;**134**:330-335.
Franchi A, Bocca S, Anderson S, Riggs R, Oehninger S. Expression of milk fat globule EGF-factor 8 (MFG-E8) mRNA and protein in the human endometrium and its regulation by prolactin. *Mol Hum Reprod* 2011;**17**:360-371.
Frank GR, Brar AK, Cedars MI, Handwerger S. Prostaglandin E2 enhances human endometrial stromal cell differentiation. *Endocrinology* 1994;**134**:258-263.
Franz C, Boing AN, Montag M, Strowitzki T, Markert UR, Mastenbroek S, Nieuwland R, Toth B. Extracellular vesicles in human follicular fluid do not promote coagulation. *Reprod Biomed Online* 2016;**33**:652-655.
Freier CP, Kuhn C, Rapp M, Endres S, Mayr D, Friese K, Anz D, Jeschke U. Expression of CCL22 and Infiltration by Regulatory T Cells are Increased in the Decidua of Human Miscarriage Placentas. *American Journal of Reproductive Immunology* 2015;**74**:216-227.
Friand V, David G, Zimmermann P. Syntenin and syndecan in the biogenesis of exosomes. *Biol Cell* 2015;**107**:331-341.
Friedler S, Ben-Ami I, Gidoni Y, Strassburger D, Kasterstein E, Maslansky B, Komarovsy D, Bern O, Ron-El R, Raziel A. Effect of seminal plasma application to the vaginal vault in in vitro fertilization or intracytoplasmic sperm injection treatment cycles-a double-blind, placebo-controlled, randomized study. *J Assist Reprod Genet* 2013;**30**:907-911.

Frolikova M, Manaskova-Postlerova P, Cerny J, Jankovicova J, Simonik O, Pohlova A, Secova P, Antalikova J, Dvorakova-Hortova K. CD9 and CD81 Interactions and Their Structural Modelling in Sperm Prior to Fertilization. *Int J Mol Sci* 2018;**19**.
Galgani M, Insabato L, Cali G, Della Gatta AN, Mirra P, Papaccio F, Santopaolo M, Alviggi C, Mollo A, Strina I *et al.* Regulatory T cells, inflammation, and endoplasmic reticulum stress in women with defective endometrial receptivity. *Fertil Steril* 2015;**103**:1579-1586 e1571.
Gangalum RK, Atanasov IC, Zhou ZH, Bhat SP. AlphaB-crystallin is found in detergent-resistant membrane microdomains and is secreted via exosomes from human retinal pigment epithelial cells. *J Biol Chem* 2011;**286**:3261-3269.
Gao H, Gao Y, Pang W, Pan C, Ji H, Dong W. Iridoviral infection can be reduced by UCHL1-loaded exosomes from the testis of Chinese giant salamanders (Andrias davidianus). *Vet Microbiol* 2018;**224**:50-57.
Garcia MA, Nelson WJ, Chavez N. Cell-Cell Junctions Organize Structural and Signaling Networks. *Cold Spring Harb Perspect Biol* 2018;**10**.
Garcia-Rodriguez A, de la Casa M, Peinado H, Gosalvez J, Roy R. Human prostasomes from normozoospermic and non-normozoospermic men show a differential protein expression pattern. *Andrology* 2018.
Gardner DK, Surrey E, Minjarez D, Leitz A, Stevens J, Schoolcraft WB. Single blastocyst transfer: a prospective randomized trial. *Fertil Steril* 2004;**81**:551-555.
Gauthier SA, Perez-Gonzalez R, Sharma A, Huang FK, Alldred MJ, Pawlik M, Kaur G, Ginsberg SD, Neubert TA, Levy E. Enhanced exosome secretion in Down syndrome brain - a protective mechanism to alleviate neuronal endosomal abnormalities. *Acta Neuropathol Commun* 2017;**5**:65.
Gellersen B, Brosens IA, Brosens JJ. Decidualization of the human endometrium: mechanisms, functions, and clinical perspectives. *Semin Reprod Med* 2007;**25**:445-453.
Gellersen B, Brosens J. Cyclic AMP and progesterone receptor cross-talk in human endometrium: a decidualizing affair. *J Endocrinol* 2003;**178**:357-372.
Gellersen B, Brosens JJ. Cyclic decidualization of the human endometrium in reproductive health and failure. *Endocr Rev* 2014;**35**:851-905.
Gerli R, Rambotti P, Nicoletti I, Orlandi S, Migliorati G, Riccardi C. Reduced number of natural killer cells in patients with pathological hyperprolactinemia. *Clin Exp Immunol* 1986;**64**:399-406.
Ghiringhelli F, Menard C, Terme M, Flament C, Taieb J, Chaput N, Puig PE, Novault S, Escudier B, Vivier E *et al.* CD4+CD25+ regulatory T cells inhibit natural killer cell functions in a transforming growth factor-beta-dependent manner. *J Exp Med* 2005;**202**:1075-1085.
Giacomini E, Vago R, Sanchez AM, Podini P, Zarovni N, Murdica V, Rizzo R, Bortolotti D, Candiani M, Vigano P. Secretome of in vitro cultured human embryos contains extracellular vesicles that are uptaken by the maternal side. *Sci Rep* 2017;**7**:5210.
Gipson IK, Blalock T, Tisdale A, Spurr-Michaud S, Allcorn S, Stavreus-Evers A, Gemzell K. MUC16 is lost from the uterodome (pinopode) surface of the receptive human endometrium: in vitro evidence that MUC16 is a barrier to trophoblast adherence. *Biol Reprod* 2008;**78**:134-142.
Girouard J, Frenette G, Sullivan R. Comparative proteome and lipid profiles of bovine epididymosomes collected in the intraluminal compartment of the caput and cauda epididymidis. *Int J Androl* 2011;**34**:e475-486.
Glasser SR, Mulholland J. Receptivity is a polarity dependent special function of hormonally regulated uterine epithelial cells. *Microsc Res Tech* 1993;**25**:106-120.

Goni FM, Alonso A. Effects of ceramide and other simple sphingolipids on membrane lateral structure. *Biochim Biophys Acta* 2009;**1788**:169-177.
Gorelik L, Constant S, Flavell RA. Mechanism of transforming growth factor beta-induced inhibition of T helper type 1 differentiation. *J Exp Med* 2002;**195**:1499-1505.
Graham CH, Lysiak JJ, McCrae KR, Lala PK. Localization of transforming growth factor-beta at the human fetal-maternal interface: role in trophoblast growth and differentiation. *Biol Reprod* 1992;**46**:561-572.
Granot I, Gnainsky Y, Dekel N. Endometrial inflammation and effect on implantation improvement and pregnancy outcome. *Reproduction* 2012;**144**:661-668.
Green EA, Gorelik L, McGregor CM, Tran EH, Flavell RA. CD4+CD25+ T regulatory cells control anti-islet CD8+ T cells through TGF-beta-TGF-beta receptor interactions in type 1 diabetes. *Proc Natl Acad Sci U S A* 2003;**100**:10878-10883.
Greening DW, Gopal SK, Xu R, Simpson RJ, Chen W. Exosomes and their roles in immune regulation and cancer. *Semin Cell Dev Biol* 2015;**40**:72-81.
Greening DW, Nguyen HP, Evans J, Simpson RJ, Salamonsen LA. Modulating the endometrial epithelial proteome and secretome in preparation for pregnancy: The role of ovarian steroid and pregnancy hormones. *J Proteomics* 2016;**144**:99-112.
Grund S, Grummer R. Direct Cell(-)Cell Interactions in the Endometrium and in Endometrial Pathophysiology. *Int J Mol Sci* 2018;**19**.
Gubbay O, Critchley HO, Bowen JM, King A, Jabbour HN. Prolactin induces ERK phosphorylation in epithelial and CD56(+) natural killer cells of the human endometrium. *J Clin Endocrinol Metab* 2002;**87**:2329-2335.
Guffanti E, Kittur N, Brodt ZN, Polotsky AJ, Kuokkanen SM, Heller DS, Young SL, Santoro N, Meier UT. Nuclear pore complex proteins mark the implantation window in human endometrium. *J Cell Sci* 2008;**121**:2037-2045.
Guiet R, Poincloux R, Castandet J, Marois L, Labrousse A, Le Cabec V, Maridonneau-Parini I. Hematopoietic cell kinase (Hck) isoforms and phagocyte duties - from signaling and actin reorganization to migration and phagocytosis. *Eur J Cell Biol* 2008;**87**:527-542.
Guillomot M, Guay P. Ultrastructural features of the cell surfaces of uterine and trophoblastic epithelia during embryo attachment in the cow. *Anat Rec* 1982;**204**:315-322.
Gupta S. Mechanisms of transmembrane signalling in human T cell activation. *Mol Cell Biochem* 1989;**91**:45-50.
Gutsche S, von Wolff M, Strowitzki T, Thaler CJ. Seminal plasma induces mRNA expression of IL-1beta, IL-6 and LIF in endometrial epithelial cells in vitro. *Mol Hum Reprod* 2003;**9**:785-791.
Hanna J, Goldman-Wohl D, Hamani Y, Avraham I, Greenfield C, Natanson-Yaron S, Prus D, Cohen-Daniel L, Arnon TI, Manaster I *et al.* Decidual NK cells regulate key developmental processes at the human fetal-maternal interface. *Nat Med* 2006;**12**:1065-1074.
Hantak AM, Bagchi IC, Bagchi MK. Role of uterine stromal-epithelial crosstalk in embryo implantation. *Int J Dev Biol* 2014;**58**:139-146.
Harper J, Jackson E, Sermon K, Aitken RJ, Harbottle S, Mocanu E, Hardarson T, Mathur R, Viville S, Vail A *et al.* Adjuncts in the IVF laboratory: where is the evidence for 'add-on' interventions? *Hum Reprod* 2017;**32**:485-491.
Hessvik NP, Llorente A. Current knowledge on exosome biogenesis and release. *Cell Mol Life Sci* 2018;**75**:193-208.
HFEA. Fertility treatment 2014 - Trends and figures. 2016. Human Fertilisation & Embryology Authority

HFEA. Fertility treatment 2014-2016 Trends and figures. 2018. Human Fertilisation & Embryology Authority
Hoog JL, Lotvall J. Diversity of extracellular vesicles in human ejaculates revealed by cryo-electron microscopy. *J Extracell Vesicles* 2015;**4**:28680.
Hori S, Nomura T, Sakaguchi S. Control of regulatory T cell development by the transcription factor Foxp3. *Science* 2003;**299**:1057-1061.
Horne AW, Lalani EN, Margara RA, Ryder TA, Mobberley MA, White JO. The expression pattern of MUC1 glycoforms and other biomarkers of endometrial receptivity in fertile and infertile women. *Mol Reprod Dev* 2005;**72**:216-229.
Horne AW, White JO, Lalani el N, Mobberley MA, Margara RA, Trew GH, Ryder TA. Analysis of epitopes on endometrial epithelium by scanning immunoelectron microscopy. *Biochem Biophys Res Commun* 2002;**292**:102-108.
Horwich A, Parker C, de Reijke T, Kataja V, Group EGW. Prostate cancer: ESMO Clinical Practice Guidelines for diagnosis, treatment and follow-up. *Ann Oncol* 2013;**24 Suppl 6**:vi106-114.
Huang SJ, Schatz F, Masch R, Rahman M, Buchwalder L, Niven-Fairchild T, Tang C, Abrahams VM, Krikun G, Lockwood CJ. Regulation of chemokine production in response to pro-inflammatory cytokines in first trimester decidual cells. *J Reprod Immunol* 2006;**72**:60-73.
Hunt JS, Pace JL, Morales PJ, Ober C. Immunogenicity of the soluble isoforms of HLA-G. *Mol Hum Reprod* 2003;**9**:729-735.
Hurley JH. ESCRT complexes and the biogenesis of multivesicular bodies. *Curr Opin Cell Biol* 2008;**20**:4-11.
Hviid MM, Macklon N. Immune modulation treatments-where is the evidence? *Fertil Steril* 2017;**107**:1284-1293.
Iaccarino L, Ghirardello A, Zen M, Villalta D, Tincani A, Punzi L, Doria A. Polarization of TH2 response is decreased during pregnancy in systemic lupus erythematosus. *Reumatismo* 2012;**64**:314-320.
Illingworth IM, Kiszka I, Bagley S, Ireland GW, Garrod DR, Kimber SJ. Desmosomes are reduced in the mouse uterine luminal epithelium during the preimplantation period of pregnancy: a mechanism for facilitation of implantation. *Biol Reprod* 2000;**63**:1764-1773.
Inada K, Shima T, Nakashima A, Aoki K, Ito M, Saito S. Characterization of regulatory T cells in decidua of miscarriage cases with abnormal or normal fetal chromosomal content. *J Reprod Immunol* 2013;**97**:104-111.
Ininns EK, Gatanaga M, Cappuccini F, Dett CA, Yamamoto RS, Granger GA, Gatanaga T. Growth of the endometrial adenocarcinoma cell line AN3 CA is modulated by tumor necrosis factor and its receptor is up-regulated by estrogen in vitro. *Endocrinology* 1992;**130**:1852-1856.
Irving JA, Lala PK. Functional role of cell surface integrins on human trophoblast cell migration: regulation by TGF-beta, IGF-II, and IGFBP-1. *Exp Cell Res* 1995;**217**:419-427.
Ishitani A, Sageshima N, Hatake K. The involvement of HLA-E and -F in pregnancy. *J Reprod Immunol* 2006;**69**:101-113.
Jansen FH, Krijgsveld J, van Rijswijk A, van den Bemd GJ, van den Berg MS, van Weerden WM, Willemsen R, Dekker LJ, Luider TM, Jenster G. Exosomal secretion of cytoplasmic prostate cancer xenograft-derived proteins. *Mol Cell Proteomics* 2009;**8**:1192-1205.

Jasper MJ, Tremellen KP, Robertson SA. Primary unexplained infertility is associated with reduced expression of the T-regulatory cell transcription factor Foxp3 in endometrial tissue. *Mol Hum Reprod* 2006;**12**:301-308.
Jin LP, Chen QY, Zhang T, Guo PF, Li DJ. The CD4+CD25 bright regulatory T cells and CTLA-4 expression in peripheral and decidual lymphocytes are down-regulated in human miscarriage. *Clin Immunol* 2009;**133**:402-410.
Joaquin Gadea JP, Junaid Kashir, Kevin Coward. The male reproductive tract and spermatogeneis. In Kevin Coward DW (ed) *Textbook of Clinical Embryology*. 2013. Cambridge University Press, USA.
Juan T, Furthauer M. Biogenesis and function of ESCRT-dependent extracellular vesicles. *Semin Cell Dev Biol* 2018;**74**:66-77.
Kabelitz D. Do CD2 and CD3-TCR T-cell activation pathways function independently? *Immunol Today* 1990;**11**:44-47.
Kabir-Salmani M, Nikzad H, Shiokawa S, Akimoto Y, Iwashita M. Secretory role for human uterodomes (pinopods): secretion of LIF. *Mol Hum Reprod* 2005;**11**:553-559.
Kahn DA, Baltimore D. Pregnancy induces a fetal antigen-specific maternal T regulatory cell response that contributes to tolerance. *Proc Natl Acad Sci U S A* 2010;**107**:9299-9304.
Kara F, Cinar O, Erdemli-Atabenli E, Tavil-Sabuncuoglu B, Can A. Ultrastructural alterations in human decidua in miscarriages compared to normal pregnancy decidua. *Acta Obstet Gynecol Scand* 2007;**86**:1079-1086.
Kehrl JH, Wakefield LM, Roberts AB, Jakowlew S, Alvarez-Mon M, Derynck R, Sporn MB, Fauci AS. Production of transforming growth factor beta by human T lymphocytes and its potential role in the regulation of T cell growth. *J Exp Med* 1986;**163**:1037-1050.
Kelly RW, Holland P, Skibinski G, Harrison C, McMillan L, Hargreave T, James K. Extracellular organelles (prostasomes) are immunosuppressive components of human semen. *Clin Exp Immunol* 1991;**86**:550-556.
Kenneth Murphy CW. *Janeway's Immunobiology*. 9th Edition edn, 2017. Garland Science, UK.
Kerr JF, Wyllie AH, Currie AR. Apoptosis: a basic biological phenomenon with wide-ranging implications in tissue kinetics. *Br J Cancer* 1972;**26**:239-257.
Keskin DB, Allan DS, Rybalov B, Andzelm MM, Stern JN, Kopcow HD, Koopman LA, Strominger JL. TGFbeta promotes conversion of CD16+ peripheral blood NK cells into CD16- NK cells with similarities to decidual NK cells. *Proc Natl Acad Sci U S A* 2007;**104**:3378-3383.
Khalil N. TGF-beta: from latent to active. *Microbes Infect* 1999;**1**:1255-1263.
Kho EM, McCowan LM, North RA, Roberts CT, Chan E, Black MA, Taylor RS, Dekker GA, Consortium S. Duration of sexual relationship and its effect on preeclampsia and small for gestational age perinatal outcome. *J Reprod Immunol* 2009;**82**:66-73.
Kim B, Kawashima A, Ryu JA, Takahashi N, Hartman RP, King BF, Jr. Imaging of the seminal vesicle and vas deferens. *Radiographics* 2009;**29**:1105-1121.
Kimura H, Fukui A, Fujii S, Yamaguchi E, Kasai G, Mizunuma H. Timed sexual intercourse facilitates the recruitment of uterine CD56(bright) natural killer cells in women with infertility. *Am J Reprod Immunol* 2009;**62**:118-124.
Klejman A, Schreiner SJ, Nieborowska-Skorska M, Slupianek A, Wilson M, Smithgall TE, Skorski T. The Src family kinase Hck couples BCR/ABL to STAT5 activation in myeloid leukemia cells. *EMBO J* 2002;**21**:5766-5774.
Klemmt PA, Carver JG, Kennedy SH, Koninckx PR, Mardon HJ. Stromal cells from endometriotic lesions and endometrium from women with endometriosis have reduced decidualization capacity. *Fertil Steril* 2006;**85**:564-572.

Kohorn EI, Rice SI, Gordon M. In vitro production of nucleolar channel system by progesterone in human endometrium. *Nature* 1970;**228**:671-672.
Kohorn EI, Rice SI, Hemperly S, Gordon M. The relation of the structure of progestational steroids to nucleolar differentiation in human endometrium. *J Clin Endocrinol Metab* 1972;**34**:257-264.
Kulkarni AB, Huh CG, Becker D, Geiser A, Lyght M, Flanders KC, Roberts AB, Sporn MB, Ward JM, Karlsson S. Transforming growth factor beta 1 null mutation in mice causes excessive inflammatory response and early death. *Proc Natl Acad Sci U S A* 1993;**90**:770-774.
Kuramoto H, Tamura S, Notake Y. Establishment of a cell line of human endometrial adenocarcinoma in vitro. *Am J Obstet Gynecol* 1972;**114**:1012-1019.
Kusama K, Nakamura K, Bai R, Nagaoka K, Sakurai T, Imakawa K. Intrauterine exosomes are required for bovine conceptus implantation. *Biochem Biophys Res Commun* 2018;**495**:1370-1375.
Laguens G, Goni JM, Jr., Laguens M, Goni JM, Laguens R. Demonstration and characterization of HLA-DR positive cells in the stroma of human endometrium. *J Reprod Immunol* 1990;**18**:179-186.
Lalancette C, Bordeleau LJ, Faure RL, Leclerc P. Bull testicular haploid germ cells express a messenger encoding for a truncated form of the protein tyrosine kinase HCK. *Mol Reprod Dev* 2006;**73**:520-530.
Lane B, Oxberry W, Mazella J, Tseng L. Decidualization of human endometrial stromal cells in vitro: effects of progestin and relaxin on the ultrastructure and production of decidual secretory proteins. *Hum Reprod* 1994;**9**:259-266.
Laouar Y, Sutterwala FS, Gorelik L, Flavell RA. Transforming growth factor-beta controls T helper type 1 cell development through regulation of natural killer cell interferon-gamma. *Nat Immunol* 2005;**6**:600-607.
Larsen JF. Electron microscopy of the uterine epithelium in the rabbit. *J Cell Biol* 1962;**14**:49-64.
Lasser C, Alikhani VS, Ekstrom K, Eldh M, Paredes PT, Bossios A, Sjostrand M, Gabrielsson S, Lotvall J, Valadi H. Human saliva, plasma and breast milk exosomes contain RNA: uptake by macrophages. *J Transl Med* 2011;**9**:9.
Ledee N, Chaouat G, Serazin V, Lombroso R, Dubanchet S, Oger P, Louafi N, Ville Y. Endometrial vascularity by three-dimensional power Doppler ultrasound and cytokines: a complementary approach to assess uterine receptivity. *J Reprod Immunol* 2008;**77**:57-62.
Ledee-Bataille N, Dubanchet S, Coulomb-L'hermine A, Durand-Gasselin I, Frydman R, Chaouat G. A new role for natural killer cells, interleukin (IL)-12, and IL-18 in repeated implantation failure after in vitro fertilization. *Fertil Steril* 2004;**81**:59-65.
Lee SK, Kim CJ, Kim DJ, Kang JH. Immune cells in the female reproductive tract. *Immune Netw* 2015;**15**:16-26.
Li MO, Wan YY, Sanjabi S, Robertson AK, Flavell RA. Transforming growth factor-beta regulation of immune responses. *Annu Rev Immunol* 2006;**24**:99-146.
Li MQ, Wang Y, Chang KK, Meng YH, Liu LB, Mei J, Wang Y, Wang XQ, Jin LP, Li DJ. CD4+Foxp3+ regulatory T cell differentiation mediated by endometrial stromal cell-derived TECK promotes the growth and invasion of endometriotic lesions. *Cell Death Dis* 2014;**5**:e1436.
Ligam P, Manuelpillai U, Wallace EM, Walker D. Localisation of indoleamine 2,3-dioxygenase and kynurenine hydroxylase in the human placenta and decidua: implications for role of the kynurenine pathway in pregnancy. *Placenta* 2005;**26**:498-504.

Lim HW, Hillsamer P, Banham AH, Kim CH. Cutting edge: direct suppression of B cells by CD4+ CD25+ regulatory T cells. *J Immunol* 2005;**175**:4180-4183.
Lindenberg S, Hyttel P, Lenz S, Holmes PV. Ultrastructure of the early human implantation in vitro. *Hum Reprod* 1986;**1**:533-538.
Lindenberg S, Hyttel P, Sjogren A, Greve T. A comparative study of attachment of human, bovine and mouse blastocysts to uterine epithelial monolayer. *Hum Reprod* 1989;**4**:446-456.
Liu JY, Li F, Wang LP, Chen XF, Wang D, Cao L, Ping Y, Zhao S, Li B, Thorne SH *et al.* CTL- vs Treg lymphocyte-attracting chemokines, CCL4 and CCL20, are strong reciprocal predictive markers for survival of patients with oesophageal squamous cell carcinoma. *Br J Cancer* 2015;**113**:747-755.
Liu W, Putnam AL, Xu-Yu Z, Szot GL, Lee MR, Zhu S, Gottlieb PA, Kapranov P, Gingeras TR, Fazekas de St Groth B *et al.* CD127 expression inversely correlates with FoxP3 and suppressive function of human CD4+ T reg cells. *J Exp Med* 2006;**203**:1701-1711.
Liu X, Liu Y, Ding M, Wang X. Reduced expression of indoleamine 2,3-dioxygenase participates in pathogenesis of preeclampsia via regulatory T cells. *Mol Med Rep* 2011;**4**:53-58.
Lletget C. *Libro Blanco Biosanitario "La Infertilidad en España: Situación actual y perspectivas"*. 2011.
Lock P, Ralph S, Stanley E, Boulet I, Ramsay R, Dunn AR. Two isoforms of murine hck, generated by utilization of alternative translational initiation codons, exhibit different patterns of subcellular localization. *Mol Cell Biol* 1991;**11**:4363-4370.
Lopata A, Bentin-Ley U, Enders A. "Pinopodes" and implantation. *Rev Endocr Metab Disord* 2002;**3**:77-86.
Lotti F, Maggi M. Ultrasound of the male genital tract in relation to male reproductive health. *Hum Reprod Update* 2015;**21**:56-83.
Lowell CA, Niwa M, Soriano P, Varmus HE. Deficiency of the Hck and Src tyrosine kinases results in extreme levels of extramedullary hematopoiesis. *Blood* 1996;**87**:1780-1792.
Lowell CA, Soriano P, Varmus HE. Functional overlap in the src gene family: inactivation of hck and fgr impairs natural immunity. *Genes Dev* 1994;**8**:387-398.
Madison MN, Jones PH, Okeoma CM. Exosomes in human semen restrict HIV-1 transmission by vaginal cells and block intravaginal replication of LP-BM5 murine AIDS virus complex. *Virology* 2015;**482**:189-201.
Madison MN, Okeoma CM. Exosomes: Implications in HIV-1 Pathogenesis. *Viruses* 2015;**7**:4093-4118.
Madison MN, Roller RJ, Okeoma CM. Human semen contains exosomes with potent anti-HIV-1 activity. *Retrovirology* 2014;**11**:102.
Maida Y, Takakura M, Nishiuchi T, Yoshimoto T, Kyo S. Exosomal transfer of functional small RNAs mediates cancer-stroma communication in human endometrium. *Cancer Med* 2016;**5**:304-314.
Malissen B, Bongrand P. Early T cell activation: integrating biochemical, structural, and biophysical cues. *Annu Rev Immunol* 2015;**33**:539-561.
Marti JJ, Herrmann U. Immunogestosis: a new etiologic concept of "essential" EPH gestosis, with special consideration of the primigravid patient; preliminary report of a clinical study. *Am J Obstet Gynecol* 1977;**128**:489-493.
Maruyama T, Yoshimura Y, Yodoi J, Sabe H. Activation of c-Src kinase is associated with in vitro decidualization of human endometrial stromal cells. *Endocrinology* 1999;**140**:2632-2636.

Mascarenhas MN, Flaxman SR, Boerma T, Vanderpoel S, Stevens GA. National, regional, and global trends in infertility prevalence since 1990: a systematic analysis of 277 health surveys. *PLoS Med* 2012;**9**:e1001356.
Matera L, Cesano A, Bellone G, Oberholtzer E. Modulatory effect of prolactin on the resting and mitogen-induced activity of T, B, and NK lymphocytes. *Brain Behav Immun* 1992;**6**:409-417.
Mati JK, Mugambi M, Muriuki PB, Thairu K. Effect of prolactin on isolated rabbit myometrium. *J Endocrinol* 1974;**60**:379-380.
Mawhinney M, Mariotti A. Physiology, pathology and pharmacology of the male reproductive system. *Periodontol 2000* 2013;**61**:232-251.
McKarns SC, Schwartz RH. Distinct effects of TGF-beta 1 on CD4+ and CD8+ T cell survival, division, and IL-2 production: a role for T cell intrinsic Smad3. *J Immunol* 2005;**174**:2071-2083.
McKelvey KJ, Powell KL, Ashton AW, Morris JM, McCracken SA. Exosomes: Mechanisms of Uptake. *J Circ Biomark* 2015;**4**:7.
Mellor AL, Chandler P, Lee GK, Johnson T, Keskin DB, Lee J, Munn DH. Indoleamine 2,3-dioxygenase, immunosuppression and pregnancy. *J Reprod Immunol* 2002;**57**:143-150.
Meseguer M, Pellicer A, Simon C. MUC1 and endometrial receptivity. *Mol Hum Reprod* 1998;**4**:1089-1098.
Meuleman T, Snaterse G, van Beelen E, Anholts JD, Pilgram GS, van der Westerlaken LA, Eikmans M, Claas FH. The immunomodulating effect of seminal plasma on T cells. *J Reprod Immunol* 2015;**110**:109-116.
Mills KH. Regulatory T cells: friend or foe in immunity to infection? *Nat Rev Immunol* 2004;**4**:841-855.
Minciacchi VR, Spinelli C, Reis-Sobreiro M, Cavallini L, You S, Zandian M, Li X, Mishra R, Chiarugi P, Adam RM *et al.* MYC Mediates Large Oncosome-Induced Fibroblast Reprogramming in Prostate Cancer. *Cancer Res* 2017;**77**:2306-2317.
Miwa N, Hayakawa S, Miyazaki S, Myojo S, Sasaki Y, Sakai M, Takikawa O, Saito S. IDO expression on decidual and peripheral blood dendritic cells and monocytes/macrophages after treatment with CTLA-4 or interferon-gamma increase in normal pregnancy but decrease in spontaneous abortion. *Mol Hum Reprod* 2005;**11**:865-870.
Miyazaki T, Tanaka S, Sanjay A, Baron R. The role of c-Src kinase in the regulation of osteoclast function. *Mod Rheumatol* 2006;**16**:68-74.
Mjosberg J, Berg G, Jenmalm MC, Ernerudh J. FOXP3+ regulatory T cells and T helper 1, T helper 2, and T helper 17 cells in human early pregnancy decidua. *Biol Reprod* 2010;**82**:698-705.
Mocsai A, Ligeti E, Lowell CA, Berton G. Adhesion-dependent degranulation of neutrophils requires the Src family kinases Fgr and Hck. *J Immunol* 1999;**162**:1120-1126.
Mohn H, Le Cabec V, Fischer S, Maridonneau-Parini I. The src-family protein-tyrosine kinase p59hck is located on the secretory granules in human neutrophils and translocates towards the phagosome during cell activation. *Biochem J* 1995;**309 (Pt 2)**:657-665.
Mortaz E, Alipoor SD, Varahram M, Jamaati H, Garssen J, Mumby SE, Adcock IM. Exosomes in Severe Asthma: Update in Their Roles and Potential in Therapy. *Biomed Res Int* 2018;**2018**:2862187.
Moy E, Kimzey LM, Nelson LM, Blithe DL. Glycoprotein hormone alpha-subunit functions synergistically with progesterone to stimulate differentiation of cultured human endometrial stromal cells to decidualized cells: a novel role for free alpha-subunit in reproduction. *Endocrinology* 1996;**137**:1332-1339.

Mselle TF, Meadows SK, Eriksson M, Smith JM, Shen L, Wira CR, Sentman CL. Unique characteristics of NK cells throughout the human female reproductive tract. *Clin Immunol* 2007;**124**:69-76.
Munn DH, Zhou M, Attwood JT, Bondarev I, Conway SJ, Marshall B, Brown C, Mellor AL. Prevention of allogeneic fetal rejection by tryptophan catabolism. *Science* 1998;**281**:1191-1193.
Munoz-Suano A, Hamilton AB, Betz AG. Gimme shelter: the immune system during pregnancy. *Immunol Rev* 2011;**241**:20-38.
Murphy CR, Swift JG, Need JA, Mukherjee TM, Rogers AW. A freeze-fracture electron microscopic study of tight junctions of epithelial cells in the human uterus. *Anat Embryol (Berl)* 1982;**163**:367-370.
Nagamatsu T, Schust DJ, Sugimoto J, Barrier BF. Human decidual stromal cells suppress cytokine secretion by allogenic CD4+ T cells via PD-1 ligand interactions. *Hum Reprod* 2009;**24**:3160-3171.
Nagashima T, Maruyama T, Uchida H, Kajitani T, Arase T, Ono M, Oda H, Kagami M, Masuda H, Nishikawa S *et al.* Activation of SRC kinase and phosphorylation of signal transducer and activator of transcription-5 are required for decidual transformation of human endometrial stromal cells. *Endocrinology* 2008;**149**:1227-1234.
Nakamura K, Kitani A, Strober W. Cell contact-dependent immunosuppression by CD4(+)CD25(+) regulatory T cells is mediated by cell surface-bound transforming growth factor beta. *J Exp Med* 2001;**194**:629-644.
Nederlof I, Meuleman T, van der Hoorn MLP, Claas FHJ, Eikmans M. The seed to success: The role of seminal plasma in pregnancy. *J Reprod Immunol* 2017;**123**:24-28.
Need JA. Pre-eclampsia in pregnancies by different fathers: immunological studies. *Br Med J* 1975;**1**:548-549.
Nejat EJ, Ruiz-Alonso M, Simon C, Meier UT. Timing the window of implantation by nucleolar channel system prevalence matches the accuracy of the endometrial receptivity array. *Fertil Steril* 2014;**102**:1477-1481.
Nejatbakhsh R, Kabir-Salmani M, Dimitriadis E, Hosseini A, Taheripanah R, Sadeghi Y, Akimoto Y, Iwashita M. Subcellular localization of L-selectin ligand in the endometrium implies a novel function for pinopodes in endometrial receptivity. *Reprod Biol Endocrinol* 2012;**10**:46.
Nicolosi A, Correa Leite ML, Musicco M, Arici C, Gavazzeni G, Lazzarin A. The efficiency of male-to-female and female-to-male sexual transmission of the human immunodeficiency virus: a study of 730 stable couples. Italian Study Group on HIV Heterosexual Transmission. *Epidemiology* 1994;**5**:570-575.
Nikas G. Pinopodes as markers of endometrial receptivity in clinical practice. *Hum Reprod* 1999;**14 Suppl 2**:99-106.
Nikas G, Makrigiannakis A. Endometrial pinopodes and uterine receptivity. *Ann N Y Acad Sci* 2003;**997**:120-123.
Nikzad H, Kabir-Salmani M, Shiokawa S, Akimoto Y, Iwashita M. Co-expression of galectin-3 and alpha v beta 3 integrin at pinopodes of human endometrium. *Iran J Reprod Med* 2010;**8**:145-152.
Nishida M. The Ishikawa cells from birth to the present. *Hum Cell* 2002;**15**:104-117.
O'Flynn K, Knott LJ, Russul-Saib M, Abdul-Gaffar R, Morgan G, Beverley PC, Linch DC. CD2 and CD3 antigens mobilize Ca2+ independently. *Eur J Immunol* 1986;**16**:580-584.
Oborna I, Novotny R, Brezinova J, Petrova P, Lichnovsky V, Fingerova H. Changes in the development of uterine pinopodes in steroid hormone supplemented cycles. *Physiol Res* 2004;**53**:423-429.

Okada H, Nakajima T, Sanezumi M, Ikuta A, Yasuda K, Kanzaki H. Progesterone enhances interleukin-15 production in human endometrial stromal cells in vitro. *J Clin Endocrinol Metab* 2000;**85**:4765-4770.
Orchard MD, Shaw TJ, Murphy CR. Junctional plaque proteins shift to the apical surface of uterine epithelial cells during early pregnancy in the rat. *Acta Histochem* 1999;**101**:147-156.
Ornellas F, Bringhenti I, Mattos B, Mandarim-de-Lacerda CA, Aguila MB. Father's obesity programs the adipose tissue in the offspring via the local renin-angiotensin system and MAPKs pathways, especially in adult male mice. *Eur J Nutr* 2018;**57**:1901-1912.
Osteen KG, Hill GA, Hargrove JT, Gorstein F. Development of a method to isolate and culture highly purified populations of stromal and epithelial cells from human endometrial biopsy specimens. *Fertil Steril* 1989;**52**:965-972.
Ostensen M, Husby G. A prospective clinical study of the effect of pregnancy on rheumatoid arthritis and ankylosing spondylitis. *Arthritis Rheum* 1983;**26**:1155-1159.
Ostensen M, Villiger PM. The remission of rheumatoid arthritis during pregnancy. *Semin Immunopathol* 2007;**29**:185-191.
Paria BC, Zhao X, Das SK, Dey SK, Yoshinaga K. Zonula occludens-1 and E-cadherin are coordinately expressed in the mouse uterus with the initiation of implantation and decidualization. *Dev Biol* 1999;**208**:488-501.
Park KH, Kim BJ, Kang J, Nam TS, Lim JM, Kim HT, Park JK, Kim YG, Chae SW, Kim UH. Ca2+ signaling tools acquired from prostasomes are required for progesterone-induced sperm motility. *Sci Signal* 2011;**4**:ra31.
Parr MB, Parr EL. Uterine luminal epithelium: protrusions mediate endocytosis, not apocrine secretion, in the rat. *Biol Reprod* 1974;**11**:220-233.
Patel P, Borkowf CB, Brooks JT, Lasry A, Lansky A, Mermin J. Estimating per-act HIV transmission risk: a systematic review. *AIDS* 2014;**28**:1509-1519.
Paterson AM, Lovitch SB, Sage PT, Juneja VR, Lee Y, Trombley JD, Arancibia-Carcamo CV, Sobel RA, Rudensky AY, Kuchroo VK *et al.* Deletion of CTLA-4 on regulatory T cells during adulthood leads to resistance to autoimmunity. *J Exp Med* 2015;**212**:1603-1621.
Pawluk-Kolc M, Zieba-Palus J, Parczewski A. Application of false discovery rate procedure to pairwise comparisons of refractive index of glass fragments. *Forensic Sci Int* 2006;**160**:53-58.
Peck A, Mellins ED. Plasticity of T-cell phenotype and function: the T helper type 17 example. *Immunology* 2010;**129**:147-153.
Pereira Suarez AL, Lopez-Rincon G, Martinez Neri PA, Estrada-Chavez C. Prolactin in inflammatory response. *Adv Exp Med Biol* 2015;**846**:243-264.
Phoonsawat W, Aoki-Yoshida A, Tsuruta T, Sonoyama K. Adiponectin is partially associated with exosomes in mouse serum. *Biochem Biophys Res Commun* 2014;**448**:261-266.
Piccirillo CA, Shevach EM. Cutting edge: control of CD8+ T cell activation by CD4+CD25+ immunoregulatory cells. *J Immunol* 2001;**167**:1137-1140.
Pinheiro JCB, D.M. . *Mixed-Effects Models in S and S-PLUS*. 2000. Springer.
Pisitkun T, Shen RF, Knepper MA. Identification and proteomic profiling of exosomes in human urine. *Proc Natl Acad Sci U S A* 2004;**101**:13368-13373.
Poh AR, O'Donoghue RJ, Ernst M. Hematopoietic cell kinase (HCK) as a therapeutic target in immune and cancer cells. *Oncotarget* 2015;**6**:15752-15771.
Poliakov A, Spilman M, Dokland T, Amling CL, Mobley JA. Structural heterogeneity and protein composition of exosome-like vesicles (prostasomes) in human semen. *Prostate* 2009;**69**:159-167.

Pons-Rejraji H, Artonne C, Sion B, Brugnon F, Canis M, Janny L, Grizard G. Prostasomes: inhibitors of capacitation and modulators of cellular signalling in human sperm. *Int J Androl* 2011;**34**:568-580.
Potter SW, Gaza G, Morris JE. Estradiol induces E-cadherin degradation in mouse uterine epithelium during the estrous cycle and early pregnancy. *J Cell Physiol* 1996;**169**:1-14.
Raab M, Pfister S, Rudd CE. CD28 signaling via VAV/SLP-76 adaptors: regulation of cytokine transcription independent of TCR ligation. *Immunity* 2001;**15**:921-933.
Radford KJ, Thorne RF, Hersey P. CD63 associates with transmembrane 4 superfamily members, CD9 and CD81, and with beta 1 integrins in human melanoma. *Biochem Biophys Res Commun* 1996;**222**:13-18.
Rahnama F, Thompson B, Steiner M, Shafiei F, Lobie PE, Mitchell MD. Epigenetic regulation of E-cadherin controls endometrial receptivity. *Endocrinology* 2009;**150**:1466-1472.
Ramchandani P, Banner MP, Pollack HM. Imaging of the seminal vesicles. *Semin Roentgenol* 1993;**28**:83-91.
Raposo G, Nijman HW, Stoorvogel W, Liejendekker R, Harding CV, Melief CJ, Geuze HJ. B lymphocytes secrete antigen-presenting vesicles. *J Exp Med* 1996;**183**:1161-1172.
Raposo G, Stoorvogel W. Extracellular vesicles: exosomes, microvesicles, and friends. *J Cell Biol* 2013;**200**:373-383.
Rarani FZ, Borhani F, Rashidi B. Endometrial pinopode biomarkers: Molecules and microRNAs. *J Cell Physiol* 2018.
Rawdanowicz TJ, Hampton AL, Nagase H, Woolley DE, Salamonsen LA. Matrix metalloproteinase production by cultured human endometrial stromal cells: identification of interstitial collagenase, gelatinase-A, gelatinase-B, and stromelysin-1 and their differential regulation by interleukin-1 alpha and tumor necrosis factor-alpha. *J Clin Endocrinol Metab* 1994;**79**:530-536.
Redman CW, Sargent IL. Circulating microparticles in normal pregnancy and pre-eclampsia. *Placenta* 2008;**29 Suppl A**:S73-77.
Redman CW, Sargent IL. Immunology of pre-eclampsia. *Am J Reprod Immunol* 2010;**63**:534-543.
Reinherz EL, Meuer S, Fitzgerald KA, Hussey RE, Levine H, Schlossman SF. Antigen recognition by human T lymphocytes is linked to surface expression of the T3 molecular complex. *Cell* 1982;**30**:735-743.
Rejraji H, Sion B, Prensier G, Carreras M, Motta C, Frenoux JM, Vericel E, Grizard G, Vernet P, Drevet JR. Lipid remodeling of murine epididymosomes and spermatozoa during epididymal maturation. *Biol Reprod* 2006;**74**:1104-1113.
Remes Lenicov F, Rodriguez Rodrigues C, Sabatte J, Cabrini M, Jancic C, Ostrowski M, Merlotti A, Gonzalez H, Alonso A, Pasqualini RA *et al.* Semen promotes the differentiation of tolerogenic dendritic cells. *J Immunol* 2012;**189**:4777-4786.
Ringden O, Baygan A, Remberger M, Gustafsson B, Winiarski J, Khoein B, Moll G, Klingspor L, Westgren M, Sadeghi B. Placenta-Derived Decidua Stromal Cells for Treatment of Severe Acute Graft-Versus-Host Disease. *Stem Cell Transl Med* 2018;**7**:325-332.
Ringden O, Erkers T, Nava S, Uzunel M, Iwarsson E, Conrad R, Westgren M, Mattsson J, Kaipe H. Fetal membrane cells for treatment of steroid-refractory acute graft-versus-host disease. *Stem Cells* 2013;**31**:592-601.
Robbins SM, Quintrell NA, Bishop JM. Myristoylation and differential palmitoylation of the HCK protein-tyrosine kinases govern their attachment to membranes and association with caveolae. *Mol Cell Biol* 1995;**15**:3507-3515.

Robertson SA, Bromfield JJ, Tremellen KP. Seminal 'priming' for protection from pre-eclampsia-a unifying hypothesis. *J Reprod Immunol* 2003;**59**:253-265.
Robertson SA, Guerin LR, Bromfield JJ, Branson KM, Ahlstrom AC, Care AS. Seminal fluid drives expansion of the CD4+CD25+ T regulatory cell pool and induces tolerance to paternal alloantigens in mice. *Biol Reprod* 2009;**80**:1036-1045.
Robertson SA, Mayrhofer G, Seamark RF. Ovarian steroid hormones regulate granulocyte-macrophage colony-stimulating factor synthesis by uterine epithelial cells in the mouse. *Biol Reprod* 1996;**54**:183-196.
Robertson SA, Moldenhauer LM. Immunological determinants of implantation success. *Int J Dev Biol* 2014;**58**:205-217.
Robertson SA, Prins JR, Sharkey DJ, Moldenhauer LM. Seminal fluid and the generation of regulatory T cells for embryo implantation. *Am J Reprod Immunol* 2013;**69**:315-330.
Robertson SA, Sharkey DJ. Seminal fluid and fertility in women. *Fertil Steril* 2016;**106**:511-519.
Robillard PY, Hulsey TC, Perianin J, Janky E, Miri EH, Papiernik E. Association of pregnancy-induced hypertension with duration of sexual cohabitation before conception. *Lancet* 1994;**344**:973-975.
Rodriguez-Boulan E, Nelson WJ. Morphogenesis of the polarized epithelial cell phenotype. *Science* 1989;**245**:718-725.
Rodriguez-Caro H, Williams SA. Strategies to reduce non-communicable diseases in the offspring: negative and positive in utero programming. *J Dev Orig Health Dis* 2018:1-11.
Ronquist G, Nilsson BO. The Janus-faced nature of prostasomes: their pluripotency favours the normal reproductive process and malignant prostate growth. *Prostate Cancer Prostatic Dis* 2004;**7**:21-31.
Ronquist G, Nilsson BO, Hjerten S. Interaction between prostasomes and spermatozoa from human semen. *Arch Androl* 1990;**24**:147-157.
Ronquist GK, Larsson A, Stavreus-Evers A, Ronquist G. Prostasomes are heterogeneous regarding size and appearance but affiliated to one DNA-containing exosome family. *Prostate* 2012;**72**:1736-1745.
Ronquist KG, Ek B, Stavreus-Evers A, Larsson A, Ronquist G. Human prostasomes express glycolytic enzymes with capacity for ATP production. *Am J Physiol Endocrinol Metab* 2013;**304**:E576-582.
Ronquist KG, Ronquist G, Carlsson L, Larsson A. Human prostasomes contain chromosomal DNA. *Prostate* 2009;**69**:737-743.
Rooney IA, Atkinson JP, Krul ES, Schonfeld G, Polakoski K, Saffitz JE, Morgan BP. Physiologic relevance of the membrane attack complex inhibitory protein CD59 in human seminal plasma: CD59 is present on extracellular organelles (prostasomes), binds cell membranes, and inhibits complement-mediated lysis. *J Exp Med* 1993;**177**:1409-1420.
Royce RA, Sena A, Cates W, Jr., Cohen MS. Sexual transmission of HIV. *N Engl J Med* 1997;**336**:1072-1078.
Ruan YC, Guo JH, Liu X, Zhang R, Tsang LL, Dong JD, Chen H, Yu MK, Jiang X, Zhang XH *et al.* Activation of the epithelial Na+ channel triggers prostaglandin E(2) release and production required for embryo implantation. *Nat Med* 2012;**18**:1112-1117.
Rubinstein E, Ziyyat A, Prenant M, Wrobel E, Wolf JP, Levy S, Le Naour F, Boucheix C. Reduced fertility of female mice lacking CD81. *Dev Biol* 2006;**290**:351-358.
Rudd CE, Raab M. Independent CD28 signaling via VAV and SLP-76: a model for in trans costimulation. *Immunol Rev* 2003;**192**:32-41.
Ruiz-Alonso M, Blesa D, Diaz-Gimeno P, Gomez E, Fernandez-Sanchez M, Carranza F, Carrera J, Vilella F, Pellicer A, Simon C. The endometrial receptivity array for diagnosis

and personalized embryo transfer as a treatment for patients with repeated implantation failure. *Fertil Steril* 2013;**100**:818-824.
Rutanen EM, Koistinen R, Wahlstrom T, Bohn H, Ranta T, Seppala M. Synthesis of placental protein 12 by human decidua. *Endocrinology* 1985;**116**:1304-1309.
Saez F, Motta C, Boucher D, Grizard G. Antioxidant capacity of prostasomes in human semen. *Mol Hum Reprod* 1998;**4**:667-672.
Saez F, Motta C, Boucher D, Grizard G. Prostasomes inhibit the NADPH oxidase activity of human neutrophils. *Mol Hum Reprod* 2000;**6**:883-891.
Saez F, Sullivan R. Prostasomes, post-testicular sperm maturation and fertility. *Front Biosci (Landmark Ed)* 2016;**21**:1464-1473.
Sahlen G, Nilsson O, Larsson A, Carlsson L, Norlen BJ, Ronquist G. Secretions from seminal vesicles lack characteristic markers for prostasomes. *Ups J Med Sci* 2010;**115**:107-112.
Sahlen GE, Egevad L, Ahlander A, Norlen BJ, Ronquist G, Nilsson BO. Ultrastructure of the secretion of prostasomes from benign and malignant epithelial cells in the prostate. *Prostate* 2002;**53**:192-199.
Saito S, Nakashima A, Shima T, Ito M. Th1/Th2/Th17 and regulatory T-cell paradigm in pregnancy. *Am J Reprod Immunol* 2010;**63**:601-610.
Saito S, Shima T, Inada K, Nakashima A. Which types of regulatory T cells play important roles in implantation and pregnancy maintenance? *Am J Reprod Immunol* 2013;**69**:340-345.
Salker M, Teklenburg G, Molokhia M, Lavery S, Trew G, Aojanepong T, Mardon HJ, Lokugamage AU, Rai R, Landles C *et al.* Natural selection of human embryos: impaired decidualization of endometrium disables embryo-maternal interactions and causes recurrent pregnancy loss. *PLoS One* 2010;**5**:e10287.
Salleh N, Giribabu N. Leukemia inhibitory factor: roles in embryo implantation and in nonhormonal contraception. *ScientificWorldJournal* 2014;**2014**:201514.
Samanta L, Parida R, Dias TR, Agarwal A. The enigmatic seminal plasma: a proteomics insight from ejaculation to fertilization. *Reprod Biol Endocrinol* 2018;**16**:41.
Sang Q, Yao Z, Wang H, Feng R, Wang H, Zhao X, Xing Q, Jin L, He L, Wu L *et al.* Identification of microRNAs in human follicular fluid: characterization of microRNAs that govern steroidogenesis in vitro and are associated with polycystic ovary syndrome in vivo. *J Clin Endocrinol Metab* 2013;**98**:3068-3079.
Sanjabi S, Oh SA, Li MO. Regulation of the Immune Response by TGF-beta: From Conception to Autoimmunity and Infection. *Cold Spring Harb Perspect Biol* 2017;**9**.
Sarani SA, Ghaffari-Novin M, Warren MA, Dockery P, Cooke ID. Morphological evidence for the 'implantation window' in human luminal endometrium. *Hum Reprod* 1999;**14**:3101-3106.
Sargent I. Reproductive Immunology. In Wells KCD (ed) *Textbook of Clinical Embryology*. 2013. Cambridge University Press, USA.
Sasaki Y, Darmochwal-Kolarz D, Suzuki D, Sakai M, Ito M, Shima T, Shiozaki A, Rolinski J, Saito S. Proportion of peripheral blood and decidual CD4(+) CD25(bright) regulatory T cells in pre-eclampsia. *Clin Exp Immunol* 2007;**149**:139-145.
Sasaki Y, Sakai M, Miyazaki S, Higuma S, Shiozaki A, Saito S. Decidual and peripheral blood CD4+CD25+ regulatory T cells in early pregnancy subjects and spontaneous abortion cases. *Mol Hum Reprod* 2004;**10**:347-353.
Sassone-Corsi P. Coupling gene expression to cAMP signalling: role of CREB and CREM. *Int J Biochem Cell Biol* 1998;**30**:27-38.
Savage ND, de Boer T, Walburg KV, Joosten SA, van Meijgaarden K, Geluk A, Ottenhoff TH. Human anti-inflammatory macrophages induce Foxp3+ GITR+ CD25+

regulatory T cells, which suppress via membrane-bound TGFbeta-1. *J Immunol* 2008;**181**:2220-2226.
Schreiner SJ, Schiavone AP, Smithgall TE. Activation of STAT3 by the Src family kinase Hck requires a functional SH3 domain. *J Biol Chem* 2002;**277**:45680-45687.
Schumacher A, Wafula PO, Bertoja AZ, Sollwedel A, Thuere C, Wollenberg I, Yagita H, Volk HD, Zenclussen AC. Mechanisms of action of regulatory T cells specific for paternal antigens during pregnancy. *Obstet Gynecol* 2007;**110**:1137-1145.
Schumacher A, Zenclussen AC. Regulatory T cells: regulators of life. *Am J Reprod Immunol* 2014;**72**:158-170.
Sentman CL, Meadows SK, Wira CR, Eriksson M. Recruitment of uterine NK cells: induction of CXC chemokine ligands 10 and 11 in human endometrium by estradiol and progesterone. *J Immunol* 2004;**173**:6760-6766.
Shankar Srinivas TW. Early embryogenesis. In Kevin Coward DW (ed) *Textbook of Clinical Embryology*. 2013. Cambridge University Press, Spain.
Shima T, Sasaki Y, Itoh M, Nakashima A, Ishii N, Sugamura K, Saito S. Regulatory T cells are necessary for implantation and maintenance of early pregnancy but not late pregnancy in allogeneic mice. *J Reprod Immunol* 2010;**85**:121-129.
Shimizu A, Maruyama T, Tamaki K, Uchida H, Asada H, Yoshimura Y. Impairment of decidualization in SRC-deficient mice. *Biol Reprod* 2005;**73**:1219-1227.
Shull MM, Ormsby I, Kier AB, Pawlowski S, Diebold RJ, Yin M, Allen R, Sidman C, Proetzel G, Calvin D *et al.* Targeted disruption of the mouse transforming growth factor-beta 1 gene results in multifocal inflammatory disease. *Nature* 1992;**359**:693-699.
Simon C, Greening DW, Bolumar D, Balaguer N, Salamonsen LA, Vilella F. Extracellular Vesicles in Human Reproduction in Health and Disease. *Endocr Rev* 2018;**39**:292-332.
Simons K, Fuller SD. Cell surface polarity in epithelia. *Annu Rev Cell Biol* 1985;**1**:243-288.
Singh H, Aplin JD. Adhesion molecules in endometrial epithelium: tissue integrity and embryo implantation. *J Anat* 2009;**215**:3-13.
Skibinski G, Kelly RW, Harkiss D, James K. Immunosuppression by human seminal plasma--extracellular organelles (prostasomes) modulate activity of phagocytic cells. *Am J Reprod Immunol* 1992;**28**:97-103.
Smyth MJ, Strobl SL, Young HA, Ortaldo JR, Ochoa AC. Regulation of lymphokine-activated killer activity and pore-forming protein gene expression in human peripheral blood CD8+ T lymphocytes. Inhibition by transforming growth factor-beta. *J Immunol* 1991;**146**:3289-3297.
Southcombe JH, Mounce G, McGee K, Elghajiji A, Brosens J, Quenby S, Child T, Granne I. An altered endometrial CD8 tissue resident memory T cell population in recurrent miscarriage. *Sci Rep* 2017;**7**:41335.
Stangelberger A, Waldert M, Djavan B. Prostate cancer in elderly men. *Rev Urol* 2008;**10**:111-119.
Stavreus-Evers A, Aghajanova L, Brismar H, Eriksson H, Landgren BM, Hovatta O. Co-existence of heparin-binding epidermal growth factor-like growth factor and pinopodes in human endometrium at the time of implantation. *Mol Hum Reprod* 2002;**8**:765-769.
Stavreus-Evers A, Nikas G, Sahlin L, Eriksson H, Landgren BM. Formation of pinopodes in human endometrium is associated with the concentrations of progesterone and progesterone receptors. *Fertil Steril* 2001;**76**:782-791.
Stefanoska I, Jovanovic Krivokuca M, Vasilijic S, Cujic D, Vicovac L. Prolactin stimulates cell migration and invasion by human trophoblast in vitro. *Placenta* 2013;**34**:775-783.

Stoikos CJ, Harrison CA, Salamonsen LA, Dimitriadis E. A distinct cohort of the TGFbeta superfamily members expressed in human endometrium regulate decidualization. *Hum Reprod* 2008;**23**:1447-1456.
Sullivan R, Frenette G, Girouard J. Epididymosomes are involved in the acquisition of new sperm proteins during epididymal transit. *Asian J Androl* 2007;**9**:483-491.
Sullivan R, Saez F. Epididymosomes, prostasomes, and liposomes: their roles in mammalian male reproductive physiology. *Reproduction* 2013;**146**:R21-35.
Sun X, Ruan YC, Guo J, Chen H, Tsang LL, Zhang X, Jiang X, Chan HC. Regulation of miR-101/miR-199a-3p by the epithelial sodium channel during embryo implantation: involvement of CREB phosphorylation. *Reproduction* 2014;**148**:559-568.
Szamatowicz M. Assisted reproductive technology in reproductive medicine - possibilities and limitations. *Ginekol Pol* 2016;**87**:820-823.
Taams LS, van Amelsfort JM, Tiemessen MM, Jacobs KM, de Jong EC, Akbar AN, Bijlsma JW, Lafeber FP. Modulation of monocyte/macrophage function by human CD4+CD25+ regulatory T cells. *Hum Immunol* 2005;**66**:222-230.
Tabanelli S, Tang B, Gurpide E. In vitro decidualization of human endometrial stromal cells. *J Steroid Biochem Mol Biol* 1992;**42**:337-344.
Tanaka N, Miyazaki K, Tashiro H, Mizutani H, Okamura H. Changes in adenylyl cyclase activity in human endometrium during the menstrual cycle and in human decidua during pregnancy. *J Reprod Fertil* 1993;**98**:33-39.
Tang B, Guller S, Gurpide E. Cyclic adenosine 3',5'-monophosphate induces prolactin expression in stromal cells isolated from human proliferative endometrium. *Endocrinology* 1993;**133**:2197-2203.
Tannetta D, Dragovic R, Alyahyaei Z, Southcombe J. Extracellular vesicles and reproduction-promotion of successful pregnancy. *Cell Mol Immunol* 2014;**11**:548-563.
Tannetta D, Masliukaite I, Vatish M, Redman C, Sargent I. Update of syncytiotrophoblast derived extracellular vesicles in normal pregnancy and preeclampsia. *J Reprod Immunol* 2017;**119**:98-106.
Tarazona R, Delgado E, Guarnizo MC, Roncero RG, Morgado S, Sanchez-Correa B, Gordillo JJ, Dejulian J, Casado JG. Human prostasomes express CD48 and interfere with NK cell function. *Immunobiology* 2011;**216**:41-46.
Teh WT, McBain J, Rogers P. What is the contribution of embryo-endometrial asynchrony to implantation failure? *J Assist Reprod Genet* 2016;**33**:1419-1430.
Terzakis JA. The nucleolar channel system of human endometrium. *J Cell Biol* 1965;**27**:293-304.
Tesarik J. Appropriate timing of the acrosome reaction is a major requirement for the fertilizing spermatozoon. *Hum Reprod* 1989;**4**:957-961.
Thie M, Denker HW. In vitro studies on endometrial adhesiveness for trophoblast: cellular dynamics in uterine epithelial cells. *Cells Tissues Organs* 2002;**172**:237-252.
Thie M, Fuchs P, Denker HW. Epithelial cell polarity and embryo implantation in mammals. *Int J Dev Biol* 1996;**40**:389-393.
Thimon V, Frenette G, Saez F, Thabet M, Sullivan R. Protein composition of human epididymosomes collected during surgical vasectomy reversal: a proteomic and genomic approach. *Hum Reprod* 2008;**23**:1698-1707.
Tompkins AJ, Chatterjee D, Maddox M, Wang J, Arciero E, Camussi G, Quesenberry PJ, Renzulli JF. The emergence of extracellular vesicles in urology: fertility, cancer, biomarkers and targeted pharmacotherapy. *J Extracell Vesicles* 2015;**4**:23815.
Trajkovic K, Hsu C, Chiantia S, Rajendran L, Wenzel D, Wieland F, Schwille P, Brugger B, Simons M. Ceramide triggers budding of exosome vesicles into multivesicular endosomes. *Science* 2008;**319**:1244-1247.

Travis MA, Sheppard D. TGF-beta activation and function in immunity. *Annu Rev Immunol* 2014;**32**:51-82.
Tremellen KP, Valbuena D, Landeras J, Ballesteros A, Martinez J, Mendoza S, Norman RJ, Robertson SA, Simon C. The effect of intercourse on pregnancy rates during assisted human reproduction. *Hum Reprod* 2000;**15**:2653-2658.
Trickett A, Kwan YL. T cell stimulation and expansion using anti-CD3/CD28 beads. *J Immunol Methods* 2003;**275**:251-255.
Tsatsanis C, Androulidaki A, Venihaki M, Margioris AN. Signalling networks regulating cyclooxygenase-2. *Int J Biochem Cell Biol* 2006;**38**:1654-1661.
UNAIDS. UNAIDS Data 2018. 2018. Joiunt United Nations Programme on HIV/AIDS (UNAIDS).
Utleg AG, Yi EC, Xie T, Shannon P, White JT, Goodlett DR, Hood L, Lin B. Proteomic analysis of human prostasomes. *Prostate* 2003;**56**:150-161.
Valdes CT, Schutt A, Simon C. Implantation failure of endometrial origin: it is not pathology, but our failure to synchronize the developing embryo with a receptive endometrium. *Fertil Steril* 2017;**108**:15-18.
Valitutti S, Muller S, Cella M, Padovan E, Lanzavecchia A. Serial triggering of many T-cell receptors by a few peptide-MHC complexes. *Nature* 1995;**375**:148-151.
van der Pol E, Coumans FA, Grootemaat AE, Gardiner C, Sargent IL, Harrison P, Sturk A, van Leeuwen TG, Nieuwland R. Particle size distribution of exosomes and microvesicles determined by transmission electron microscopy, flow cytometry, nanoparticle tracking analysis, and resistive pulse sensing. *J Thromb Haemost* 2014;**12**:1182-1192.
van Mourik MS, Macklon NS, Heijnen CJ. Embryonic implantation: cytokines, adhesion molecules, and immune cells in establishing an implantation environment. *J Leukoc Biol* 2009;**85**:4-19.
van Niel G, Bergam P, Di Cicco A, Hurbain I, Lo Cicero A, Dingli F, Palmulli R, Fort C, Potier MC, Schurgers LJ *et al.* Apolipoprotein E Regulates Amyloid Formation within Endosomes of Pigment Cells. *Cell Rep* 2015;**13**:43-51.
van Niel G, Charrin S, Simoes S, Romao M, Rochin L, Saftig P, Marks MS, Rubinstein E, Raposo G. The tetraspanin CD63 regulates ESCRT-independent and -dependent endosomal sorting during melanogenesis. *Dev Cell* 2011;**21**:708-721.
van Niel G, D'Angelo G, Raposo G. Shedding light on the cell biology of extracellular vesicles. *Nat Rev Mol Cell Biol* 2018;**19**:213-228.
Varghese B, Maher JE, Peterman TA, Branson BM, Steketee RW. Reducing the risk of sexual HIV transmission: quantifying the per-act risk for HIV on the basis of choice of partner, sex act, and condom use. *Sex Transm Dis* 2002;**29**:38-43.
Vashisht M, Rani P, Onteru SK, Singh D. Curcumin Encapsulated in Milk Exosomes Resists Human Digestion and Possesses Enhanced Intestinal Permeability in Vitro. *Appl Biochem Biotechnol* 2017;**183**:993-1007.
Verma S, Hiby SE, Loke YW, King A. Human decidual natural killer cells express the receptor for and respond to the cytokine interleukin 15. *Biol Reprod* 2000;**62**:959-968.
Vernazza PL, Eron JJ, Fiscus SA, Cohen MS. Sexual transmission of HIV: infectiousness and prevention. *AIDS* 1999;**13**:155-166.
Vinketova K, Mourdjeva M, Oreshkova T. Human Decidual Stromal Cells as a Component of the Implantation Niche and a Modulator of Maternal Immunity. *J Pregnancy* 2016;**2016**:8689436.
von Wolff M, Rosner S, Germeyer A, Jauckus J, Griesinger G, Strowitzki T. Intrauterine instillation of diluted seminal plasma at oocyte pick-up does not increase the IVF

pregnancy rate: a double-blind, placebo controlled, randomized study. *Hum Reprod* 2013;**28**:3247-3252.
von Wolff M, Wang X, Gabius HJ, Strowitzki T. Galectin fingerprinting in human endometrium and decidua during the menstrual cycle and in early gestation. *Mol Hum Reprod* 2005;**11**:189-194.
Wang H, Pilla F, Anderson S, Martinez-Escribano S, Herrer I, Moreno-Moya JM, Musti S, Bocca S, Oehninger S, Horcajadas JA. A novel model of human implantation: 3D endometrium-like culture system to study attachment of human trophoblast (Jar) cell spheroids. *Mol Hum Reprod* 2012;**18**:33-43.
Wang HS, Perry LA, Kanisius J, Iles RK, Holly JM, Chard T. Purification and assay of insulin-like growth factor-binding protein-1: measurement of circulating levels throughout pregnancy. *J Endocrinol* 1991;**128**:161-168.
Wathes DC, Wooding FB. An electron microscopic study of implantation in the cow. *Am J Anat* 1980;**159**:285-306.
Way DL, Grosso DS, Davis JR, Surwit EA, Christian CD. Characterization of a new human endometrial carcinoma (RL95-2) established in tissue culture. *In Vitro* 1983;**19**:147-158.
Welton JL, Webber JP, Botos LA, Jones M, Clayton A. Ready-made chromatography columns for extracellular vesicle isolation from plasma. *J Extracell Vesicles* 2015;**4**:27269.
Whitby S, Salamonsen LA, Evans J. The Endometrial Polarity Paradox: Differential Regulation of Polarity Within Secretory-Phase Human Endometrium. *Endocrinology* 2018;**159**:506-518.
White HD, Crassi KM, Givan AL, Stern JE, Gonzalez JL, Memoli VA, Green WR, Wira CR. CD3+ CD8+ CTL activity within the human female reproductive tract: influence of stage of the menstrual cycle and menopause. *J Immunol* 1997;**158**:3017-3027.
White TE, di Sant'Agnese PA, Miller RK. Human endometrial cells grown on an extracellular matrix form simple columnar epithelia and glands. *In Vitro Cell Dev Biol* 1990;**26**:636-642.
WHO. Current practices and controversies in assisted reproduction. 2002. World Health Organization.
WHO. Reproductive Health Indicators. Guidelines for their generation, interpretation and analysis for global monitoring. 2006. World Health Organization.
Wilcox AJ, Baird DD, Weinberg CR. Time of implantation of the conceptus and loss of pregnancy. *N Engl J Med* 1999;**340**:1796-1799.
Wilczynski JR. Th1/Th2 cytokines balance--yin and yang of reproductive immunology. *Eur J Obstet Gynecol Reprod Biol* 2005;**122**:136-143.
Winger EE, Reed JL. Low circulating CD4(+) CD25(+) Foxp3(+) T regulatory cell levels predict miscarriage risk in newly pregnant women with a history of failure. *Am J Reprod Immunol* 2011;**66**:320-328.
Wira CR, Rodriguez-Garcia M, Patel MV. The role of sex hormones in immune protection of the female reproductive tract. *Nat Rev Immunol* 2015;**15**:217-230.
Wu F, Chen X, Liu Y, Liang B, Xu H, Li TC, Wang CC. Decreased MUC1 in endometrium is an independent receptivity marker in recurrent implantation failure during implantation window. *Reprod Biol Endocrinol* 2018;**16**:60.
Wynn RM. Ultrastructural development of the human decidua. *Am J Obstet Gynecol* 1974;**118**:652-670.
Wynn RM, Woolley RS. Ultrastructural cyclic changes in the human endometrium. II. Normal postovulatory phase. *Fertil Steril* 1967;**18**:721-738.

Xu G, Guimond MJ, Chakraborty C, Lala PK. Control of proliferation, migration, and invasiveness of human extravillous trophoblast by decorin, a decidual product. *Biol Reprod* 2002;**67**:681-689.
Yanez-Mo M, Siljander PR, Andreu Z, Zavec AB, Borras FE, Buzas EI, Buzas K, Casal E, Cappello F, Carvalho J *et al.* Biological properties of extracellular vesicles and their physiological functions. *J Extracell Vesicles* 2015;**4**:27066.
Yang H, Qiu L, Chen G, Ye Z, Lu C, Lin Q. Proportional change of CD4+CD25+ regulatory T cells in decidua and peripheral blood in unexplained recurrent spontaneous abortion patients. *Fertil Steril* 2008;**89**:656-661.
Yang Y, Liu L, Liu B, Li Q, Wang Z, Fan S, Wang H, Wang L. Functional Defects of Regulatory T Cell Through Interleukin 10 Mediated Mechanism in the Induction of Gestational Diabetes Mellitus. *DNA Cell Biol* 2018;**37**:278-285.
Yeaman GR, Guyre PM, Fanger MW, Collins JE, White HD, Rathbun W, Orndorff KA, Gonzalez J, Stern JE, Wira CR. Unique CD8+ T cell-rich lymphoid aggregates in human uterine endometrium. *J Leukoc Biol* 1997;**61**:427-435.
Yi H, Zhen Y, Jiang L, Zheng J, Zhao Y. The phenotypic characterization of naturally occurring regulatory CD4+CD25+ T cells. *Cell Mol Immunol* 2006;**3**:189-195.
Zanders ED, Lamb JR, Feldmann M, Green N, Beverley PC. Tolerance of T-cell clones is associated with membrane antigen changes. *Nature* 1983;**303**:625-627.
Zervomanolakis I, Ott HW, Hadziomerovic D, Mattle V, Seeber BE, Virgolini I, Heute D, Kissler S, Leyendecker G, Wildt L. Physiology of upward transport in the human female genital tract. *Ann N Y Acad Sci* 2007;**1101**:1-20.
Zhang D, Ma C, Sun X, Xia H, Zhang W. S100P expression in response to sex steroids during the implantation window in human endometrium. *Reprod Biol Endocrinol* 2012;**10**:106.
Zhang J, Dunk C, Croy AB, Lye SJ. To serve and to protect: the role of decidual innate immune cells on human pregnancy. *Cell Tissue Res* 2016;**363**:249-265.
Zhang J, Salamonsen LA. Tissue inhibitor of metalloproteinases (TIMP)-1, -2 and -3 in human endometrium during the menstrual cycle. *Mol Hum Reprod* 1997;**3**:735-741.
Zhu H, Hou CC, Luo LF, Hu YJ, Yang WX. Endometrial stromal cells and decidualized stromal cells: origins, transformation and functions. *Gene* 2014;**551**:1-14.
Zihni C, Mills C, Matter K, Balda MS. Tight junctions: from simple barriers to multifunctional molecular gates. *Nat Rev Mol Cell Biol* 2016;**17**:564-580.
Zijlstra C, Stoorvogel W. Prostasomes as a source of diagnostic biomarkers for prostate cancer. *J Clin Invest* 2016;**126**:1144-1151.